Norwegian University of Science and Technology

Doctoral Thesis

Ultra-high frame rate tissue Doppler imaging, technical feasibility and first clinical experiences

Author:
Lars Christian Naterstad Lervik, MD

Supervisors:
Asbjørn Støylen, Prof. Dr. Med. and
Brage Amundsen, MD PhD

A thesis submitted in fulfilment of the requirements for the degree of Philosophiae Doctor

in the

Ultrasound Group
Department of Circulation and Medical Imaging

"Cherish those who seek the truth but beware of those who find it"

François-Marie Arouet, Voltaire

NORWEGIAN UNIVERSITY OF SCIENCE AND TECHNOLOGY

Abstract

Faculty of Medicine and Health Sciences
Department of Circulation and Medical Imaging

Philosophiae Doctor

Ultra-high frame rate tissue Doppler imaging, technical feasibility and first clinical experiences

by Lars Christian Naterstad Lervik, MD

Echocardiography has become an important tool in the diagnosis of heart disease. It is non-invasive and tolerable and can be used to assess both cardiac structure and function. In the late 1980s, tissue Doppler imaging (TDI) was added to the tools of echocardiography, which made it possible to quantify myocardial motion by measuring tissue velocities. This has proven useful, especially in the assessment of left ventricular function. The frame rate is of great interest when measuring myocardial motion with TDI. Conventional colour TDI can typically sample 150 images of the left ventricle per second. The frame rate may be increased to 250 images per second by focusing on a single ventricular wall. This may, however, not be sufficient to resolve all of the mechanical events in a cardiac cycle. At NTNU we have developed a method for acquisition of tissue Doppler data with a frame rate of 1200 fps and 500 fps in two- and three-dimensions (2D and 3D), respectively. The aims of this thesis were therefore to evaluate the technical feasibility and describe the first clinical experiences with Ultra-high Frame Rate Tissue Doppler Imaging. In the first paper, *Ultra-high Frame Rate Tissue Doppler Imaging*, we examined the technical feasibility of 2D UFR-TDI. In this study, we found that use of UFR-TDI is feasible with a frame rate of 1200 fps. The method showed good agreement with conventional TDI in peak velocity measurements, and provided additional information about the mechanical events in early systole.

In the second paper, *Detection of mechanical activation in an open chest porcine model by three-dimensional UFR-TDI, a feasibility study*, we describe a method for detection of mechanical activation in the left ventricle with UFR-TDI in two and three dimensions in an open chest pig model with epicardial pacing. The delay from onset of electrical to mechanical activation was shorter in the segments corresponding to the pacing electrodes both in 2D and 3D UFR-TDI. Our findings indicate that detection of onset of mechanical activation may be feasible, both with 2D and 3D UFR-TDI.

In the third paper, *Myocardial Strain Rate by Anatomic Doppler Spectrum: First Clinical Experience Using Retrospective Spectral Tissue Doppler from Ultra-High Frame Rate imaging*, we describe a new method for evaluating tissue deformation by tissue Doppler; Anatomic Doppler Spectrum (ADS). ADS enables retrospective spectral analysis of tissue deformation from Doppler data from the entire ventricular wall without the influence of clutter. We found that deformation analysis by ADS was feasible in more segments and was able to differentiate segmental distribution of scar tissue compared to color TDI.
In the fourth paper, *Color Tissue Doppler Imaging in Contrast Echocardiography - a Feasibility Study*, we explore the reproducibility of tissue Doppler velocity parameters after injection of ultrasound contrast medium. We found that the intra- and inter-observer repeatability in post-contrast measurements was non-inferior compared to pre-contrast measurements.

The results warrant further study and improvement of existing technology is needed for clinical benefit.

NORGES TEKNISK-NATURVITENSKAPELIGE UNIVERSITET

Sammendrag

Fakultet for medisin og helsevitenskap
Institutt for sirkulasjon og bildediagnostikk

Philosophiae Doctor

Vevsdoppler med ultra-høy tidsoppløsning, teknisk gjennomførbarhet og første kliniske erfaringer

by Lars Christian Naterstad Lervik, MD

Ekkokardiografi er blitt et viktig verktøy i diagnostikk av hjertesykdom. Det er ikke-invasivt og tolerabelt, og kan brukes til å vurdere både hjertets struktur og funksjon. På slutten av 80-tallet ble vevsDoppler (TDI) introdusert i ekkokardiografi, noe som gjorde det mulig å kvantifisere myokardbevegelse ved å måle vevhastigheter. Dette har vist seg nyttig, spesielt i funksjonsvurderingen av venstre ventrikkel. Bildefrekvens er viktig når man måler myokardbevegelse med TDI. Konvensjonell TDI kan typisk fange 150 bilder av venstre ventrikkel per sekund. Frekvensens kan økes til 250 bilder per sekund ved kun å fokusere på en ventrikulær vegg. Dette er imidlertid ikke tilstrekkelig for analyse av de raske mekaniske hendelsene i hjertesyklus. Ved NTNU har vi utviklet en metode for opptak av Doppler-data med en bildefrekvens på 1200 og 500 bilder per sekund, i henholdsvis 2- og 3-dimensjoner. Målene med denne avhandlingen var derfor å evaluere den tekniske egnetheten og gjennomførbarheten, og beskrive de første kliniske erfaringene med Ultra-High Frame Rate Tissue Doppler Imaging (UFR-TDI).

I den første artikkelen, *Ultra-high Frame Rate Tissue Doppler Imaging*, undersøkte vi teknisk gjennomførbarhet for 2D UFR-TDI. I denne studien fant vi at bruk av UFR-TDI er mulig med en bildefrekvens på 1200 fps. Metoden viste godt samsvar med konvensjonelle maksimale TDI hastighetsmål, og ga ny informasjon om de mekaniske hendelsene i tidlig systole.
I den andre artikkelen, *Detection of mechanical activation in an open chest porcine model by three-dimensional UFR-TDI, a feasibility study*, beskriver vi en metode for påvisning av mekanisk aktivering i venstre ventrikkel med UFR-TDI i to og tre dimensjoner (2D og 3D) i en "open chest" grisemodell med epikardiell pacing. Tidsforsinkelsen fra start av elektrisk til mekanisk aktivering var kortere i segmentene svarende til pacemaker elektrodene både i 2D og 3D UFR-TDI. Våre funn indikerer at deteksjon av mekanisk aktivering kan være mulig både med 2D og 3D UFR-TDI.

I den tredje artikkelen, *Myocardial Strain Rate by Anatomic Doppler Spectrum: First Clinical Experience Using Retrospective Spectral Tissue Doppler from Ultra-High Frame Rate imaging*, beskriver vi en ny metode for å evaluere vevsdeformasjon med vevsdoppler, Anatomisk Doppler Spectrum (ADS). ADS tillater retrospektiv spektralanalyse av vevsdeformasjon fra Doppler-data fra hele ventrikkelveggen uten påvirkning av støy. Vi fant at deformasjonsanalysen med ADS var mulig i flere segmenter og var i stand til å differensiere segmental utbredelse av arrvev sammenlignet med farge TDI.
I den fjerde artikkelen, *Color Tissue Doppler Imaging in Contrast Echocardiography - a Feasibility Study*, undersøker vi reproduserbarheten av vevsdoppler hastighetsparametere etter injeksjon av ultralyd kontrast. Vi fant at intra- og inter-observatør-repeterbarheten i målingene etter kontrast var uendret sammenlignet med pre-kontrastmålinger.

Resultatene indikerer at videre studier og forbedring av eksisterende teknologi er nødvendig for klinisk nytte.

Acknowledgements

Firstly, thanks to Asbjørn Støylen, main project promoter and motivator. His insight, experience in the field and professional standing has been invaluable to my work. Brage Amundsen has been my second promotor during the PhD period and his thoroughness and hardworking attitude has encouraged me to improve my work alot. His calm and pleasant personality has been uplifting during hard periods of the PhD. Birger Brekke has taught me LaTeX and some basic Matlab, he also tried to introduced me to python and GitBash (without success). Birgers relaxed and focused attitude helped me to focus my energy when needed. Joakim Lund has been a great support during the entire PhD period. He has always made time to provide feedback, assist in analysis and writing, and his knowledge and thoroughness has been greatly appreciated. Further, his humble and polite personality made him a delight to work with. Svein Arne Aase has been my go-to technical person, always available for questions providing solutions for most of them, a true problemsolver and engineer. A greath thanks to Jan D'hooge and the entire Leuven team which made paper II possible. Their contribution was invaluable.

To my daughter, Nora, thanks for being my greatest motivation and allowing me to forget the hospital, patients and thesis! To my wife, Trine, thanks for the patience! You have listened to endless frustrations and, most of the time, appear to be interested and helpful! Thanks to my parents, my mom who actually debugged some code and my dad who has proof read some of my work! You have been a great support and motivation! Also thanks to Stein Haugen for proof reading and providing valuable feedback.

Finally thanks to the Department of Circulation and Medical Imaging and Medical Imaging Lab for the funding which made this thesis possible.

List Of Papers

The following papers are included in this thesis titled, 'Ultra-high frame rate tissue Doppler imaging, technical feasibility and first clinical experiences'

Paper I Birger Brekke, Lars C L Nilsen, Joakim Lund, Hans Torp, Tore Bjastad, Brage H Amundsen, Asbjorn Stoylen, and Svein Aase. Ultra-high frame rate tissue Doppler imaging. Ultrasound in medicine & biology, 40(1):222 31, jan 2014. ISSN 1879- 291X. doi: 10.1016/j.ultrasmedbio.2013.09.012. [1]

Paper II LCN Lervik, B Brekke, C Missant, P Haemers, L Tong, A Ortega, H Torp, A Stoylen, GR Sutherland and J D'hooge. Detection of left ventricular mechanical activation by three-dimensional ultra-high frame rate tissue Doppler imaging in an open-chest porcine model, a feasibility study. Manuscript submitted for review in Echocardiography [2]

Paper III LCN Lervik, B Brekke, SA Aase, MT Lønnebakken, D Stensvåg, BH Amundsen, H Torp, and A Stoylen. Myocardial Strain Rate by Anatomic Doppler Spectrum: First Clinical Experience Using Retrospective Spectral Tissue Doppler from Ultra-High Frame Rate imaging. Ultrasound in medicine & biology - doi: 10.1016/j.ultrasmedbio.2017.05.016 [3]

Paper IV MT Lønnebakken, LCN Lervik and A Støylen. Tissue Doppler Imaging in Contrast Echocardiography a feasibility study. - Manuscript [4]

Contents

List of Figures

Abbreviations

ACEI	Angiotensin Converting Enzyme Inhibitor
ADS	Anatomic Doppler Spectrum
ADS SR Slope	Anatomic Doppler Spectrum Mid-systolic Segmental Strain Rate
ADS SR Visual	Anatomic Doppler Spectrum Visual Mid-systolic Segmental Strain Rate
ARB	Angiotensin II Receptor blocker
CRT	Cardiac Resynchronization Therapy
CW	Continious Wave
CX	Circumflex Coronary Artery
DSE	Dobutamine Stress Echo
EF	Ejection Fraction
LAD	Left Anterior Descending Artery
LGE-MRI	Late Gadolinium Enhanced Magnetic Resonance Imaging
LV	Left Ventricle
LVOT	Left Ventricular Outflow Tract
MLA	Multi Line Acquisition
MRI	Enhanced Magnetic Resonance Imaging
NYHA	New York Heart Association
PCI	Percutaneous Coronary Intervention
PSSR	Peak Systolic Strain Rate
PW	Pulsed Wave
RCA	Right Coronary Artery
SR	Strain Rate
STEMI	ST-Elevation myocardial infarction
TD	Tissue Doppler
TDI	Tissue Doppler Imaging

UC	Ultrasound Contrast
UFR-TDI	Ultra-high Frame Rate Tissue Doppler Imaging

Chapter 1

Introduction and background

Echocardiography has become a valuable clinical tool in cardiac diagnostics. It is non-invasive, cheap and has very few contraindications. It is also portable, making it available bedside. As the technology develops, the areas of use are continuously expanding. The background for this thesis was to explore the technical and clinical feasibility of deformation imaging by ultra-high frame rate tissue Doppler imaging (UFR-TDI). Chapter 1 includes a brief history of ultrasound, an introduction to ultrasound, tissue Doppler and deformation imaging and its current state, along with a section regarding technical aspects and clinical potential of high frame rate imaging. Chapter 2 includes the hypothesis on which the thesis is based. Materials and methods for technical and clinical feasibility studies are described in Chapter 3. The results are summarized in Chapter 4. Discussion and limitations are provided in Chapters 5 and 6, respectively. Finally a conclusion and future directions are provided in Chapters 7 and 8, respectively.

1.1 Echocardiography - a brief historical summary

1.1.1 The history of ultrasound

Ultrasound has been used in the clinic since the late 50s, but the concept of echolocation was described as early as in the 18th century by Lazzaro Spellanzani, who found that the bats navigation relied on soundwaves [5]. In the late 19th century, Pierre and Paul-Jacques Curie described piezoelectricity [6]. Piezoelectricity is the property by

which electrical charge is created by the mechanical deformation of a crystal [7]. These two discoveries aided the first commercial use of ultrasonic waves in 1912. The sinking of Titanic motivated Lewis Richardson to develop and patent both airborne and underwater echolocation systems intended for iceberg-detection. His work also aided the development of the ASDIC, later know as SONAR (Sound Navigation And Ranging), by Langewin and Boyle in 1915, which was used during World War I to detect enemy submarines [8, p.10]. Between the world wars, ultrasound techniques were applied to detect flaws in metal. The machines were called reflectoscopes or flaw detectors [9, 10] and contributed to the development of medical diagnostic ultrasound.

1.1.2 Ultrasound in medicine and cardiology

In 1942, Karl Theodore Dussik and his brother, Frederick Dussik, attempted to use ultrasound to locate brain tumors and the cerebral ventricles by measuring the transmission of a ultrasound beam through the scull [11]. They termed their procedure hyperphonography. They recorded the first ever diagnostic ultrasound image of a living human being in 1947, and presented it at a meeting in Mount Sinai Hospital in New York in 1951 [12]. In 1950, Wolf-Dieter Keidel described recordings of ultrasonic intensity variations synchronous to the heart in his attempt to quantify percussion [1] [12–14]. During the 50s several independent research groups attempted to use reflected ultrasound in diagnostics [12]. In 1953 in Lund in Sweden, Edler and Herz met to discuss the possibility of using ultrasound in diagnosis of mitral regurgitation [12]. They managed to visualize moving cardiac structures by ultrasound, and later developed the m-mode [15].

1.1.3 Development of Doppler Imaging in Trondheim

The Doppler-effect was first theoretically derived by Christian Doppler for light in 1843 [16]. Later Ballot empirically verified the Doppler effect for sound waves [17]. The Doppler effect describes the change in frequency of a wave from a source moving relative to the observer. This effect was utilized in the development of PEDOF (Pulsed Echo Doppler Frequency), which was developed at The Norwegian Institute of Technology in cooperation with the section of Cardiology at the university hospital, now known

[1] The principle of percussion is that a pulse transmitted from the body surface, is reflected with different frequency and amplitude. It is still used in the clinic today, and was first introduced in 1761 by Leopold Auenbrugger

as NTNU and St. Olavs Hospital respectively. Initially PEDOF was used to record velocities in the ascending and descending Aorta with a mean and a maximum flow velocity estimator. The maximum flow estimator was non-directional and detected the maximal frequency Doppler signal. The mean estimator was able to discern direction of the blood flow, showing flow reversal in the descending aorta in aortic regurgitation [18]. In Oslo, Jarle Holen was able to use the Bernoulli equation to non-invasively estimate pressure based on the blood flow ($4v^2$) [19, 20]. This equation was implemented on the PEDOF, and it was validated against invasive pressure measurements in Trondheim in 1978 by Hatle et al. [21]. Several developments in non-invasive diagnostics of valvular and structural disease was accomplished by this group which pioneered cardiac Doppler ultrasound [22–27]. In the late 1980s, pulsed tissue Doppler imaging (TDI) was added to the tools of echocardiography [28] This led to the development of colour TDI [29].

1.2 Introduction to Ultrasound

Sources for this section are Guyton and Hall [30], Holm [31], Szabo [7] & Stoylen [32].

Ultrasound is defined as sound waves with frequencies above the upper limit of the audible range of humans (>20 000 Hz) [30]. A sound wave is a mechanical wave which results from back and forth vibration of the particles of the medium through which the sound wave is moving. Because of the longitudinal motion of the particles, there are regions where the particles are compressed together, and other regions where the particles are spread apart. These regions are known as compressions and refractions, respectively. The wavelength of a sound wave is the distance from one compression to the next. The wavelength λ is related to the frequency f by the sound velocity c as shown in equation (1.1).

$$\lambda = \frac{c}{f} \tag{1.1}$$

The sound frequencies audible by the human ear are between 20 to 20 000 Hz [30, p. 657], while diagnostic ultrasound uses frequencies in the megahertz range. Transcutaneous ultrasound uses between 1-12 MHz, and intravascular uses up to 30 MHz. The speed of sound differs depending on the material in which it is transmitted (Table 1.1), and for human soft tissue as in diagnostic ultrasound, a speed of 1540 m/s is assumed.

Ultrasound is generated by applying electric current to piezoelectric ceramics with electrodes on each side. When current is applied, the ceramics start to compress and decompress (vibrate), and this motion is transferred to the medium to which it is applied. This vibration is used to generate an ultrasonic wave, which is commonly referred to as an ultrasound pulse. Inversely, if an external force is applied to the crystal, it will generate current. When an ultrasound pulse is applied to the body surface through ultrasound gel, the pulse is reflected from the tissue and produces subtle vibration in the ceramics. The same piezoelectric ceramics used for generating the transmitted ultrasound pulse also samples the reflected ultrasound pulse, and a current is generated and processed to an ultrasound signal.

By measuring the time delay between the transmitted and received reflected ultrasound pulse, the distance to the reflector can be estimated.

1.2.1 How is an ultrasound image generated?

In basic ultrasound, the amplitude of the reflected wave is used to generate an image. When a pulse meets a reflector, it is partly reflected and partly transmitted to deeper tissues (Figure 1.1). The amplitude of the reflected wave depends on the difference in the density of the tissue it traverses, *i.e.* the higher density the stronger reflection (higher amplitude). In grayscale imaging, the amplitude of the reflected wave is represented as grayscale intensities (Figure 1.1). A full sector b-mode consists of several ultrasound pulses consecutively transmitted and received to cover a sector. The data acquired from the reflected waves of each transmit is then combined to produce one image (Figure 1.2).

Material	Velocity (m/s)
Air	330
Water	1497
Fat	1440
Average soft tissue	1540
Blood	1570
Muscle	1500 - 1630
Bone	2700 - 4100
Metal	3000 - 6000

TABLE 1.1: Speed of sound in various materials. [32]

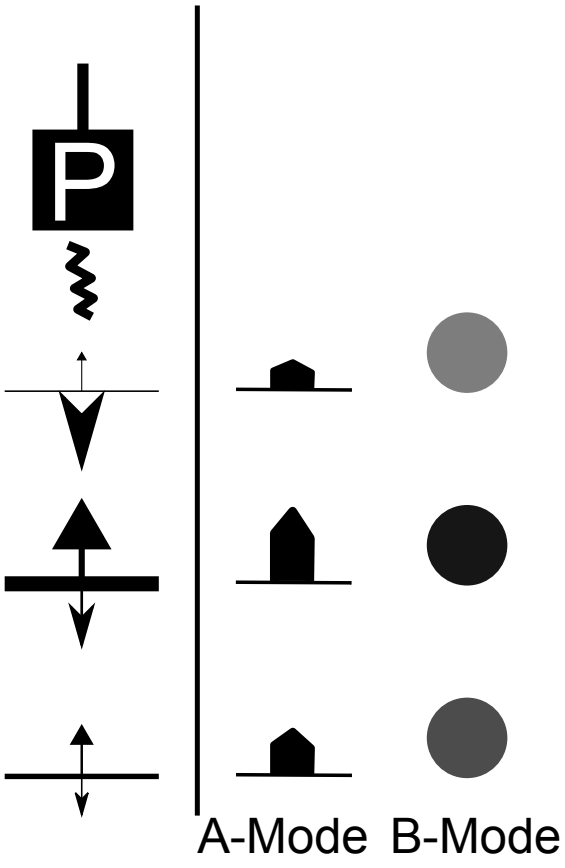

FIGURE 1.1: A pulse is transmitted from the probe (P) and reflected at different depths. Each reflected wave has a different amplitude and is visualized differently in both A-mode and B-mode. A-Mode (Amplitude-Mode) - Shows depth and amplitude of reflected signal. B-Mode (Brightness mode) - Amplitude is shown as grayscale intensity. The amplitude of the reflected beam depends on the difference in density of the tissues the pulse traverses.

1.3 The Doppler effect and Doppler Imaging

The Doppler effect is the change in frequency of a wave for an observer, when the source is moving relative to the observer (Illustrated in Figure 1.3). This change in frequency is called the Doppler shift, and is used to estimate velocities of blood and tissue. In ultrasound the Doppler shift for the reflected ultrasound pulse is described in Equation (1.2).

$$f_d = 2f_0\frac{v}{c}cos\theta \tag{1.2}$$

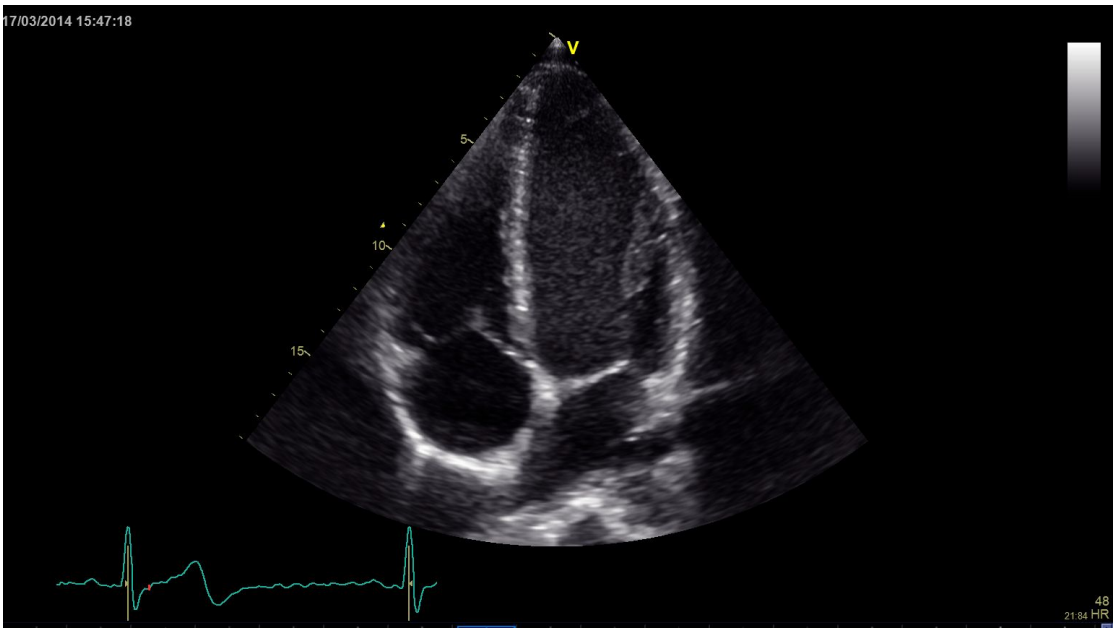

FIGURE 1.2: B-Mode grayscale image from a healthy volunteer. Apical 4-chamber acquisition.

In the equation the frequency shift f_d is the result of a signal with frequency f_0 being reflected from an object with the velocity $v << c$ (v is the velocity of the object, c is the velocity of sound) moving at an angle θ to the insonation soundwave. This equation is used to calculate the velocity of an object moving relative to the observer.

In echocardiography Doppler was first used to determine the speed of blood (Section 1.1.3). Continuous Wave Doppler (CW) was used for estimation of flow velocities. In CW Doppler the transducer is usually split in two, with one part for transmit and the other part for reception. A signal is continuously transmitted and received, and the received signal is compared with the transmitted signal. By measuring the Doppler shift between transmit and receive, the velocity of the blood is estimated. The signals are then processed with the help of Hilbert transform [2] and fast Fourier transform [3] to produce velocity spectra. The phase shifts are used to separate signals forward and reverse flow for stereo audio enjoyment (which produces the familiar Doppler sound). When using CW Doppler all reflected echos from the entire depth of the signal are

[2] A linear operator which takes a function, $u(t)$, and produces a function $H(u)(t)$ with the same domain. It i s a basic tool in Fourier analysis

[3] Fourier analysis approximate general functions by sums of simpler trigonometric functions. In ultrasound the received signal is decomposed to sine/cosine waves as a part of data compression

FIGURE 1.3: Doppler effect of water flow around a swan. Image by Zátonyi Sándor / [CC-BY-SA-3.0]

received, which produces a range ambiguity. This modality remains useful for high velocity measurements such as peak flow and assessment of stenoses [33].

1.3.1 Pulsed Wave Doppler (PW)

To overcome the range ambiguity of CW, Pulsed Wave Doppler was developed. In PW, pulses of a given length are transmitted with a time delay, and the frequency shift in the reflected pulse is measured after a certain time compared to the corresponding transmitted pulse. This frequency shift is used to determine the velocity of the reflective object. The delay chosen between the transmit and receive determines the depth at which the velocity data is gathered. A potential problem with the pulsed Doppler technology is aliasing. Aliasing is a directional ambiguity introduced when phase shifts exceeds one phase, which may be the case for high velocities. This results in a limitation of the maximal velocity that can be measured, a limitation given by the Nyquist limit [34].

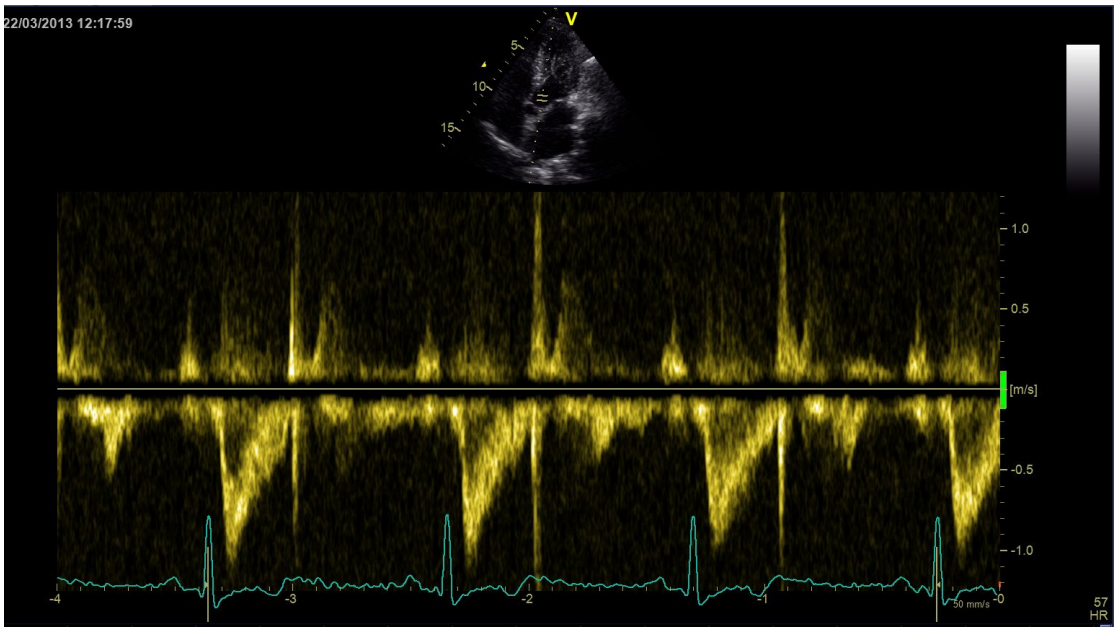

FIGURE 1.4: Pulsed Wave Doppler with region of interest superimposed on a b-mode image - bloodflow data from the left ventricular outflowtract

This limitation can be overcome by adjusting wavelength, pulse repetition frequency or baseline.

Both CW and PW Doppler is commonly combined with b-mode for navigational and diagnostic purposes (Figure 1.4).

1.3.2 Tissue Doppler Imaging

Traditionally Doppler was used in estimation of flow velocities, and for these applications the semi-stationary signals from the myocardium were considered as clutter [4] and therefore attempted to be filtered out. However it was soon suggested that this information could be of clinical value, and by altering the focus, gain and filters, tissue velocities could be acquired [35]. The signal from blood and tissue are typically of different intensity and velocity, this difference is favorable when filtering the signals (Figure 1.5). Tissue Doppler imaging is based on Pulsed wave Doppler, and uses pulsed wave packet acquisition to estimate velocities in the myocardium [28, 29, 36]. A packet consists of two or more pulses sent in the same direction. Several packets are transmitted to cover

[4] Clutter is a common denotation of unwanted noise in echocardiography, in flow imaging it refers to reflections from stationary and semi-stationary tissue, while in Tissue Doppler Imaging it often refers to reverberations

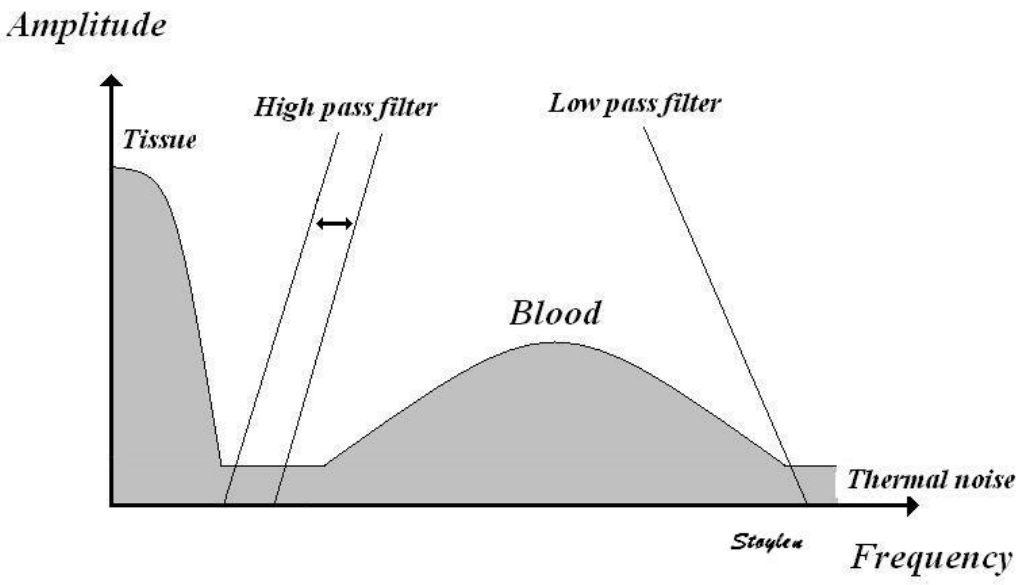

FIGURE 1.5: The distribution of Doppler frequencies. The signal from tissue has high amplitude and low frequency, while the signal from blood has a lower amplitude and a higher frequency. Reproduced with permission from Stoylen [32]

the desired sector (Figure 1.6), the received signals are sampled at different time-delays to cover different depths. An autocorrelation algorithm is then used to determine the phase-shift, and velocities are estimated for each packet. The velocities estimated are commonly color-coded and superimposed on b-mode data (Figure 1.7). Spatial and temporal resolution are inversely dependent on the number of packets (and packet size) used to cover a sector. This means that better spatial resolution comes at the cost of worse temporal resolution, and vise versa. Several techniques has been proposed to overcome these limitations, some of which are explained in Section 1.6 and discussed in the first paper, *Ultra-high Frame Rate Tissue Doppler Imaging* (UFR-TDI). By applying these techniques, conventional tissue Doppler imaging can reach about 250 frames per second. In this thesis, we use UFR-TDI which can reach 1200 frames per second in 2D, and 500 frames per second in 3D. The technical aspects of this acquisition technique are explained in Section 3.1.2.1 and 3.1.2.2.

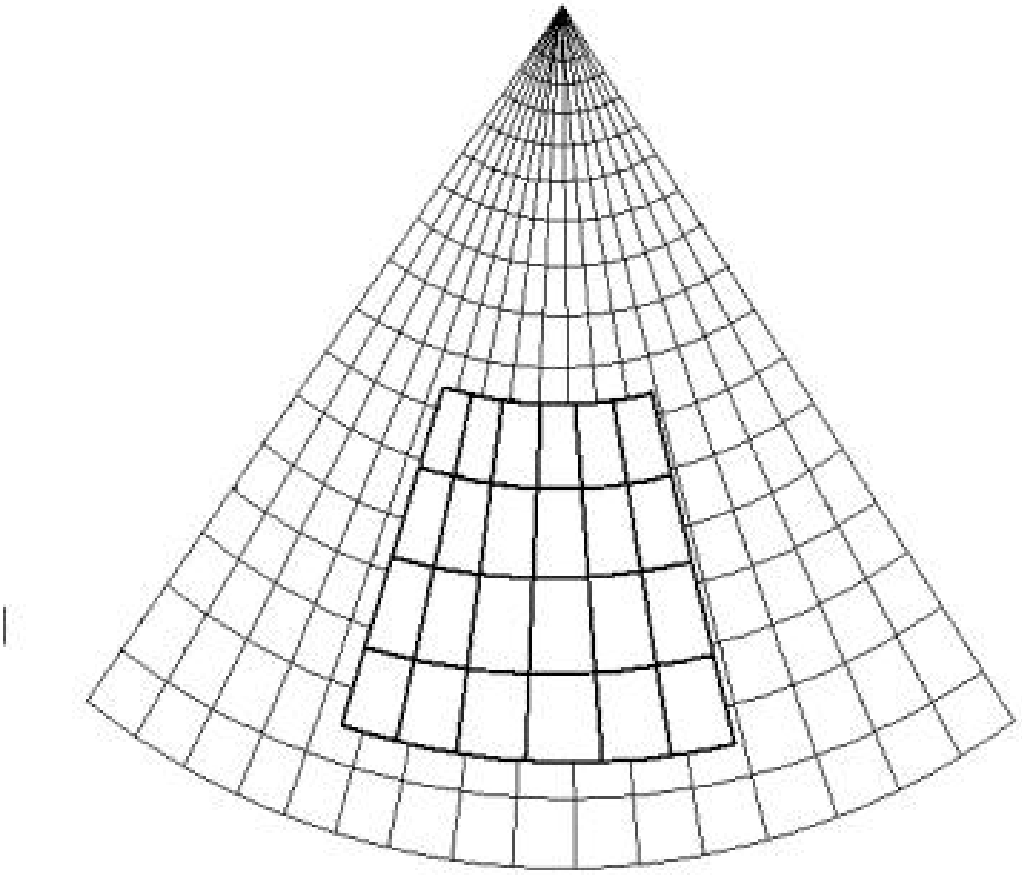

FIGURE 1.6: Each square represents one packet, several packets are needed to cover an entire 2D-sector. Reproduced with permission from Stoylen [32]

1.3.2.1 Limitations of tissue Doppler

The main source for this section is Aase [36].

A well-known limitation of all Doppler-based modalities is the angle dependency. Angle dependency makes interpretation of segments perpendicular to the insonation pulse impossible, and interpretation of segments not aligned with the ultrasound beam a challenge. This makes tissue Doppler most suitable for measurement of longitudinal motion of the heart from the apical view. These two limitations can seemingly be overcome with the use of speckle tracking, which tracks speckles from b-mode images to estimate velocities. However, speckle tracking requires better spatial resolution for proper tracking of speckles, and therefore provides lower frame rates.

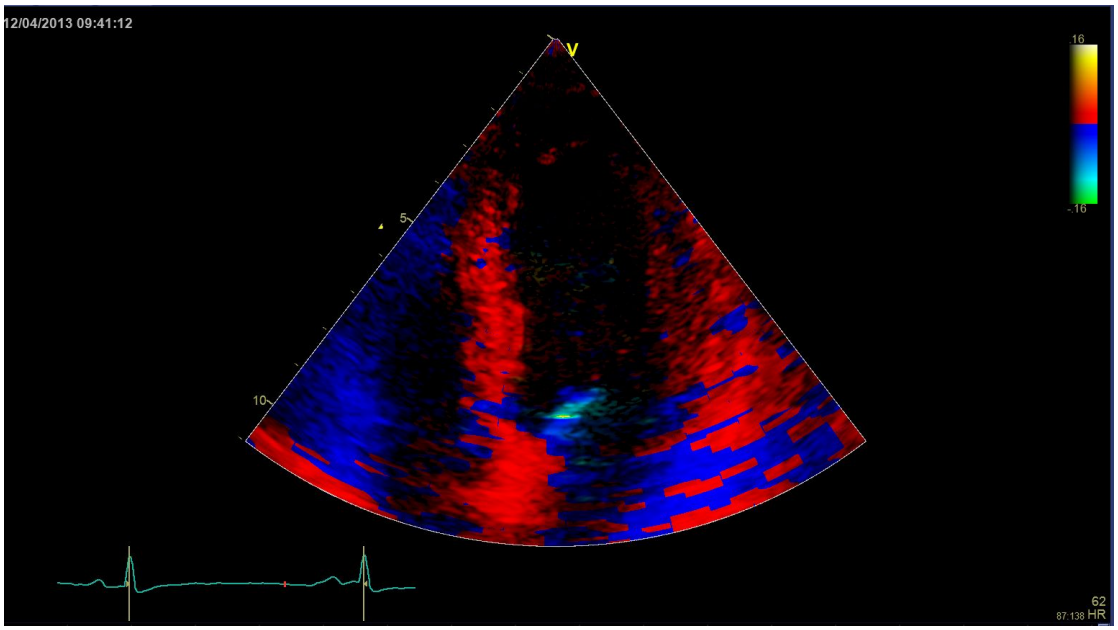

FIGURE 1.7: Tissue Doppler data superimposed on a b-mode cine, 4-chamber apical view. Blue color represent movement away from probe, while red represents movement towards the probe.

1.4 Evaluation of regional myocardial function with ultrasound

Myocardial infarction (MI) impairs the contractile abilities in the affected myocardium. Infarct size has proven a good prognostic marker, and is strongly correlated with outcome in post-MI patients [37–39]. Currently, the gold standard for quantifying infarct size is Magnetic Resonance Imaging (MRI) with the use of Gadolinium contrast. MRI is both costly and time-consuming, which motivates the use of other imaging modalities for evaluation of myocardial scar and regional function. Ultrasound is relatively cheap, portable, less time-consuming and it offers a better temporal resolution than MR. To be able to evaluate regional function, one must discern between wall motion (displacement and velocity) and wall deformation (strain and strain rate) [40]. Wall motion does not differentiate between active and passive motion, in other words, a basal segment can be pulled by a more apical segment even though it is not contracting. This mechanism is commonly referred to as tethering. Tethering makes evaluation of regional function a challenge, as non-contracting segments may be masked by healthy segments. Wall deformation (strain and strain rate) is not sensitive to tethering, and is therefore more

suitable for regional functional measurements [41]. Studies suggest that deformation imaging has incremental value in evaluation of regional myocardial function [42].

1.4.1 Deformation imaging

Deformation in laymen terms can be explained as a quantitative measurement of stretch and compression. In echocardiography, deformation of the myocardium can be translated to contraction and relaxation, and can be quantified with strain and strain rate [43].

1.4.1.1 Strain and strain rate explained

The term myocardial strain was introduced by Mirsky and Parmley [44] and is defined as a dimensionless quantity which is produced by the application of stress. It represents the fractional or the percent change from the original or unstressed dimensions. This is demonstrated in Equation (1.3)

$$\epsilon = \frac{L - L_0}{L_0} = \frac{\Delta L}{L_0} \tag{1.3}$$

Where ϵ is the strain, L_0 is unstressed dimension, L is the dimension at the time of measurement and ΔL is the difference between L and L_0. This provides a quantitative measurement of deformation, and is commonly expressed as a percentage (%). The strain can also be expressed relative to the length at a previous time instance (Eulerian strain) [40]. For myocardial imaging, eulerian strain is best suited, as it is not as reliant on the initial length L_0. This is true for one-dimensional deformation. 2D strain however, has four components; Two normal strains, and two shear strains [40, 43, 45] (Figure 1.8). Tissue Doppler based deformation imaging can provide one-dimensional measurements, and does not permit simultaneous measurement of shear strain components.

Strain rate is the rate by which this deformation occurs (deformation per time unit) commonly expressed s^{-1}. The local rate of deformation or strain per time unit equals the velocity difference per unit length (1.4)

$$\dot{\epsilon} = \frac{\epsilon}{\Delta t} = \frac{\Delta L / L_0}{\Delta t} = \frac{\Delta L / \Delta t}{L_0} = \frac{\Delta V}{L_0} \tag{1.4}$$

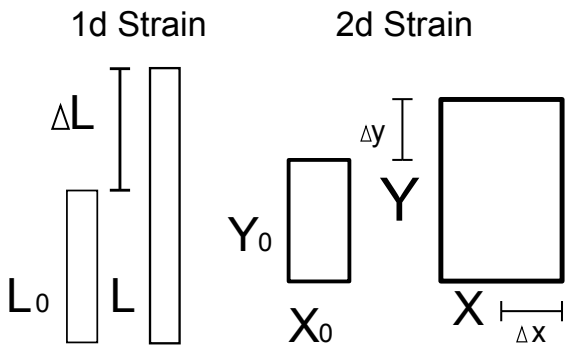

FIGURE 1.8: One dimensional and 2D strain demonstrated.

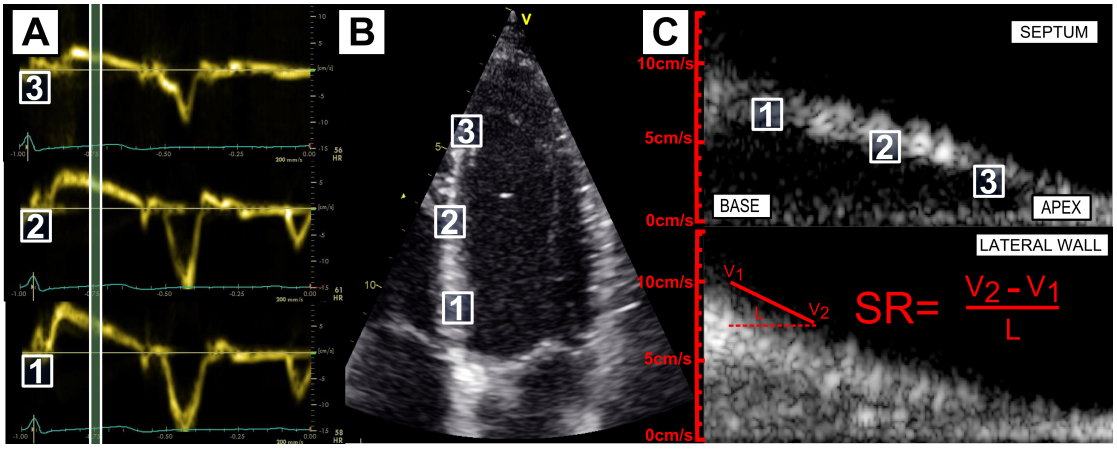

FIGURE 1.9: Anatomic Doppler Spectrum in a healthy subject. (a) Pulsed Wave Spectral Doppler traces from the regions of interest indicated in (b). Mid-systole, which is the time point used as basis for the Anatomic Doppler Spectrum (ADS), is demarcated with green. (b) B-mode, with regions of interest demarcated as 1, 2 and 3 respectively. (c) Anatomic Doppler Spectrum from the septum and lateral wall of the same subject. The highest velocities are present at the base of the ventricle, and gradually become lower towards the apex. The slope of the spectral envelope represents the velocity gradient in the ventricular wall, and is used to determine strain rate in the segment of interest. This is illustrated with the formula (V2-V1)/L. Signal can easily be separated from the stationary components around zero in the septum, however, in the lateral wall, signal can be separated from the stationary component around zero only by tracing the spectral envelope. V1 = Velocity 1, V2 = Velocity 2, L = Segment length, SR – Strain Rate.

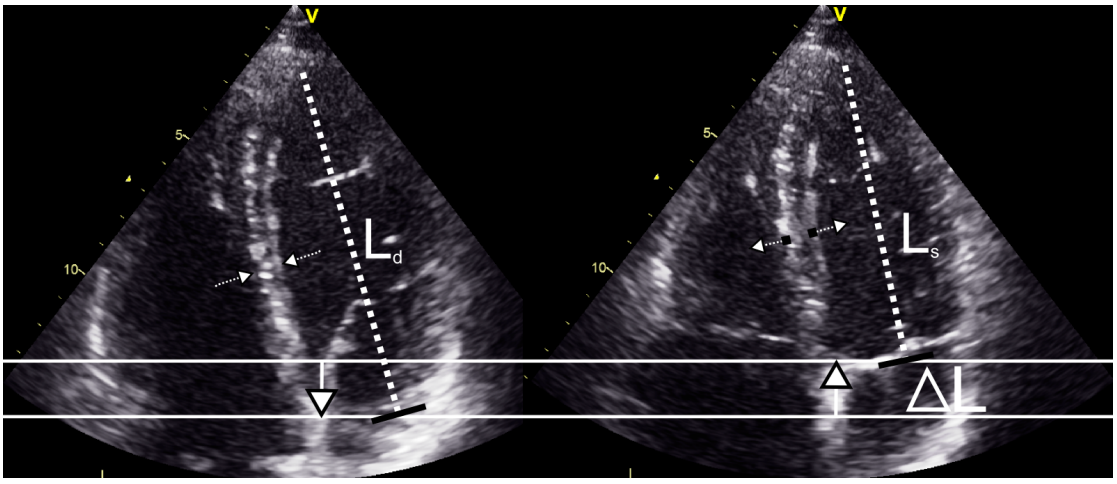

FIGURE 1.10: Longitudinal motion of the heart in systole and diastole. L_d represents diastolic dimensions, L_s represents systolic dimensions and ΔL represents relative shortening.

where ΔV is the velocity gradient in the segment. The relation between velocity gradient and strain rate is demonstrated in equation (1.4); in *Myocardial Strain Rate by Anatomic Doppler Spectrum: First Clinical Experience Using Retrospective Spectral Tissue Doppler from Ultra-High Frame Rate imaging* [3], we utilize this in estimation of deformation from retrospective tissue Doppler data based on visualization of the velocity gradient (Figure 1.9). The velocity gradient can be used for strain rate calculations, and it has the same direction as strain (negative=shortening, positive=lengthening).

1.4.1.2 Strain and Strain Rate - Clinical use and limitations

Contracting myocardium shortens and thickens, while relaxing myocardium lengthens and becomes thinner (Figure 1.10). Deformation imaging can quantify shortening and lengthening and is therefore suitable for evaluating contraction and relaxation of the myocardium. It has proven to be of clinical value when investigating myocardial function [45–52]. The main limitation for deformation imaging by tissue Doppler is suboptimal reproducibility, and vulnerability to noise [53]. Further, there is a substantial variation in a healthy population which complicates interpretation of this parameter [54].

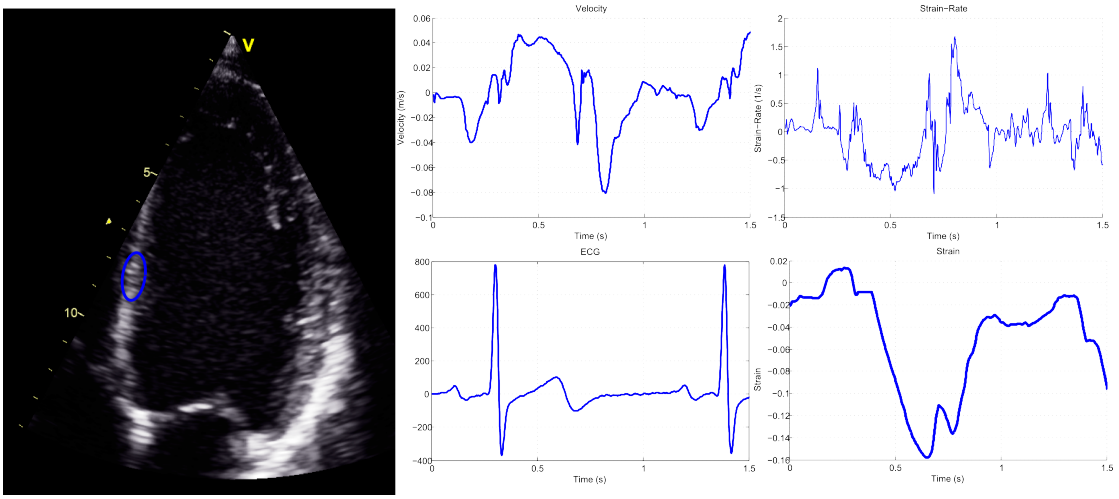

FIGURE 1.11: Relation between Velocities, Strain and Strain rate from UFR-TDI: Velocity and deformation curves from the ROI demarcated in b-mode image in a healthy subject. In the upper right panel you can see the strain rate profile. One can discern two systolic strain rate spikes, the first occurring during the pre-ejection period. This was the spike used as basis for the parameter of mechanical activation in the 3D data in *Detection of mechanical activation in an open chest porcine model by three-dimensional UFR-TDI, a feasibility study.*

1.4.1.3 Deformation imaging by tissue Doppler

As described in Section 1.4, strain and strain rate can be derived from velocity gradients. This makes tissue Doppler imaging suitable for deformation analysis. By analyzing the velocity gradients, strain rate data can be extracted. By integrating the strain rate data, one can calculate the strain value. The relation between velocities, strain and strain rate is illustrated in Figure 1.11. Strain rate by tissue Doppler allows for a high sampling rate as it uses the velocity gradients.

1.4.2 Contrast enhanced ultrasound

Ultrasound contrast is a method used to compensate for the attenuation of signal, overcome noise and enhance the wall-definition [55] in patients with poor acoustic windows. However, using contrast, the destruction of microbubbles by the ultrasound causes the signal to decorrelate, rendering tissue Doppler by autocorrelation unfeasible. Previous studies combining TDI and ultrasound contrast has been disappointing and the combination of ultrasound contrast and TDI has in general not been recommended [56–58]. In *Color Tissue Doppler Imaging in Contrast Echocardiography - a Feasibility Study* [4], we

compare the inter- and intra-observer repeatability TDI velocity indices before injection of ultrasound contrast and after 10 minutes continuous scanning.

1.5 Mechanical activation of the myocardium

In a healthy heart the mechanical activation is initiated by an electrical impulse originating from the sinoatrial node traveling through the AV-node, finaly depolarizing the left ventricular myocardium through the purkinje system (Figure 1.12). The speed of depolarization in the purkinje fibers ranges from 1.5-4 m/s [30, p. 117]. Due to the distribution of this system, the depolarizing signals are spread throughout the ventricles in about 30ms [30, p. 117]. After it reaches the myocardium, cell-cell transmission rate is about 1.0-1.5 m/s [59]. There is a delay between electrical and mechanical activation of cardiomyocytes, termed electromechanical delay, which has been shown to be 20-50ms at the cellular level [60]. To be able to capture such events, echocardiographic equipment with high temporal resolution must be used. In *Detection of mechanical activation in an open chest porcine model by three-dimensional UFR-TDI, a feasibility study* [2], we explore the ability of UFR-TDI to detect origin of mechanical activation in a paced open-chest porcine model.

1.6 Ultra-high Frame Rate Tissue Doppler Imaging

There have been several developments within fast cardiac imaging during the last decade, however the systems currently available in the clinic can offer a frame rate of up to 250 frames per second with a narrow sector. There are two main acquisition modulations which can increase the frame rate; reducing the number of transmits needed per sector, and limiting the sector itself. A method used to reduce the number of transmits is multi-line acquisition (MLA); MLA was introduced by Shattuck et al. [61] and allowed for several receive lines per transmit (Figure 1.13). This method is well established in the clinic, and in daily use in conventional Tissue Doppler Imaging. Other strategies have focused on narrow [62] or sparse sector scans [63]. Several other strategies have been employed to increase frame rates in echocardiography [64–71]. UFR-TDI utilizes both the narrow sector and MLA for realization of ultra-high frame rates.

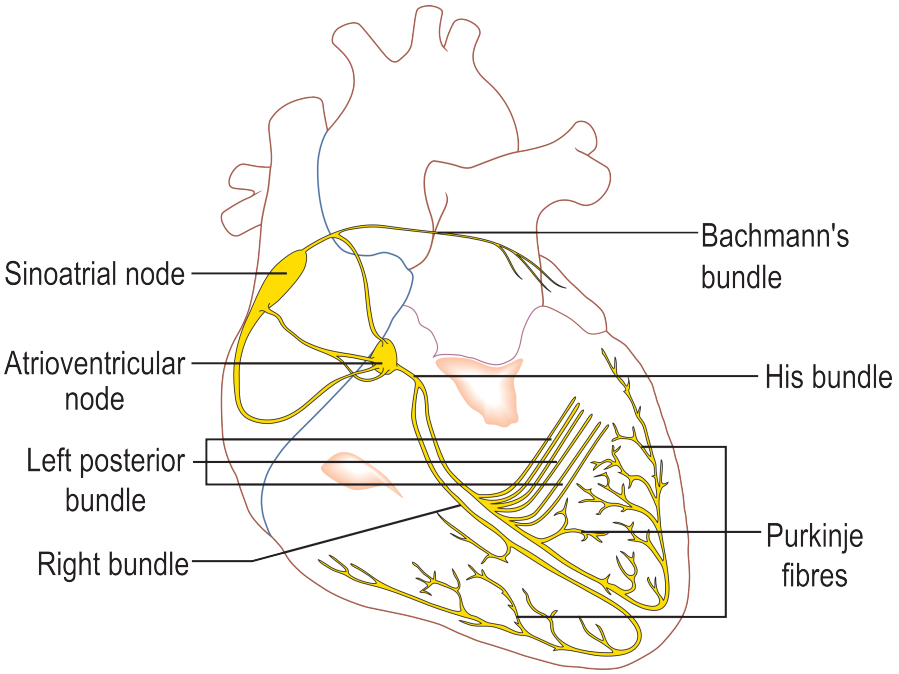

FIGURE 1.12: The purkinje system with branches. Image by Madhero88 / [CC-BY-SA-3.0]

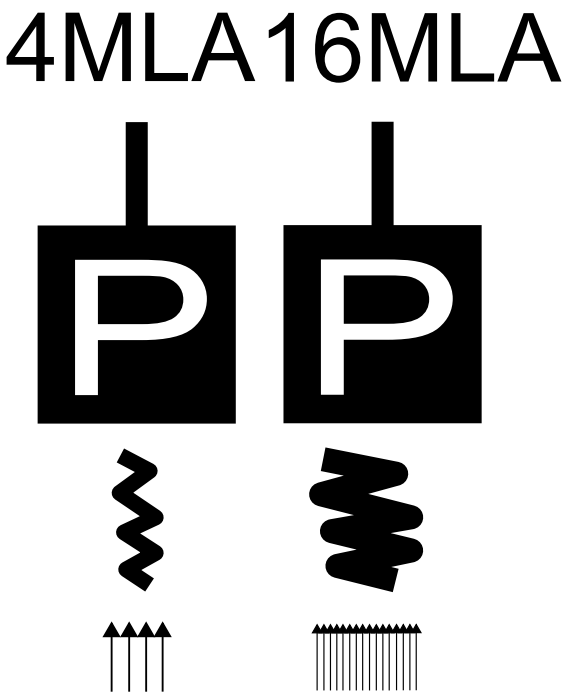

FIGURE 1.13: Conventional Multi-line acquisition acquisition versus UFR-TDI Multi-line acquisition. Left: Conventional 4MLA with four received pulses per transmit. Right: UFR-TDI 16MLA with 16 received pulses per transmit. As demonstrated with the use of MLA, a full sector can be covered with a reduced number of transmit events.

The need for high frame rate has been documented in several papers and guidelines [72–74], especially for 3D-imaging. UFR-TDI is a new acquisition technique developed at NTNU, which can be implemented on a GE Vingmed Vivid E9 (GE Vingmed, Horten, Norway). UFR-TDI can acquire data in both 2D and three dimensions (3D) with a frame rate of 1200 and 500, respectively. The studies currently available are few in number and experimental. This means that the clinical potential remains to be explored. The state of the art regarding high frame rate cardiac imaging has recently been covered in Cikes et al. [75]. They suggest potential benefits, such as mapping mechanical activation, resolution of deformation profiles and improvement of deformation imaging. In this thesis we explore the use of UFR-TDI in these contexts.

1.6.1 Improvement of deformation imaging

Deformation imaging by tissue Doppler currently suffers from sub-optimal variability and reproducibility [46, 54]. A higher amount of samples per unit of time would allow for smoothing over more samples which should improve signal-to-noise ratio. This in turn, could decrease variability and improve reproducibility of deformation imaging by tissue Doppler. This is investigated in Section 5.3.2.

1.6.2 Anatomic Doppler Spectrum - Retrospective spectral Doppler

Ultra high frame rates allow retrospective extraction of spectral tissue Doppler data from the complete sector. This has previously not been possible. The application has the benefits of PW Doppler as it enables visualization of the spatial velocity gradient in a spectral fashion allowing separation of reverberations from myocardial signal. In addition, Anatomic Doppler Spectrum enables simultaneous visualization of data from the entire left ventricle simultaneously, as color Doppler, enabling spectral analysis of myocardial deformation. This potentially realizes more robust estimation of deformation, as well as improving the feasibility in less echogenic patients. The method is described in paper III, *Myocardial Strain Rate by Anatomic Doppler Spectrum: First Clinical Experience Using Retrospective Spectral Tissue Doppler from Ultra-High Frame Rate imaging* [3].

1.6.3 Mechanical Activation

Mechanical activation is one application of high frame rate imaging currently investigated by several groups [76–82]. Some feasibility studies have been performed and results show promise [77, 78, 83]. These studies suggest that ultra-high frame rates can be used to track the mechanical activation throughout the heart by detailed resolution of the systolic deformation profile. The use of UFR-TDI for detection of onset of mechanical activation of the left ventricle is discussed in paper II, *Detection of mechanical activation in an open chest porcine model by three-dimensional UFR-TDI, a feasibility study* [2]. If feasible, such application could potentially be used in monitoring of CRT-Response, and characterization of arrhythmias, e.g. evaluation of patients pre-ablation.

1.6.4 Resolution of Pre-ejection period

It has been shown that ventricular contraction starts before mitral valve closure [84]. However, as this period only lasts for 100ms, high frame-rate is required to resolve the physiological aspects involved. This is further investigated in paper I, *Ultra-high Frame Rate Tissue Doppler Imaging* [1], where we attempt to resolve the pre-ejection velocity profile at 1200 frames per second.

Chapter 2

Objectives and hypothesis

The thesis builds on five hypothesis:

First - 2D and 3D tissue Doppler imaging with ultra-high frame rates is feasible with adequate quality

Second - 2D and 3D tissue Doppler imaging with ultra-high frame rate may improve feasibility of deformation imaging by tissue Doppler

Third - 2D and 3D tissue Doppler imaging with ultra-high frame rate allows detailed resolution of the pre-ejection contraction period

Fourth - 2D and 3D tissue Doppler imaging with ultra-high frame rate enables analysis of mechanical activation in the left ventricle

Fifth - TDI velocity measurements are feasible and reproducible after injection of ultrasound contrast medium and contrast destruction by 10 minutes of continuous ultrasound scanning

In Paper I, *Ultra-high Frame Rate Tissue Doppler Imaging* [1], we examine the feasibility of UFR-TDI in velocity estimation. The pre-ejection period is also resolved with a velocity profile from UFR-TDI data with 1200 frames per second.

In Paper II, *Detection of mechanical activation in an open chest porcine model by three-dimensional UFR-TDI, a feasibility study* [2], we examine the detection of mechanical

activation in an open-chest pig model by strain rate with 2D and 3D ultra-high frame rate tissue Doppler imaging.

In Paper III, *Myocardial Strain Rate by Anatomic Doppler Spectrum: First Clinical Experience Using Retrospective Spectral Tissue Doppler from Ultra-High Frame Rate imaging* [3], we describe a new method for evaluating tissue deformation by tissue Doppler, Anatomic Doppler Spectrum (ADS). ADS enables retrospective spectral analysis of tissue deformation from Doppler data without the influence of clutter.

In Paper IV, *Color Tissue Doppler Imaging in Contrast Echocardiography - a Feasibility Study* [4], we explore the reproducibility of tissue Doppler velocity parameters after injection of ultrasound contrast medium and contrast destruction by 10 minutes of continuous ultrasound scanning.

Chapter 3

Materials and methods

3.1 Paper I - Technical feasibility

The frame rate is of great interest when measuring myocardial motion with TDI. Several groups are investigating ultrafast cardiac imaging and its clinical potential [75]. Several methods have been developed to increase the frame rate in echocardiography. Most of which entail limiting the number of transmit events needed to cover a complete sector [85], limiting the sector itself [62], or a combination of both.

3.1.1 Study population

In Paper I, *Ultra-high Frame Rate Tissue Doppler Imaging*, 10 young healthy volunteers (25-43y) and one patient with atrial fibrillation were included.

3.1.2 Echocardiographic acquisition

A GE Vingmed Vivid E9 (GE Vingmed, Horten, Norway) was used for acquisition. UFR-TDI and conventional data was acquired from the apex in the standard 2-, 4-chamber and apical long-axis views. The ECG leads from the Vivid E9 was aligned with the electrical vector showing the earliest deflection in QRS.

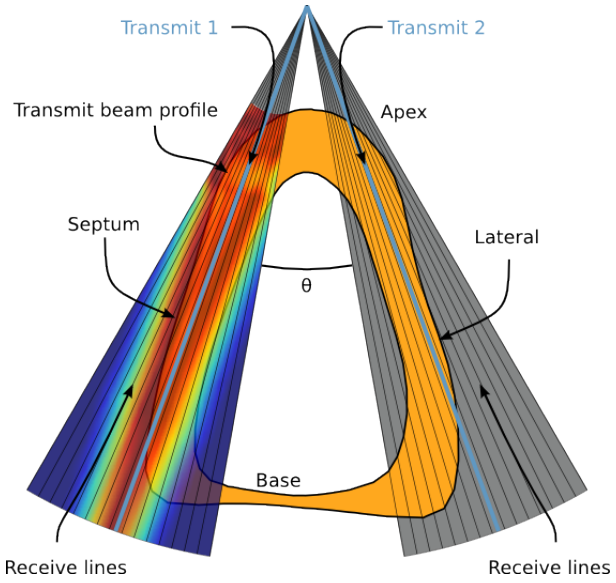

FIGURE 3.1: UFR-TDI acquisition 2D - Beamprofile

The electrical vector was identified in a 12-lead ECG which was obtained from all subjects. Care was taken to identify the lead showing the earliest deflection in QRS. The difference between the leads may be as great as 40 ms (the duration of a normal Q-wave).

We also performed an ECG latency test to estimate the time delay between the scanner ECG and UFR-TDI acquisition. The test is described in Sutherland et al. [86]. The results of this test showed that there was a delay of 5.5 ms between the two modalities. This delay was corrected for in all measurements.

3.1.2.1 2D UFR-TDI

In our UFR-TDI acquisition set-up, we cover the two left ventricular walls in each view with only two broad transmit beams, only covering the myocardium, excluding the myocardial cavity. In addition, we use 16 receive lines per transmit. The acquisition set-up is illustrated in Figure 3.1. By utilizing this acquisition methodology we achieve a frame rate of 1200 fps. The acquisition methodology was implemented on a Vivid E9 (GE Vingmed, Horten, Norway), and the recordings were made with a M5S-D (GE Vingmed, Horten, Norway) phased array cardiac probe. The method is further described in Brekke et al. [1].

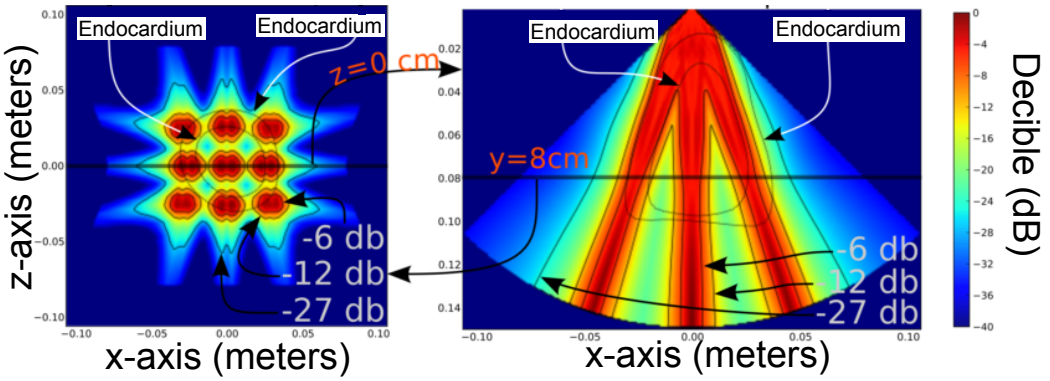

FIGURE 3.2: UFR-TDI acquisition 3D - Beamprofile

3.1.2.2 3D UFR-TDI

A similar strategy to 2D was employed to reduce the number of transmit events needed to cover the entire sector while capturing 3D data. MLA is used and the set-up consists of 3x3 transmit beams to cover the entire ventricle, as demonstrated in Figure 3.2. For each of the 9 transmit beams, 16 (4x4) lines are received. This set-up allows a sampling rate of 500 volumes per second. The acquisition consists of one cardiac cycle with 3D b-mode data, immediately followed by one full-volume 3D UFR-TDI cine. The trig-points used were peak R of the QRS complex. The set-up was implemented on a Vivid E9, and recordings were done with a 4V (GE Vingmed, Horten, Norway) phased array probe. This method is further described in Brekke et al. [87].

3.1.3 Data analysis

All conventional echo-data were analyzed in EchoPAC Ver. 112 Rev. 13 (GE Vingmed AS, Horten, Norway). UFR-TDI data was analyzed in dedicated post-processing software developed in Matlab R2011a (The MathWorks, Natick, MA, USA). UFR-TDI data can be visualized in a curved anatomical M-mode presenting tissue velocities, accelerations, deformation (strain or strain rate) or Doppler spectrum. An example from the 2D and 3D UFR-TDI post processing tools is seen in figure 3.3 and 3.4, respectively.

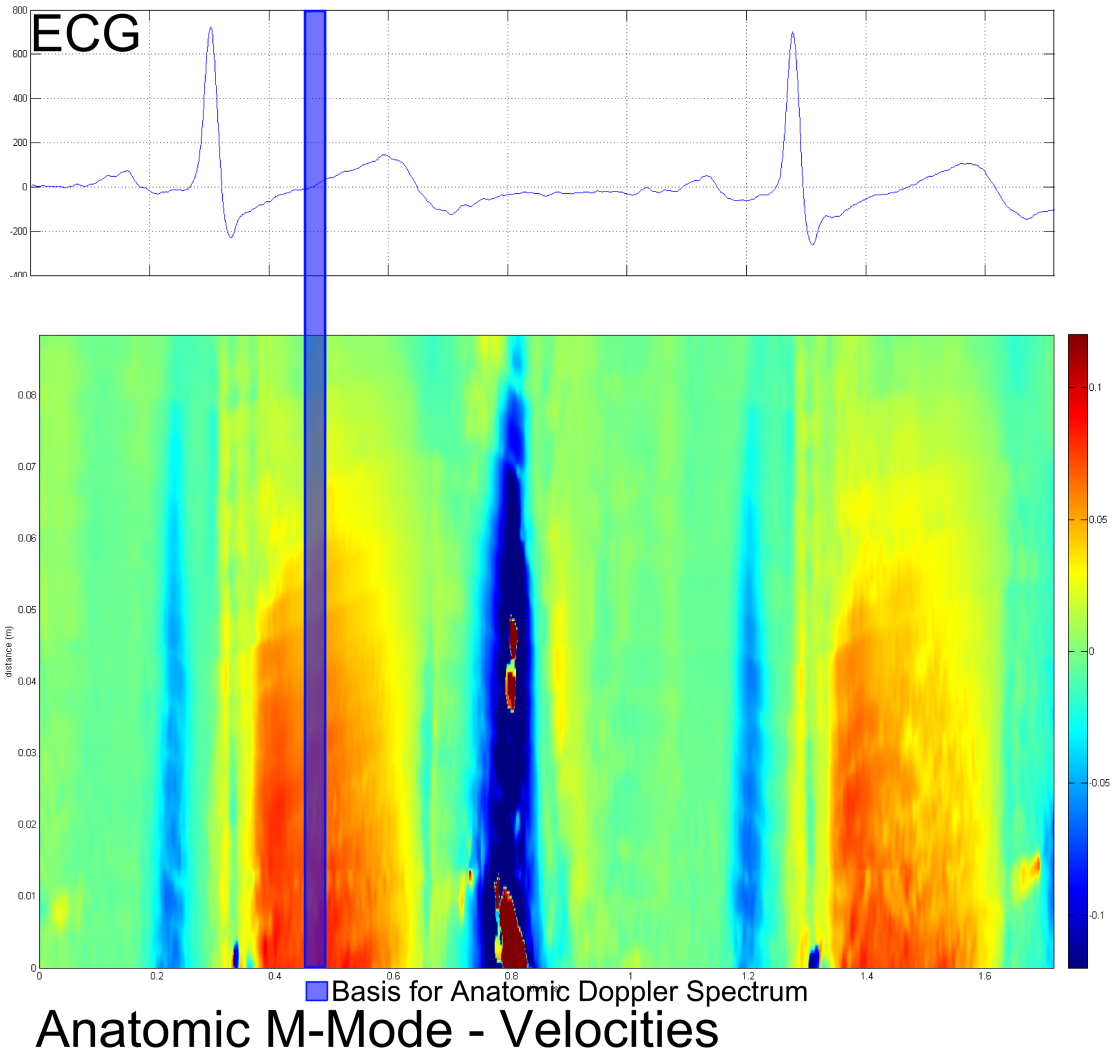

FIGURE 3.3: 2D UFR-TDI Post-processing analysis tool developed in MATLAB (The MathWorks, Natick, MA, USA). Anatomic M-mode presenting tissue velocity data from the septum of the left ventricle in a healthy volunteer. Above, the ECG from the same patient is presented. In this case the tool was used for selection of time of interest in Anatomic Doppler Spectrum [3]. The colormap is indicated in meters per second. Mid-systole is indicated as basis for ADS measurements.

3.1.3.1 Agreement with conventional TDI

Peak annular velocities *S', e' and a'* (where *S'* = peak systolic myocardial velocity, *e'* = peak early diastolic myocardial velocity and *a'* = peak late diastolic myocardial velocity) were acquired from mitral annulus in the septal and lateral walls of the left ventricle. Acquisition was made with UFR-TDI and conventional color TDI, and inter- and intra-method agreement and reproducibility were compared.

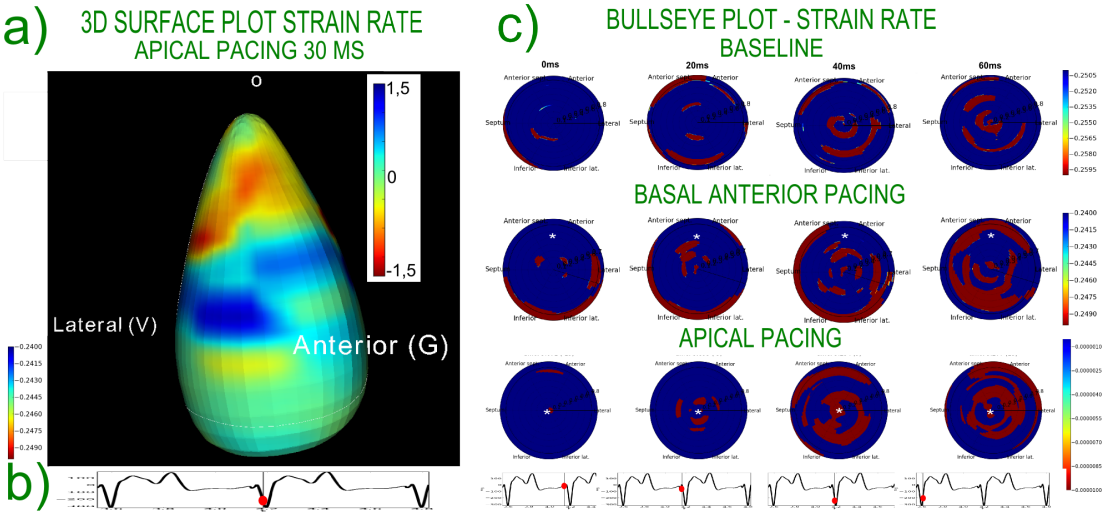

FIGURE 3.4: 3D UFR-TDI data: a: 3D model of the left ventricle during inferior pacing with 3D UFR-TDI Strain Rate data superimposed on its surface. b: ECG c: Bull's eye Plot with UFR-TDI Strain rate data from the left ventricle presented at 20 ms increments from the onset of QRS. Red indicates shortening (SR<-0.25 s^{-1}), Blue indicates SR values >-0.25 s^{-1}. At baseline the onset of shortening is found inferoseptally and spreads inferiorly and anteriorly. During basal anterior pacing, the onset of shortening starts anteriorly before it spreads laterally and septally. During apical pacing, the onset of shortening is found apically in both anterior and inferior wall, after which it spreads inferiolaterally and anteriorly. Asterisk: Segment corresponding with pacing electrode

3.1.3.2 Pre-ejection period

The pre-ejection period is defined as the period from the first deflection in the QRS complex to the start of ejection [88]. In our study, the first deflection in QRS was assessed from the aligned lead in the ECG recording. The start of ejection was defined as the onset of the *S'* wave in the velocity curves, extracted from the mitral annulus of the septum in UFR-TDI data. The onset of the *S'* wave has previously been shown to correlate well with aortic valve opening [89]. We measured the time intervals between the events observed in the pre-ejection period (Fig. 4.1). Mitral valve closure was manually determined in a reconstructed M-mode created from the UFR-TDI data of a selected receive line crossing the mitral valve. Determination of which of the 32 receive lines crosses the mitral valve was also performed manually. Figure 3.5 illustrates an M-mode crossing the mitral valve.

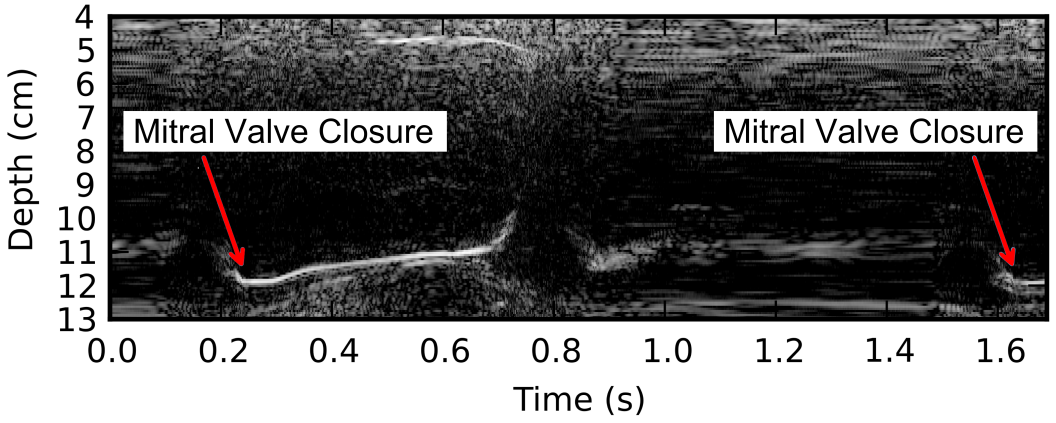

FIGURE 3.5: Detection of mitral valve closure from a reconstructed M-mode UFR-TDI B-mode data.

3.1.4 Statistical analysis

All statistical calculations were made in SPSS for Windows 2010 (IBM Corp. in Armonk, NY.). Values are expressed as mean ± standard deviations (SD) unless otherwise noted. Bland-Altman analysis and paired t-tests with Bonferroni correction were used to compare measurements of peak annular velocities. Paired t-tests were used to compare measurements of time from electrical activation to peak systolic velocity. The level of significance was set at 0.05.

3.2 Paper II - Experimental Animal Study

3.2.1 Animal preparation

Four pigs with target weight 30-35kg were included. Anesthesia regimen was as follows: Initially the animals were premedicated with Zoletil ($8mg/kgI.M.$) and Xylazine ($2.5mg/kgI.M.$), after which anesthesia was induced with Propofol ($2mg/kgI.V.$) and Sufentanil (0.25 μg/kg/h). Anesthesia was maintained with a continuous infusion of Propofol ($10mg/kg/h$) and Sufentanil (1 μg/kg/h) via an ear vein. The animals were ventilated with a mixture of oxygen and room air to maintain normocapnia and normoxia (tidal volume of 8 ml/kg and respiratory rate of 12 times/minute). The animals

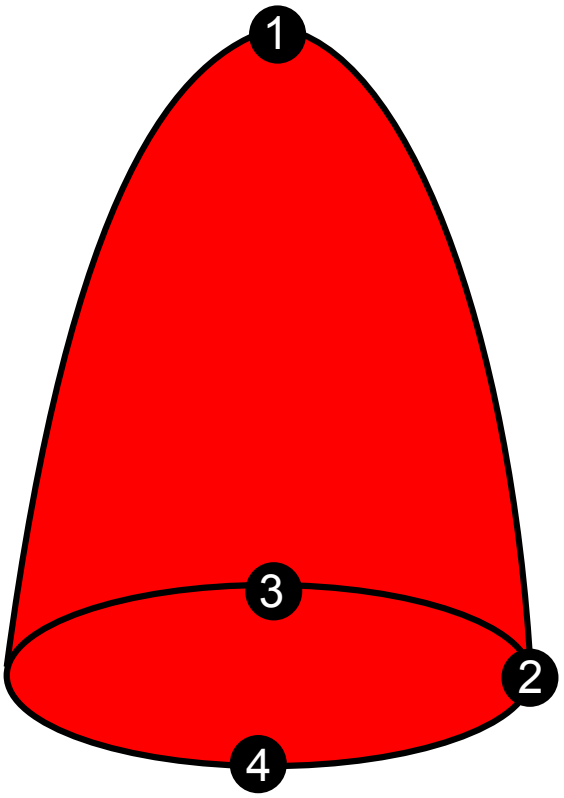

FIGURE 3.6: Schematic view of the left ventricle. The placement of pacing electrodes: 1 - apical, 2 – lateral, 3 – inferior and 4 – anterior

were kept hydrated with Lactated Ringer's solution at a rate of 8 mL/kg/h. A neuromuscular blocker was infused to prevent spontaneous respiration (Nimbex or Esmeron). Sternotomy was performed and the heart was suspended in a pericardial cradle. Four uni-polar electrodes were epicardially implanted at the apex, basal lateral-, anterior- and inferior-wall (Figure 3.6 and 3.7). Vascular access was gained through the left jugular vein (assessment of central venous pressure and administration of drugs) and right carotid artery in order to insert a micromanometer (Millar, Houston, TX, USA) into the left ventricle to record instantaneous left ventricular pressure. The experiments were conducted at Leuven university hospital, Belgium, in cooperation with Myocardial Imaging Lab. The study was approved by the local ethics committee at Leuven university hospital, Belgium.

3.2.2 Acquisition protocol

UFR-TDI was implemented on a GE Vingmed Vivid E9, an M5S-D phased array probe and a 4V probe was used for 2D and 3D acquisitions respectively (GE Vingmed, Horten,

Norway). The imaging methods have previously been described [1, 87]. The acquisition was performed in the following steps:

1. Baseline acquisition of 2D b-mode data followed by 2D UFR-TDI data from the standard apical views, i.e. two- and four-chamber and apical long-axis view.
2. Baseline recording of 3D UFR-TDI data from the apical view
3. Implantation of pacing electrodes (Fig. 3.7)
4. Acquisition of 2D b-mode data followed by UFR-TDI data from the three apical views
5. Acquisition of 3D UFR-TDI data from the apical view
6. Steps 4 and 5 were repeated during pacing from each of the basal and one apical electrode

A liver was used as a stand-off between the myocardium and the probe for both 2D and 3D acquisition. Typical frame rates for URF-TDI data were 1250-1310 Hz and 500 Hz in 2D and 3D respectively.

3.2.2.1 2D UFR-TDI analysis

The 2D data was analyzed with in-house software developed in Matlab 2011b (The MathWorks, Natick, MA, USA). The analysis of the 2D-UFR-TDI data was performed in the following steps:

1. A curved anatomic M-mode was drawn in the wall of interest
2. An anatomic M-mode presenting strain rates from the curved anatomic m-mode was generated (Figure 3.8)
3. The time of onset of QRS was detected in the ECG plot
4. The time from the onset of QRS to strain rate zero-cross for all depths along the anatomic curve was automatically estimated and the median time to zero-cross was provided for each segment (basis, middle and apex)

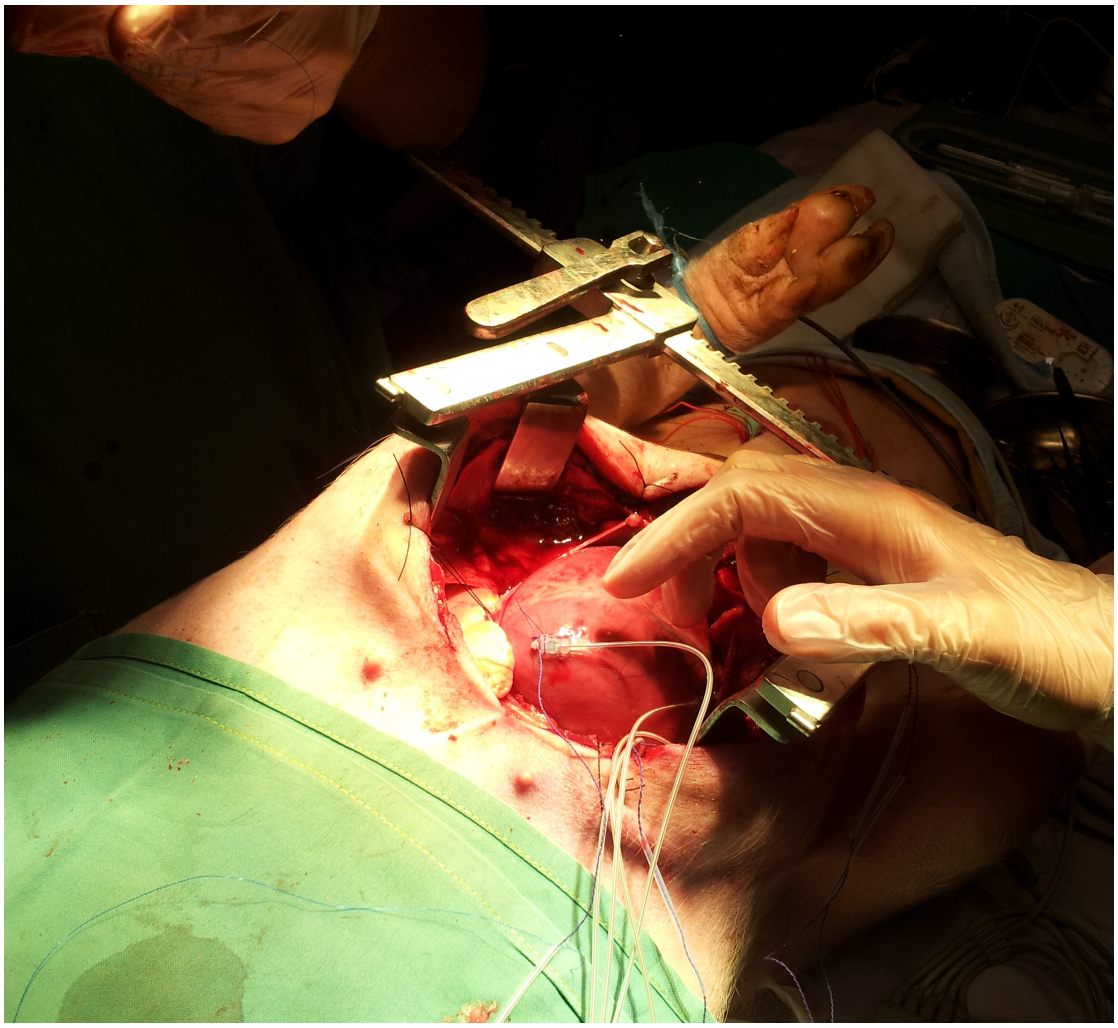

FIGURE 3.7: Animal preparation with pacing electrode sutured/glued to the epicardium.

The onset of QRS was defined as the first deflection of Q- or R-wave. First negative strain rate was defined as first zero-crossing from a positive to a negative strain rate value after the onset of QRS. The length of a segment was typically 15-25 mm depending on the length of the ventricle. The temporal averaging was 10 ms and the sample volume was 6 mm x 3 mm. A Butterworth clutter filter with cut-off at 0.5 cm/s was applied to minimize noise. Strain rate was calculated with linear regression over a strain length of 16 mm. For the basal measurements, the electrodes were assigned the corresponding segment in the 18 segment model based on its placement, i.e. anterior – anterior from apical two chamber view, inferior – inferior from apical two-chamber view, lateral – inferolateral from apical long axis view. For the apical pacing, the segment with the shortest time interval was used. Care was taken during acquisition to make sure that

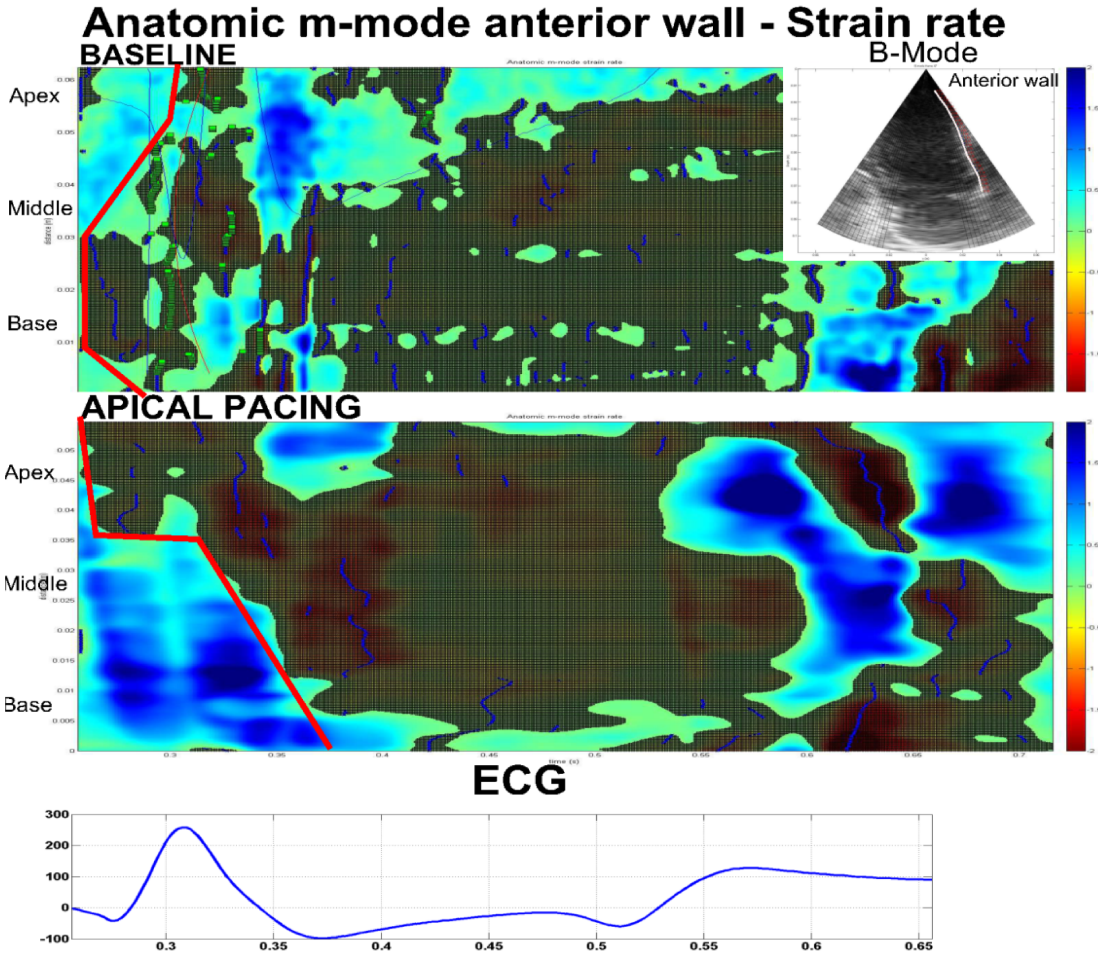

FIGURE 3.8: 2D UFR-TDI - mean segmental strain rate. Upper two panels shows anatomic M-mode presenting strain rate from the anterior during natural pacing and apical pacing. The onset of shortening can be seen in the middle segment during natural pacing, and in the apical segment during apical pacing. Below the ECG from the natural pacing. In the upper right panel, B-mode apical two-chamber view with anatomic curve that forms basis for anatomical M-mode superimposed

proper imaging planes were recorded and that the segment corresponding to pacing electrode was within the field of view.

3.2.2.2 3D UFR-TDI

3D-data was analyzed with in-house developed software based on Orderud et al. [90]. The 3D UFR-TDI data was presented in a bull's eye plot and as a 3D mesh-model of the left-ventricle with color coded strain rate (Figure 3.4). The strain rate data in the bull's eye plot was coded dichotomously with strain rate values above or below $-0.25\,s^{-1}$. The

distribution of the strain rate was visually assessed in the bull's eye plot; when more than 50% of a segment presented strain rates more negative than $<-0.25\,s^{-1}$ it was defined as mechanically activated The cut-off value of $< -0.25\,s^{-1}$ was determined by measuring peak pre-ejection strain rate from 4-chamber views in 10 healthy volunteers (Figure 1.11). Half of the median value in these measurements was used as a cut-off for mechanical activation. The pre-ejection velocity spikes have previously been shown to be closely related to mechanical activation [84], and pre-ejection strain rate was therefore chosen as a surrogate for mechanical activation. Temporal smoothing in the 3D data was set to 10 ms. The spatial smoothing was set to 20 mm x 8 mm x 8 mm (Circumferential x Longitudinal x Endo-epicardial). The analysis was performed in the following steps:

1. Software based on Orderud et al. [90] was applied to the 3D b-mode data to chose region for extraction of 3D UFR-TDI data
2. Strain rate data was visualized on a 3D model of the left ventricle based on the region of interest determined in step 1 and in a bull's eye plot (Figure 3.4)
3. The time of onset of QRS was selected as starting point for analysis
4. Each segment in the bull's eyeplot (18 segment model) was then analyzed in increments of 2 ms and the time interval from onset of QRS to mechanical activation in >50% of the segment of interest was measured

3.2.3 Feasibility

In the 2D UFR-TDI data, 100 segments were feasible for analysis, 8 segments were excluded due to reverberations, random noise or dropouts. In the 3D UFR-TDI data 107 segments were feasible for analysis, 1 segment was excluded due to dropouts.

3.3 Paper III and IV - Clinical Feasibility

3.3.1 Study population

Ten healthy volunteers and twenty patients at least three weeks after their first ST-elevation myocardial infarction were enrolled in the study. Inclusion criteria were: less

than 75 years old, peak Troponin T $> 1000ng/l$, estimated glomerular filtration rate $>$ 60ml/min and NYHA functional class <III. Exclusion criteria were previous MI, contraindications to MR-contrast/ultrasound contrast, severe heart failure, and chronic atrial fibrillation. No patients were excluded due to poor echocardiographic quality. All patients had been examined with acute coronary angiography, and Percuteaneous Coronary Intervention (PCI) was performed as appropriate during the acute phase. The control group consisted of ten healthy volunteers. The control group was not examined with LGE MRI. Population characteristics are found in Table 3.1. Informed consent was obtained from all study participants. The study was approved by the regional ethics committee for medical research ethics and conducted according to the Helsinki declaration.

Patient characteristics	MI patients (n=20)	Healthy volunteers (n=10)
Mean age	60 (±5.9) years	34 (±15.2) years
Male	18	10
Days from infarct to ultrasound examination	146 (21-356)	-
Days from infarct to LGE MRI examination	296 (101-436)	-
Troponin T Peak - ng/l	5842(1240 – 10000)	-
Hypertension	25%	-
Diabetes	0%	-
STEMI	100%	-
Single vessel disease	50%	-
Culprit lesion		
- LAD	40%	-
- CX	25%	-
- RCA	35%	-
Current medication		
- Asprin	100%	-
- Clopidogrel/Ticagrelor	100%	-
- Betablocker	85%	-
- Statin	100%	-
- ACEI/ARB	60%	-
Infarct Size - % LGE	12.11 (± 4.94) %	-
Left Ventricular Ejection Fraction - BiPlane	56 (±8) %	54 (± 6) %

TABLE 3.1: Patient Characteristics - Paper III and IV. STEMI - ST-Elevation Myocardial Infarction, LAD - Left anterior descending coronary artery, CX - Circumflex coronary artery, RCA - Right Coronary Artery, ACEI - Angiotensin converting enzyme inhibitor, ARB - Angiotensin II receptor blockers, LGE - Late Gadolinium Enhancement

3.3.2 Echocardiographic Acquisition

Both UFR-TDI and conventional echocardiographic data was acquired with a Vivid E9 (GE Vingmed, Horten, Norway). The 2D and 3D data was acquired with a phased array probe, M5S-D and 4V, respectively (GE Vingmed, Horten, Norway). Conventional and UFR-TDI data was acquired from the three apical views (2-, 4-chamber and apical long axis view). The technical aspects of the UFR-TDI acquisition technique is described in Brekke et al. 1.

In Paper III, *Myocardial Strain Rate by Anatomic Doppler Spectrum: First Clinical Experience Using Retrospective Spectral Tissue Doppler from Ultra-High Frame Rate imaging*, the acquisition was performed in the following steps:

1. Conventional tissue Doppler data from the three apical views was acquired
2. B-mode data from the three apical views was acquired
3. UFR-TDI data from the three apical views was acquired

In Paper IV, *Color Tissue Doppler Imaging in Contrast Echocardiography - a Feasibility Study*, the acquisition was performed in the following steps:

1. TDI data was acquired in the apical 4-chamber view and two cardiac cycles were digitally stored for post-processing
2. Intravenous injection of 2 ml bolus of UC, SonoVue® (Bracco, Italy) and flushed by 10 ml of saline in a peripheral decubital vein
3. 10 minutes of continuous ultrasound scanning with a mechanical index of 0.8
4. A *second* TDI dataset was acquired in the apical 4-chamber view and two cardiac cycles were digitally stored for post-processing

3.3.3 Anatomic Doppler Spectrum

Anatomic Doppler Spectrum (ADS) (Figure 1.9) is constructed by calculating the spectral data for one time instance at all the spatial points along an anatomical curve drawn along the ventricular wall. It can be constructed in the post-processing from UFR-TDI

data. The spectral data was computed with a Hamming window of 100 ms [1]. ADS allow visualization of the velocity gradient in the ventricular wall without influence of reverberations by tracing the spectral envelope (Figure 1.9c). Strain rate was estimated from the velocity gradient in the region of interest, as demonstrated in Figure 1.9. A steep negative slope of the spectral envelope indicates rapid shortening (contraction) and was defined as normokinetic, slight slope was defined as hypokinetic, no slope of the spectral envelope was defined as akinetic, and positive slope was defined as dyskinetic (lengthening). The region of interest was adjusted to fit the segment of interest, ranging from 15-25 mm in length (Figure 3.9c). The time of interest used for estimation of strain rate was mid-systole. Mid-systole is more reproducible than a peak value and has previously proved suitable for evaluation of myocardial function [42].

The analyses were performed in the following steps:

1. An anatomic curve was drawn from the base to the apex of the ventricular wall. The wall definition was determined in UFR-TDI verified by conventional B-Mode data(Figure 3.9a)
2. An anatomic M-mode presenting tissue velocities was generated with UFR-TDI data from the anatomic curve described in 1 (Figure 3.3)
3. The time of interest was selected, mid-systole for SR estimation and peak S' for comparison with PW velocities (Figure 3.3)
4. ADS was constructed from the time of interest (Figure 3.9c)

The velocity gradient in the ventricular wall was semi-quantitatively and quantitatively assessed (Figure 3.9c). Care was taken to minimize the gain setting while maintaining a consistent spectral envelope. The measurements were done at the peak of the spectrum.

3.3.4 Echocardiographic Analysis

In Paper III - *Myocardial Strain Rate by Anatomic Doppler Spectrum: First Clinical Experience Using Retrospective Spectral Tissue Doppler from Ultra-High Frame Rate imaging* the analysis was performed as follows. All conventional echodata was analyzed

[1] A hamming window is an averaging technique which minimizes sidelobes

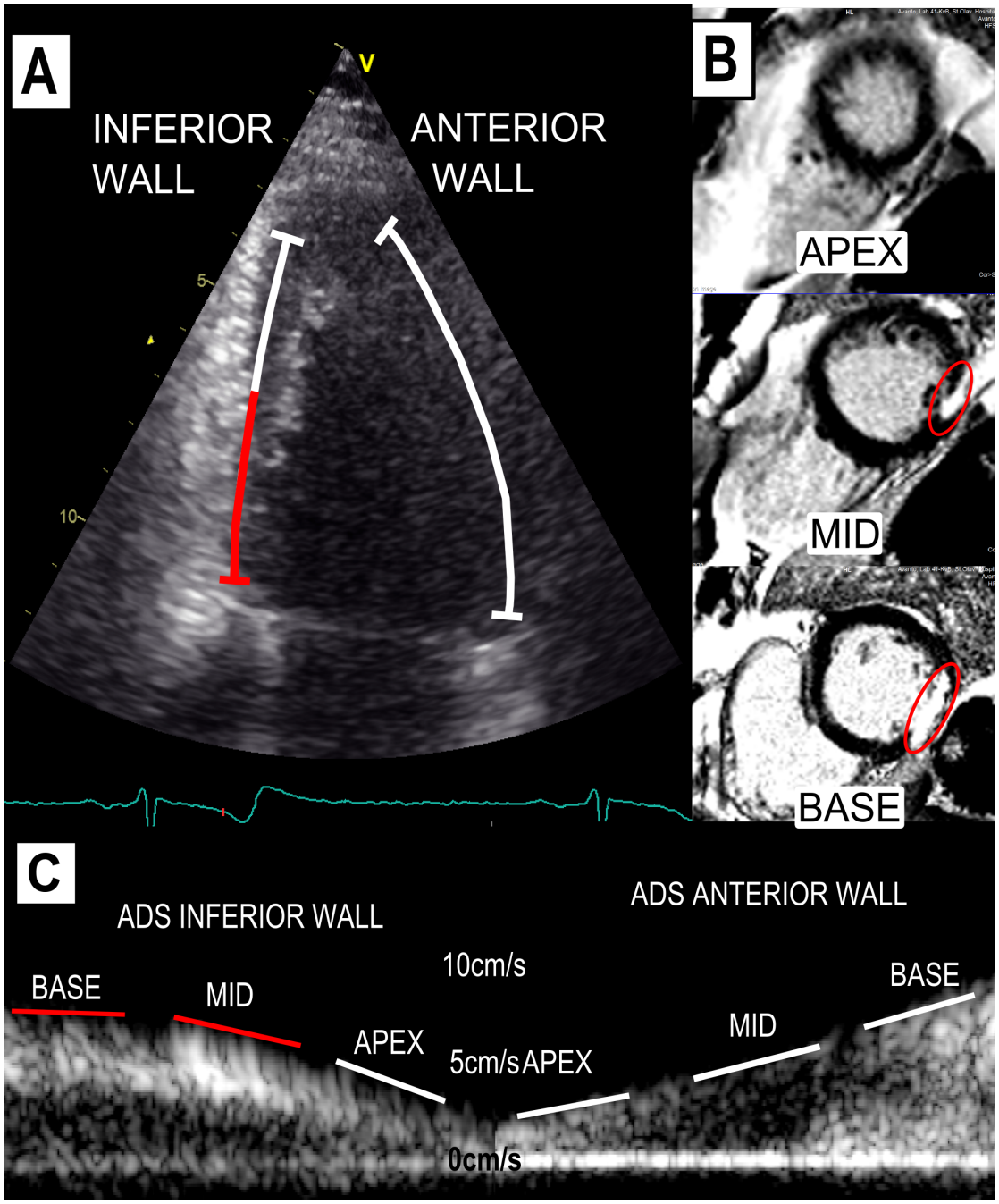

FIGURE 3.9: Anatomic Doppler Spectrum from anterior and inferior wall in a patient with an inferior wall infarction: A: B-mode image and anatomical curve forming the basis for Anatomic Doppler Spectrum. B: Late gadolinium-enhanced MRI from the same patient. The infarcted area is visible as enhanced scar in the basal and midventricular inferior wall (demarcated with red ring). C: The Anatomic Doppler Spectrum shows nearly the same slope in all anterior segments, despite low signal (lung or bone shadow). In the inferior wall there is almost no slope in the basal segment, reduced slope in the middle, and normal slope in the apical segment. This corresponds with the scar distribution seen on the late gadolinium-enhanced MRI to the right.

in Echopac Ver. 112 Rev. 13 (GE Vingmed, Horten, Norway). 2D UFR-TDI data was analyzed with in-house developed software in Matlab 2011a (The MathWorks, Natick, MA, USA). 3D UFR-TDI data was analyzed with in-house developed software based on GE 4D Auto LVQ software (GE Vingmed, Horten, Norway).

SR was measured in an 18 segment model. For global parameters 18 segments were adapted to a 16 segments model by averaging the apical segments, antero- and inferoseptal, and antero- and inferolateral respectively, the mean of the 16 segments was then calculated. Subjects with > 12 eligible segments were included in the analysis of global parameters. The following parameters were assessed:

Anatomic Doppler spectrum: Mid-systolic segmental strain rate (ADS SR Slope): Steps 1-4 described in Anatomic Doppler Spectrum were used. The mid-systolic slope of the spectral envelope in the segment of interest was measured and strain rate was extracted (Figure 3.9c).

Anatomic Doppler spectrum: Visual mid-systolic segmental strain rate (ADS SR Visual): Steps 1-4 described in Anatomic Doppler Spectrum was used. The slope of the spectral envelope was visually assessed and scored on a scale from 1 to 4 (1 – normokinetic, 2 – hypokinetic, 3 – akinetic and 4 - dyskinetic).

Mitral annular velocities were measured to evaluate the accuracy of the new UFR-TDI method: *Anatomic Doppler spectrum S'* - The time of peak S' was detected in UFR-TDI velocity curves from the septal and lateral mitral annulus respectively, thereafter steps 1-4 described in Anatomic Doppler Spectrum was followed. Peak S' velocity was then measured at the septal and lateral mitral annulus in an ADS. *PW TDI S'* - A 6 mm sample volume was placed at the septal and lateral mitral annulus. The peak systolic mitral annular velocities in the septum and lateral walls were measured.

Ejection fraction (EF): EF was measured using the modified biplane Simpson method (4- and 2-chamber views).

Peak systolic strain rate by TDI (TDI PSSR): TDI PSSR was measured in an 18 segment model from the apical 2-, 4-chamber and long axis view with conventional TDI. A sample volume of 6 mm x12 mm was placed in the mid-myocardium in each segment, Gaussian smoothing of 40 ms was used.

UFR-TDI was used for estimation of ADS SR Slope, ADS SR Visual and ADS S'. Conventional acquisition was used for PW TDI S', EF and TDI PSSR.

In Paper IV, *Color Tissue Doppler Imaging in Contrast Echocardiography - a Feasibility Study*, the analysis was performed as follows: Following the joint European Association of Echocardiography and American Society of Echocardiography recommendations for left ventricular segmentation and to avoid random noise, only the 2 basal and 2 mid LV segments in the apical 4 chamber view was analyzed. Systolic tissue Doppler velocities, *S', e'* and *a'*, were assessed in the 4 different LV segments in 2 consecutive heart beats by two readers blinded to each other's results.

3.3.5 Magnetic Resonance Imaging

The examinations were performed with a 1.5 T Siemens Avanto (Siemens Medical, Erlangen, Germany) with a 6-channel radio frequency coil. A Gadolinium based contrast agent, Gadoterate meglumine (0.15 mmol/kg DOTAREM, Guerbet LLC,) was then administered and contrast enhanced images were acquired ten minutes later using a phase-sensitive inversion recovery balanced steady-state free precession sequence [91]. A Look-Locker sequence was used to determine the appropriate T inversion time. Firstly, a short-axis stack of the left ventricle was acquired (slice thickness 8 mm and interslice gap 2 mm), then long-axis images were acquired (2-, 4-chamber and long axis views). The images were acquired during end-expiratory breath hold (10-15 seconds), in end-diastole before atrial contraction. Typical image parameters for Gadolinium enhanced acquisition was: Acquisition matrix:256*127 pixels with in-plane resolution of 1.3 mm x 1.3 mm, 45 degree flip angle and inversion time 290–310 ms. LGE MRI was performed in 20 patients. One patient was excluded due to claustrophobia. The analysis was performed in Segment v1.9.r2959 Segment v1.9.r2959(http://segment.heiberg.se) [92, 93]. The myocardial and infarct border was semi-automatically traced on each short axis slice (Figure 3.10 & 3.11). Short axis slices where myocardium occupied >2/3 of the circumference was included in the analysis. Papillary muscles were excluded from the volume. A pixel intensity of 1.8 standard deviataions greater than healthy myocardium was considered as infarcted [94]. The results were reported in a 16 segment model corresponding to the model used for conventional echocardiographic parameters. The segments were divided in three groups based on fraction of gadolinium enhanced myocardium (LGE);

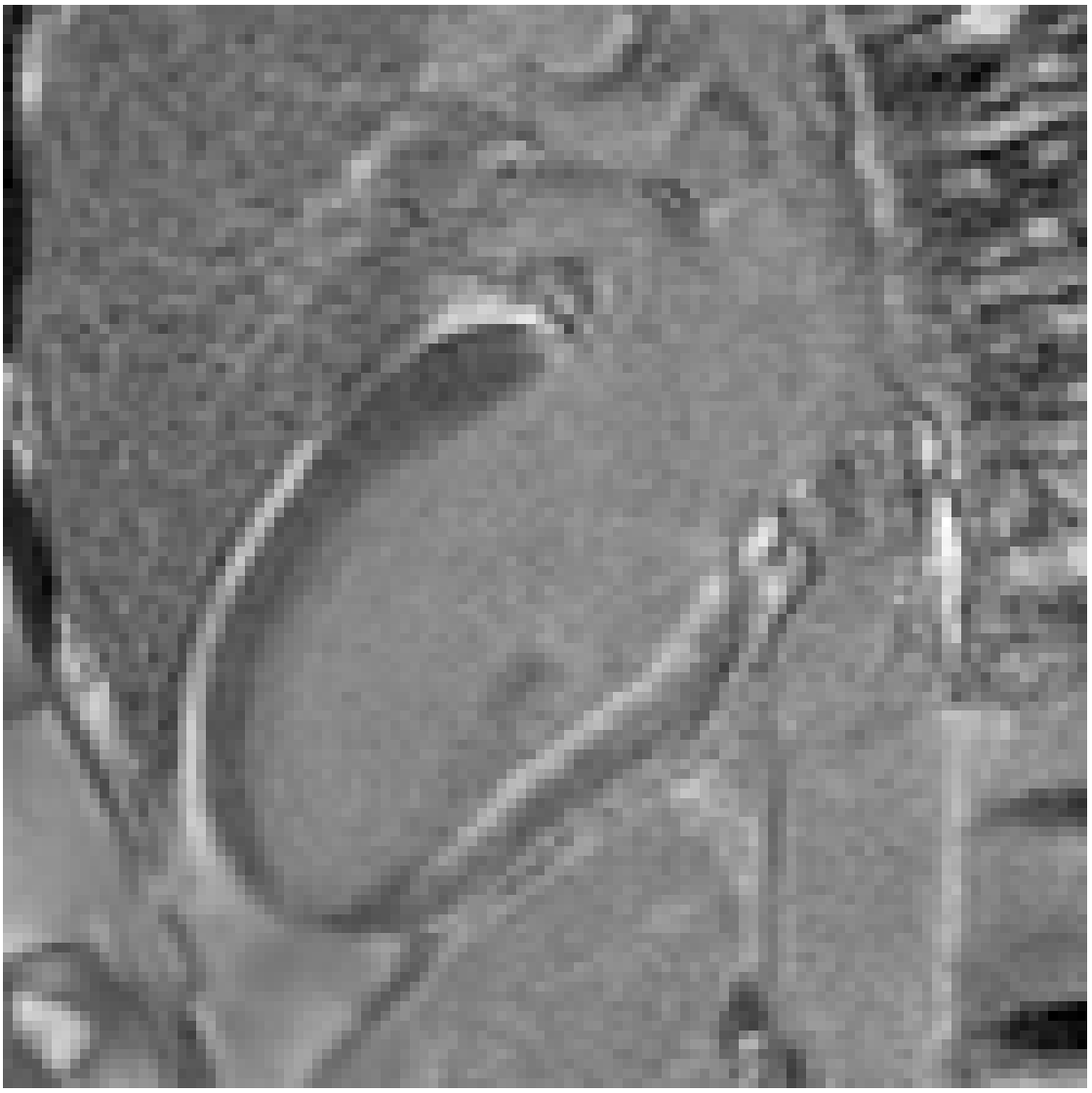

FIGURE 3.10: LGE MRI myocardial infarct

0%, 0-50% and >50% [95]. The patients were divided based on median infarct size; $< 12\%$ and $> 12\%$.

3.3.6 Statistical analysis

All statistical calculations were made in SPSS for Windows 2010 (IBM Corp. in Armonk, NY.). Continuous variables are presented as mean ± standard deviations (SD) or median (range) and categorical variables as percentages unless otherwise noted. A p-value $<.05$ was considered significant unless otherwise noted.

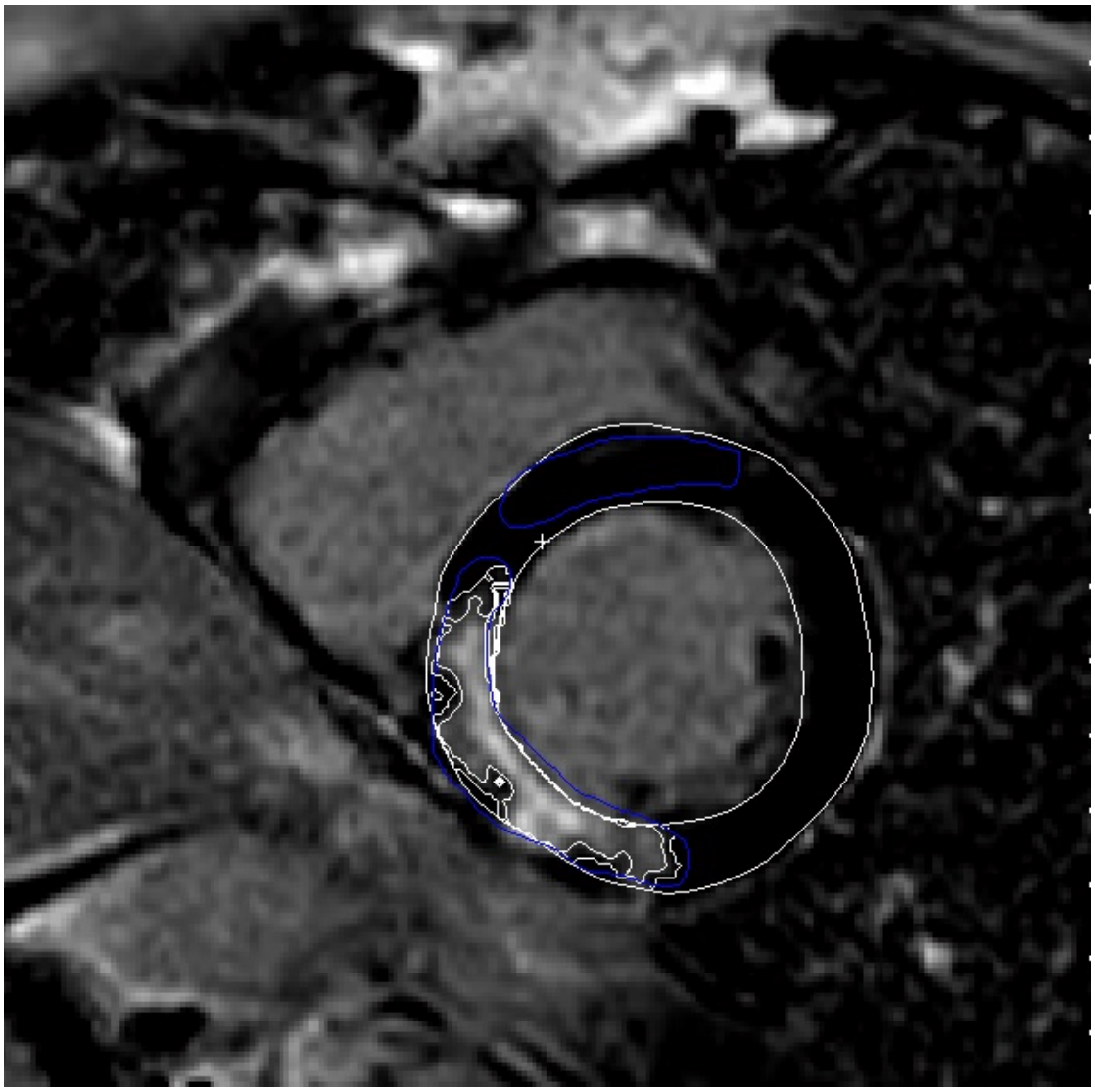

FIGURE 3.11: Semi-automatic infarct area detection in Segment

In *Myocardial Strain Rate by Anatomic Doppler Spectrum: First Clinical Experience Using Retrospective Spectral Tissue Doppler from Ultra-High Frame Rate imaging*, the comparison of means within segmental parameters and global parameters was performed with one-way ANOVA with Bonferroni post hoc test. Homogeneity of variances was tested with Levene's test[96]. In case homogeneity of variances could not be assumed, Welch ANOVA with Games-Howell post-hoc test was used. The correlation between global parameters (Mean ADS visual SSR and Mean ADS SSR) and myocardial infarct size was tested with Pearson's correlation coefficient. Cochran's Q test was used to compare the proportion of analyzed segments by each method. Agreement between peak S' measurements by the two methods was assessed with Bland Altman analysis [97].

Inter- and intra-observer reproducibility of ADS Strain rate parameters were assessed according to Bland Altman [97], and is expressed as coefficient of repeatability (COR). COR represents 1.96 x SD of the mean inter- or intra-observer difference. Further, Mean Error was estimated, which represents the absolute inter- and intra-observer difference divided by parameter mean.

In *Color Tissue Doppler Imaging in Contrast Echocardiography - a Feasibility Study* tissue Doppler velocities prior to and after UC injection was compared using paired t-test. Equality of variance of TDI velocities before and after UC was tested by Levine's test. Inter- and intra-observer reproducibility of velocity measurements before UC, after UC and between measurements before UC was compared to measurements after UC, and was tested by intraclass correlations and presented as Bland-Altman plots including limits of agreement.

Chapter 4

Summary of results

4.1 Paper I - Technical Feasibility

The aim of this study was to evaluate feasibility of 2D UFR-TDI. The study showed that tissue Doppler was feasible with a frame rate of 1200 fps. The tissue velocities measured with UFR-TDI were in agreement with velocities measured by conventional TDI. The pre-ejection period was resolved in high detail (Figure 4.1).

4.1.1 Agreement with TDI

In assessment of peak annular velocities, paired t-tests with Bonferroni correction indicated no significant differences between UFR-TDI and conventional TDI or between repeated conventional TDI recordings. Bland-Altman analysis of inter-method variability and conventional TDI intra-method variability revealed comparable limits of agreement (Tables 4.1 and 4.2). With respect to time to peak *S'*, paired t-tests indicated no significant differences between UFR-TDI and conventional TDI (p=0.163) or between repeated conventional TDI recordings (p=0.279).

4.1.2 Pre-Ejection period

The pre-ejection period had a mean total duration of 91.0±13.1 ms. In this period, there were two spikes of positive velocity in the basal septum before the onset of the *S'* wave. The interval from the first deflection of QRS to the start of spike 1 was 22.7±13.0 ms,

	S-'wave		*e*'-wave		*a*'-wave	
	Lateral	Septal	Lateral	Septal	Lateral	Septal
Average for UFR-TDI (cm/s)	8.32	7.15	13.58	10.19	5.51	6.70
Average for conventional TDI (cm/s)	8.68	7.34	13.55	10.45	4.80	6.38
Average difference (cm/s)	-0.36	-0.19	0.03	-0.26	0.71	0.32
Limits of agreement (cm/s)	(-2.27,1.56)	(-1.13,0.75)	(-1.43,1.48)	(-3.20,2.67)	(-1.18,2.61)	(-1.49,2.13)
t-test p-value	0.28	0.23	0.91	0.59	0.05	0.30

TABLE 4.1: Agreement between UFR-TDI and conventional TDI

	S'-wave		*e*'-wave		*a*'-wave	
	Lateral	Septal	Lateral	Septal	Lateral	Septal
Average for UFR-TDI (cm/s)	8.68	7.34	13.55	10.45	4.80	6.38
Average for conventional TDI (cm/s)	8.54	7.48	13.43	10.20	5.20	6.61
Average difference (cm/s)	0.14	-0.14	0.12	0.25	-0.40	0.23
Limits of agreement (cm/s)	(-0.90,1.18)	(-1.05,0.77)	(-1.83,2.06)	(-1.83,2.32)	(-1.47,0.67)	(-2.19,1.73)
t-test p-value	0.42	0.38	0.72	0.48	0.04	0.48

TABLE 4.2: Intra-method agreement between UFR-TDI and conventional TDI

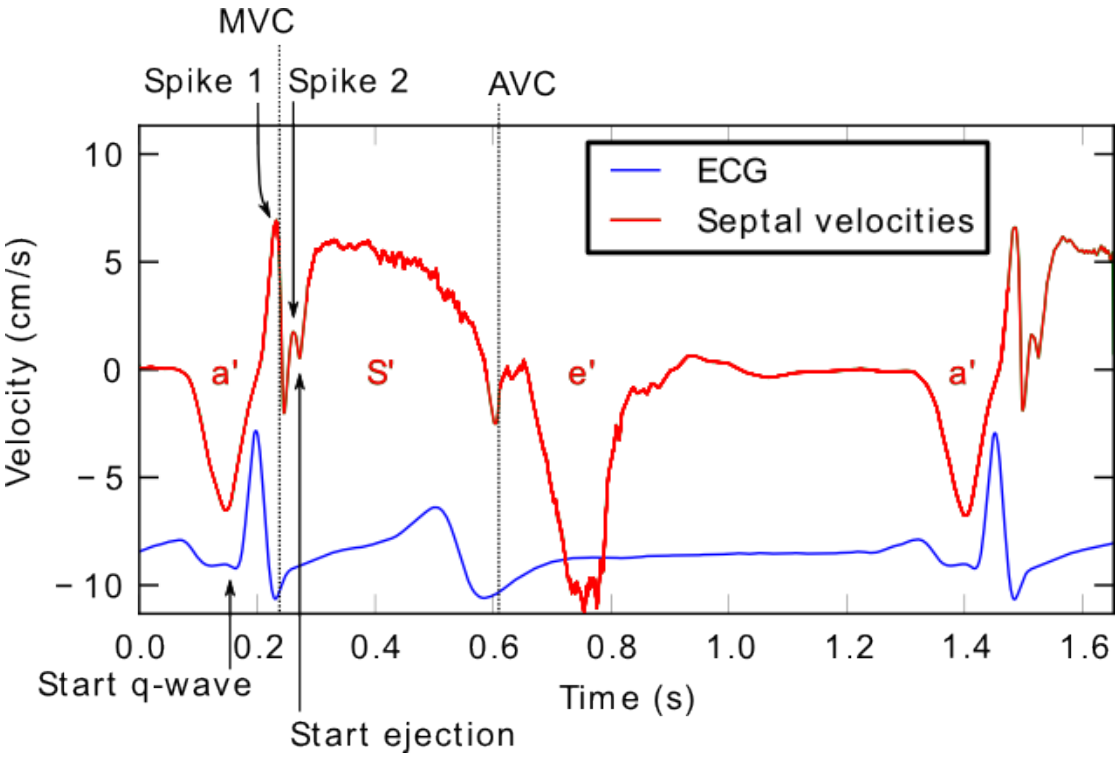

FIGURE 4.1: The events during the pre-ejection period from 1200 fps UFR-TDI data

and to the start of spike 2, 67.0±14 ms. The interval between the start of velocity spike 1 and mitral valve closure was 29.6±16.1 ms. The isovolumic contraction period (mitral valve closure to ejection) had a mean duration of 39.1±17.5 ms. The second spike was not seen in the lateral wall, where the initial positive spike was followed by a negative spike. The time intervals in the pre-ejection period are illustrated in Figure 4.1

Wall	Segment	Baseline (ms)	Apical Pacing (ms)	Anterior pacing (ms)	Lateral pacing (ms)
Inferoseptum	Basal	16	10	89	28
	Mid	78	30	79	62
	Apex	36	32	107	121
Anterolateral	Basal	57	39	84	19
	Mid	22	19	99	56
	Apex	101	11	122	55
Anterior	Basal	68	67	63	28
	Mid	36	54	28	28
	Apex	10	39	76	60
inferior	Basal	31	-	121	72
	Mid	256	-	89	35
	Apex	22	-	92	42
Anteroseptal	Basal	77	57	79	211
	Mid	98	76	84	114
	Apex	14	75	227	106
Inferolateral	Basal	11	86	52	159
	Mid	6	89	98	32
	Apex	58	56	156	74

TABLE 4.3: 2D-UFR-TDI data Mean time interval Onset QRS – First negative strain rate

4.2 Paper II - Experimental Animal Study

The results from the experiments showed that the time to negative strain rate is shorter in the paced segments than the unpaced in both 2D and 3D measurements. The findings are summarized in table 4.3 and 4.4, and as a scatterplot in figure 4.2.

4.2.1 2D UFR-TDI - Time to shortening:

The mean time interval from onset QRS to onset of shortening (negative SR) was 35 ± 23 ms in the segments corresponding to the placement of the pacing electrodes, and 70.2 ± 38.9 ms in the remaining segments, and 73 ± 64 ms in all segment combined.

4.2.2 3D UFR-TDI - Time to shortening:

The mean interval from onset of QRS to onset of shortening ($<-0.25\,s^{-1}$) was 41 ± 15 ms in the corresponding to the placement of the pacing electrodes, and 69 ± 52 ms in remaining segments. Pearsons R for correlation between the methods was r = 0.14 (p=ns) after removal of four outliers.

Wall	Segment	Baseline (ms)	Apical Pacing (ms)	Anterior pacing (ms)	Lateral pacing (ms)
Inferoseptum	Basal	62	298	48	67
	Mid	78	54	62	78
	Apex	46	40	-	85
Anetrolateral	Basal	120	68	90	44
	Mid	42	32	48	58
	Apex	26	28	148	83
Anterior	Basal	112	38	52	66
	Mid	48	54	148	87
	Apex	120	-	11	88
Inferior	Basal	78	232	48	47
	Mid	59	32	62	54
	Apex	34	22	-	84
Anteroseptal	Basal	228	56	44	51
	Mid	46	66	82	101
	Apex	73	24	98	39
Inferolateral	Basal	44	66	92	46
	Mid	45	30	62	62
	Apex	24	-		68

TABLE 4.4: 3D-UFR-TDI data Mean time interval Onset QRS – strain rate $-0.25\,s^{-1}$

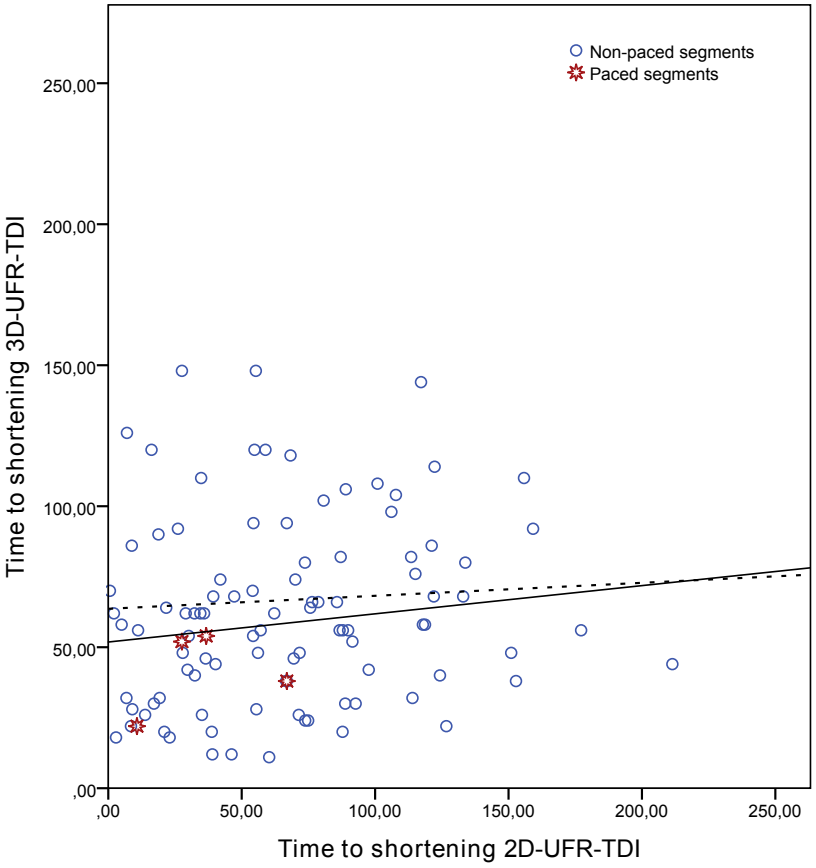

FIGURE 4.2: : Y-axis represents mean time to shortening measured in a given segment X-axis represents time to shortening in corresponding segment measured in from 3D-UFR-TDI. Unit is milliseconds.

Global correlation with LGE MRI		
Method	Pearsons correlation coefficient - r	p -value
LGE MRI - Mean ADS SR Visual	0.68*	<.001
LGE MRI - Mean ADS SR Slope	0.50*	0.006
LGE MRI - Mean TDI Peak systolic strain rate	0.23	0.30
LGE MRI - Mean spectral S' (lateral and septal)	-0.56	0.002
LGE MRI - Mean ADS S' (lateral and septal)	-0.56	0.002
LGE-MRI - EF	-0.3	0.1

TABLE 4.5: Global correlation with LGE MRI - ADS SR Visual – Anatomic Doppler Spectrum Visual mid-systolic segmental strain rate, ADS SR Slope – Anatomic Doppler Spectrum mid-systolic strain rate, ADS S' - Anatomic Doppler Spectrum peak systolic velocity, TDI PSSR – Peak systolic strain rate Tissue Doppler Imaging, EF – Ejection fraction.

4.3 Clinical Feasibility

4.3.1 Paper III - Anatomic Doppler Spectrum

4.3.1.1 Feasibility

The feasibility for the segmental ADS methods were better than the feasibility for TDI PSSR (ADS SR Slope 95%, ADS SR Visual 96%, TDI PSSR 87% (Q(3) = 54.4, p<0.001). The inter- and intra-observer reproducibility of the ADS SR Slope measurements are given in Table 4.6 and figure 4.3.

4.3.1.2 Segmental parameters

For the comparison of segments with different fraction of viable myocardium, we found that ADS SR visual was the only method that was able to differentiate between the three categories of segmental scar (Table 4.7). All methods were able to differentiate healthy from scarred myocardium.

4.3.1.3 Global parameters

When averaging the segmental measurements, ADS SR Visual, ADS SR Slope and Peak S' showed a significant correlation with infarct size, PSSR TDI did not (r=0.68 p<0.001, r=0.50 p=0.006, r=-0.56 p=0.002, and r=0.23 p=0.30). No method was able to differentiate between 0-12% LGE and >12% LGE. The results are summarized in tables 4.5 & 4.7, and scatterplots provided in figure 4.4.

Inter- and intra-observer reproducibility					
Method	Mean	Mean difference ± SD	Limits of agreement	COR	Mean error (%)
Inter-observer Segmental ADS SR Slope	-0.69s-1	0.070 ± .38	-0.68 to 0.82	0.76	42 %
Inter-observer Mean ADS SR Slope	-0.71s-1	0.037 ± .05	-0.06 to 0.14	0.10	6 %
Intra-observer Segmental ADS SR Slope	-0.75s-1	0.163 ± .31	-0.29 to 0.77	0.62	37 %
Intra-observer Mean ADS SR Slope	-0.76s-1	0.172 ± .09	-0.01 to 0.35	0.18	22%

TABLE 4.6: Inter- and intra-observer reproducibility Anatomic Doppler Spectrum - Limits of agreement is presented as mean±1.96 SD, ADS SR,Slope – Anatomic Doppler Spectrum mid-systolic strain rate, SD – Standard,Deviation, COR – Coefficient of repeatability

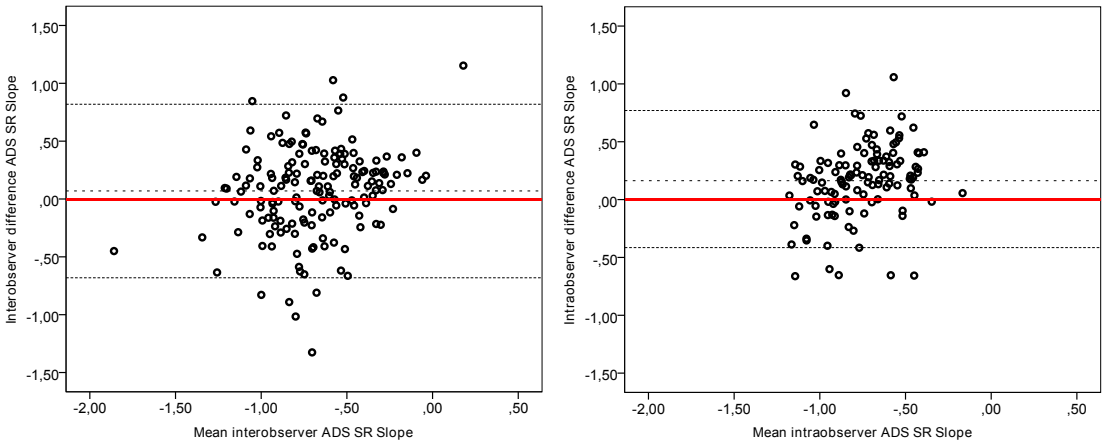

FIGURE 4.3: : The left panel presents Bland Altman plot for inter-observer ADS SR Slope measurements, the right presents Bland Altman plot for intra-observer ADS SR Slope measurements. The unit on the x- and y-axis in both panels are s^{-1}.

4.3.1.4 Peak systolic mitral velocities (S') measured by PW Doppler and ADS

S' by PW TDI was 8.0 ± 2.3 cm/s and by ADS was 7.6 ± 2.2 cm/s. The data are presented in a Bland Altman Plot (Fig. 4.4). The mean difference was 0.35 cm/s, limits of agreement was -2.1 cm/s to 2.76 cm/s.

4.3.1.5 Late gadolinium enhanced magnetic resonance imaging

LGE MRI were performed in 19 patients, 304 segments were analyzed, of which 151 segments showed no scar tissue, 108 segments showed 0% - 50% and 45 segments showed >50%. No segments were discarded from the analysis due to image quality. Mean LV infarct size was 12.1 ± 4.9 %. Scar tissue was identified in all patients.

Segmental parameters			
Parameter- Mean (SD)	Healthy (n=311)	0-50% LGE MRI (n=108)	>50% LGE MRI (n=45)
ADS SR Visual	1.20 (±0.46)a	1.51 (±0.65)b	1.88 (±0.72)
ADS SR Slope	-0.73 (±0.35)c	-0.66 (±0.45)	-0.51 (±0.43)
TDI peak systolic strain rate	-1.06 (±0.49)d	-0.92(±0.44)	-0.91(±0.56)
Global parameters			
	Healthy (n=10)	0-12% LGE MRI (n=8)	>12% LGE MRI (n=11)
Mean ADS SR Visual (n=29)	1.03 (±0.05)e	1.48 (±0.27)	1.52 (±0.21)
Mean ADS SR Slope (n=28)	-0.79 (±0.09)f	-0.67 (±0.15)	-0.60 (±0.13)
Mean TDI PSSR (n=22)	-1.1 (±0.22)	-0.99 (±0.15)	-0.97(±0.23)

TABLE 4.7: ADS SR Visual – Anatomic Doppler Spectrum Visual mid-systolic segmental strain rate, ADS SR Slope – Anatomic Doppler Spectrum mid-systolic segmental strain rate, TDI PSSR – Tissue Doppler Imaging peak systolic strain rate a-Significantly different from 0-50% and >50% (p=<0.001) b-Significantly different from >50% (p=<0.05) c-Significantly different from >50% (p=<0.01) d-Significantly different from 0-50% (p=<0.05) e- Significantly different from 0-12% and >12% (p=<0.001) f- Significantly different from >12% (p=<0.01)

Variables	Before contrast	After contrast	p-value	ICC (95% CI)
S' (cm/s)	5.02±1.52	4.96±1.36	0.683	0.82 (0.71-0.89)
e' (cm/s)	-6.05±1.90	-5.90±1.76	0.359	0.84 (0.75-0.90)
a' (cm/s)	-5.90±2.12	-5.80±1.96	0.517	0.89 (0.82-0.93)

TABLE 4.8: Reproducibility of Tissue velocity before and 10 minutes after contrast injection

4.3.2 Paper IV - Color Tissue Doppler Imaging in Contrast Echocardiography - a Feasibility Study

4.3.2.1 Feasibility

In 7% of LV segments image quality did not allow TDI velocity measurement and had to be excluded from the analysis. The number of segments with poor image quality did not differ prior and after contrast injection.

4.3.2.2 TDI reproducibility

There was no significant intra-observer variability for *S'*, *e'* & *a'* in repeated measurements pre- and post-contrast injection. Further, there was no significant inter-observer variability for *S'* and *e'* in repeated measurements pre- and post-contrast. There was however a significant Inter-observer variation for *a'* both in the pre- and post-contrast measurements. The findings show similar reproducibility in pre- and post-contrast measurements (Table 4.8).

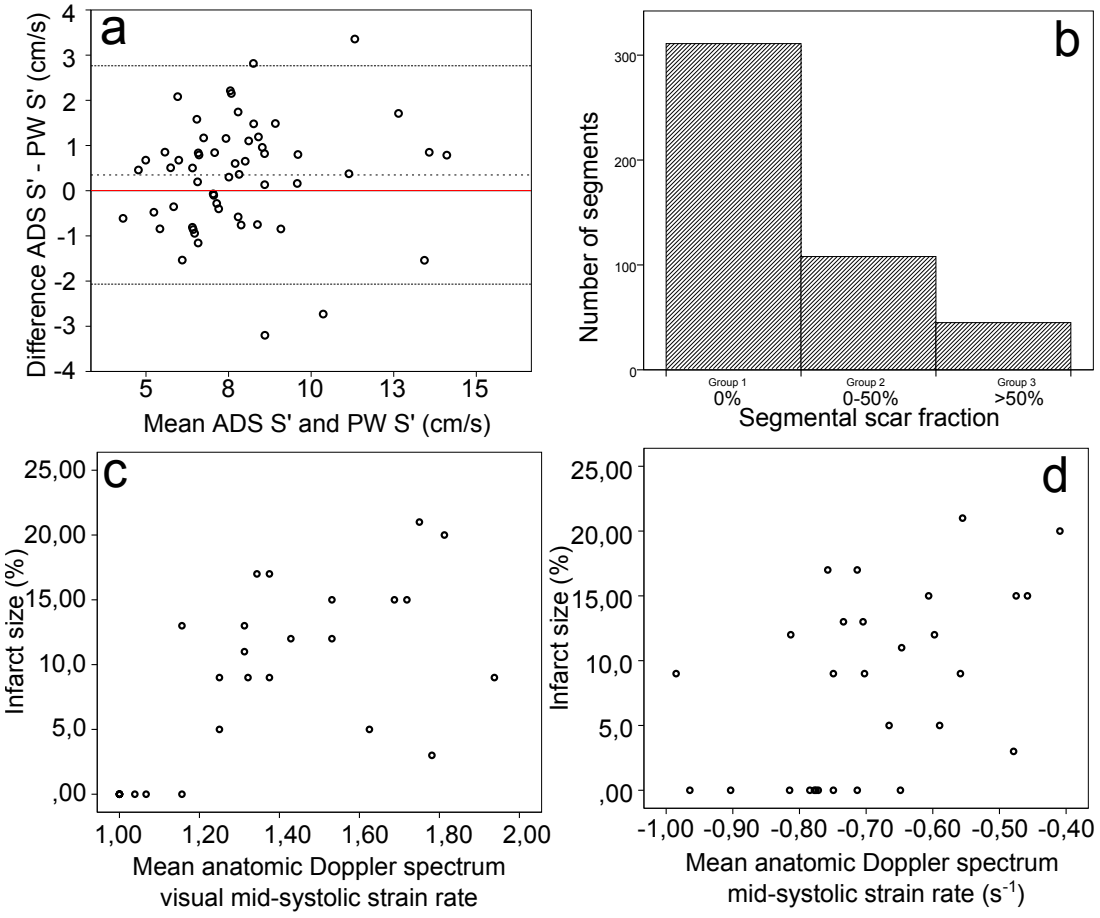

FIGURE 4.4: : (a) Bland Altman plot: pulsed wave Doppler peak annular velocities and ADS Peak annular velocities (*S'*). (b) Segmental infarct fraction measured with gadolinium enhanced magentic resonance imaging (LGE-MRI). Y-axis shows number of segments, x-axis shows the different Groups: Group 1 - 0%, Group 2 - $0 - 50\%$ and group 3 - $> 50\%$ LGE-MRI. (c) Scatterplot with infarct size measured with LGE-MRI on y-axis and mean ADS SR Visual on the x-axis. (d) Scatterplot with infarct size measured with LGE-MRI on y-axis and mean ADS SR Slope on the x-axis. Scatterplot with infarct size measured with LGE MRI on y-axis and mean ADS SR Visual on the x-axis.

Chapter 5

Discussion

The main findings in this thesis are:

1. Estimation of velocities and deformation with frame rates of 1200 fps in 2D and 500 fps in 3D is feasible with UFR-TDI
2. Strain rate analysis by 2D UFR-TDI with ADS was feasible in more segments compared to strain rate by conventional TDI, further, 2D UFR-TDI showed better repeatability of strain rate measurements than conventional TDI
3. The pre-ejection period was resolved in 2D UFR-TDI in 1200 fps, making new information available in early systole
4. Mechanical activation in the left ventricle can be detected with 2D and 3D UFR-TDI
5. TDI based velocity measurements was feasible after injection of ultrasound contrast

5.1 Technical feasibility - main findings and discussion

5.1.1 Paper I - Ultra-high Frame Rate Tissue Doppler Imaging

In *Ultra-high Frame Rate Tissue Doppler Imaging* we demonstrated that tissue Doppler imaging is feasible with a frame rate of 1200 fps. Such high temporal resolution makes

new information available in both early and late systole. Comparison of velocity measurements with conventional TDI indicates that our sensitivity is sufficient for estimating velocities.

UFR-TDI utilizes multi-line acquisition to realize ultra-high frame rates. Multi-line acquisition has some disadvantages, the most important being line artifacts visible in B-mode imaging when using a large number of parallel receive beams [98]. For tissue Doppler imaging with parallel receive, the main disadvantage is lowered sensitivity for the outermost receive beams. In our method, the receive lines furthest from the transmit direction have 20-dB-reduced power compared with the center receive lines at 10-cm depth. This results in lower intensity signal with side lobes toward the transmit direction. Suggested technical improvements to minimize these issues are described in Brekke et al. [1]. The frame-rates provided by UFR-TDI do not allow good B-mode image quality, as demonstrated in Figure 5.2. However, the image quality was sufficient for anatomic orientation when recording and analyzing tissue Doppler data. Because we only image the ventricular walls within two relatively narrow sectors, it is necessary that the sectors are well positioned. Currently, the visual support during acquisition is limited to showing the total sector, which includes both receive sectors and the hole in the middle. Thus, some training is required for the user. Furthermore, as the ventricular walls should be aligned with the transmit direction, the method is best suited for apical recordings. In the parasternal views, the heart walls are perpendicular to the transmit beams, and the method will not be able to cover the ventricular walls entirely.

5.1.1.1 Pre-Ejection period

During the pre-ejection period, ventricular depolarization spreads along the Purkinje system, after which mechanical activation of the ventricles occurs. The delay between electrical excitation and mechanical activation has been reported to be about 30 ms at the cellular level [60]. Moreover, previous studies have found that mechanical activation starts before mitral valve closure [84, 99]. With the high frame rate in the present method, we see that the onset of QRS in the ECG precedes the onset of the initial tissue velocities by 22.7 ms, on the same order of magnitude as the delay reported on a cellular level by Cordeiro et al. [60]. Thus, it seems that the high frame rate makes it possible to measure electromechanical delay. We also find that the initial velocity spikes precede

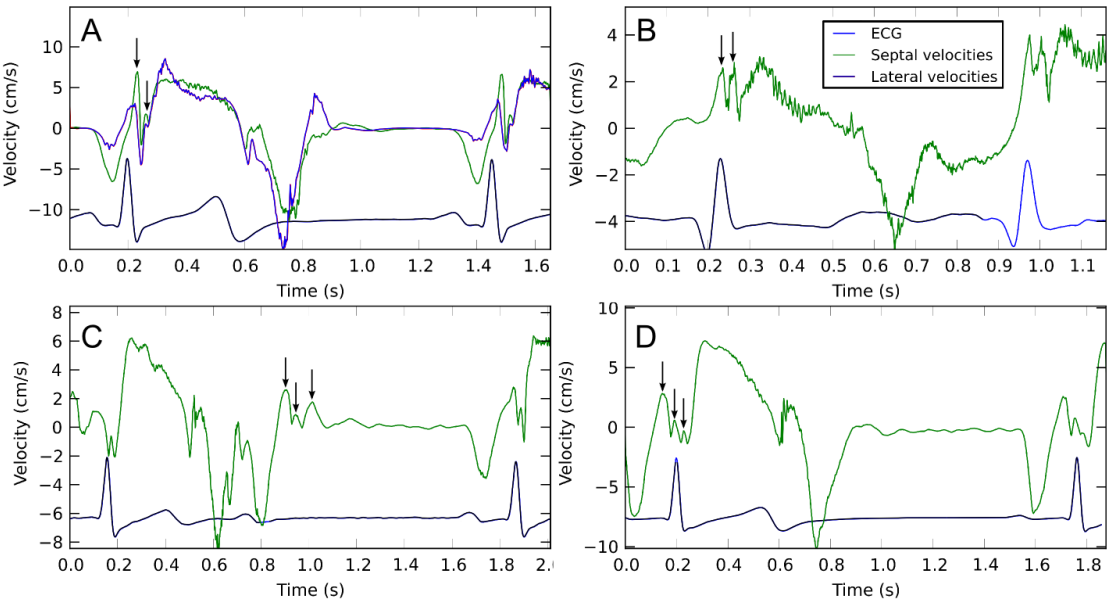

FIGURE 5.1: UFR-TDI Velocity curves: Examples of annular velocity curves recorded with ultra-high frame rate tissue Doppler imaging (UFR-TDI). (a) Velocities in the septal and lateral walls of a normal subject, showing two positive spikes in the septal wall. In the lateral wall there is a biphasic spike, with positive velocity during spike 1 and negative velocity during spike 2. (b) Velocities in the basal septum of a patient with atrial fibrillation. This subject has no substantial atrial contraction; however, the two spikes are still evident. (c) Velocities in a subject with Wenckebach block, indicating an atrial systole not followed by ventricular systole. The velocity curve shows several spikes after the a' wave, even though there is no ventricular activa- tion. (d) Velocities in the basal part of the septum in a subject with a long PQ interval (230 ms). The first spike after a' precedes the onset of QRS. ECG: electrocardiogram

mitral valve closure. This is in accordance with the studies by Remme et al. [84], Tsakiris et al. [99] & Goetz et al. [100]. Pre-ejection velocities have previously been studied by pulsed tissue Doppler as well as color Doppler with high frame rates [101–104]. However, to our knowledge, only Kanai [105] has examined the basal velocities from the apical view at similar frame rates. Kanai found two positive velocity spikes in the basal septum, similar to our findings, although with a different proposed explanation. The pre-ejection velocities in the lateral wall, on the other hand exhibit a biphasic pattern with a positive, followed by a negative spike (Fig. 5.1a). This has been described by several authors [101, 106]. The origin of the initial pre-ejection velocity spike has been suggested both to be ventricular [84], representing the start of ventricular mechanical activation, and to be atrial, representing recoil after ventricular elongation caused by atrial contraction. In our study, the initial double spike was also present in a subject with atrial fibrillation (Fig. 5.1b), indicating that the spike should be of ventricular origin. Velocities of atrial origin can be seen in Wenckebach block (Fig. 5.1c) or long PQ interval (Fig. 5.1d), so

atrial recoil may contribute. The information obtained by velocities, however, is limited. Because of tethering, actively contracting parts of the ventricle (in this case the earliest activated parts) may pull along more basal parts that are not yet activated. This means that it would be difficult to describe the electromechanical activation sequence from velocities alone. Strain rate imaging [45] would eliminate the tethering effects and can be measured with UFR-TDI (Fig. 5.2).

5.2 Paper II - Detection of mechanical activation in an open chest porcine model by three-dimensional UFR-TDI, a feasibility study

In *Ultra-high Frame Rate Tissue Doppler Imaging* we demonstrated that we were able to measure the electromechanical delay. In the experimental animal study, *Detection of mechanical activation in an open chest porcine model by three-dimensional UFR-TDI, a feasibility study*, we demonstrated that detection of onset of mechanical activation by 2D and 3D UFR-TDI deformation data in an open chest pig model is feasible. We measured the time delay from onset of QRS to onset of shortening. Time to mechanical activation was shorter in the segments corresponding to the pacing electrodes than in the remaining segments in 3D UFR-TDI data for all pacing sites, further the time intervals were in the same order of magnitude as found in the 2D UFR-TDI data.

The detection of electromechanical activation by deformation imaging is complex. There is continuously active and passive deformation throughout the ventricle, and differentiation remains a challenge. Peak negative strain rate signals shortening. During pre ejection time, this will most probable be active, while neighbouring, non-activated areas will be stretched. However, recoil from atrial systole may complicate this measurement by compressing some of myocardium.

The time intervals measured in 3D UFR-TDI are in the same order of magnitude as the 2D UFR-TDI data. There is however a large spread in both the 2D-, and 3D-UFR-TDI data, and time to shortening does differ between the 2D- and 3D-data for corresponding non-pacing segments (Fig. 4.2). A possible explanation for this is that the method used for detection of onset of shortening differs. 2D UFR-TDI uses automatic detection of

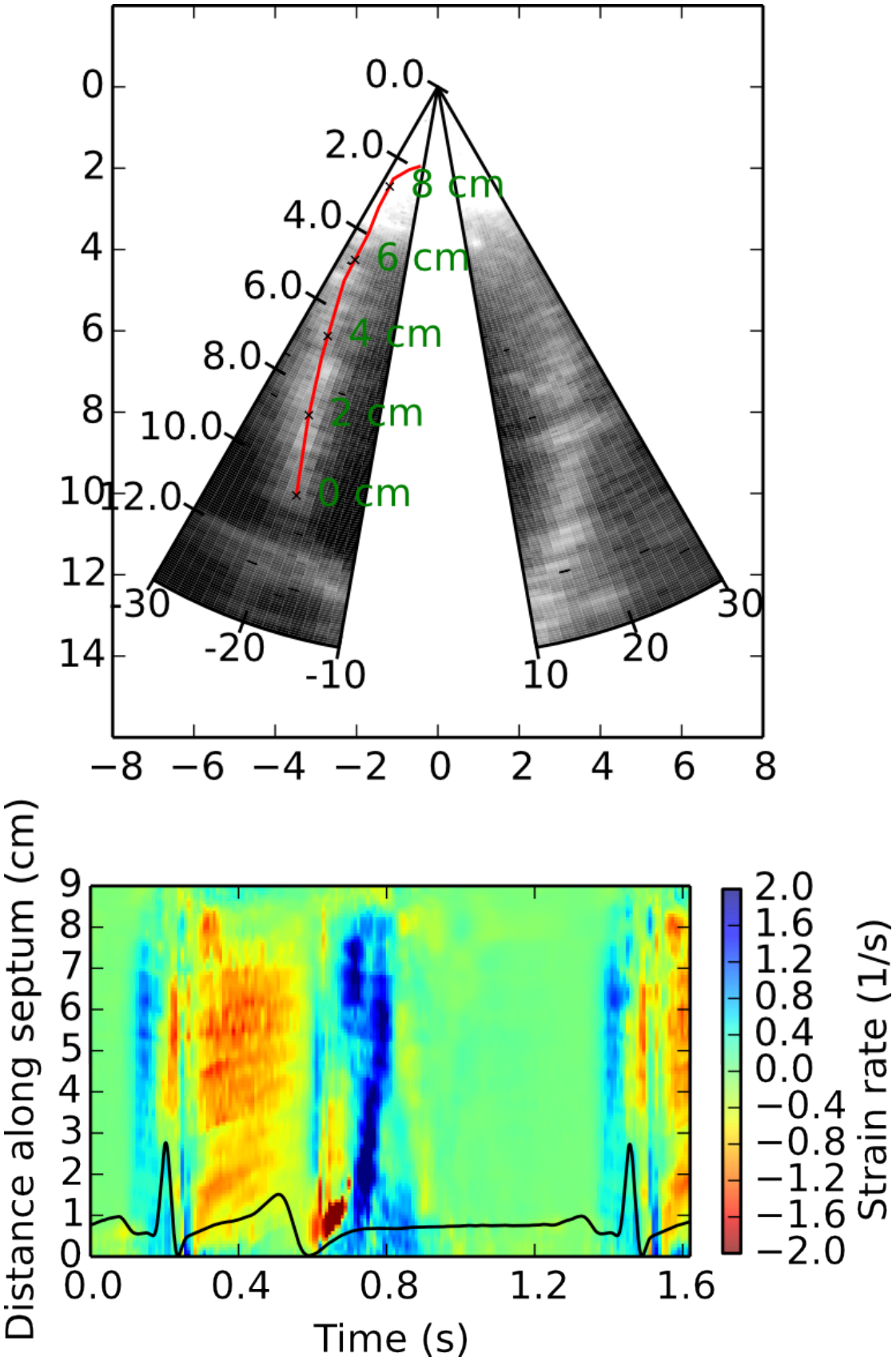

FIGURE 5.2: Upper panel: B-Mode of the septal and lateral walls showing the selected anatomic curve. Lower panel: Curved anatomic M-mode with septal wall strain rates from one cardiac cycle. Contraction during systole and relaxation during diastole are seen as negative and positive strain rates, respectively. The black line in the Anatomic M-mode represents the ECG

zero-cross and provides median value from each segment, while 3D UFR-TDI uses a dichotomous semiquantitative approach.

Further, the number of segments discarded from analysis due to noise was higher than 2D than in 3D. The segments were excluded due to noise and drop-outs. The origin of the noise could be the implanted crystals and catheter which may affect Doppler quality, or heterogeneity of the liver used as standoff. The visualization of strain rate in an anatomic m-mode in the 2D-UFR-TDI analysis allows a more detailed evaluation of data quality. Such visualization allows exclusion of clutter with more confidence. Such evaluation is not possible in the 3D UFR-TDI data in its current state which could explain the difference between 2D and 3D.

The time delays measured are in the same order of magnitude as the delays measured at the cellular level [107], and in recent experimental studies [83, 108, 109]. The time interval measured was similar for the 2D and 3D methods.

The results indicate that onset of negative strain rate corresponds with the onset of mechanical activation from pacing electrodes and that the segment from which the mechanical activation originates can be detected with UFR-TDI. However, the small sample size and study limitations do not allow us to extrapolate results to human studies with any confidence. The main findings seem to support that strain rate imaging by UFR-TDI is able to detect the onset of mechanical activation, but for reliability, further improvement in noise reduction is necessary. The large spread in the activation times in the non-pacing segments, and the sometimes ambiguous interpretation of 3D data indicates that further development of clutter suppression algorithm, improvement of analysis software and further validation studies including simultaneous electrophysiological mapping could provide additional information needed before the method can be tested in a clinical setting. Other groups have recently published studies showing promise in this regard [69, 77, 80, 81, 108], and their findings should be taken into consideration before pursuit and further development of the described method. If such method is further developed, it could prove useful in estimation of dyskinesia and dyssynchrony.

5.3 Clinical feasibility: Evaluation of myocardial function

We investigated strain rate measurements by UFR-TDI with ADS in Paper III *Myocardial Strain Rate by Anatomic Doppler Spectrum: First Clinical Experience Using Retrospective Spectral Tissue Doppler from Ultra-High Frame Rate imaging.* Feasibility for performing tissue Doppler velocity measurements after injection of ultrasound contrast were investigated in Paper IV *Color Tissue Doppler Imaging in Contrast Echocardiography - a Feasibility Study.* The findings are discussed in the following section.

5.3.1 Paper III - Myocardial Strain Rate by Anatomic Doppler Spectrum: First Clinical Experience Using Retrospective Spectral Tissue Doppler from Ultra-High Frame Rate imaging

In this study we demonstrated that strain rate by ADS was able to identify scarred myocardium and differentiate transmural from non-transmural distribution of myocardial scar on a segmental level (Table 4.7). Furthermore, we demonstrated that analysis of strain rate by ADS was feasible in a higher number of segments compared with strain rate by conventional TDI. Tissue velocities measured by ADS indicate good accuracy compared with spectral Doppler velocity measurements by PW TDI with a minor bias.

Spectral Doppler data has several advantages compared to analyzing velocity traces based on autocorrelation estimates. As autocorrelation only gives one velocity trace, signal as well as noise and dropouts are averaged into the trace. As the entire spectrum of velocities rather than a weighted average can be visualized by spectral Doppler, data quality can easily be assessed. Furthermore, such visualization makes it possible to separate reverberation noise from signal from moving tissue (Fig. 5.3). Finally, such spectral presentation of tissue velocity data makes estimation of the velocity gradient, i.e. SR, feasible without influence of noise, as it relies on tracing the spectral envelope which remains visible in the presence of clutter (Figs. 1.9c & 5.4).

We correlated SR with scar tissue distribution determined by LGE-MRI. SR is a parameter of function rather than scar tissue. Dysfunction may be seen in peri-infarct areas, where scar is not detected by LGE-MRI. Therefore LGE-MRI is sub-optimal as reference method in comparison with SR. However, LGE-MRI is the gold-standard for imaging myocardial scar-distribution, and as extent of myocardial scarring correlates

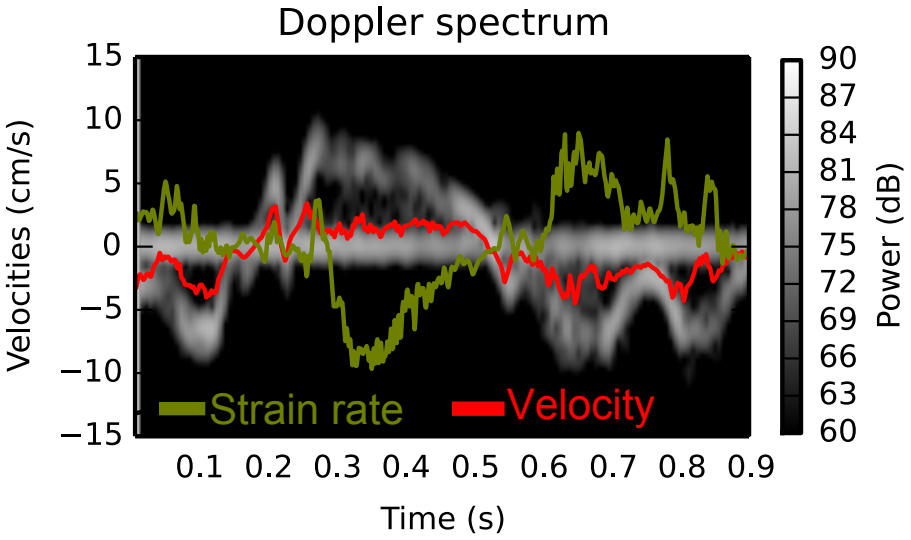

FIGURE 5.3: Doppler spectrum with velocity and strain rate estimations by autocorrelation from the basal septum. The Doppler spectrum was calculated with a window length of 30 ms. The velocity and strain rate measurements were estimated with plain autocorrelation. The velocity curves is biased towards zero due to clutter and the strain rate curve is noisy.

with reduced myocardial function [48], it was chosen as reference method in this study. This may have contributed to the poor correlation between SR and scar at the segmental level. Both ADS methods showed significant correlation with LGE-MRI findings at the global level and between-group differences at the segmental level, however, the scatterplot shows that there is a substantial variation in the measurements, and that some of the large infarcts have high SR (Figure 4.4). This indicates that there are still pitfalls to overcome with SR imaging by TDI, and that SR remains a useful addition in an echocardiographic examination rather than its mainstay.

TDI PSSR has previously showed better correlation with transmurality of myocardial scar ($r=0.63$ $p<0.05$)[51] compared to our findings ($r=0.23$ $p>0.05$). This difference may be a result of the variability of deformation by conventional TDI [47, 110], as well as misalignment of the LGE-MRI segments compared with ultrasound, or poor image quality. Also, Zhang et al. [51] investigated larger infarcts (range of 5-45 % vs

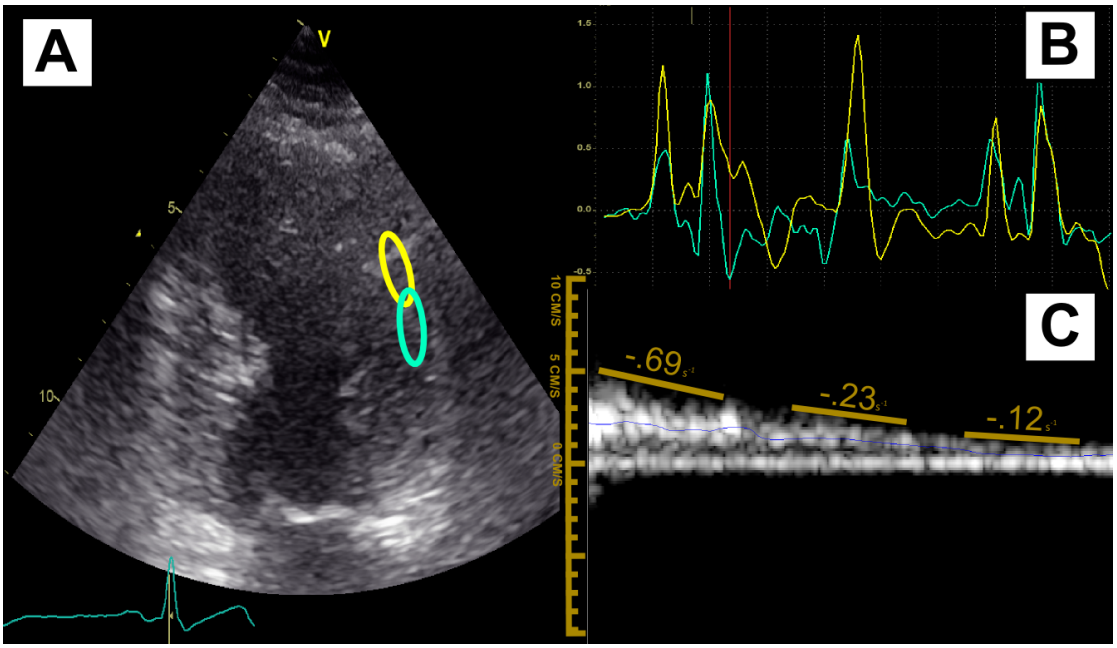

FIGURE 5.4: Strain rate estimated by ADS in patient with MRI confirmed anterior wall infarction. A: Two-chamber b-mode showing the inferior and anterior ventricular wall in a patient with MRI confirmed anterior wall infarction. Region of interests are demarcated with turqoise and yellow. In the apical segmen, one can se reverberation, within the yellow ROI. B: The strain rate curves from TDI data in ROIs from A. The interpretation of such strain rates are ambigious as the curves are heavily influenced by noise. C: ADS from the anterior wall in the same patient, the noise can be visualized as the signals between the sepctral envelope and zero, however, as the spectral envelope can easily be visualized, the velocity gradient can be measured without the influence of the clutter signal. While the value is normal in the basal segment, low strain rates is found in the middle and apical segments, which corresponds to extent of infarct by MRI.

3-21%), and performed image acquisition within 6 days of infarct potentially including stunned myocardium. This differs from our study and may have contributed to the observed difference. Finally, using conventional strain rate imaging, segments with noise is conventionally excluded, thus increasing correlations of the analyzable segment. Thus, differences between studies in correlation coefficients, may reflect differences in exclusion rate.

The results indicate that the semi-quantitative method, ADS SR Visual, correlated better with scar than the quantitative methods, ADS SR Slope (p=ns) and TDI PSSR (p=0.006). This indicates that visual assessment of the Doppler spectrum might be superior to quantitative measurement of SR data. This is in line with previous studies, where semi-quantitative methods has proven superior to quantitative methods [111]. A possible explanation for this could be that the semi-quantitative assessment of the slope

also allows visual assessment of relative change in deformation between the adjacent segments in the same patient (Fig. 3.9). As there is a substantial variation in peak systolic SR by tissue Doppler, even in healthy subjects selected with optimal image quality [54], the quantitative reduction in deformation in ischemic myocardium with preserved contractile function may be hard to measure. A quantitative method does not take into account such between-patient variations, and might therefore not be as suitable for evaluation of regional myocardial function as the semi-quantitative approach.

Mitral annular velocities (peak S') was measured with ADS and PW TDI in the same population. There was a small bias of 0.35 cm/s ($p=0.04$). A possible explanation for this bias may be the length of the time window (i.e. temporal smoothing) used for ADS (100 ms). A longer time window will reduce peak values [112].

The inter- and intra-observer COR and the Mean error of global inter-observer ADS SR Slope measurements is in the same order of magnitude as previous findings [113]. The mean error of segmental ADS SR Slope, and intra-observer global mean ADS SR Slope was however poorer. Comparable values from Thorstensen et al. [113] were based on speckle tracking rather than tissue Doppler, and included healthy subjects, which may explain some of the difference. Our findings are however in the same order of magnitude as described by Ingul et al. [47], a study based on infarct subjects and TDI strain rate data. Some of the variation in our findings may be attributed to the difference in time point chosen as basis for ADS, mid-systole is selected from an anatomic m-mode in a cine consisting of three cardiac cycles. Further the difference in strain length and gain settings may also contribute to some variation in measurements.

This study demonstrates the feasibility of strain rate by retrospective construction of spectral tissue Doppler. This has to our knowledge not been demonstrated earlier. ADS based strain rate correlate better with scar morphology than strain rate measurements from conventional TDI. Analysis of ADS based deformation is also viable in more segments compared with convetional TDI ($p<0.05$). This indicates potential use in patients with poor acoustic windows.

5.3.2 Repeatability of strain rate measurements, conventional vs UFR-TDI

TDI currently used in the clinic has a temporal resolution between 100-150 frames per second (fps) in a full sector view. As UFR-TDI enables acquisition of TDI data at 1200fps, it makes temporal smoothing feasible over far more samples than in conventional TDI. To investigate if this smoothing affects the repeatability of SR measurements, we examined inter-observer repeatability of systolic strain rate measurements in 30 patients with UFR-TDI and conventional TDI [114].

Mean absolute percentage error and Coefficient of repeatability (COR) are reported to evaluate repeatability. The COR is computed in the same units as the assessment tool and sets the boundary of the minimally detectable true change that can be measured [115]. The mean absolute percentage error was similar for both methods in septum (27.6% vs 26.3%), but was lower for UFR-TDI in the lateral wall (19.2% vs 44.9%). The results are found in Table 5.1 and presented as Bland-Altman plots in Figures 5.5 and 5.6

Dalen et al. [54] present similar findings, however the authors use a method that combines speckle tracking and tissue Doppler in a healthy population, where the COR for segmental peak systolic strain rate was found to be $-0.5s^{-1}$, which is similar to our findings in the healthy population where COR for UFR-TDI was $-0.46s^{-1}$. Further, the findings are on the same order of magnitude as Thorstensen et al. [113], where COR for speckle tracking based 2D strain rate is $-0.5s^{-1}$. Finally, similar results was presented by Schmid et al. [116], this study however, looked at the TDI based measurements from both systole and diastole. This indicates non-inferiority of UFR-TDI method in terms of curve-based strain rate measurements. The repeatability was better for UFR-TDI based SR measurements in the lateral wall compared to conventional TDI ($p<.05$) (table 5.1). A possible explanation for this may be that the lateral wall in general has higher velocities and variability, and therefore an increased sampling-rate improves estimation. There was no difference between the septal wall measurements.

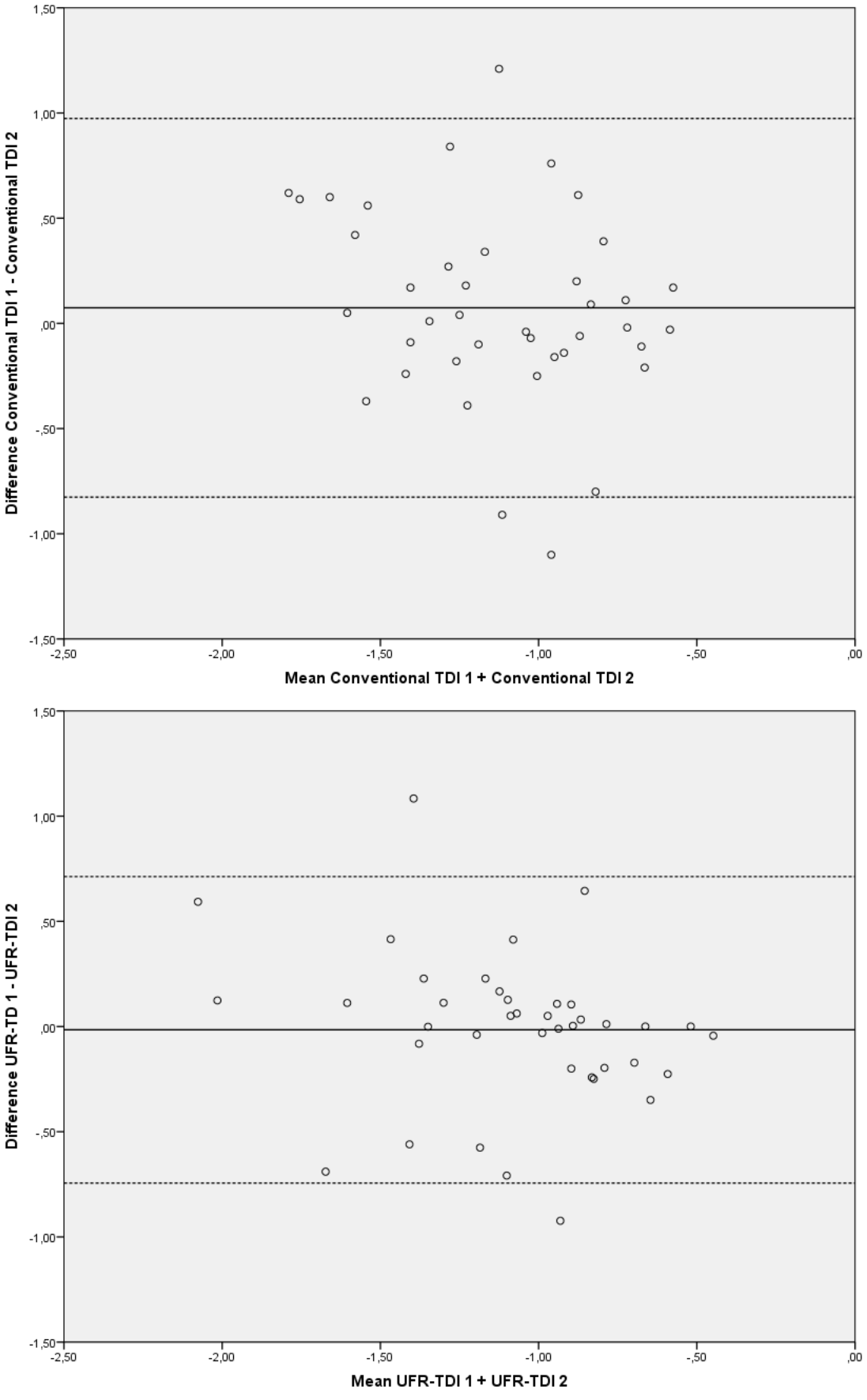

FIGURE 5.5: Bland-Altman plot for Infarcted population illustrating mean difference and limits of agreement (mean ± 1.96 SD) - Left: Conventional TDI 1-2 Right: UFR-TDI 1-2

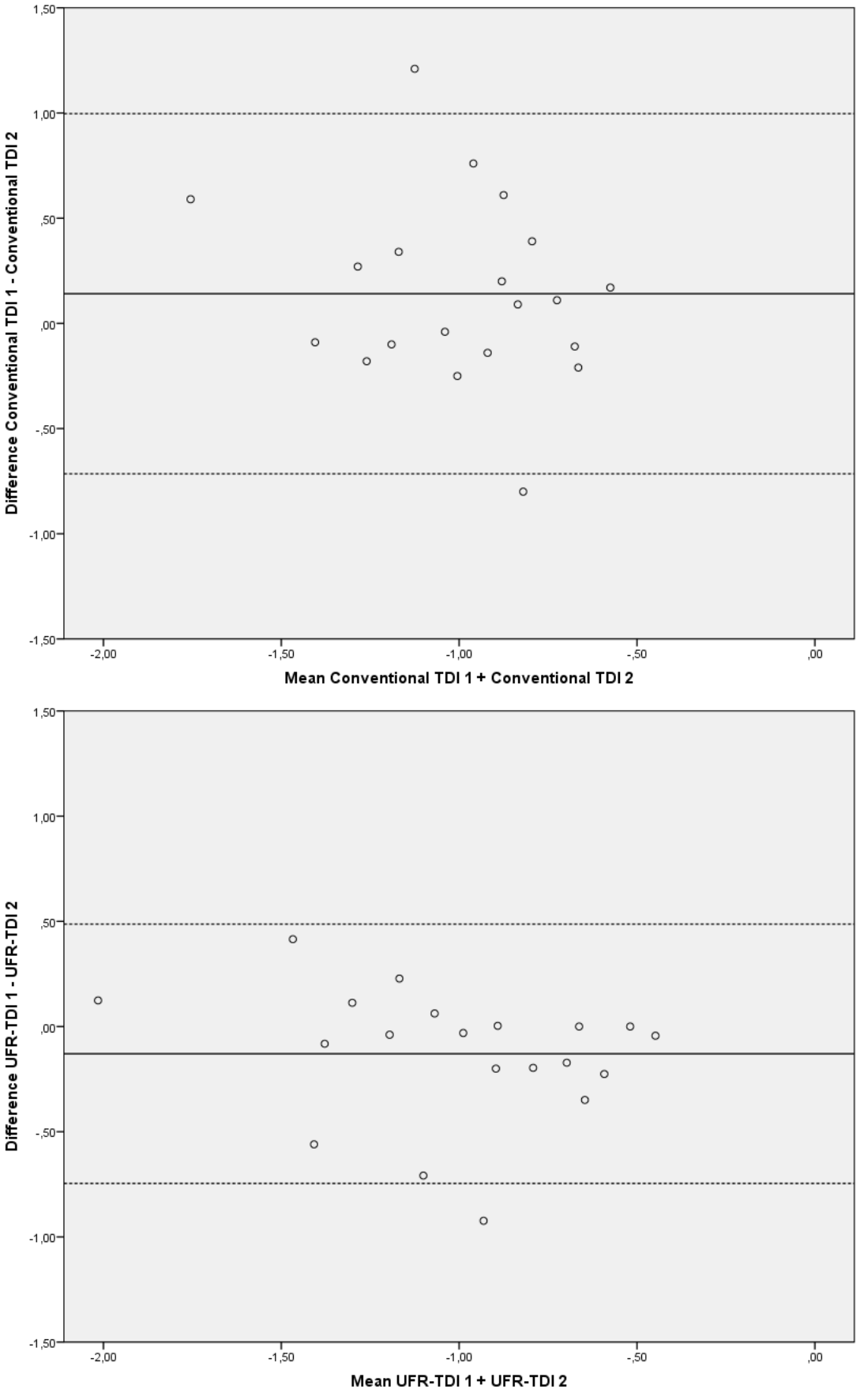

FIGURE 5.6: Bland-Altman plot for lateral wall in Infarcted population illustrating mean difference and limits of agreement (mean ± 1.96 SD) - Left: Conventional TDI Lateral 1-2 Right: UFR-TDI Lateral 1-2

	Healthy subjects (n=10)					
	Conventional TDI			UFR-TDI		
	PSSR s^{-1}	MAPE	COR s^{-1}	PSSR s^{-1}	MAPE	COR s^{-1}
Septum	$-1.19s^{-1}$	23.27 %	$0.79s^{-1}$	$-1.28s^{-1}$	19.66 %	$0.48s^{-1}$
Lateral Wall	$-1.33s^{-1}$	17.04 %	$0.51s^{-1}$	$-1.59s^{-1}$	11.03 %	$0.46s^{-1}$
	Infarcted Patients (n=20)					
	Conventional TDI			UFR-TDI		
Septum	$-1.26s^{-1}$	26.32 %	$0.95s^{-1}$	$-1.15s^{-1}$	27.63 %	$0.78s^{-1}$
Lateral Wall	$-1.00s^{-1}$	44.87 %	$0.86s^{-1}$	$-1.01s^{-1}$	19.21 %	$0.62s^{-1*}$

TABLE 5.1: PSSR: Peak Systolic Strain Rate MAPE: Mean Absolute Percentage Error COR: Coefficient of repeatability * p $\leq$ 0.05 for comparison between methods

5.3.3 Feasibility

The intra- and inter-observer variability of TDI based SR measurements is substantial [53]. The feasibility is in the end determined by the degree of uncertainty deemed acceptable by the observer. This in turn is affected by the observer's experience. The interpretation of strain rate curves requires extensive training and experience to make decisions with confidence. The spectral presentation of the data, as suggested in our article, *Myocardial Strain Rate by Anatomic Doppler Spectrum: First Clinical Experience Using Retrospective Spectral Tissue Doppler from Ultra-High Frame Rate imaging*, could make interpretation of TDI based strain rate data available also for the less experienced user. In our study the feasibility of TDI based SR measurements were 87%, which is in line with previous findings where Ingul et al. [47, 117] present 92% and 86% feasibility, respectively. The ADS demonstrated a significant improvement in this regard, by allowing analysis of 95% of the segments.

5.3.4 Paper IV - Color Tissue Doppler Imaging in Contrast Echocardiography - a Feasibility Study

Ultrasound contrast has the ability to enhance Doppler signals [118] and improvement of Doppler signals are one of the recommended indications for adding UC in clinical echocardiography, in particularly when evaluating valvular heart disease [119, 120], and in vascular ultrasound [121]. Previous experimental and clinical studies have documented that UC biases the autocorrelation phase shift of tissue Doppler velocity measurements causing velocity overestimation [56–58]. Consequently, UC has become a

contraindication to perform TD velocity measurements. Recently, in line with our results, Nagy et al. [122], report that both TD and speckle tracking based myocardial deformation imaging is feasible during contrast echocardiography . This is in line with our findings. Our study adds to this by directly demonstrating a good reproducibility of TD velocity measurement comparing tissue velocities before UC injection and 10 minutes after UC injection followed by continuous ultrasound scanning to potentiate UC destruction. According to previous studies, reproducibility of TD velocity measurements is good [113, 123], and the intra- and inter-observer reproducibility of this study were in line with these finding both prior to and 10 minutes after UC injection. Whether TD velocity can contribute to improve diagnosis in ischemic heart disease, is partly limited by image quality. Poor image quality and noise, in particularly in the apical and inferior wall of LV, may cause misinterpretation. When comparing reproducibility of TD velocity measurements after UC, we therefore excluded LV regions known to be most prone to noise, and assessed velocities only in the mid- and basal 4 LV segments in the 4-chamber view (inferoseptal and anterolateral wall).

Chapter 6

Limitations

6.1 Paper I - Ultra-high Frame Rate Tissue Doppler Imaging

Larger sample sizes are needed to draw any firm conclusions about feasibility and diagnostic accuracy. The general limitations of tissue Doppler also apply to UFR-TDI. This includes angle dependency [53, 124], which is a known issue and may be problematic, especially when interpreting data in the apical, as well as inferolateral regions. As UFR-TDI utilizes MLA-technique to minimize the number of transmit events needed to cover the sector, broad transmit beams are used. The broad transmit beams renders the signals more vulnerable to stationary reverberations than a set-up with narrower transmit beams. Further, the broad transmit beams causes side-lobes on the 16 MLA recieve (Figure 6.1), which may distort velocity measurements in neighboring receive lines. Accordingly the high temporal resolution comes at the cost of lower spatial resolution. The acquisition set-up is designed for apical recordings, and not parasternal. This means that data is captured from two 20 degree fields corresponding to the ventricular walls. Parasternal recordings will be difficult due to the fact that the entire sector is not covered, and the method does not allow estimation of vectors perpendicular to the insonation beam.

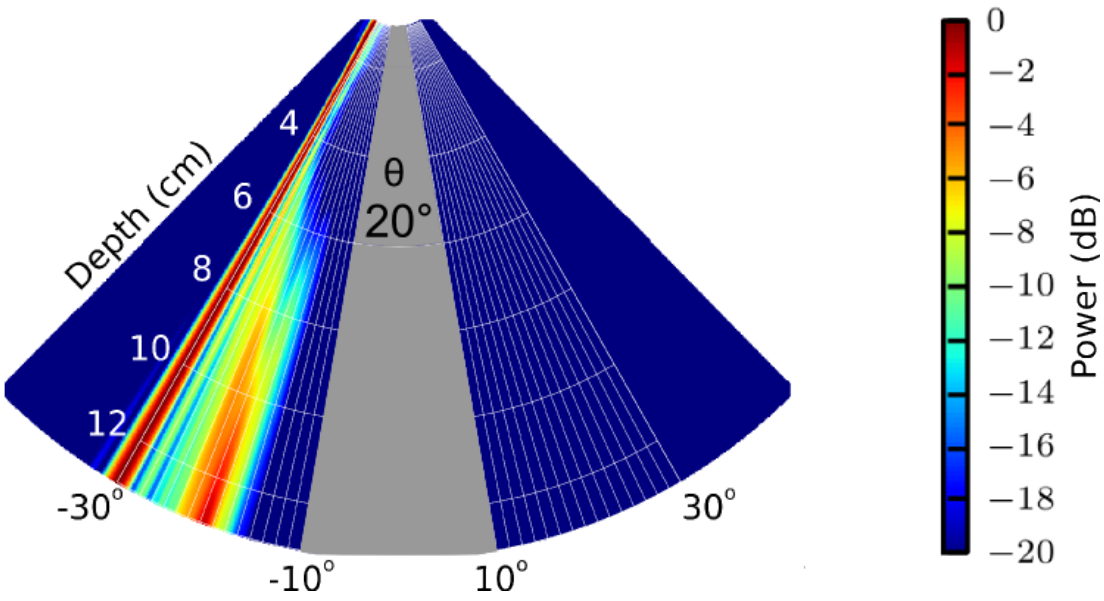

FIGURE 6.1: Transmit-receive beam profile for the utmost receive line in a scan setup with θ 20 degrees.

6.2 Paper II - Detection of mechanical activation in an open chest porcine model by three-dimensional UFR-TDI, a feasibility study

The sample size is too small to perform any relevant significance testing which can be extrapolated to human studies. The results can only give us an indication, and does not allow us to draw any firm conclusions.

The porcine heart proved vulnerable to instrumentation, including a high susceptibility to arrhythmias in an open chest model. In retrospect, an ovine or canine model might have been better suitable for such study due to the presence of collateral arterial supply [125].

The ECG was not aligned with the electrical vector, this leaves a possible "blackout" of 40 ms initially (duration of a q-wave). The reason for this is as the pacing site changes, the vector also changes, and realigning the electrodes for each pacing site was not feasible in the protocol.

The 3D method acquires data over two cardiac cycles, first one b-mode for navigational purposes for regions of data extraction, then 3D UFR-TDI data is acquired. The trigger for recording is peak of the R-wave. As the event we are trying to capture, mechanical

activation, has onset before and ends after the peak of the R-wave, it would be beneficial to introduce a different triggerpoint, in example end systole, for analysis of the mechanical activation. Further, the 3D model does not offer visualization of the left ventricular outflow tract, this could introduce bias, as velocities from the corresponding segment could disturb velocities in adjacent segments.

The UFR-TDI method only allows for acquisition from the apical view, furthermore only of one ventricle simultaneously. This limits the methods potential use for mapping of activation sequences beyond the ventricles in its current state.

6.3 Paper III - Myocardial Strain Rate by Anatomic Doppler Spectrum: First Clinical Experience Using Retrospective Spectral Tissue Doppler from Ultra-High Frame Rate imaging

ADS represents velocities from a limited time window, events preceding or following the time of interest cannot be detected. Mid-systole has, however, previously proven suitable for evaluation of infarct size [42]. The angle dependence of TDI also applies to ADS. The study has a small sample size and the control group was not matched on age. The variation in time delay from infarction to image acquisition, and from LGE MRI to ultrasound acquisition is large, which may introduce some bias, however, since image acquisitions was performed after the acute phase the bias should be minimal. As the technology develops, speckle tracking emerges as the most used method for deformation imaging, albeit, strain imaging and not strain rate. The frame rate is so far not considered sufficient for strain rate, although speckle tracking based strain rate was implemented in the earlier versions, this has now been disallowed in the present versions of the software.

6.4 Paper IV - Color Tissue Doppler Imaging in Contrast Echocardiography - a Feasibility Study

The sample size is small and larger studies should be performed to substantiate findings. Our findings indicate that color Doppler systolic velocities can be used with non-inferior intra- and inter-observer repeatability compared to measurements without contrast.

Chapter 7

Conclusion

In this thesis we demonstrated the feasibility of UFR-TDI in both 2D and 3D.

We found that mechanical activation could be detected with UFR-TDI in an open chest pig-model in both 2D and 3D. The time intervals measured were in the same order of magnitude as the electromechanical delay measured on the cellular level.
Further our findings suggest that the repeatability of deformation measurements by UFR-TDI was better compared with conventional TDI, however, the repeatability of UFR-TDI was on par with repeatability by combined methods reported in other studies. Repeatability, however, depends on many factors, among others the spatial resolution. Limiting deformation analysis to a mean of a whole segment as was done in some of the previous methods, will improve repeatability at the expense of spatial resolution.

We demonstrated the feasibility of retrospective spectral tissue Doppler based deformation. This has to our knowledge not previously been described. We evaluated regional myocardial function with ADS and global function as a composite of the segmental parameters. Visualization of the spatial distribution of the velocity gradient enabled quantitative and semi-quantitative estimation of strain rate without the influence of clutter; further it allowed detection of myocardial scar with better correlation compared to conventional TDI. However the investigative software is still experimental and should be revised before a possible introduction to the clinical setting. Finally, we found that tissue Doppler measurements could be performed without bias after introduction of ultrasound contrast. This is also in agreement with previous findings.

However, all studies in this thesis are feasibility studies with relatively small sample size, and larger studies are required to substantiate our findings. Directions for future studies along with suggestions for improvement of currently investigated methods are provided in Chapter 8. The potential of ultrafast cardiac imaging is still not exhausted, and the technology has unrealized potential which warrants further research.

Tissue Doppler based deformation imaging remains an important addition to established methods, however, it remains an additional diagnostic tool rather than mainstay of routine echo protocol.

Chapter 8

Implications for future work - UFR-TDI - where to go from here?

In this chapter I will provide some experiences and recommendation for future development of the described methods, and discuss some areas which should be of emphasis in future studies.

8.1 UFR-TDI

A tracking algorithm which enables measurement of deformation from the same ROI throughout the cardiac cycle would be useful, and possibly contribute to improved segmental measurements. However, the spatial resolution when using 16 MLA is limited, and the effect might also be limited. This is substantiated by Dalen et al. [54] which compared TDI with fixed ROI and tracked ROI, finding no significant differences between the two methods. The method should be developed further, to include full sector 2D acquisition. This would expand the use of the method further. It would also enable analysis of radial events, i.e. shear waves along the myocardial septum, from the parasternal view, in addition, it will improve the user-friendliness for the clinician.

8.2 Mechanical Activation

The relation between ischemia and alternation in myocardial contraction has been known for several decades [126]. Several methods for quantifying such abnormal contraction pattern has been introduced [127–134], and some of the more recent developments include mechanical dispersion, using strain [135] and strain rate [136, 137], with prediction of ventricular arrhythmia and adverse cardiac events following cardiac resynchronization therapy (CRT), respectively. Most of these methods, with a few exceptions, use timing of peaks to quantify this abnormal contraction pattern. Peak values represent peak contraction, and should therefore be more suitable for estimation of variation in peak contraction, rather than onset of contraction. When evaluating the electromechanical activation, the onset of contraction rather than peak values should be investigated and time to onset of shortening should be used. It has been shown that electrical activation in infarcted myocardium is significantly delayed [138], and that time to peak myocardial velocities is increased [139, 140]. As the Purkinje system is located sub-endocardially, it could indicate that patients with sub-endocardial ischemia would demonstrate delayed onset of contraction, as described in Ashikaga et al. [138]. The frame rates made available by UFR-TDI enabled resolution of the pre-ejection period in great detail, visualizing two velocity spikes in the ventricular septum corresponding to the area of earliest mechanical activation in the healthy left ventricle. The findings indicate that the primary spike represents mechanical activation as the delay we measure corresponds to the electromechanical delay measured on the cellular level [60]. In Paper II [2] we propose a method for estimating the electromechanical activation based on these findings.

Dyssynchrony can be an effect of a failing heart or a consequence of an underlying alteration of the electromechanical activation pattern. It means that the heart does not contract synchronously, which may cause inefficient pumping of blood to the body. It often requires CRT, which involves implantation of a pacemaker with leads that are attached to the myocardium. There are two areas of potential use in this context; Firstly, the decision regarding whether to implant a CRT Device is complicated, and additional parameters of function which aid in this decission-making is needed. Several of the methods currently available are indirect measurements of dyssynchrony, e.g. by measuring time to peak values [127–133]. The results reported by Chung et al. [127] in a multi-center study evaluating several echocardiographic parameters efficacy in prediction

of CRT-response (PROSPECT study) demonstrated the need for novel methods, as the study showed relatively poor performance for all parameters. The parameters that had a modest performance included PW Doppler based pre-ejection period duration, and TDI measurement of time to onset of systolic velocity. This indicates that measuring time of onset rather than peak values could be beneficial. Since such time intervals have duration in tens of milliseconds, adequate temporal resolution is essential. This is an area in which further studies should be performed, and some already show promise in this regard [108]. Secondly, the placement of pacing leads in healthy, and not scarred myocardium is crucial for the efficacy of CRT. The efficacy of the treatment is evaluated with ultrasound. If electromechanical mapping proves feasible, the spread of mechanical activation from pacemaker lead could be identified, and as such, aid in evaluation of efficacy of treatment.

The results are promising in regards of detection of mechanical activation. The findings indicate that the method was able to detect mechanical activation in both 2D and 3D. However, the method did not allow mapping an electromechanical wave due to the lack of validation, and limitations in UFR-TDI method, i.e. angle-dependency and limited sector acquisition. Suggested alterations to study design is mentioned in Section 5.2. Also, improvement in clutter-suppression could aid analysis.

Suggested improvements to current software:

- LVOT in 3D model - A possibility for visualization of the left ventricular outflow-tract on the model itself. It would improve usability of 3D analysis tool.
- Integrate b-mode images - An integration or simultaneous visualization of the 3D b-mode images in the model would also improve usability and aid navigation.
- Isochronous map - An isochronous visualization of activation sequence based on time to threshold in each segment would improve the model and facilitate analysis.

8.3 Anatomic Doppler Spectrum

ADS shows promise in semi-quantitative and quantitative estimation of deformation by retrospective spectral UFR-TDI. However the investigative software is still experimental and should be revised before possible introduction to clinic. The emphasis of future work

could be on evaluating the method in a more selected patient group segregated by quality of acquisition and acoustic window to further substantiate the usefulness of the method.

8.4 Tissue Doppler velocity estimates after injection of ultrasound contrast

The study performed in this thesis only demonstrates non-inferiority of intra- and inter-observer repeatability of tissue Doppler velocity estimates prior to and after 10 minutes of continious ultrasound scanning with a mechanical index of 0.8. These findings are not directly transferable to DSE protocols which could be an area of use. Further studies should be performed during DSE protocols to further evaluate the findings. Finally, strain and strain rate measurements should be included in further studies, as they are tools frequently used during DSE protocols. In addition, the acquisition of UFR-TDI data (high FR IQ data), allows retrospective spectral Doppler instead of only autocorrelation traces. This mode is far less sensitive to the distortion induced by ultrasound contrast, and may present an additional method for simultaneous contrast and deformation imaging. However, the much higher velocities of blood, combined with the low lateral resolution of the present set up, may present a challenge.

Appendix A

Paper I - Ultra-high Frame Rate Tissue Doppler Imaging

Ultrasound in Med. & Biol., Vol. 40, No. 1, pp. 222–231, 2014

0301-5629/$ - see front matter

http://dx.doi.org/10.1016/j.ultrasmedbio.2013.09.012

● *Original Contribution*

ULTRA-HIGH FRAME RATE TISSUE DOPPLER IMAGING

Birger Brekke,* Lars C. L. Nilsen,* Joakim Lund,* Hans Torp,* Tore Bjastad,†
Brage H. Amundsen,*‡ Asbjorn Stoylen,*‡ and Svein A. Aase†

*MI Lab and Department of Circulation and Medical Imaging, Norwegian University of Science and Technology, Trondheim, Norway; †GE Vingmed Ultrasound, Horten, Norway; and ‡Department of Cardiology, St. Olav Hospital, Trondheim, Norway

(*Received* 8 *October* 2012; *revised* 17 *July* 2013; *in final form* 11 *September* 2013)

Abstract—We describe a new tissue Doppler imaging (TDI) method, ultra-high frame rate tissue Doppler imaging (UFR-TDI). With two broad transmit beams covering only the ventricular walls, we achieve 1200 frames/s in a four-chamber apical view. We examined 10 healthy volunteers to study the feasibility of this method. Ultra-high-frame-rate TDI provided peak annular velocities and time to peak S' intervals in good agreement with those measured with conventional TDI. Moreover, UFR-TDI provided additional information in early and late systole: In all subjects, the method was able to separate the timing of electrical activation, start of mechanical contraction, mitral valve closure and start of ejection. The earliest mechanical activation was seen before mitral valve closure. The method was also able to measure the propagation speed of the mechanical wave created by aortic valve closure. (E-mail: birger.brekke@ntnu.no) © **2014 World Federation for Ultrasound in Medicine & Biology.**

Key Words: **Echocardiography, Myocardium function, Continuous acquisition, Plane wave imaging, Multi-line acquisition, Mechanical wave propagation, Pre-ejection period, Aortic valve closure.**

INTRODUCTION

Echocardiography has become an important tool in the diagnosis of heart disease. It is non-invasive and tolerable and can be used to assess both cardiac structure and cardiac function. In the late 1980s, tissue Doppler imaging (TDI) was added to the tools of echocardiography (Isaaz et al. 1989). TDI made it possible to measure myocardial motion quantitatively. This has proven useful, especially in the assessment of left ventricular function.

The frame rate is of great interest when measuring myocardial motion with TDI. Conventional TDI can typically sample 150 images of the left ventricle per second. The frame rate may be increased to 250 images per second when focusing on a single ventricular wall. This may, however, not be sufficient to resolve all of the mechanical events in a cardiac cycle. Examples of such events are the spread of electromechanical activation throughout the ventricle (Katz 2010), and mechanical waves caused by aortic valve closure (Kanai 2005), which propagate in the heart with velocities of 0.3–1.0 and 1–7 m/s, respectively. Higher frame rates may be beneficial for characterization of such events.

Several methods have been developed to increase the frame rate in echocardiography. In the 1980s, Shattuck et al. (1984) introduced multi-line acquisition, in which multiple receive lines are acquired for each wide transmit beam. Lateral resolution and field of view can thereby be maintained at higher frame rates. Electrocardiogram (ECG)-gated stitching over multiple cardiac cycles is another method used to improve temporal and spatial resolution. These techniques are currently used in daily practice.

Many other methods have been developed and implemented on research scanners during the last 20 y. Most of these methods involve reducing the number of transmit events. D'hooge et al. (2002) reduced the number of transmit beams by imaging a narrow sector, whereas Kanai et al. (1993) used a sparse sector scan. Methods further developing the concept of multi-line acquisition have been extensively studied (Cheng and Lu 2006; Hasegawa and Kanai 2011; Honjo et al. 2008, 2010; Lu et al. 2006; Provost et al. 2011, 2012; Tanter et al. 2002). Other strategies for increasing the frame rate include modulated excitation and synthetic aperture (Misaridis and Jensen 2005).

Address correspondence to: Birger Brekke, Norwegian University of Science and Technology 7491, Trondheim, Norway. E-mail: birger.brekke@ntnu.no

Conflicts of Interest: Svein Arne Aase and Tore Bjastad were previously employed by MI Lab, but are now employed by GE Vingmed AS. Hans Torp is partly employed by GE Vingmed AS. Brage H. Amundsen is employed by MI Lab. GE Vingmed is a partner in MI Lab.

These recent advances in increasing frame rate have added new possibilities to cardiac ultrasound, such as the visualization of electromechanical activation (Provost et al. 2011) and the propagation of mechanical waves in the myocardium (Kanai 2005). However, the full clinical potential of high frame rate has probably not been determined yet. Clinical studies are few in number, and the availability of high frame rate is limited. To explore the clinical potential of high frame rate further, new methods should be developed and the availability must improve. New ultra-high frame rate methods that are easily implemented on commercial scanners may thus be valuable additions to high frame rate cardiac ultrasound.

In this article, we propose a new ultra-high frame rate TDI method. The new concept behind this method is imaging of only the ventricular walls. By excluding the ventricular cavity, an image of the left ventricle can be acquired with only two wide transmit beams. For each wide transmit beam, 16 receive lines are acquired. Our method, ultra-high frame rate tissue Doppler imaging (UFR-TDI), can image two walls of the left ventricle simultaneously with 16 receive lines on each wall at ~1200 frames/s (fps) from the apical view. To our knowledge, such performance has not previously been described for human tissue Doppler imaging. Moreover, the method can be implemented on a commercial ultrasound scanner, which is a major advantage.

This study had two main objectives. The first was to test UFR-TDI with beam-profile simulations. The second objective was to implement UFR-TDI on a commercial ultrasound scanner and study the feasibility of using this method on healthy human subjects. To study the feasibility of UFR-TDI, we examined how well it agreed with conventional TDI on tissue velocity measurements. Moreover, we examined whether UFR-TDI could provide additional information about the mechanical events in the pre-ejection period and measure the propagation speed of the mechanical wave created by aortic valve closure. Under Methods, we describe the UFR-TDI technology, the *in vivo* acquisition and the data analysis. Results from beam-profile simulations and data analysis of *in vivo* acquisitions are described under Results. Feasibility, potential applications and limitations are considered in the Discussion.

METHODS

Ultra-high frame rate acquisition

In our UFR-TDI acquisition setup, we transmit in only two directions. In the case of the left ventricle, this would be the lateral and septal walls in a four-chamber view. Plane waves are used for transmit. From each transmit, 16 receive lines are acquired. Figure 1 illustrates the transmit and receive directions for a scan of the left ventricle from an apical view. The spacing angle between the two transmit directions, θ, is adjustable. The receive lines for each transmit are equally distributed over a sector centered in the transmit direction.

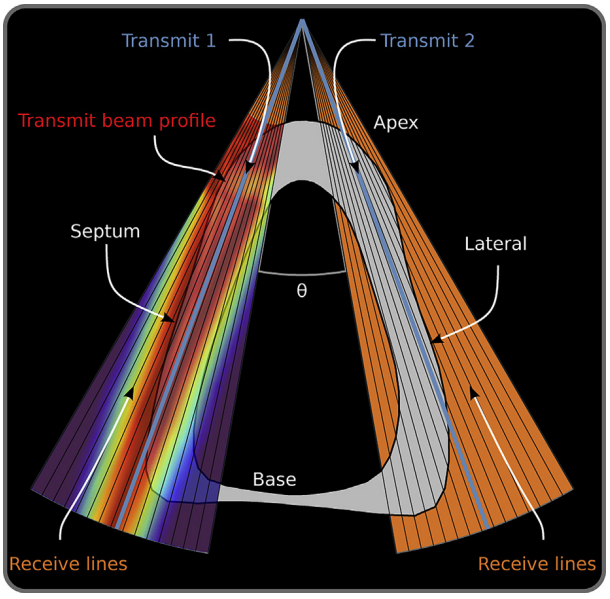

Fig. 1. Transmit and receive directions for a scan setup of the left ventricle from an apical four-chamber view.

Furthermore, only one transmit is sent in each direction per frame. Both tissue Doppler and B-mode images are acquired. Whereas the TDI transmits cover only the ventricular walls, the B-mode transmits are equally distributed over the entire sector. The transmit sequence is illustrated in Figure 2 and given by $T_1 - - T_2 - - B_1 - T_1 - - T_2 - B_2 - \ldots - T_1 - - T_2 - B_N -$, where T_i is TDI transmit direction i, B_k is B-mode transmit direction k, N is the number of transmits for a B-mode frame, and "—" is a pause of ~0.2 ms. The pause is equal to $2d/c$, where d is the scanning depth, and c is the speed of sound in soft tissue. There are four pauses between TDI transmits for a given angle. Hence, the TDI frame rate is equal to c/(8d). To reduce B-mode influence on frame-to-frame TDI estimates, we have limited the B-mode transmit aperture to 0.9 mm. TDI transmits were focused at 30 cm, resembling plane waves. Additional scan parameters are listed in Table 1. The acquisition method was implemented on a Vivid E9 scanner with an M5S-D probe (GE Vingmed Ultrasound AS, Horten, Norway).

Simulations

Transmit-receive beam profiles were simulated in a scan setup with $\theta = 20°$. The simulations were performed with the ultrasound simulation software Field II (Jensen 1996). Scan parameters are listed in Table 1.

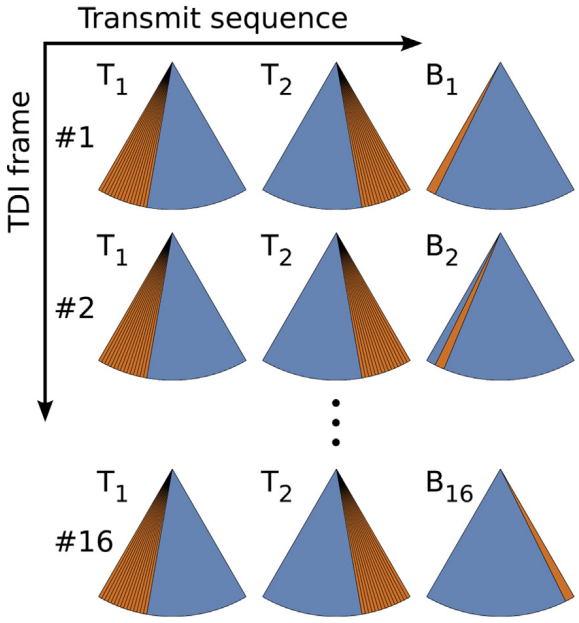

Fig. 2. Transmit sequence for ultra-high frame rate tissue Doppler imaging (UFR-TDI). Sixteen TDI frames are acquired for each B-mode frame.

Post-processing

Post-processing was performed in MATLAB (The MathWorks, Natick, MA, USA). Beamformed IQ-demodulated data (IQ) were extracted from the ultrasound recordings with in-house developed software. Tissue Doppler velocity, v, was estimated using frame-to-frame autocorrelation (Bjaerum et al. 2001) and included the following steps:

1. Clutter filtering of IQ
2. $R1(i) = IQ^*(i) \bullet IQ(i+1)$, where i is the frame index; that is, R1 is the autocorrelation of IQ with temporal lag one
3. Spatial and temporal averaging on R_1 by moving average
4. $v(i) = \angle R1(i)/\pi \cdot v_{nyquist}$, where $v_{nyquist} = c/(4f_c) \bullet$ fps is the Nyquist velocity, f_c is the center frequency and c is the speed of sound in soft tissue.

Table 1. Scan setup for ultra-high frame rate tissue Doppler imaging

Parameter	Value
Center frequency	2.44 MHz
Number of transmit beams	2
Number of receive lines	32
Number of receive lines per transmit beam	16
Receive beam spacing	1.33°
Transmit aperture size azimuth	22 mm
Transmit aperture size elevation	13 mm
Number of elements	192
Receive aperture	Expanding
Transmit apodization	Rectangular
Receive apodization	Rectangular
Transmit focus	30 cm
Receive focus	Dynamic
Pulse length	1.2 μs
Probe	M5S-D

In echocardiography, clutter is unwanted echo signals such as stationary reverberations and echoes from surrounding tissue. In tissue Doppler imaging, clutter will bias the velocity estimates toward zero. A clutter filter can reduce this effect (Heimdal et al. 1998). The UFR-TDI method is vulnerable to clutter because the wide transmit beams cover more surrounding tissue. Clutter filtering is therefore important for accurate velocity estimation in this method. Clutter filtering was employed when generating velocity curves for peak velocity measurements. It was not used in measurements of time to peak S', pre-ejection period and mechanical wave measurements. The clutter filter was a second-order high-pass Butterworth filter with a cutoff frequency corresponding to $0.08 \times v_{nyquist}$, which is 1.5 cm/s for a 1200 fps acquisition. Figure 3 provides an example illustrating the effect of our clutter filter.

ECG latency test

When recording both ECG and Doppler data with an ultrasound scanner, a time delay between the two modalities may occur. To be able to adjust for this discrepancy, we measured the delay between ECG and ultrasound data acquisition. The test was performed as follows: Two ECG electrodes were connected to the probe, while the third electrode remained lowered in a water basin. A thin copper wire passing over the probe footprint connected the two ECG electrodes attached to the probe. The probe was then immersed in the basin. The time delay between the first ECG deflection, and the first sign of water contact in the UFR-TDI recordings was

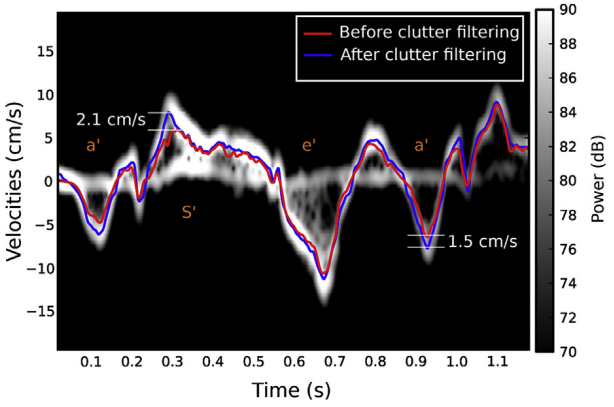

Fig. 3. Velocity curves before and after clutter filtering, in a Doppler spectrum from the basal septum. The spectrum shows clutter noise around the baseline. In this example, the effect of the clutter filter is most evident in the S' and a' waves.

measured in 13 immersions. A similar test has been described by Sutherland et al. (2006).

In vivo acquisition

Ten healthy male volunteers (25–43 y) and one patient with atrial fibrillation were examined using a Vivid E9 ultrasound scanner with an M5S-D probe. The study was approved by the regional ethics committee, and all subjects gave informed consent. The study was performed at NTNU, Trondheim, Norway.

A 12-lead ECG was obtained from all subjects. Care was taken to identify the lead showing the earliest deflection in QRS, as the difference between the leads may be as great as 40 ms (the duration of a normal Q wave). The electrodes on the scanner were then aligned with the vector of this lead.

Four cine loops were recorded with the Vivid E9 scanner in the following sequence:

1. TDI-1: An apical four-chamber view with conventional TDI (150 fps)
2. UFR-TDI-1: An apical four-chamber view with UFR-TDI (1000–1200 fps)
3. TDI-2: An (second) apical four-chamber view with conventional TDI (150 fps)
4. UFR-TDI-2: A narrow sector septum and mitral valve view with UFR-TDI (1200 fps)

Data analysis

All UFR-TDI data were analyzed with post-processing software developed in MATLAB, whereas conventional TDI data were analyzed with EchoPAC (GE Vingmed AS, Horten, Norway).

Agreement with conventional TDI. Peak annular velocities S', e' and a' (where S' = peak systolic myocardial velocity, e' = peak early diastolic myocardial velocity and a' = peak late diastolic myocardial velocity) were acquired from the basal part of the septal and lateral walls of the left ventricle, with UFR-TDI-1 and conventional TDI (TDI-1 and TDI-2). Spatial averaging was performed over a 6 × 6-mm (lateral × longitudinal) region of interest for both UFR-TDI and conventional TDI. Temporal averaging of 5 ms was used for UFR-TDI, and 30 ms for conventional TDI. Agreement between UFR-TDI and conventional TDI was assessed and compared with intra-method variability for conventional TDI (TDI-1 and TDI-2). According to the Bonferroni correction, a p-value $<0.05/6$ (0.008) was considered to indicate significance (6 = number of comparisons).

The time of peak systolic velocity in the septal annulus (S') was detected in the velocity curves in TDI-1, TDI-2 and UFR-TDI-1. The earliest deflection in the QRS complex was detected in the ECG. The time interval between the two events was measured. Inter-method (UFR-TDI and TDI-1) and intra-method (TDI-1 and TDI-2) agreement was assessed. A mean difference with a p-value <0.05 was considered significant.

Pre-ejection period. The pre-ejection period is defined as the period from the first deflection in the QRS complex to the start of ejection (Weissler et al. 1968). In our study, the first deflection in QRS was assessed from the aligned lead in the ECG recording. The start of ejection was defined as the onset of the S' wave in the velocity curves, extracted from the basal part of the septum in UFR-TDI-2. The onset of the S' wave has previously been shown to correlate well with aortic valve opening (Pai and Gill 1998). We measured the time intervals between the events observed in the pre-ejection period (see Fig. 4).

Mitral valve closure was manually determined in a reconstructed M-mode, created from the UFR-TDI-2 data of a selected receive line crossing the mitral valve. Determination of which of the 32 receive lines crosses the mitral valve was also performed manually. Figure 5 illustrates an M-mode crossing the mitral valve.

Mechanical wave created by aortic valve closure. A mechanical wave created by aortic valve closure has previously been described by Kanai (2005) and Pernot et al. (2007). To measure the propagation speed of this wave with UFR-TDI, a curved anatomic M-mode was extracted from the septal wall in the UFR-TDI-1 recording. The velocities were transformed into acceleration values, using first-order forward difference (Fig. 6). The point of peak acceleration after ejection before the e' wave was manually detected. This point has been found

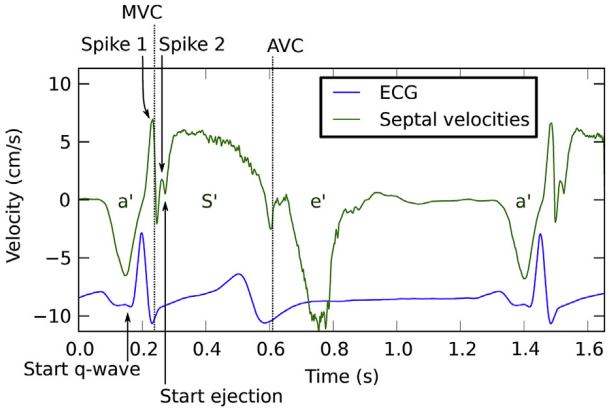

Fig. 4. Velocity curve from the basal septum in a normal subject. In the pre-ejection period, two positive velocity spikes, spike 1 and spike 2, can be seen. S' = peak systolic myocardial velocity, e' = peak early diastolic myocardial velocity, a' = peak late diastolic myocardial velocity. AVC = aortic valve closure; ECG = electrocardiogram; MVC = mitral valve closure.

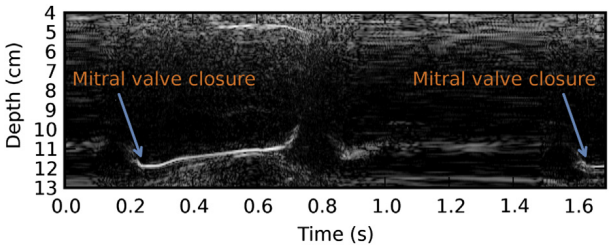

Fig. 5. Reconstructed M-mode from a receive line crossing the mitral valve.

to coincide with aortic valve closure (Aase et al. 2008). A straight line was aligned with the peak acceleration signal in the anatomic M-mode (Fig. 6d), and the slope of this line was interpreted as the propagation velocity of the mechanical wave created by aortic valve closure.

Statistics

Time intervals and velocities are expressed as means ± standard deviations (SD). Bland-Altman analysis and paired t-tests with Bonferroni correction were used to compare measurements of peak annular velocities. Paired *t*-tests were used to compare measurements of time from electrical activation to peak systolic velocity. The level of significance was set at 0.05.

RESULTS

Simulations

Simulated transmit-receive beam profiles of eight receive lines are illustrated in Figure 7a. The angle of maximum power for each of the receive lines was shifted slightly toward the transmit direction at –20°. The half-power beam widths at 10-cm depth were between 2.03° and 2.62°, with a mean value of 2.34° (SD = 0.14°). This gives an average lateral resolution of 4.1 mm at 10-cm depth. The axial resolution, Δz, is given by $\Delta z = c_0 T/2$, where c_0 = 1540 m/s is the speed of sound in soft tissue, and T is the pulse length. Our transmit pulse has a pulse length of 1.2 μs, which gives an axial resolution of 0.92 mm. Figure 7b is a simulated transmit-receive beam profile for one of the receive lines. The side lobes were mainly unilateral and oriented toward the transmit direction. The side lobe level, which is the ratio between the peak side lobe and the main lobe, increased with increasing depth and increasing angle from the transmit direction.

Strain rate example

As seen in Figure 8, strain rate can be derived from UFR-TDI data. In this example, strain rate was estimated with linear regression and a strain length of 16 mm.

ECG latency test

The ECG test revealed an average delay of 5.5 ms (n = 13, SD = 1.3 ms) from the start of the ECG signal to the start of tissue Doppler data acquisition on the Vivid E9 scanner. The time discrepancy between ECG data and tissue Doppler data was corrected for.

Agreement with conventional TDI

In assessment of peak annular velocities, paired *t*-tests with Bonferroni correction indicated no significant

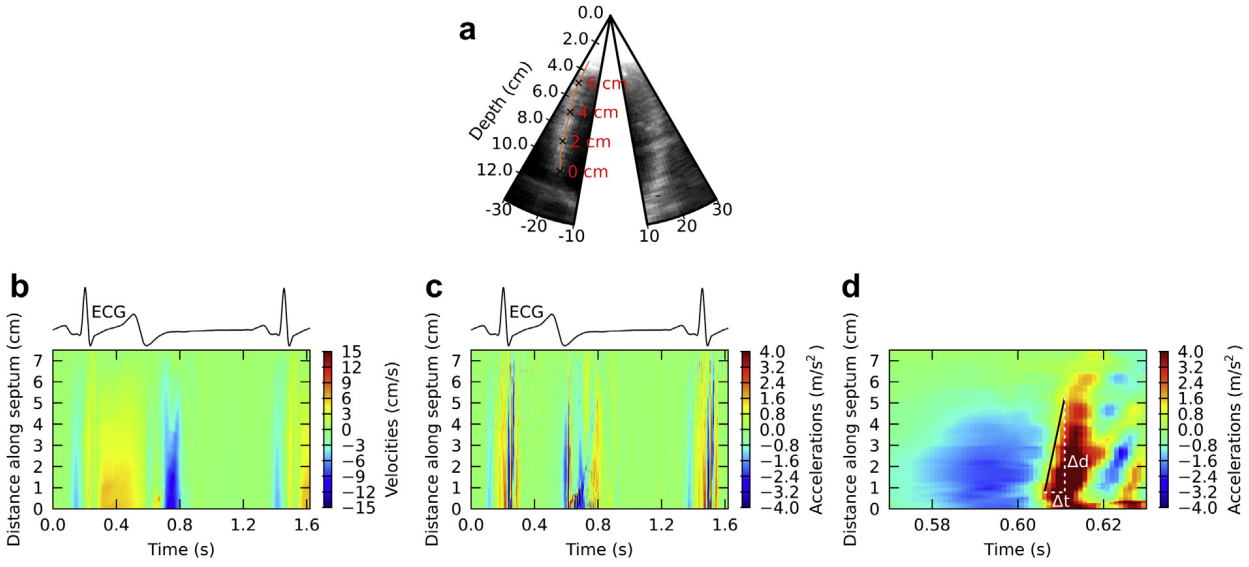

Fig. 6. (a) B-Mode of the septal and lateral walls showing the selected anatomic curve. (b) Curved anatomic M-mode with septal wall velocities from one cardiac cycle. (c) Acceleration values calculated from the velocities in (a). (d) Close-up of the time interval around aortic valve closure marked in (b). Peak acceleration before the e' wave was detected, and the straight line following this point along the wall was drawn to measure the slope ($\Delta d/\Delta t$). This slope equaled the propagation velocity of the event along the wall. ECG = electrocardiogram.

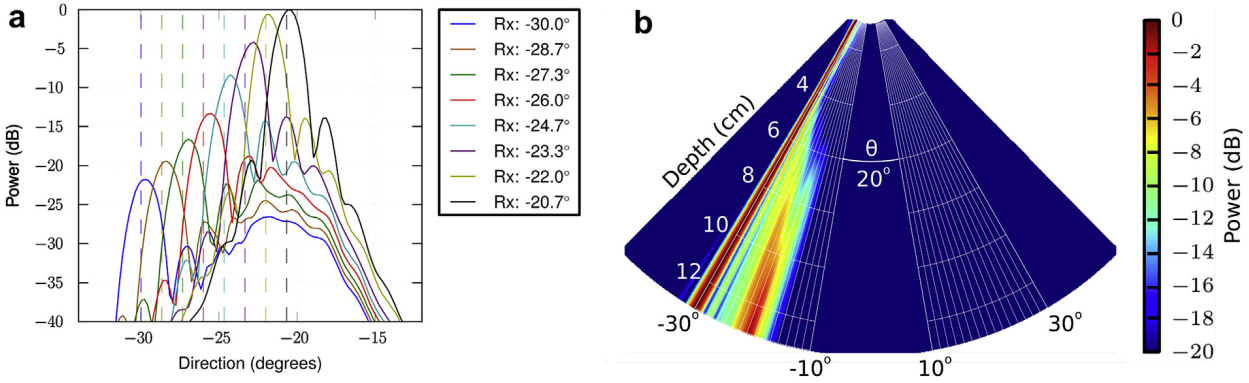

Fig. 7. (a) Transmit-receive beam profile at 10-cm depth for the eight lateral receive lines in one sector with transmit direction at −20°. (b) Transmit-receive beam profile for the utmost receive line in a scan setup with $\theta = 20°$. ECG = electrocardiogram.

differences between UFR-TDI and conventional TDI (UFR-TDI-1 and TDI-1) or between repeated conventional TDI recordings (TDI-1 and TDI-2) (Tables 2 and 3). Bland-Altman analysis of inter-method variability and conventional TDI intra-method variability revealed comparable limits of agreement (Tables 2 and 3).

With respect to time to peak S', paired t-tests indicated no significant differences between UFR-TDI and conventional TDI (UFR-TDI-1 and TDI-1, $p = 0.163$) or between repeated conventional TDI recordings (TDI-1 and TDI-2, $p = 0.279$).

Pre-ejection period

The pre-ejection period had a mean total duration of 91.0 ms (SD = 13.1 ms). In this period, there were two spikes of positive velocity in the basal septum before the onset of the S' wave. The interval from the first deflection of QRS to the start of spike 1 was 22.7 ms (SD = 13.0 ms), and to the start of spike 2, 67.0 ms (SD = 14 ms). The interval between the start of velocity spike 1 and mitral valve closure was 29.6 ms (SD = 16.1 ms). The isovolumic contraction period (mitral valve closure to ejection) had a mean duration of 39.1 ms (SD = 17.5 ms). The second spike was not seen in the lateral wall, where the initial positive spike was followed by a negative spike. The time intervals in the pre-ejection period are illustrated in Figure 4.

Mechanical wave created by aortic valve closure

At the expected time of aortic valve closure, the UFR-TDI method was able to measure the propagation speed of a mechanical wave along the septum in all 10 subjects. The average propagation speed was 5.41 m/s (n = 10, SD = 1.28 m/s).

DISCUSSION

We have illustrated that tissue Doppler imaging is feasible with a frame rate of ∼1200 fps. This high temporal resolution makes new information available in both early and late systole.

Comparison of velocity measurements with conventional TDI indicates that our sensitivity is sufficient for estimating velocities. Tissue Doppler has previously

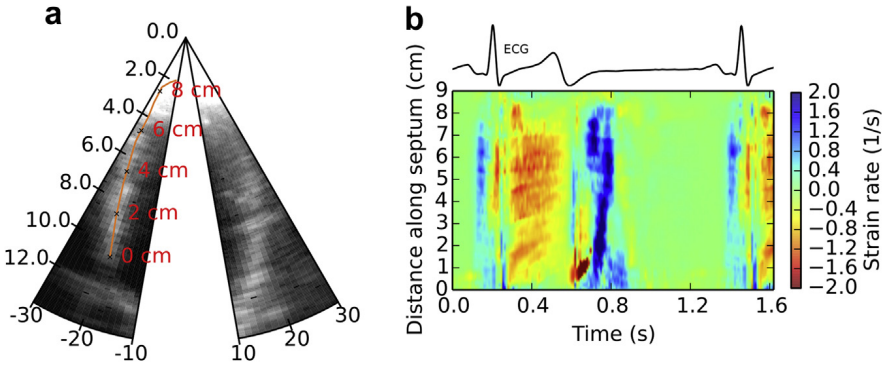

Fig. 8. (a) B-Mode of the septal and lateral walls showing the selected anatomic curve. (b) Curved anatomic M-mode with septal wall strain rates from one cardiac cycle. Contraction during systole and relaxation during diastole are seen as negative and positive strain rates, respectively. ECG = electrocardiogram.

Table 2. Agreement between UFR-TDI and conventional TDI

	S' wave		e' wave		a' wave	
	Lateral	Septal	Lateral	Septal	Lateral	Septal
Average for UFR-TDI (cm/s)	8.32	7.15	13.58	10.19	5.51	6.70
Average for conventional TDI (cm/s)	8.68	7.34	13.55	10.45	4.80	6.38
Average difference (cm/s)	−0.36	−0.19	0.03	−0.26	0.71	0.32
Limits of agreement (cm/s)	(−2.27,1.56)	(−1.13,0.75)	(−1.43,1.48)	(−3.20,2.67)	(−1.18,2.61)	(−1.49,2.13)
t-test *p*-value	0.28	0.23	0.91	0.59	0.05	0.30

UFR-TDI = ultra-high frame rate tissue Doppler imaging.

been validated against phantom (Fleming et al. 1994), B-mode (Fleming et al. 1996), and ultra-sonomicrometry in animal experiments (Gorcsan et al. 1997).

Multi-line acquisition has some disadvantages, the most important being line artifacts visible in B-mode imaging when using a large number of parallel receive beams (Bjastad et al. 2007). For tissue Doppler imaging with parallel receive, the main disadvantage is lowered sensitivity for the outermost receive beams. In our method, the receive lines furthest from the transmit direction have 20-dB-reduced power compared with the center receive lines at 10-cm depth. This results in lower intensity signal with side lobes toward the transmit direction. Also, the angle of maximum power for each of the receive lines is shifted slightly toward the transmit direction.

A suggested improvement is use of Hamming apodization instead of rectangular apodization on receive. This would reduce the side lobes, but increase the main lobe beam width by 30%–50%.

Our clutter filter was designed for peak velocities by selecting a high cutoff frequency. Such a filter can cause noisier velocity estimates for lower velocities ($< \sim$1.5 cm/s). However, this was not a problem in our study because we used clutter filtering only for estimation of peak annular velocities (S', e' and a').

We used a small transmit aperture (0.9 mm) and, thus, unfocused waves on B-mode transmits. The motivation for using this approach was to reduce the effect B-mode transmits might have on the frame-to-frame tissue Doppler estimates. Using a small transmit aperture reduces B-mode image quality. However, the image quality was sufficient for anatomic orientation when recording and analyzing tissue Doppler data.

Because we only image the ventricular walls within two relatively narrow sectors, it is necessary that the sectors are well positioned. Currently, the visual support during acquisition is limited to showing the total sector, which includes both receive sectors and the hole in the middle. Thus, some training is required for the user. Furthermore, as the ventricular walls should be aligned with the transmit direction, the method is best suited for apical recordings. In the parasternal views, the heart walls are perpendicular to the transmit beams, and the method will not be able to cover the ventricular walls entirely.

Pre-ejection period

During the pre-ejection period, ventricular depolarization spreads along the Purkinje system, after which mechanical activation of the ventricles occurs. The delay between electrical excitation and mechanical activation has been reported to be about 30 ms at the cellular level (Cordeiro et al. 2004). Moreover, previous studies have found that mechanical activation starts before mitral valve closure (Remme et al. 2008; Tsakiris et al. 1978).

With the high frame rate in the present method, we see that the onset of QRS in the ECG precedes the onset of the initial tissue velocities by 22.7 ms, on the same order of magnitude as the delay reported by Cordeiro et al. (2004). Thus, it seems that the high frame rate makes it possible to measure electromechanical delay. We also find that the initial velocity spikes precede mitral valve closure. This is in accordance with the studies by Remme et al. (2008), Tsakiris et al. (1978) and Goetz

Table 3. Intra-method agreement for conventional TDI

	S' wave		e' wave		a' wave	
	Lateral	Septal	Lateral	Septal	Lateral	Septal
Average for conventional TDI-1 (cm/s)	8.68	7.34	13.55	10.45	4.80	6.38
Average for conventional TDI-2 (cm/s)	8.54	7.48	13.43	10.20	5.20	6.61
Average difference (cm/s)	0.14	−0.14	0.12	0.25	−0.40	−0.23
Limits of agreement (cm/s)	(−0.90,1.18)	(−1.05,0.77)	(−1.83,2.06)	(−1.83,2.32)	(−1.47,0.67)	(−2.19,1.73)
t-test *p*-value	0.42	0.38	0.72	0.48	0.04	0.48

et al. (2005). Pre-ejection velocities have previously been studied by pulsed tissue Doppler as well as color Doppler with high frame rates (Garcia et al. 1996; Pellerin et al. 1997; Pislaru et al. 2001; Sengupta 2005). However, to our knowledge, only Kanai (2009) has examined the basal velocities from the apical view at similar frame rates. Kanai found two positive velocity spikes in the basal septum, similar to our findings, although with a different proposed explanation. The pre-ejection velocities in the lateral wall, on the other hand exhibit a biphasic pattern with a positive, followed by a negative spike (Fig. 9a). This has been described by several authors (Garcia et al. 1996; Marciniak et al. 2008).

The origin of the initial pre-ejection velocity spike has been suggested both to be ventricular (Remme et al. 2008), representing the start of ventricular mechanical activation, and to be atrial, representing recoil after ventricular elongation caused by atrial contraction. In our study, the initial spike was also present in a subject with atrial fibrillation (Fig. 9b), indicating that the spike may be of ventricular origin. Velocities of atrial origin can be seen in Wenckebach block (Fig. 9c) or long PQ interval (Fig. 9d), so atrial recoil may contribute.

The information obtained by velocities, however, is limited. Because of tethering, actively contracting parts of the ventricle may pull along more basal parts that are not yet activated. This means that it would be difficult to describe the electromechanical activation sequence from velocities alone. Strain rate imaging (D'hooge 2000) would eliminate the tethering effects and can be measured with UFR-TDI (Fig. 8). However, as strain rate imaging has a less favorable signal-to-noise ratio, the feasibility of its use requires further study.

Mechanical wave created by aortic valve closure

A mechanical wave created by aortic valve closure has previously been described by Kanai (2005) and Pernot et al. (2007). Such a wave was also found in our study, in septal anatomic M-modes with acceleration values. The wave propagated along the septum from base to apex, with a mean velocity of 5.41 m/s. This is in agreement with the findings presented by Kanai (2005), with propagation velocities on the same order of magnitude.

Several factors may affect the velocity of mechanical waves in the myocardium. Whereas few studies have examined the wave created by aortic valve closure, numerous studies have examined artificially induced shear waves and what determines their velocities. The effect of myocardial contraction has been reported in animal studies, where shear waves have been found to travel faster in systole than in diastole (Pernot et al. 2011; Pislaru et al. 2009). The effect of tissue properties has been examined in hepatology, where studies have reported increased velocities in liver fibrosis (Kuroda et al. 2010; Osaki et al. 2010). However, shear wave velocity in myocardial fibrosis has not to our knowledge been examined with ultrasound in humans. Wall thickness and load conditions may also influence shear wave velocity. However, with respect to load conditions,

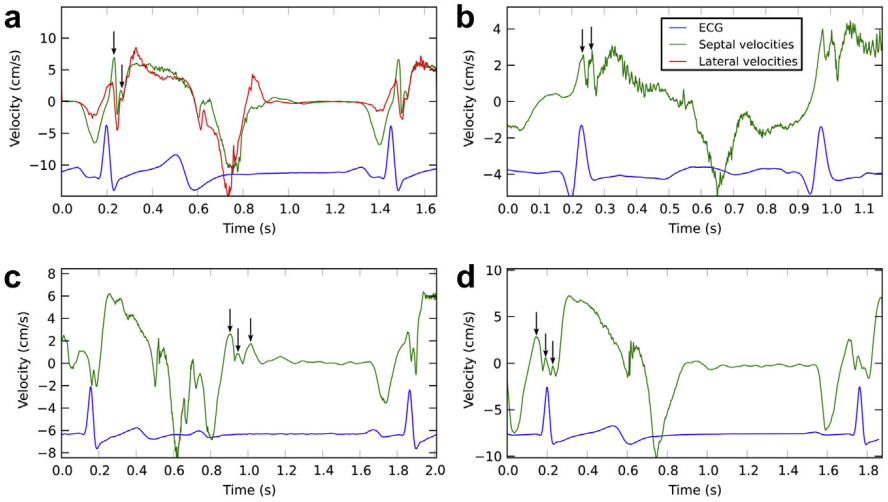

Fig. 9. Examples of annular velocity curves recorded with ultra-high frame rate tissue Doppler imaging (UFR-TDI). (a) Velocities in the septal and lateral walls of a normal subject, showing two positive spikes in the septal wall. In the lateral wall there is a biphasic spike, with positive velocity during spike 1 and negative velocity during spike 2. (b) Velocities in the basal septum of a patient with atrial fibrillation. This subject has no substantial atrial contraction; however, the two spikes are still evident. (c) Velocities in a subject with Wenckebach block, indicating an atrial systole not followed by ventricular systole. The velocity curve shows several spikes after the a' wave, even though there is no ventricular activation. (d) Velocities in the basal part of the septum in a subject with a long PQ interval (230 ms). The first spike after a' precedes the onset of QRS. ECG = electrocardiogram.

one study revealed that altering pre-load has only a modest effect on shear wave velocity (Pernot et al. 2011).

Future studies should assess mechanical wave velocity in hearts with abnormal relaxation, myocardial fibrosis, hypertrophy and diastolic failure. The present study suggests that the mechanical wave created by aortic valve closure can be measured with a commercial ultrasound scanner and may thus be used in such studies.

CONCLUSIONS

In this study, we found that use of UFR-TDI is feasible with a frame rate of 1200 fps: The method exhibited good agreement with conventional TDI in peak velocity measurements, and provided additional information about the mechanical events in early and late systole. The method can be implemented on a commercial ultrasound scanner and may become a valuable investigation tool in clinical studies.

Acknowledgments—The study has been supported by a grant from the Norwegian Research Council, through the Centre for Research Based Innovation, to MI Lab. GE Vingmed AS is a partner in MI Lab.

REFERENCES

Aase SA, Torp H, Stoylen A. Aortic valve closure: Relation to tissue velocities by Doppler and speckle tracking in normal subjects. Eur J Echocardiogr 2008;9:555–559.

Bjaerum S, Torp H, Kristoffersen K. High frame rate tissue Doppler imaging. Vol. 2. New York, IEEE, 2001:1417–1421.

Bjastad T, Aase S, Torp H. The impact of aberration on high frame rate cardiac B-mode imaging. IEEE Trans Ultrason Ferroelectr Freq Control 2007;54:32–41.

Cheng J, Lu JY. Extended high-frame rate imaging method with limited-diffraction beams. IEEE Trans Ultrason Ferroelectr Freq Control 2006;53:880–899.

Cordeiro JM, Greene L, Heilmann C, Antzelevitch D, Antzelevitch C. Transmural heterogeneity of calcium activity and mechanical function in the canine left ventricle. American Journal of Physiology - Heart and Circulatory Physiology 2004;286:H1471–H1479.

D'hooge J. Regional strain and strain rate measurements by cardiac ultrasound: Principles, implementation and limitations. Eur J Echocardiogr 2000;1:154–170.

D'hooge J, Konofagou E, Jamal F, Heimdal A, Barrios L, Bijnens B, Thoen J, Van de Werf F, Sutherland G, Suetens P. Two-dimensional ultrasonic strain rate measurement of the human heart in vivo. IEEE Trans Ultrason Ferroelectr Freq Control 2002;49:281–286.

Fleming A, McDicken W, Sutherland G, Hoskins P. Assessment of colour Doppler tissue imaging using test-phantoms. Ultrasound Med Biol 1994;20:937–951.

Fleming A, Palka P, McDicken W, Fenn L, Sutherland G. Verification of cardiac Doppler tissue images using grey-scale M-mode images. Ultrasound Med Biol 1996;22:573–581.

Garcia MJ, Rodriguez L, Ares M, Griffin BP, Klein AL, Stewart WJ, Thomas JD. Myocardial wall velocity assessment by pulsed doppler tissue imaging: Characteristic findings in normal subjects. Am Heart J 1996;132:648–656.

Goetz WA, Lansac E, Lim HS, Weber PA, Duran CMG. Left ventricular endocardial longitudinal and transverse changes during isovolumic contraction and relaxation: A challenge. Am J Physiol 2005;289: H196–H201.

Gorcsan J, Strum DP, Mandarino WA, Gulati VK, Pinsky MR. Quantitative assessment of alterations in regional left ventricular contractility with color-coded tissue Doppler echocardiography: Comparison with sonomicrometry and pressure-volume relations. Circulation 1997;95:2423–2433.

Hasegawa H, Kanai H. High-frame-rate echocardiography using diverging transmit beams and parallel receive beamforming. J Med Ultrason 2011;38:129–140.

Heimdal A, D'hooge J, Bijnens B, Sutherland G, Torp H. Effect of stationary reverberations and clutter filtering in strain rate imaging. In: Proceedings, 1998 Ultrasonics Symposium, Sendai, Japan, Vol. 2. New York: IEEE, 1998:1361–1364.

Honjo Y, Hasegawa H, Kanai H. Accurate ultrasonic measurement of myocardial regional strain rate at high temporal and spatial resolutions. In: Proceedings, 2008 Ultrasonics Symposium, Beijing, China. New York: IEEE, 2008:1995–1998.

Honjo Y, Hasegawa H, Kanai H. Two-dimensional tracking of heart wall for detailed analysis of heart function at high temporal and spatial resolutions. Jpn J Appl Phys 2010;49:07HF14.

Isaaz K, Thompson A, Ethevenot G, Cloez JL, Brembilla B, Pernot C. Doppler echocardiographic measurement of low velocity motion of the left ventricular posterior wall. Am J Cardiol 1989;64:66–75.

Jensen JA. Field: A program for simulating ultrasound systems. In: Proceedings, 10th Nordic-Baltic Conference on Biomedical Engineering. Med Biol Eng Comput 1996;4(Suppl 1, Part 1):351–353.

Kanai H. Propagation of spontaneously actuated pulsive vibration in human heart wall and in vivo viscoelasticity estimation. IEEE Trans Ultrason Ferroelectr Freq Control 2005;52:1931–1942.

Kanai H. Propagation of vibration caused by electrical excitation in the normal human heart. Ultrasound Med Biol 2009;35:936–948.

Kanai H, Satoh H, Hirose K, Chubachi N. A new method for measuring small local vibrations in the heart using ultrasound. IEEE Trans Biomedical Engineering 1993;40:1233–1242.

Katz A. Physiology of the heart. Philadelphia: Lippincott Williams & Wilkins; 2010:402.

Kuroda H, Kakisaka K, Tatemichi Y, Sawara K, Miyamoto Y, Oikawa K, Miyasaka A, Takikawa Y, Masuda T, Suzuki K. Non-invasive evaluation of liver fibrosis using acoustic radiation force impulse imaging in chronic hepatitis patients with hepatitis C virus infection. Hepatogastroenterology 2010;57(102–103):1203–1207.

Lu JY, Cheng J, Wang J. High frame rate imaging system for limited diffraction array beam imaging with square-wave aperture weightings. IEEE Trans Ultrason Ferroelectr Freq Control 2006;53:1796–1812.

Marciniak M, Bijnens B, Baltabaeva A, Marciniak A, Parsai C, Claus P, Sutherland GR. Interventricular interaction as a possible mechanism for the presence of a biphasic systolic velocity profile in normal left ventricular free walls. Heart 2008;94:1058–1064.

Misaridis T, Jensen J. Use of modulated excitation signals in medical ultrasound. Part III: High frame rate imaging. IEEE Trans Ultrason Ferroelectr Freq Control 2005;52:208–219.

Osaki A, Kubota T, Suda T, Igarashi M, Nagasaki K, Tsuchiya A, Yano M, Tamura Y, Takamura M, Kawai H, Yamagiwa S, Kikuchi T, Nomoto M, Aoyagi Y. Shear wave velocity is a useful marker for managing nonalcoholic steatohepatitis. World J Gastroenterol 2010;16:2918–2925.

Pai RG, Gill KS. Amplitudes, durations, and timings of apically directed left ventricular myocardial velocities: I. Their normal pattern and coupling to ventricular filling and ejection. J Am Soc Echocardiogr 1998;11:105–111.

Pellerin D, Cohen L, Larrazet F, Pajany F, Witchitz S, Veyrat C. Preejectional left ventricular wall motion in normal subjects using Doppler tissue imaging and correlation with ejection fraction. Am J Cardiol 1997;80:601–607.

Pernot M, Couade M, Mateo P, Crozatier B, Fischmeister R, Tanter M. Real-time assessment of myocardial contractility using shear wave imaging. J Am Coll Cardiol 2011;58:65–72.

Pernot M, Fujikura K, Fung-Kee-Fung SD, Konofagou EE. ECG-gated, mechanical and electromechanical wave imaging of cardiovascular tissues in vivo. Ultrasound Med Biol 2007;33:1075–1085.

Pislaru C, Bruce CJ, Belohlavek M, Seward JB, Greenleaf JF. Intracardiac measurement of pre-ejection myocardial velocities estimates the transmural extent of viable myocardium early after reperfusion in acute myocardial infarction. J Am Coll Cardiol 2001;38: 1748–1756.

Pislaru C, Urban M, Nenadic I, Greenleaf J. Shear wave dispersion ultrasound vibrometry applied to in vivo myocardium. In: Proceedings, Annual International Conference of the IEEE Engineering in Medicine and Biology Society. New York: IEEE, 2009:2891–2894.

Provost J, Nguyen VTH, Legrand D, Okrasinski S, Costet A, Gambhir A, Garan H, Konofagou EE. Electromechanical wave imaging for arrhythmias. Phys Med Biol 2011;56:L1–L11.

Provost J, Thiébaut S, Luo J, Konofagou EE. Single-heartbeat electromechanical wave imaging with optimal strain estimation using temporally unequispaced acquisition sequences. Phys Med Biol 2012;57:1095–1112.

Remme EW, Lyseggen E, Helle-Valle T, Opdahl A, Pettersen E, Vartdal T, Ragnarsson A, Ljosland M, Ihlen H, Edvardsen T, Smiseth OA. Mechanisms of preejection and postejection velocity spikes in left ventricular myocardium. Circulation 2008;118:373–380.

Sengupta PP. Biphasic tissue Doppler waveforms during isovolumic phases are associated with asynchronous deformation of subendocardial and subepicardial layers. J Appl Physiol 2005;99:1104–1111.

Shattuck DP, Weinshenker MD, Smith SW, von Ramm OT. Explososcan: A parallel processing technique for high speed ultrasound imaging with linear phased arrays. J Acoust Soc Am 1984;75:1273–1282.

Sutherland G, Hatle L, Claus P, Herbots L, Šeparović J. Normal Data. In: Sutherland G, Hatle L, Claus P, D'hooge J, Bijnens BH, (eds). Doppler myocardial imaging. Hasselt: BSWK BVBA; 2006. p. 62.

Tanter M, Bercoff J, Sandrin L, Fink M. Ultrafast compound imaging for 2-D motion vector estimation: Application to transient elastography. IEEE Trans Ultrason Ferroelectr Freq Control 2002;49:1363–1374.

Tsakiris AG, Gordon DA, Padiyar R, Frechette D. Relation of mitral valve opening and closure to left atrial and ventricular pressures in the intact dog. Am J Physiol 1978;234:H146–H151.

Weissler AM, Harris WS, Schoenfeld CD. Systolic time intervals in heart failure in man. Circulation 1968;37:149–159.

Appendix B

Paper II - Detection of mechanical activation in an open chest porcine model by three-dimensional UFR-TDI, a feasibility study

Detection of left ventricular mechanical activation by three-dimensional ultra-high frame rate tissue Doppler imaging in an open-chest porcine model, a feasibility study

Lars Christian N. Lervik, M.D,1, Birger Brekke, MSc.,1, Carlo Missant Prof. M.D, Ph.D., 3, Peter Haemers, M.D, 3 Ling Tong, MSc Ph.D. 3, Alejandra Ortega, MSc Ph.D. 3, Hans, Torp. Prof. Dr. Ing, MSc. 1, Asbjørn Støylen M.D, Prof. Dr. Med., 1and2, George Sutherland, M.D, Prof. Dr. Med., 3, Jan D'hooge, Prof. MSc. Ph.D, 1,3

1: MI Lab and Department of Circulation and Medical Imaging, Norwegian University of Science and Technology, Trondheim, Norway;

2: Department of Cardiology, St Olavs Hospital/Trondheim University Hospital, Trondheim, Norway

3: Department of Cardiovascular Sciences, University of Leuven, Leuven, Belgium

Corresponding author:

Lars Christian Naterstad Lervik

Lars.c.nilsen@ntnu.no / larschr.lervik@gmail.com

Tel: +47 91853697 FAX: +47 73 59 53 10

Postal address:

Department of Circulation and Medical Imaging

Norwegian University of Science and Technology

Postboks 8905

7491 Trondheim

Norway

Running head: Detection of mechanical activation with 3D-UFR-TDI

Brekke and Lervik was funded by MI Lab. MI Lab was a Centre for Research-based Innovation (SFI) appointed by the Research Council of Norway for the 8-year period 2007-2015. GE Vingmed was a partner in MI-Lab. SA Aase is employed by GE Vingmed. D'hooge was funded by a grant from European Research Council (Grant agreement 281748).

Abstract

Ultra-high frame rate tissue Doppler imaging (UFR-TDI) realizes three-dimensional (3D) TDI acquisitions from the left ventricle with a frame rate of more than 500 volumes per second. Such frame rates enable analysis of short-lived mechanical events during the cardiac cycle. In this study we examined the feasibility of detecting mechanical activation of the left ventricle by 3D-UFR-TDI in an open-chest porcine model with epicardial pacing. The time interval from onset of QRS to negative strain rate was measured in an 18 segment model. We compared our findings with high frame rate two-dimensional (2D) data. The mean time interval from onset QRS to onset of shortening was shorter in the segments corresponding to the pacing electrodes for both 2D- and 3D-UFR-TDI data. The results indicate that detection of onset of mechanical activation with 3D-UFR-TDI may be feasible.

Keywords:

Tissue and strain Doppler echocardiography

Strain rate imaging

Three-dimensional echocardiography

Color Doppler three-dimensional

Temporal resolution

Electromechanical coupling

Introduction:

Ultra-fast cardiac imaging is an area which is evolving and its potential is currently being investigated by several groups worldwide [1]. Conventional two-dimensional (2D) tissue Doppler (TDI) acquisition technology allows frame rate of about ~300 Hz by narrowing the sector and depth to a minimum, while three-dimensional (3D) acquisition enables ~25 volumes per second, respectively [2,3]. New technological developments enable high frame rates of ~1000 Hz and above in 2D[1]. However the availability of high frame rate 3D acquisition technology is limited[1,4].

The rationale for high frame rate imaging in many of the ongoing studies has been the analysis of short lived mechanical events such as shear waves or mechanical activation waves in the myocardium [5–8]. Such application could prove valuable when identifying areas of conduction delay, such as areas with subendocardial ischemia; and in planning and evaluating cardiac resynchronization therapy. 2D imaging of the mechanical activation wave has recently been validated [9]. However, to our knowledge, no data is available for 3D imaging of this mechanical activation wave by high frame rate volumetric TDI.

High frame rate 3D TDI data from left ventricle could enable detection of the first local sign of contraction and a more detailed evaluation of the propagation of such event. Further, the main part of systolic shortening is tied to the ejection period, and marks the opening of the aortic valve and the deformation due to ejection. Eventual propagation of this event is purely mechanical. During isovolumic contraction, there is pressure increase, but very little deformation. However, mechanical activation in the septum starts before the closure of the mitral valve [10,11] which is the cause of the pre-ejection velocity spike [12]. Tissue Doppler can detect such spikes, however contracting myocardium will cause neighboring tissue motion due to tethering, which renders velocity estimates less suitable for mapping such mechanical event. Strain rate imaging will subtract the effects of tethering [13], and is therefore more suitable for identifying areas of early contraction.

Ultra-high frame rate tissue Doppler imaging (UFR-TDI) realizes acquisition of 3D-tissue Doppler data with 500 volumes per second [11,14] and could be able to detect ultrafast events, such as mechanical activation. Furthermore, strain rates can be produced from 3D-UFR-TDI data which makes it suitable for mapping such mechanical event. The aim of this study was therefore to examine if detection of the onset of mechanical activation of the left ventricle in an open chest porcine model with epicardial pacing using 3D-UFR-TDI was feasible by comparing our findings with 2D-UFR-TDI data.

Materials and methods:

Animal preparation - Two pigs with target weight 30-35kg were included. Anesthesia regimen were as follows: Initially the animals were premedicated with Zoletil (8 mg/kg I.M.) and Xylazine (2.5 mg/kg I.M.), after which anesthesia was induced with Propofol (2 mg/kg I.V.) and Sufentanil (0.25 μg/kg/h). Anesthesia was maintained with a continuous infusion of Propofol (10 mg/kg/h) and Sufentanil (1 μg/kg/h) via an ear vein. The animals were ventilated with a mixture of oxygen and room air to maintain normocapnia and normoxia (tidal volume of 8 ml/kg and respiratory rate of 12 times/minute). The animals were kept hydrated with Lactated Ringer's solution at a rate of 8 mL/kg/h. A neuromuscular blocker was infused to prevent spontaneous respiration (Nimbex or Esmeron). Sternotomy was performed and the heart was suspended in a pericardial cradle. Four uni-polar electrodes were epicardially implanted at the apex, basal lateral-, anterior- and inferior-wall (Fig. 1). Vascular access was gained through the left jugular vein (assessment of central venous pressure and administration of drugs) and right carotid artery in order to insert a micromanometer (Millar, Houston, TX, USA) into the left ventricle to record instantaneous left ventricular pressure.
The study was approved by the local ethics committee of the University of Leuven, Belgium.

Acquisition protocol - UFR-TDI was implemented on a GE Vingmed Vivid E9, an M5S-D phased array probe and 4V probe was used for 2D- and 3D-acquisition respectively (GE Vingmed, Horten,

Norway). The imaging methods have previously been described [11,14]. The acquisition was performed in the following steps:

1. Baseline acquisition of 2D B-mode data followed by 2D-UFR-TDI data from the standard apical views, i.e. two- and four-chamber and apical long-axis view.
2. Baseline recording of 3D-UFR-TDI data from the apical view
3. Implantation of pacing electrodes
4. Acquisition of 2D B-mode data followed by UFR-TDI data from the three apical views
5. Acquisition of 3D-UFR-TDI data from the apical view
6. Steps 4 and 5 were repeated during pacing from each of the basal and one apical electrode

A piece of liver was used as a stand-off between the myocardium and the probe for both 2D- and 3D-acquisition. Typical frame rates for UFR-TDI data were 1250-1310 Hz and 500 Hz in 2D and 3D respectively.

Echocardiographic analysis

2D-UFR-TDI - The 2D data was analyzed with in-house software developed in Matlab 2011b (The MathWorks, Natick, MA, USA). The analysis was performed in the following steps:

1. A curved anatomic M-mode was drawn in the wall of interest (Fig. 2)
2. An anatomic M-mode presenting strain rates was generated (Fig. 2)
3. The time of onset of QRS was detected in the synchronously recorded ECG
4. The time from the onset of QRS to the strain rate zero-crossing for all depths along the anatomic M-mode was automatically estimated and the median time to zero-crossing was provided for each segment (basis, middle and apex) (Fig. 2)

The onset of QRS was defined as the first deflection of Q- or R-wave. First negative strain rate was defined as first zero-crossing from a positive to a negative strain rate value after the onset of QRS. The length of a segment was 15-25 mm depending on the length of the ventricle. The temporal averaging was 10 ms and the sample volume was 6 mm x 3 mm. A Butterworth clutter filter with cut-off at 0.5 cm/s was applied to minimize noise. Strain rate was calculated with linear regression over a strain

length of 16 mm. For the basal measurements, the electrodes were assigned the corresponding segment in the 18 segment model based on its placement, *i.e.* anterior – anterior from apical two chamber view, inferior – inferior from apical two-chamber view, lateral – inferolateral from apical long axis view. For the apical pacing, the segment with the shortest time interval was used. Care was taken during acquisition to make sure that proper imaging planes were recorded and that the segment corresponding to the pacing electrode was within the field of view.

3D-UFR-TDI - 3D-data was analyzed with in-house developed software based on Orderud et al [15]. The 3D-UFR-TDI data was presented in a bull's eye plot and as a 3D-mesh-model of the left-ventricle with colour coded strain rate (Fig. 3). The strain rate data in the bull's eye plot was coded dichotomously with strain rate values above or below $-0.25s^{-1}$. The distribution of the strain rate was visually assessed in the bull's eye plot; when more than 50% of a segment presented strain rates more negative than $-0.25s^{-1}$ it was defined as mechanically activated. The time from onset of QRS to mechanical activation was then measured. The cut-off value of $-0.25s^{-1}$ was determined by measuring peak pre-ejection strain rate from 4-chamber views in 10 healthy volunteers. Half of the median value in these measurements was used as a cut-off for mechanical activation. The pre-ejection velocity spikes have previously been shown to be closely related to mechanical activation [12], pre-ejection strain rate was therefore chosen as a surrogate for mechanical activation. Temporal smoothing in the 3D-data was set to 10 ms. The spatial smoothing was set to 20 mm x 8 mm x 8 mm (Circumferential x Longitudinal x Radial).

The analysis was performed in the following steps:

1. Software based on Orderud et al [15] was applied to the 3D B-mode data to choose the region for extraction of 3D-UFR-TDI data (Fig. 4)
2. Strain rate data was visualized on a 3D model of the left ventricle based on the region of interest determined in step 1 and in a bull's eye plot (Fig. 3)
3. The time of onset of QRS on a synchronously recorded ECG was selected manually as starting point for analysis

4. Each segment in the bull's eye plot (18 segment model) was then analyzed in increments of 2ms and the time interval from onset of QRS to mechanical activation in >50% of the segment of interest was measured (Fig. 3).

Statistics

All values are expressed as mean ± standard deviation. Students t-test was used for comparison of activation times from the 2D- and 3D-data, a *p*-value <0.05 was considered significant.

Results:

Feasibility

In the 2D-UFR-TDI data, 100 segments were feasible for analysis, 8 segments were excluded due to reverberations, random noise or dropouts. In the 3D UFR-TDI data 107 segments were feasible for analysis, 1 segment was excluded due to dropouts.

Time to shortening

2D-UFR-TDI data - The mean time interval from onset QRS to onset of shortening was 35 ± 23 ms in the segments corresponding to the placement of the pacing electrodes, 73 ± 64 ms in the remaining segments.

3D-UFR-TDI data - The mean interval from onset of QRS to onset of shortening was 41 ± 15 ms in the segments corresponding to the placement of the pacing electrodes, and 69 ± 52 ms in remaining segments.

Pearsons R for correlation between the methods was 0.14 (p=ns) after removal of four outliers.

The results are presented in Tables 1 and 2, and Figures 5 and 6.

Discussion

The findings from this feasibility study suggest that detection of onset of mechanical activation of the left ventricle with 3D-UFR-TDI by deformation imaging may be feasible. Time to mechanical

activation was shorter in the segments corresponding to the pacing electrodes than in the remaining segments in 3D-UFR-TDI data for all pacing sites, further the time intervals was in the same order of magnitude as found in the 2D-UFR-TDI data.

There is a large spread in both the 2D-, and 3D-UFR-TDI data, and time to shortening does differ between the 2D- and 3D-data for corresponding non-pacing segments (Fig. 5). A possible explanation for this is that the method used for detection of onset of shortening differs. 2D-UFR-TDI uses automatic detection of zero-cross and provides median value from each segment, while 3D-UFR-TDI uses a dichotomous semiquantitative approach.

Further, the number of segments discarded from analysis due to noise was higher than 2D than in 3D. The segments were excluded due to noise and dropouts. The origin of the noise could be the implanted crystals and catheter which may affect Doppler quality, or heterogeneity of the liver used as standoff. The visualization of strain rate in an anatomic m-mode in the 2D-UFR-TDI analysis allows a more detailed evaluation of data quality. Such visualization allows exclusion of clutter with more confidence. Such evaluation is not possible in the 3D-UFR-TDI data in its current state which contribute to the difference between 2D and 3D. In addition, as the 2D data is acquired from part of the ventricular wall, while the 3D data acquires data from the entire ventricle simultaneously, the activation may differ between the 3D segment and corresponding 2D slice. Finally, as the 2D and 3D data were not acquired simultaneously, some physiological beat-beat variability may also contribute to the difference in the activation times.

The detection of electromechanical activation by deformation imaging is complex. There is continuously active and passive deformation throughout the ventricle, and differentiation remains a challenge. Peak negative strain rate represents fast shortening. During pre-ejection time, this will most probable be active, while neighbouring, non activated areas will be stretched. However, recoil from atrial systole may complicate this measurement by compressing some of the myocardium.

The time delays measured are in the same order of magnitude as the delays measured at the cellular level [17] and in recent experimental studies [8,9,18]. Further the time interval measured was similar for the 2D and 3D methods.

Limitations

The sample size is too small to perform any relevant significance testing which can be extrapolated to human studies. The results can only give us indication, and does not allow us to draw any firm conclusions. Nevertheless, the obtained data showed the feasibility of fast 3D imaging to extract information on activation waves from a single heart beat.

The porcine heart proved vulnerable to instrumentation and susceptible to arrhythmias in an open chest model, as a result the study protocol was not performed to completion in the two experiments, as a result no corresponding data from the inferior electrode was captured. A possible explanation for this is the lack collateral blood supply [19]. An ovine or canine model might have been better suitable for such study.

The ECG was not aligned with the electrical vector, this leaves a possible “blackout” of up to 40 ms initially (duration of a q-wave). The reason for this is as the pacing site changes, the vector also changes, and realigning the electrodes for each pacing site was not feasible in the protocol. This should be considered if method is developed further.

The 3D method acquires data over two cardiac cycles, first one b-mode for navigational purposes for regions of data extraction (Fig 4), then 3D-UFR-TDI data is acquired. The trigger for recording is peak of the R-wave. As the event we are trying to capture, mechanical activation, has onset before and ends after the peak of the R-wave, it would be beneficial to introduce a different triggerpoint, in example end systole, for analysis of the mechanical activation.

Conclusion

This preliminary study shows that the onset of negative strain rate corresponds with the onset of mechanical activation from pacing electrodes and that the segment from which the mechanical

activation originates can be detected with 3D-UFR-TDI. The 3D-UFR-TDI data did however not correlate with the 2D UFR-TDI data. Albeit, when grouping elements in paced and non-paced segments, each method separately showed the same trends towards lower activation times in the segments corresponding to the pacing electrodes. This trend indicates that detection of mechanical activation with 3D UFR-TDI may be feasible; however a larger sample size is needed to substantiate findings.

Acknowledgements

Brekke and Lervik was funded by MI Lab. MI Lab was a Centre for Research-based Innovation (SFI) appointed by the Research Council of Norway for the 8-year period 2007-2015. GE Vingmed was a partner in MI-Lab. SA Aase is employed by GE Vingmed. D'hooge was funded by a grant from European Research Council (Grant agreement 281748).

Bibliography

1. Cikes M, Tong L, Sutherland GR, D'hooge J. Ultrafast cardiac ultrasound imaging: Technical principles, applications, and clinical benefits. JACC Cardiovasc. Imaging. 2014;7:812–23.

2. Badano LP. The Clinical Benefits of Adding a Third Dimension to Assess the Left Ventricle with Echocardiography. Scientifica (Cairo). 2014;2014:1–18.

3. Chien-Chia Wu V, Takeuchi M. Three-Dimensional Echocardiography: Current Status and Real-Life Applications. 2017;107–18.

4. Provost J, Papadacci C, Arango JE, Imbault M, Fink M, Gennisson J-L, et al. 3D ultrafast ultrasound imaging in vivo. Phys. Med. Biol. 2014;59:L1–13.

5. Provost J, Lee W-N, Fujikura K, Konofagou EE. Imaging the electromechanical activity of the heart in vivo. Proc. Natl. Acad. Sci. U. S. A. 2011;108:8565–70.

6. Pernot M, Konofagou E. Electromechanical imaging of the myocardium at normal and pathological states. IEEE Ultrason. Symp. Proc. 2005;0:1091–4.

7. Pernot M, Fujikura K, Fung-Kee-Fung SD, Konofagou EE. ECG-gated, mechanical and electromechanical wave imaging of cardiovascular tissues in vivo. Ultrasound Med. Biol. 2007;33:1075–85.

8. Bunting E, Lambrakos L, Kemper P, Whang W, Garan H, Konofagou E. Imaging the Propagation of the Electromechanical Wave in Heart Failure Patients with Cardiac Resynchronization Therapy. Pacing Clin. Electrophysiol. 2017;40:35–45.

9. Grondin J, Costet A, Bunting E, Gambhir A, Garan H, Wan E, et al. Validation of electromechanical wave imaging in a canine model during pacing and sinus rhythm. Hear. Rhythm. 2016;13:2221–7.

10. Tsakiris AG, Gordon DA, Padiyar R, Fréchette D. Relation of mitral valve opening and closure to left atrial and ventricular pressures in the intact dog. Am. J. Physiol. 1978;234:H146-51.

11. Brekke B, Nilsen LCL, Lund J, Torp H, Bjastad T, Amundsen BH, et al. Ultra-high Frame Rate Tissue Doppler Imaging. Ultrasound Med. Biol. 2014;40:222–31.

12. Remme EW, Lyseggen E, Helle-Valle T, Opdahl A, Pettersen E, Vartdal T, et al. Mechanisms of preejection and postejection velocity spikes in left ventricular myocardium: interaction between wall deformation and valve events. Circulation. 2008;118:373–80.

13. Heimdal A, D'hooge J, Bijnens B, Sutherland G, Torp H. Effect of stationary reverberations and clutter filtering in strain rate imaging. IEEE Ultrason. Symp. 1998. 1998;1361–4.

14. Brekke B, Torp H, Bjastad T, Stoylen A, Aase SA. 3D Tissue Doppler imaging with ultra high frame rate. 2011 IEEE Int. Ultrason. Symp. IEEE; 2011. p. 717–20.

15. Orderud F, Kiss G, Torp HG. Automatic coupled segmentation of endo- and epicardial borders in 3D echocardiography. 2008 IEEE Ultrason. Symp. IEEE; 2008. p. 1749–52.

16. D'hooge J, Heimdal A, Jamal F, Kukulski T, Bijnens B, Rademakers F, et al. Regional strain and strain rate measurements by cardiac ultrasound: principles, implementation and limitations. Eur. J. Echocardiogr. 2000;1:154–70.

17. Cordeiro JM, Greene L, Heilmann C, Antzelevitch D, Antzelevitch C. Transmural heterogeneity of calcium activity and mechanical function in the canine left ventricle. Am. J. Physiol. Heart Circ. Physiol. 2004;286:H1471-9.

18. Costet A, Wan E, Bunting E, Grondin J, Garan H, Konofagou E. Electromechanical wave imaging (EWI) validation in all four cardiac chambers with 3D electroanatomic mapping in canines *in vivo*. Phys. Med. Biol. IOP Publishing; 2016;61:8105–19.

19. Seiler C. Collateral Circulation of the Heart. London: Springer London; 2009.

Table1: 2D-UFR-TDI data Mean time interval *Onset QRS – First negative strain rate*

Wall	Segment	Baseline (ms)	Apical Pacing (ms)	Anterior pacing (ms)	Lateral pacing (ms)
Inferoseptum	Basal	16	10	89	28
	Mid	78	30	79	62
	Apex	36	32	107	121
Anterolateral	Basal	57	39	84	19
	Mid	22	19	99	56
	Apex	101	11	122	55
Anterior	Basal	68	67	63	28
	Mid	36	54	28	28
	Apex	10	39	76	60
Inferior	Basal	31	-	121	72
	Mid	256	-	89	35
	Apex	22	-	92	42
Anteroseptal	Basal	77	57	79	211
	Mid	98	76	84	114
	Apex	14	75	227	106
Inferolateral	Basal	11	86	52	159
	Mid	6	89	98	32
	Apex	58	56	156	74

Table 2: 3D-UFR-TDI data Mean time interval *Onset QRS – strain rate <-0.25 s^{-1}*

Wall	Segment	Baseline (ms)	Apical Pacing (ms)	Anterior pacing (ms)	Lateral pacing (ms)
Inferoseptum	Basal	62	298	67	48
	Mid	78	54	78	62
	Apex	36	40	85	86
Anterolateral	Basal	120	68	44	90
	Mid	42	32	58	48
	Apex	26	28	83	148
Anterior	Basal	112	38	66	52
	Mid	48	54	87	148
	Apex	69	20	88	11
Inferior	Basal	78	232	47	48
	Mid	59	32	54	62
	Apex	34	22	84	74
Anteroseptal	Basal	228	56	51	44
	Mid	46	66	101	82
	Apex	73	24	39	98
Inferolateral	Basal	44	66	46	92
	Mid	45	30	62	62
	Apex	24	28	68	80

Figure 1: Schematic view of the left ventricle. The placement of pacing electrodes: 1 - apical, 2 – lateral, 3 – inferior and 4 – anterior.

Figure 2: 2D-UFR-TDI: The upper panel shows a curved anatomic m-mode presenting strain rate from the anterior wall at natural pacing. The onset of shortening can be seen in the middle and basal segment. The middle panel shows a curved anatomic m-mode presenting strain rates from the anterior wall during apical pacing. The onset of shortening has been shifted more apically. The lower panel shows the ECG from the natural pacing. Upper right panel shows B-mode with curve that forms basis for anatomical m-mode. UFR-TDI – Ultra-high frame rate tissue Doppler imaging.

Figure 3: 3D-UFR-TDI data: a) Bull's eye Plot with UFR-TDI Strain rate data from the left ventricle presented at 20 ms intervals from the onset of QRS. Red indicates shortening ($SR<-0.25\ s^{-1}$), Blue indicates SR values $>-0.25\ s^{-1}$. At baseline the onset of shortening is found inferoseptally and spreads inferiorly and anteriorly. During basal anterior pacing, the onset of starts anteroseptally and further the interpretation becomes ambigious. During apical pacing, the onset of shortening is found apically in both anterior and inferior wall, after which it spreads inferiolaterally and anteriorly. Asterisk: Segment corresponding with pacing electrode b) 3D model of the left ventricle during apical pacing with 3D-UFR-TDI Strain Rate data superimposed on its surface 30 ms after onset of pacing. One can see apical and anterolateral activated myocardium. c) ECG. UFR-TDI – Ultra-high frame rate tissue Doppler imaging.

Figure 4: The software showing b-mode images with areas for extraction of 3D-UFR-TDI data. The yellow lines demarcate the borders of the data included for 3D analysis. UFR-TDI – Ultra-high frame rate tissue Doppler imaging.

Figure 5: Box plot presenting paced versus non-paced data. Y axis unit is in milliseconds. X axis shows the distribution time to shortening for the 2D-, and 3D-UFR-TDI paced and non-paced segments.

Figure 6: 2D-, and 3D-UFR-TDI data scatterplot. Blue points presenting corresponding non-paced segments, red points presenting corresponding paced segments. Unit is milliseconds. Dotted line presents regression line and the solid line presents regression line after removal of four outliers. Y-axis

represents time to shortening by the 3D-UFR-TDI method in milliseconds. X-axis represents time to shortening by the 2D-UFR-TDI method in milliseconds.

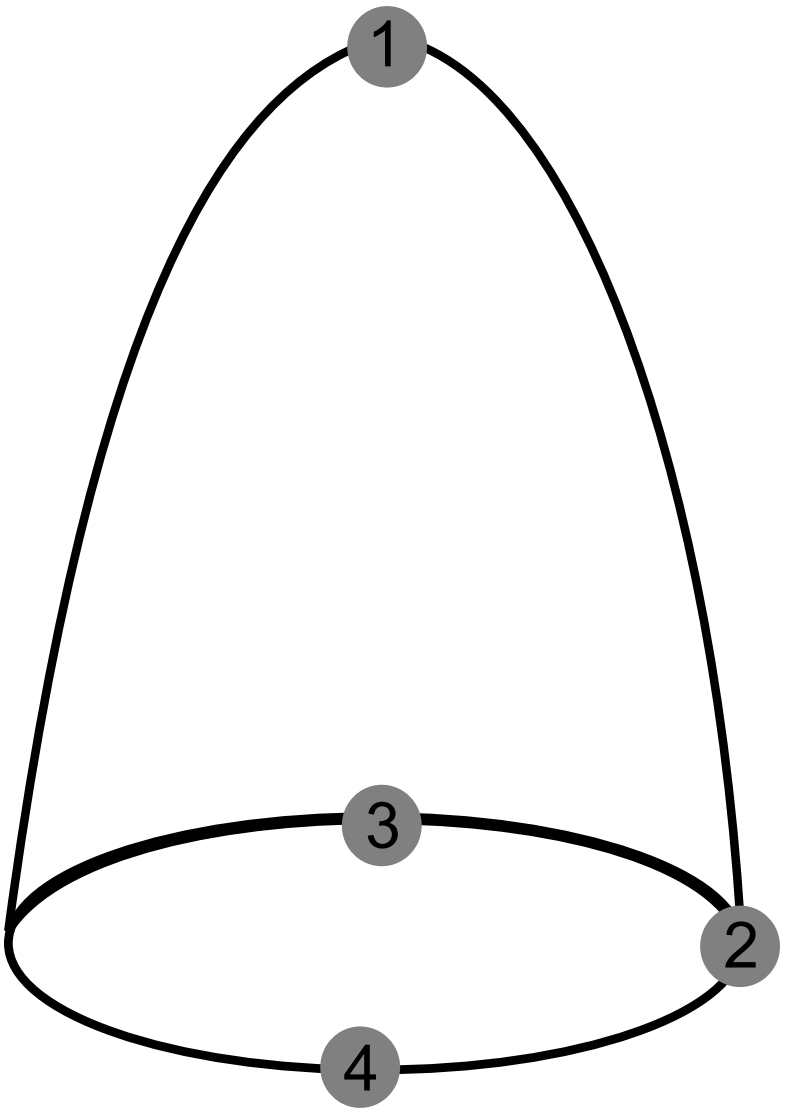
1
3
2
4

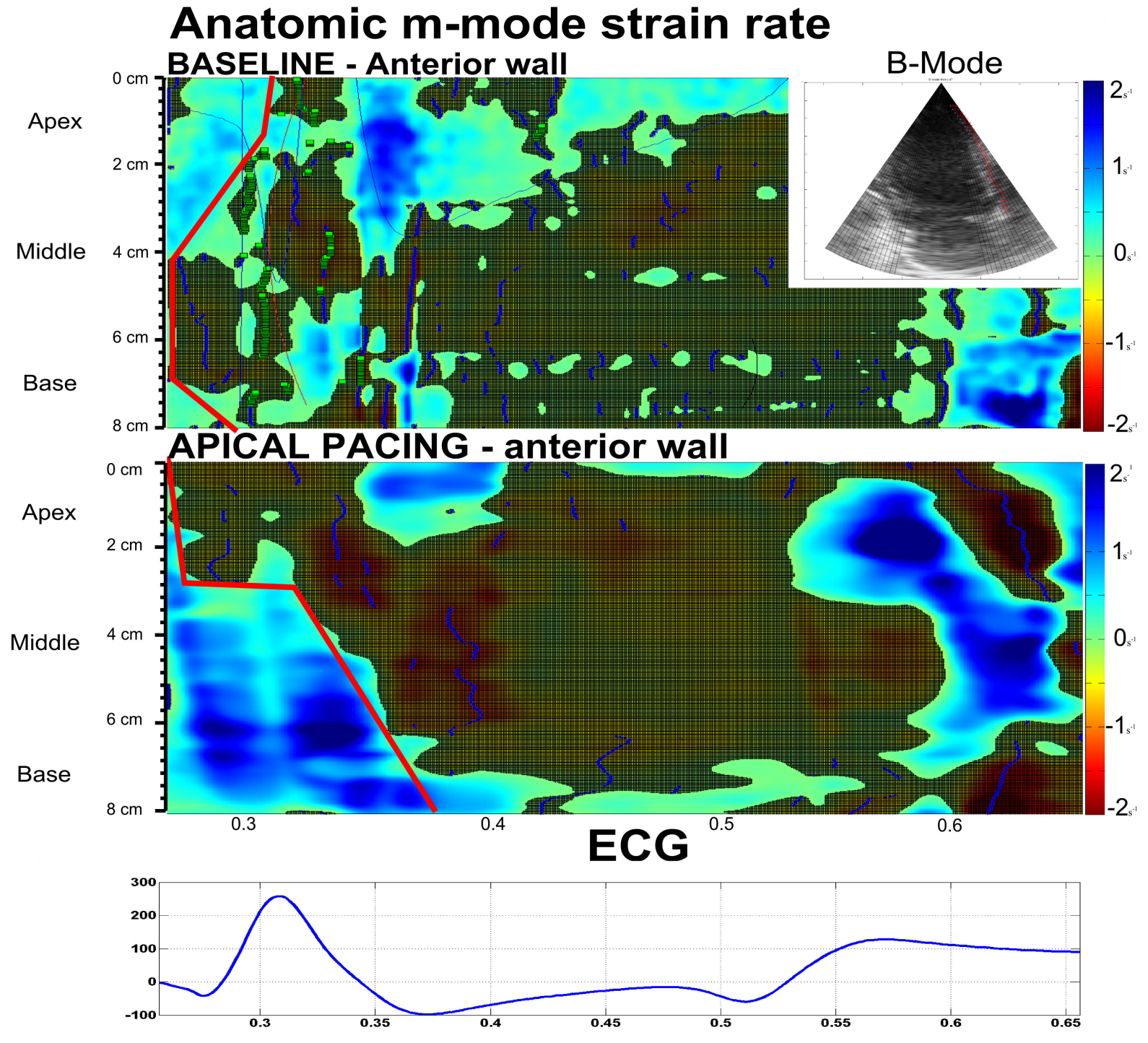
Anatomic m-mode strain rate
BASELINE - Anterior wall
B-Mode
Apex
Middle
Base
0 cm
2 cm
4 cm
6 cm
8 cm
2 s-1
1 s-1
0 s-1
-1 s-1
-2 s-1
APICAL PACING - anterior wall
0.3
0.4
0.5
0.6
ECG
300
200
100
0
-100
0.35
0.45
0.55
0.65

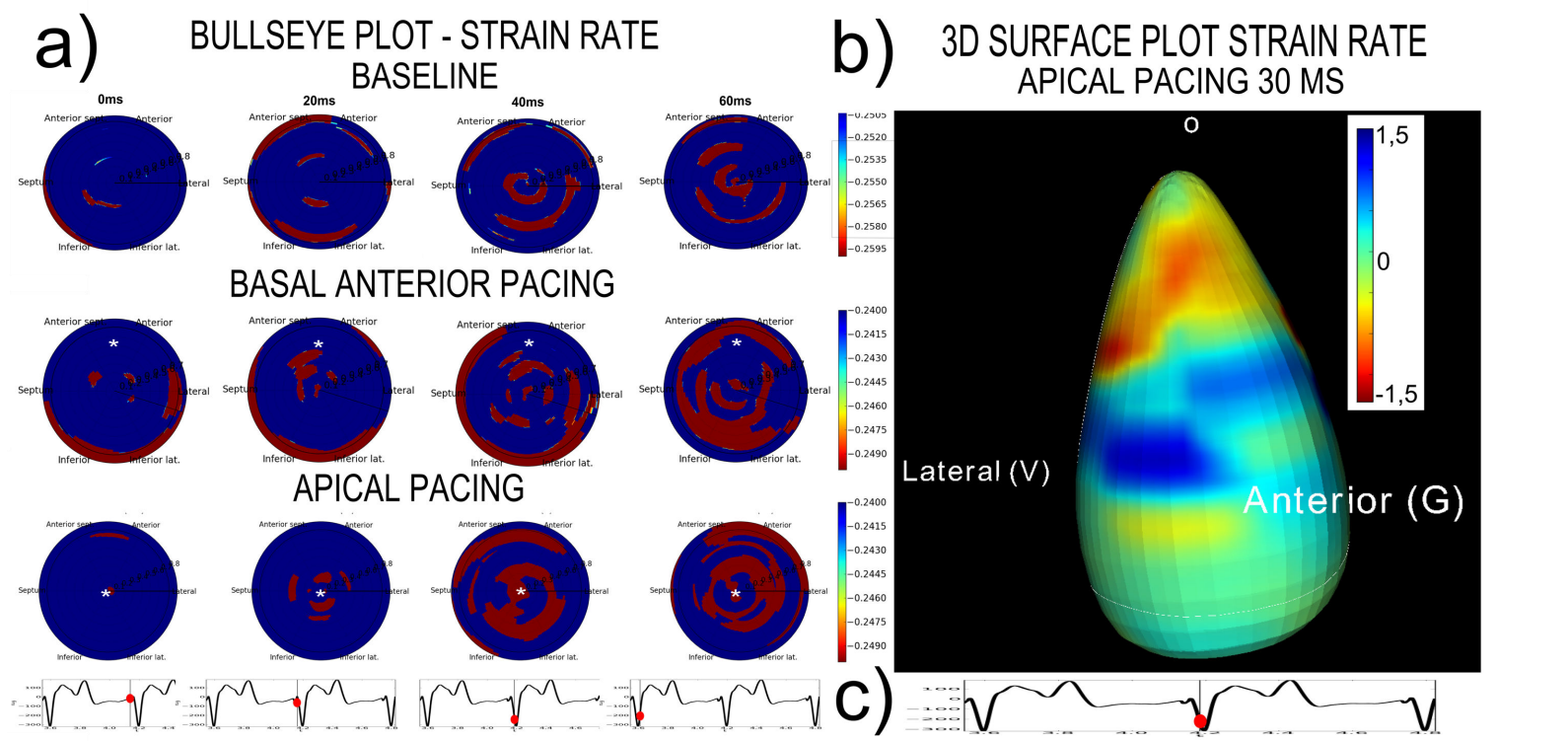
a)
BULLSEYE PLOT - STRAIN RATE
BASELINE
0ms
20ms
40ms
60ms
BASAL ANTERIOR PACING
APICAL PACING
b)
3D SURFACE PLOT STRAIN RATE
APICAL PACING 30 MS
1,5
0
-1,5
Lateral (V)
Anterior (G)
c)

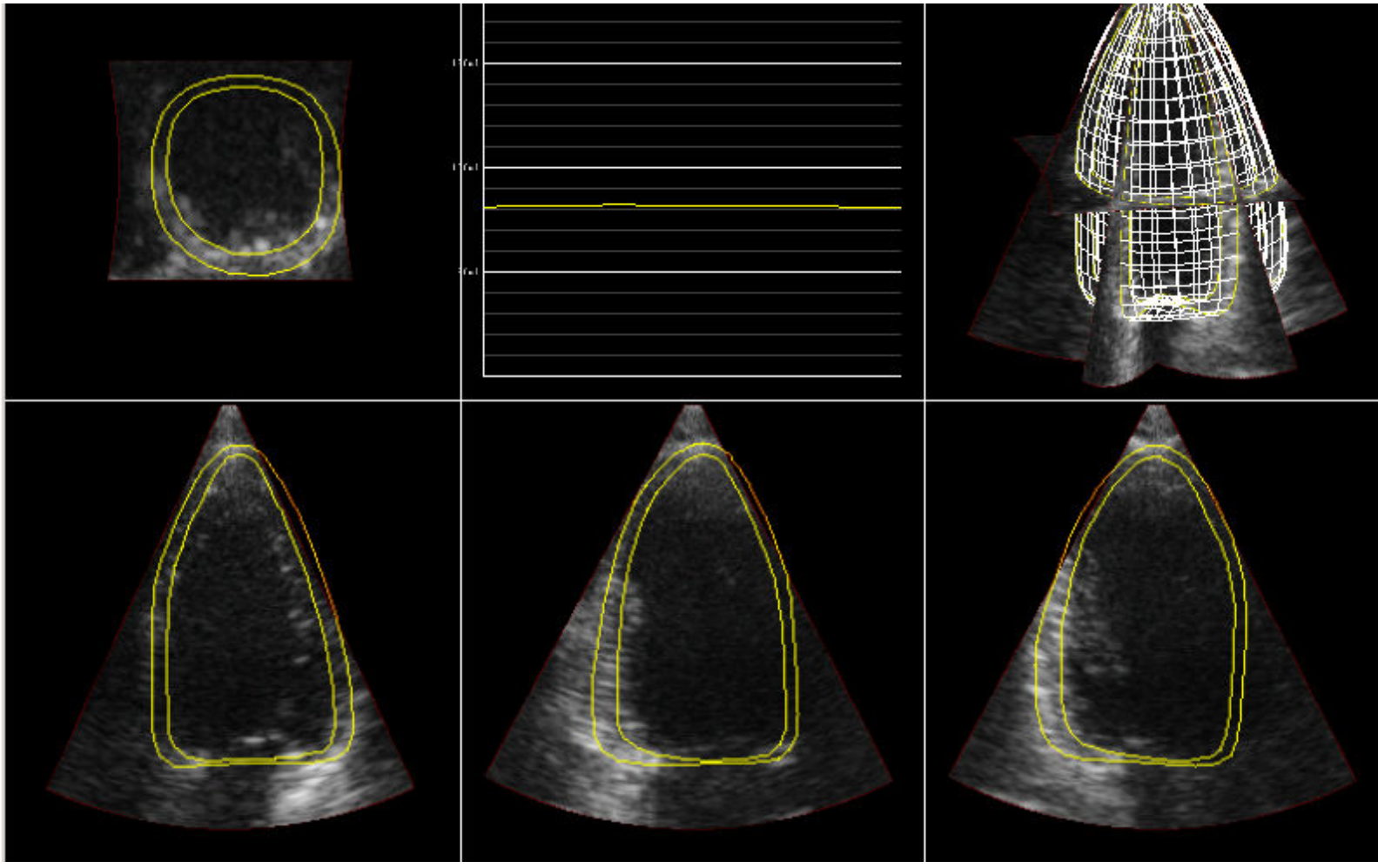

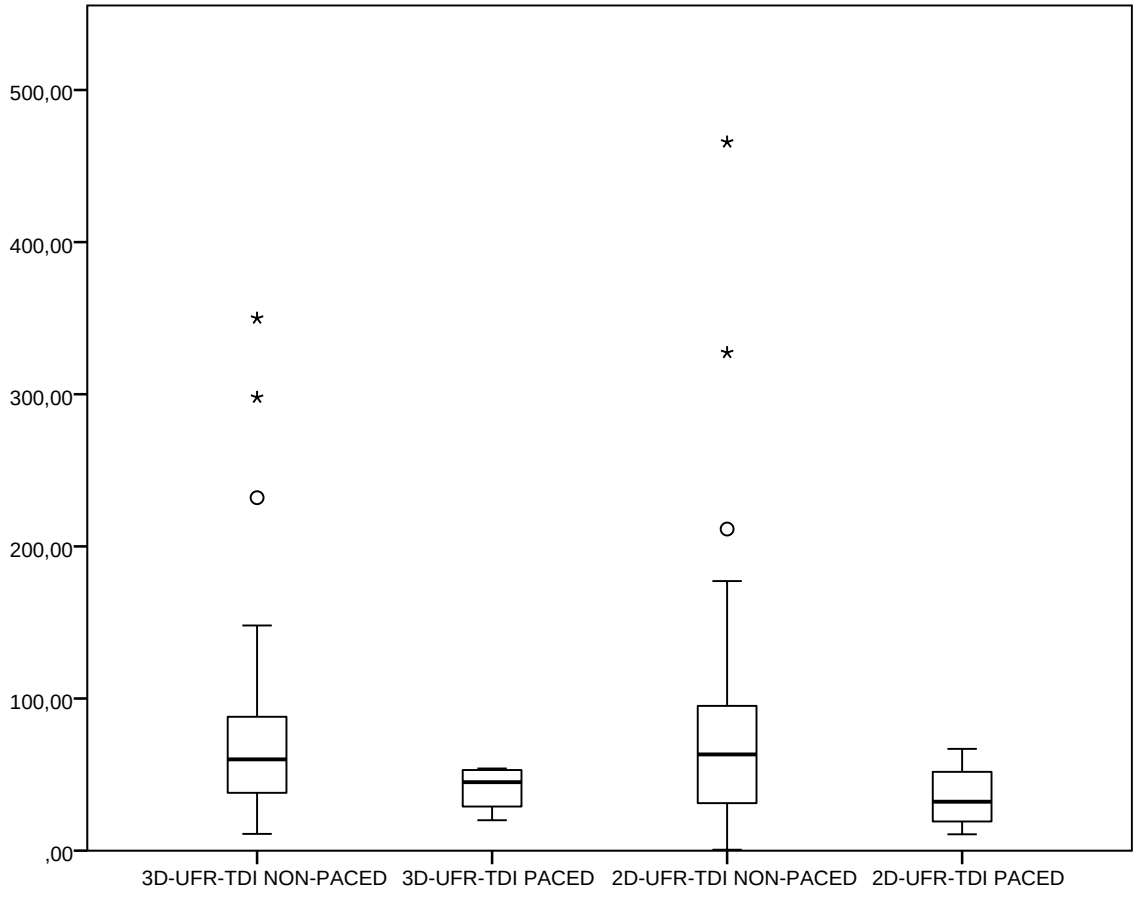
500,00
400,00
300,00
200,00
100,00
,00
3D-UFR-TDI NON-PACED
3D-UFR-TDI PACED
2D-UFR-TDI NON-PACED
2D-UFR-TDI PACED

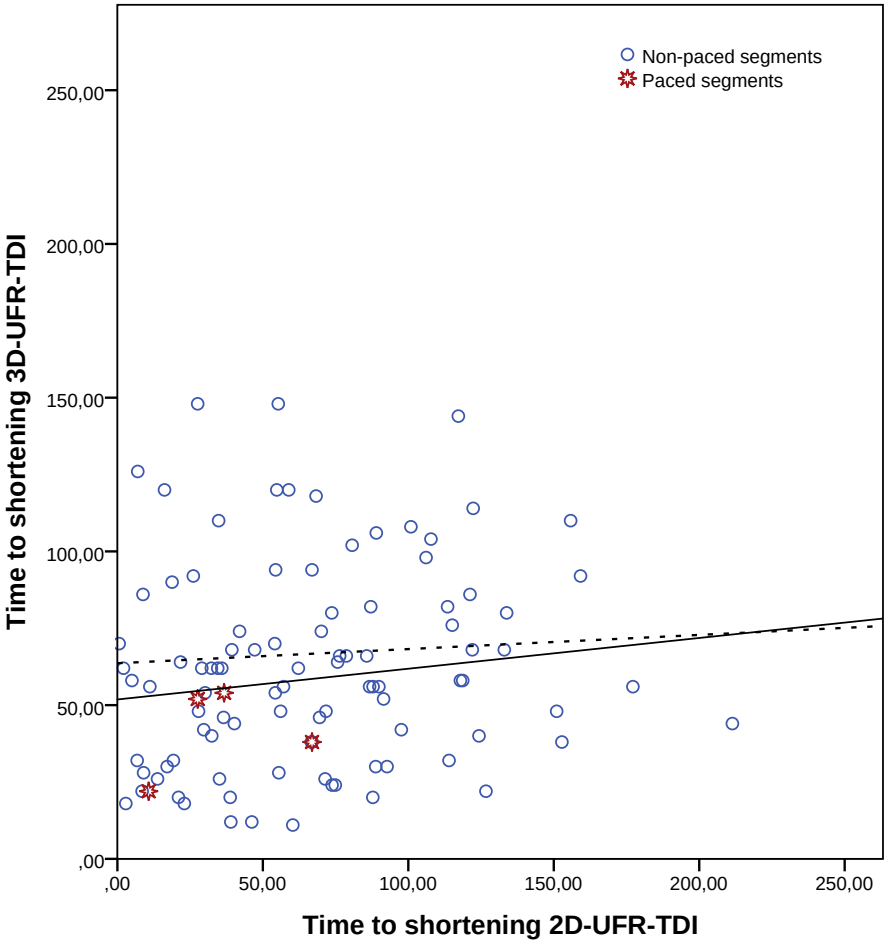
Non-paced segments
Paced segments
250,00
200,00
150,00
100,00
50,00
,00
Time to shortening 3D-UFR-TDI
,00
50,00
100,00
150,00
200,00
250,00
Time to shortening 2D-UFR-TDI

Appendix C

Paper III - Myocardial Strain Rate by Anatomic Doppler Spectrum: First Clinical Experience Using Retrospective Spectral Tissue Doppler from Ultra-High Frame Rate imaging

Ultrasound in Med. & Biol., Vol. 43, No. 9, pp. 1919–1929, 2017

0301-5629/$ - see front matter

http://dx.doi.org/10.1016/j.ultrasmedbio.2017.05.016

● *Original Contribution*

MYOCARDIAL STRAIN RATE BY ANATOMIC DOPPLER SPECTRUM: FIRST CLINICAL EXPERIENCE USING RETROSPECTIVE SPECTRAL TISSUE DOPPLER FROM ULTRA-HIGH FRAME RATE IMAGING

Lars Christian Naterstad Lervik,* Birger Brekke,* Svein Arne Aase,† Mai Tone Lønnebakken,‡ Dordi Stensvåg,§ Brage H. Amundsen,*¶ Hans Torp,* and Asbjorn Støylen*¶

*Department of Circulation and Medical Imaging, Norwegian University of Science and Technology, Trondheim, Norway; †GE Vingmed Ultrasound, Trondheim, Norway; ‡Department of Clinical Science, University of Bergen, Bergen, Norway; §Department of Radiology, St. Olav Hospital, Trondheim, Norway; and ¶Department of Cardiology, St. Olav Hospital, Trondheim, Norway

(*Received* 7 *December* 2016; *revised* 5 *May* 2017; *in final form* 15 *May* 2017)

Abstract—Strain rate imaging by tissue Doppler (TDI) is vulnerable to stationary reverberations and noise (clutter). Anatomic Doppler spectrum (ADS) presents retrospective spectral Doppler from ultra-high frame rate imaging (UFR-TDI) data for a region of interest, that is, ventricular wall or segment, at one time instance. This enables spectral assessment of strain rate (SR) without the influence of clutter. In this study, we assessed SR with ADS and conventional TDI in 20 patients with a recent myocardial infarction and 10 healthy volunteers. ADS-based SR correlated with fraction of scarred myocardium of the left ventricle ($r = 0.68, p < 0.001$), whereas SR by conventional TDI did not ($r = 0.23, p = 0.30$). ADS identified scarred myocardium and ADS Visual was the only method that differentiated transmural from non-transmural distribution of myocardial scar on a segmental level ($p = 0.002$). Finally, analysis of SR by ADS was feasible in a larger number of segments compared with SR by conventional TDI ($p < 0.001$). (E-mail: Lars.c.nilsen@ntnu.no) **© 2017 World Federation for Ultrasound in Medicine & Biology.**

Key Words: **Strain rate, Deformation imaging, Infarct diagnostics, Tissue Doppler imaging, Regional myocardial function, Retrospective spectral tissue Doppler, Anatomic Doppler spectrum, Ultra-high frame rate tissue Doppler imaging, Ultrafast cardiac imaging.**

INTRODUCTION

Regional myocardial function is important in assessment of coronary artery disease (Montalescot et al. 2013). The introduction of tissue Doppler imaging (TDI) (Isaaz et al. 1989) enabled estimation of myocardial velocities. Peak annular velocities proved to be a useful prognostic tool in patients with cardiovascular disease (Hoffmann et al. 2011). Tissue velocities are suitable for estimation of global myocardial function; however, as contracting myocardium will cause the neighboring tissue to move because of tethering (Heimdal et al. 1998b), differentiation between active and passive motion is a challenge. Such a limitation renders tissue velocity estimates less suitable for evaluation of regional myocardial function. This motivated the introduction of deformation imaging for quantification of regional left ventricular function (Heimdal et al. 1998b; Smiseth et al. 2004; Stoylen et al. 1999; Urheim et al. 2000; Voigt et al. 2000).

Strain and strain rate (SR) by TDI quantify relative wall deformation, that is, shortening and lengthening, and can be used for evaluation of regional myocardial function. As SR is an estimate of wall deformation rather than wall motion, it subtracts the effects of tethering (Heimdal et al. 1998a). SR is therefore more suitable for evaluation of regional function and viability than tissue velocities alone (Gjesdal et al. 2008; Jamal et al. 2001; Kaluzynski et al. 2001; Weidemann et al. 2003). SR can be estimated from tissue velocities by the velocity gradient in a given segment (Fleming et al. 1994) and represents deformation per unit of time.

The new Doppler acquisition method, ultra-high frame rate tissue Doppler imaging (UFR-TDI)

Address correspondence to: Lars Christian Naterstad Lervik, Department of Circulation and Medical Imaging, Norwegian University of Science and Technology, Postboks 8905, 7491 Trondheim, Norway. E-mail: Lars.c.nilsen@ntnu.no

(Brekke et al. 2014), enables acquisition of TDI data at a frame rate of 1200 frames/s. The method allows retrospective extraction of spectral TDI data from two ventricular walls simultaneously in an apical view (Figs. 1c and 2). Consequently, the Doppler spectrum along the ventricular wall from a given time point can be visualized in an anatomic Doppler spectrum (ADS) (Fig. 2c). This enables analysis of the spatial distribution of tissue velocities, that is, the velocity gradient along the ventricular wall, by tracing the spectral envelope in ADS (Fig. 2). The velocity gradient can be expressed as shortening per unit of time, that is, SR (Sagberg et al. 2004), and can be visualized and measured with ADS. As ADS allows visualization of the Doppler spectrum, it also enables separation of clutter and signal in the same manner as pulsed wave (PW) spectral Doppler (Fig. 1b). Because clutter will appear as low velocities near zero, signal can easily be separated from noise by ADS (Fig. 2), allowing estimation of SR without the influence of clutter. This potentially overcomes some of the limitations of SR from conventional TDI, which is vulnerable to noise and suffers from high variability (Ingul et al. 2005) caused by stationary reverberations (clutter) (Aase et al. 2008) (Fig. 3).

The aims of this study were therefore to investigate if SR by ADS can be used for detection of myocardial scar in patients who have had a myocardial infarction and to compare the number of segments feasible for analysis with ADS and conventional TDI. We also compared mitral annular velocities measured by ADS and PW spectral Doppler. Finally, we correlated our findings with myocardial scar detected with late gadolinium-enhanced magnetic resonance imaging (LGE-MRI).

METHODS

Study population

Ten healthy volunteers and 20 patients at least 3 wk past their first ST-elevation myocardial infarction (MI) were subsequently enrolled in the study. The inclusion criteria were age <75 y, peak troponin T > 1000 ng/L, estimated glomerular filtration rate >60 mL/min and New York Heart Association functional class <III. Exclusion criteria were previous MI, contraindications to MR contrast/ultrasound contrast, severe heart failure and chronic atrial fibrillation. No patients were excluded for poor echocardiographic quality. One patient was excluded from the analysis as the patient could not complete the LGE-MRI examination because of claustrophobia. All patients had been examined with acute coronary angiography, and percutaneous coronary intervention (PCI) was performed in all patients as appropriate during the acute phase. The control group consisted of 10 healthy volunteers. The control group was not examined with LGE-MRI. Population characteristics are outlined in Table 1. Informed consent was obtained from all study participants. The study was approved by the regional ethics committee for medical research ethics and conducted according to the Helsinki Declaration.

Echocardiographic acquisition

All echocardiographic data were acquired by experienced sonographers using a Vivid E9 with a M5S-D probe (GE Vingmed Ultrasound AS, Horten, Norway), and data were acquired from the three apical views (two-chamber, four-chamber and apical long-axis). Conventional TDI was analyzed in Echopac 112 (GE Vingmed Ultrasound AS).

Ultra-high frame rate tissue Doppler imaging

Ultra-high frame rate tissue Doppler imaging data were analyzed with in-house developed software in MATLAB 2011a (The MathWorks, Natick, MA, USA). UFR-TDI acquires TDI data at 1200 frames/s. The setup uses two wide transmit beams to cover the ventricular walls from the apical view. The transmit beams cover the two 20° outermost subsectors of the acquired sector. The sector width was manually adjusted to cover the left ventricular walls within the two subsectors.

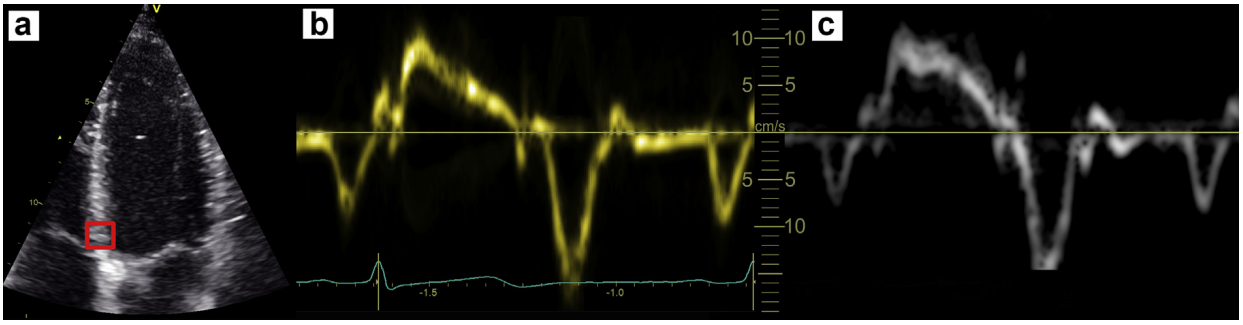

Fig. 1. (a) B-Mode with sample volume. (b) Conventional pulsed wave tissue Doppler from sample volume in (a). (c) Retrospective spectral Doppler from ultrahigh-frame-rate tissue Doppler imaging data from sample volume in (a).

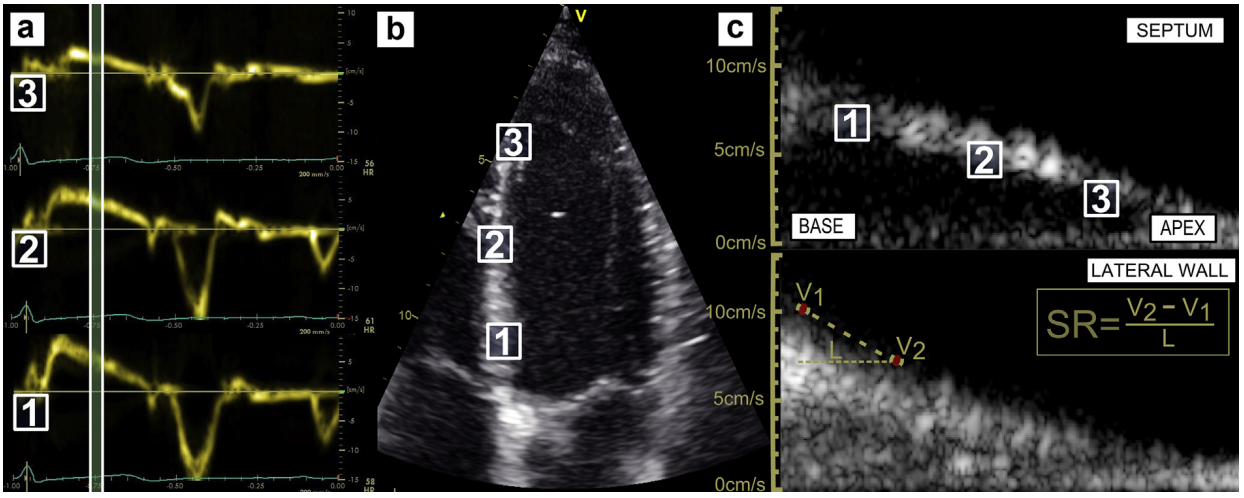

Fig. 2. Anatomic Doppler spectrum (ADS) in a healthy subject. (a) Pulsed wave spectral Doppler traces from the regions of interest indicated in (b). Midsystole, which is the time point used as basis for the ADS, is demarcated in green. (b) B-Mode, with regions of interest demarcated as 1, 2 and 3 respectively. (c) ADS from the septum and lateral wall of the same subject with regions of interest in (b) demarcated as 1, 2 and 3. The highest velocities are present at the base of the ventricle, and gradually become lower toward the apex. The slope of the spectral envelope represents the velocity gradient in the ventricular wall, and is used to determine strain rate in the segment of interest. This is illustrated with the formula $(V_2 - V_1)/L$. Signal can easily be separated from the stationary components around zero in the septum; however, in the lateral wall, signal can be separated from the stationary component around zero only by tracing the spectral envelope. V_1 = velocity 1; V_2 = velocity 2; L = segment length; SR = strain rate.

The method uses 16 receive lines for each wide transmit. Data from the ventricular cavity are not acquired. The setup is described in detail in Brekke et al. (2014). The velocity data from UFR-TDI can be visualized in a curved anatomic M-mode presenting tissue velocities (Fig.4), accelerations, deformation (strain or SR) or a Doppler spectrum (Fig. 1c). The analysis was performed blinded to patients' infarct status.

Anatomic Doppler spectrum

An ADS is constructed by calculating the spectral data for one time instance at all the spatial points along an anatomic curve drawn along the ventricular wall. It can be constructed in post-processing from UFR-TDI data. The spectral data were computed with a Hamming window of 100 ms. A Hamming window is an averaging technique that minimizes sidelobes. ADS allows

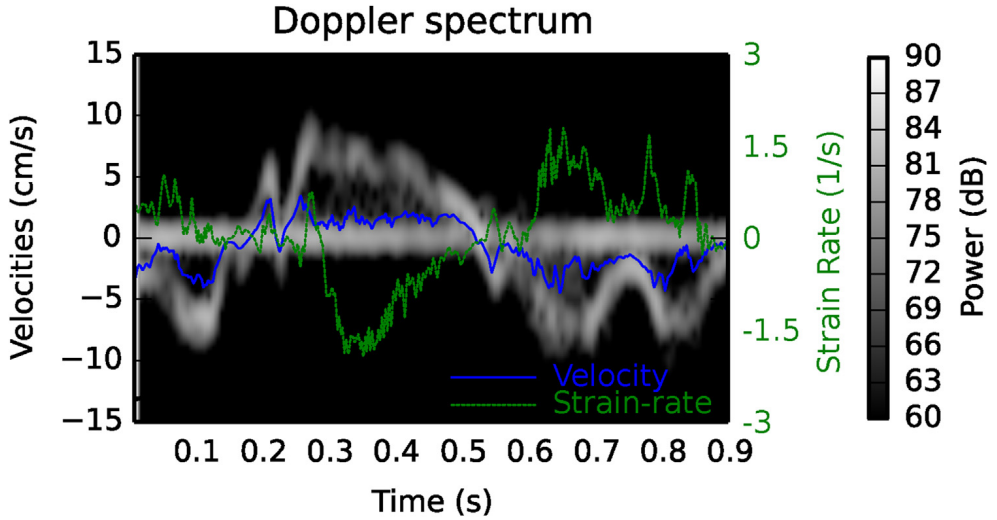

Fig. 3. Doppler spectrum with velocity (*blue*) and strain rate (*green*) estimations by autocorrelation from the basal septum. The Doppler spectrum was calculated with a window length of 30 ms. The velocity and strain rate measurements were estimated with plain autocorrelation. The velocity curve is biased toward the clutter signal, and the strain rate curve is noisy.

Table 1. Population characteristics

Characteristic	MI patients (n = 20)	Healthy volunteers (n = 10)
Mean age (y)	60 ± 5.9	34 ± 15.2
No. of males	18	10
Days from infarct to US examination	146 (21–356)	—
Days from infarct to LGE-MRI	296 (101–436)	—
Days from MR to ultrasound examination	135 (46–206)	—
Troponin T peak (ng/L)	5431 (1240–10,000)	—
Hypertension	25%	—
Single-vessel disease	50%	—
Culprit lesion		—
LAD	40%	—
CX	25%	—
RCA	35%	—
Current medication		—
Aspirin	100%	—
Clopidogrel/ticagrelor	100%	—
Beta blocker	85%	—
Statin	100%	—
ACEI/ARB	60%	—
Infarct size (LGE)	12.1 ± 4.9%	—
Left ventricular ejection fraction	56 ± 8%	54 ± 6%

LAD = left anterior descending coronary artery; CX = circumflex coronary artery; RCA = right coronary artery; ACEI = angiotensin converting enzyme inhibitor; ARB = angiotensin II receptor blockers; LGE-MRI = late gadolinium-enhanced magnetic resonance imaging; US = ultrasound.

visualization of the velocity gradient in the ventricular wall without the influence of reverberations by tracing the spectral envelope (Fig. 5c). SR was estimated from the velocity gradient in the region of interest (ROI), as illustrated in Figure 2c. A steep negative slope of the spectral envelope indicates rapid shortening (contraction) and was defined as normokinetic, a slight slope was defined as hypokinetic, no slope of the spectral envelope

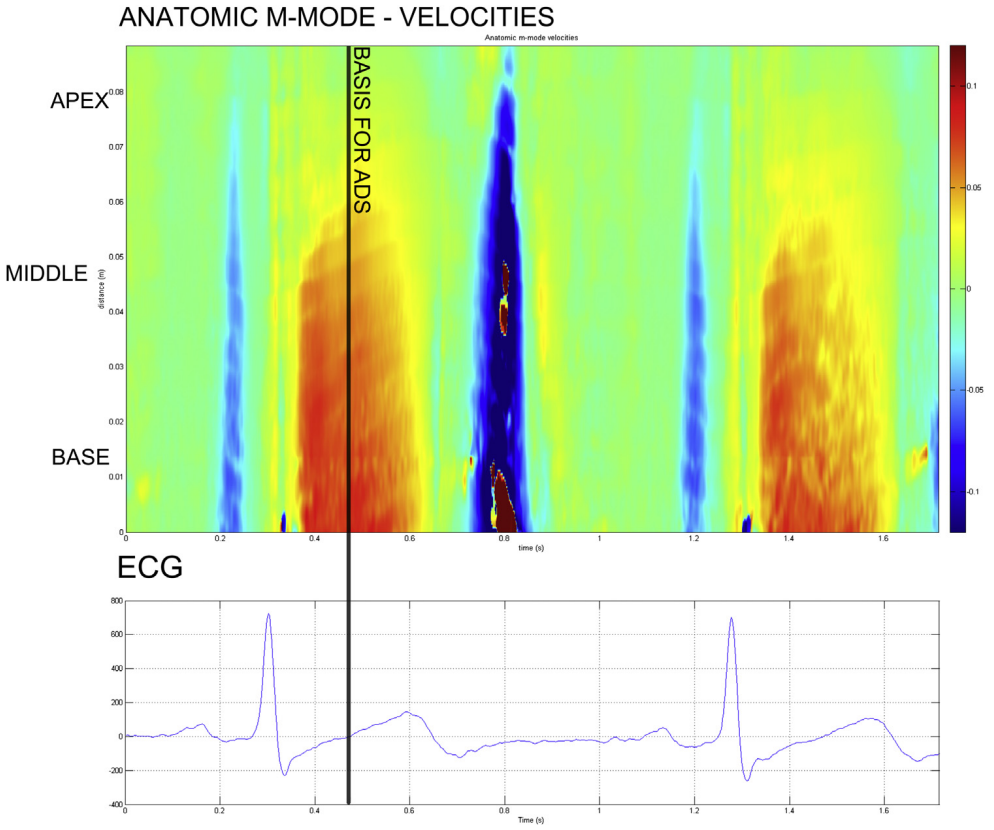

Fig. 4. Curved anatomic M-mode ultrahigh-frame-rate tissue Doppler imaging velocity data from the ventricular septum in a healthy volunteer. The midsystole is selected as basis for the anatomic Doppler spectrum. The scale for the color map is in meters per second.

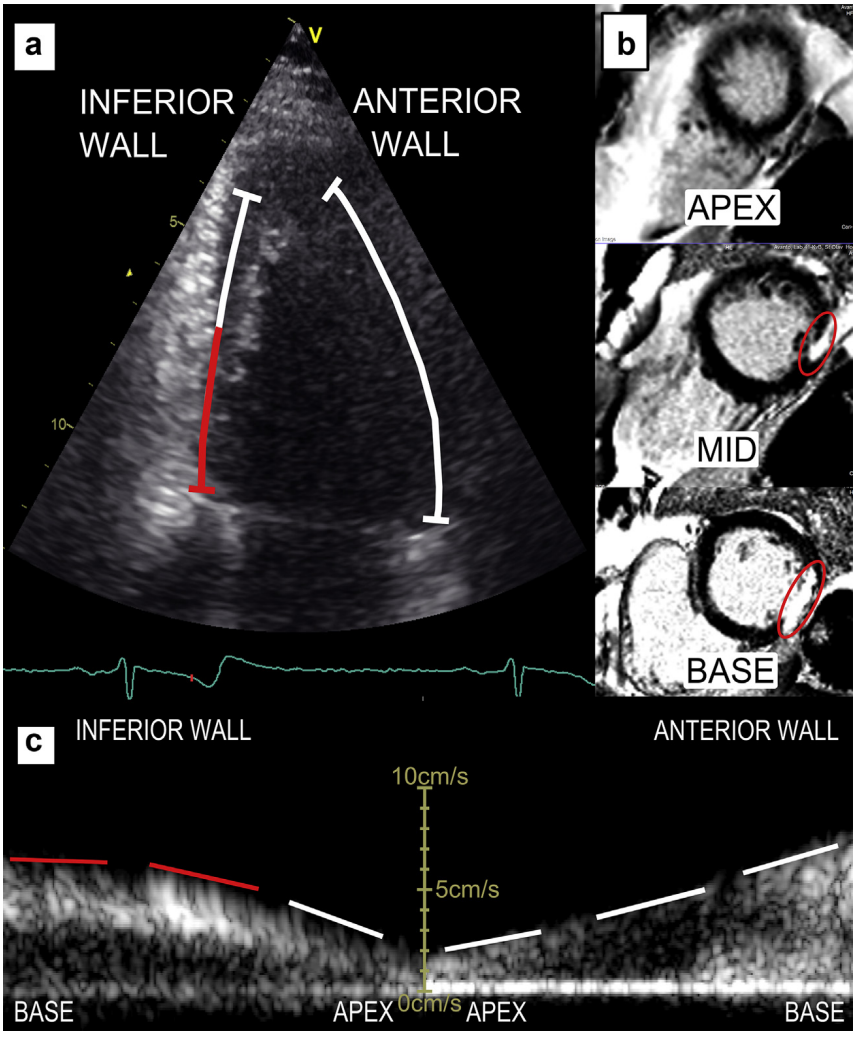

Fig. 5. Anatomic Doppler spectrum (ADS) from anterior and inferior wall in a patient with an inferior wall infarction. (a) B-Mode image and anatomic curve forming the basis for the ADS. (b) Late gadolinium-enhanced magnetic resonance image from the same patient. The infracted area is visible as enhanced scar in the basal and midventricular inferior wall (demarcated with *red ring*). (c) The ADS has nearly the same slope in all anterior segments, despite low signal (lung or bone shadow). In the inferior wall, there is almost no slope in the basal segment, reduced slope in the middle and normal slope in the apical segment. This corresponds to the scar distribution seen on the late gadolinium-enhanced magnetic resonance image to the right.

was defined as akinetic and a positive slope was defined as dyskinetic (lengthening). The ROI was adjusted to fit the segment of interest, ranging from 15 to 25 mm in length. The time of interest used for estimation of SR was midsystole. Midsystole is more reproducible than a peak value and has previously proved suitable for evaluation of myocardial function (Thorstensen et al. 2012). The analysis was comprised of the following steps:

1. An anatomic curve was drawn from the base to the apex of the ventricular wall. The wall definition was determined in UFR-TDI verified by conventional B-mode data (Fig. 5a).
2. A curved anatomic M-mode presenting tissue velocities was generated with UFR-TDI data from the anatomic curve described in step 1 (Fig. 4).
3. The time of interest was selected: midsystole for SR estimation and peak S' for comparison with PW velocities (Fig. 4).
4. ADS was constructed from the time of interest (Fig. 5c).

Care was taken to minimize the gain setting while maintaining a consistent spectral envelope. The measurements were done at the peak of the spectrum.

Echocardiograpic analysis

Strain rate was measured in an 18-segment model. For global parameters, 18 segments were adapted to a 16-segment model by averaging the apical segments antero- and inferoseptal and antero- and inferolateral, respectively; the mean of the 16 segments was then calculated.

Patients with >12 eligible segments were included in the analysis of global parameters. For *ADS SR Slope*, steps 1-4 under Anatomic Doppler Spectrum were used. The midsystolic slope of the spectral envelope in the segment of interest was measured, and SR was extracted (Fig. 5c). For *ADS SR Visual*, steps 1–4 were also used. The slope of the spectral envelope was visually assessed and scored on a scale from 1 to 4 (1 = normokinetic, 2 = hypokinetic, 3 = akinetic and 4 = dyskinetic).

Mitral annular velocities were measured to evaluate the accuracy of the new UFR-TDI method. For *ADS S′*, the time of peak *S′* was detected in UFR-TDI velocity curves from the septal and lateral mitral annuli, respectively; thereafter steps 1–4 described under Anatomic Doppler Spectrum were followed. Peak *S′* velocity was then measured at the septal and lateral mitral annuli in an ADS. For *PW TDI S′*, a 6-mm sample volume was placed at the septal and lateral mitral annuli. The peak systolic mitral annular velocities in the septum and lateral walls were measured. *Ejection fraction (EF)* was measured using the modified biplane Simpson method (four- and two-chamber views). The *peak systolic SR by TDI (TDI PSSR)* was measured in an 18-segment model from the apical two-chamber, four-chamber and long-axis views with conventional TDI. A sample volume of 6 × 12 mm was placed in the mid-myocardium in each segment; Gaussian smoothing of 40 ms was used. UFR-TDI was used for estimation of ADS SR Slope, ADS SR Visual and ADS *S′*. Conventional acquisition was used for PW TDI *S′*, EF and TDI PSSR.

Magnetic resonance image acquisition and analysis

The examinations were performed with a 1.5-T Siemens Avanto (Siemens Medical, Erlangen, Germany) with a six-channel radiofrequency coil. A gadolinium-based contrast agent, gadoterate meglumine (0.15 mmol/kg DOTAREM, Guerbet LLC, Bloomington, IN, USA) was then administered, and contrast-enhanced images were acquired 10 min later using a phase-sensitive inversion–recovery balanced steady-state free precession sequence (Lockie et al. 2009). A Look-Locker sequence was used to determine the appropriate T inversion time. First, a short-axis stack of the left ventricle was acquired (slice thickness 8 mm and interslice gap 2 mm), then long axis images were acquired (two-chamber, 4-chamber and long-axis views). The images were acquired during end-expiratory breath hold (10–15 s), in end-diastole before atrial contraction. Typical image parameters for gadolinium-enhanced acquisition were as follows: acquisition matrix, 256 × 127 pixels with in-plane resolution of 1.3 × 1.3 mm; 45° flip angle; inversion time, 290–310 ms. LGE-MRI was performed in 20 patients. The analysis was performed in Segment Version 1.9.r2959 (available at: http://segment.heiberg.se) (Cain et al. 2005; Heiberg et al. 2005). The myocardial and infarct borders were semi-automatically traced on each short-axis slice (Fig. 6). Short-axis slices on which myocardium occupied greater than two-thirds of the circumference were included in the analysis. Papillary muscles were excluded from the myocardial volume. An area with a pixel intensity 1.8 SD greater than that of the healthy myocardium was considered infarcted (Heiberg et al. 2008). The results were reported in a 16-segment model corresponding to the model used for ADS. The segments were divided in to three groups based on fraction of gadolinium-enhanced myocardium (LGE): 0%, 0–50% and >50% (Kim et al. 2000). The patients were divided based on median infarct size: <12% and >12% of total left ventricle mass.

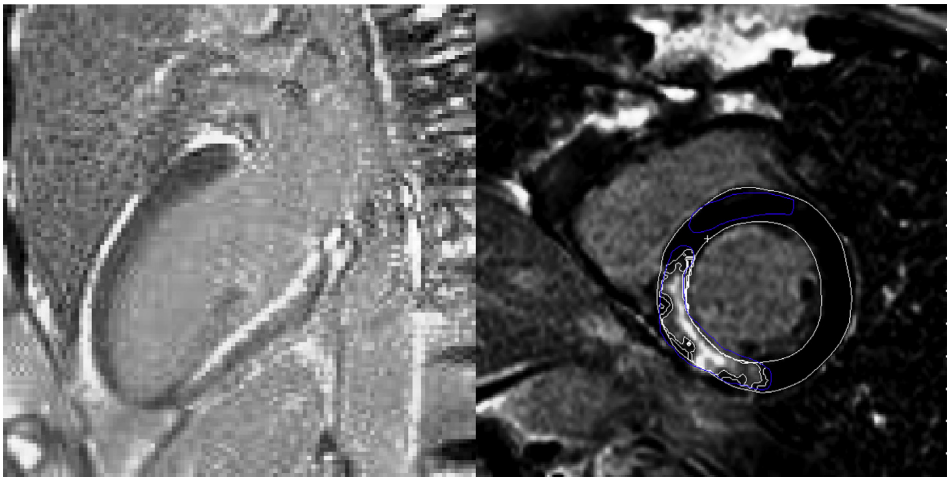

Fig. 6. Late gadolinium-enhanced magnetic resonance image of a patient who had a myocardial infarction. Semiautomatic scar detection in segment demarcated to the right.

Inter- and intra-observer reproducibility

A subset of 10 randomly selected patients (5 with infarcts and 5 healthy) were analyzed two times by L.C.N.L. Further, a randomly selected subset of 7 patients (5 with infarcts and 2 healthy) were analyzed by another observer, AS. The inter- and intra-observer reproducibility was analyzed.

Statistics

The comparison of means within segmental parameters and global parameters was performed with one-way analysis of variance (ANOVA) with a Bonferroni *post hoc* test. Homogeneity of variances was tested with Levene's test (Levene 1960). If homogeneity of variances could not be assumed, a Welch ANOVA with Games–Howell *post hoc* test was used. The correlation between global parameters (mean ADS SR Visual and mean ADS SR Slope) and myocardial infarct size was tested with Pearson's correlation coefficient. Cochran's *Q*-test was used to compare the proportions of segments analyzed by each method. Agreement between peak S' measurements obtained by the two methods was assessed with Bland–Altman analysis (Bland and Altman 1986). A p value < 0.05 was considered a marker of statistical significance. Values are expressed as the mean ± standard deviation or median (range). All statistical analyses were performed in SPSS Statistics for Windows, Version 19.0 (IBM, Armonk, NY, USA). Inter- and intra-observer reproducibility of ADS strain rate parameters was assessed according to Bland and Altman (1986), and is expressed as the coefficient of repeatability (COR). COR represents 1.96 × SD of mean inter- or intra-observer difference. Mean error was also estimated, and represents the absolute inter- and intra-observer difference divided by the parameter mean.

RESULTS

Segmental parameters

For the comparison of segments with different degrees of viable myocardium, we found that ADS SR Visual was the only method that could detect significant differences between the three categories of segmental scar (Table 2). All methods differed significantly between healthy and scarred myocardium.

Global parameters

When averaging the segmental measurements, ADS SR Visual, ADS SR Slope and Peak S' were significantly correlated with infarct size; TDI PSSR was not ($r = 0.68$, $p < 0.001$; $r = 0.50$, $p = 0.006$; $r = -0.56$, $p = 0.002$; and $r = 0.23$, $p = 0.30$). No method was able to differentiate differences between 0–12% LGE and >12% LGE. The results are summarized in Tables 3 and 4, and scatterplots are provided in Figure 7.

Peak systolic mitral velocities (S′) measured by PW Doppler and ADS

S' by PW TDI was 8.0 ± 2.3 cm/s, and by ADS, 7.6 ± 2.2 cm/s ($p = 0.04$). The data are presented in a Bland-Altman plot (Fig. 7). The mean difference was 0.35 cm/s, and the limits of agreement were −2.1 to 2.8 cm/s.

Late gadolinium-enhanced magnetic resonance imaging

Late gadolinium-enhanced MRI was performed in 19 patients; 304 segments were analyzed, of which 151 segments exhibited no infarcted tissue, 108 segments >0% to <50% infarcted tissue and 45 segments >50% infarcted tissue (Fig. 6). No segments were discarded from the analysis because of image quality. Mean left ventricular infarct size was 12.1 ± 4.9%. Scar tissue was identified in all patients.

Feasibility and reproducibility

The feasibility for use of the segmental ADS methods was better than the feasibility for use of TDI PSSR (ADS SR Slope 95%, ADS SR Visual 96%, TDI PSSR 87%; $Q[3] = 54.4$ $p < 0.001$). The inter- and intra-observer reproducibility of the ADS SR Slope measurements are listed in Table 5 and illustrated in Figure 8.

Table 2. Segmental parameters

Parameter	Healthy (n = 311)	0–50% LGE-MRI (n = 108)	>50% LGE-MRI (n = 45)
ADS SR Visual	1.20 ± 0.46*	1.51 ± 0.65†	1.88 ± 0.72
ADS SR Slope	−0.73 ± 0.35‡	−0.66 ± 0.45	−0.51 ± 0.43
TDI PSSR	−1.06 ± 0.49§	−0.92 ± 0.44	−0.91 ± 0.56

LGE-MRI = late gadolinium-enhanced magnetic resonance imaging; ADS SR Visual = anatomic Doppler spectrum visual midsystolic segmental strain rate; ADS SR Slope = anatomic Doppler spectrum midsystolic segmental strain rate; TDI PSSR = tissue Doppler imaging peak systolic strain rate.

Values are expressed as the mean ± standard deviation.

* Significantly different from 0–50% and >50% ($p < 0.001$).

† Significantly different from >50% ($p < 0.001$).

‡ Significantly different from >50% ($p = 0.002$).

§ Significantly different from 0–50% ($p = 0.48$).

Table 3. Global parameters

Parameter	Healthy (n = 10)	0-12% LGE-MRI (n = 10)	>12% LGE-MRI (n = 9)
Mean ADS SR Visual (n = 29)	1.03 ± 0.05*	1.48 ± 0.23	1.52 ± 0.23
Mean ADS SR Slope (n = 28)	−0.79 ± 0.09†	−0.67 ± 0.15	−0.60 ± 0.13
Mean TDI PSSR (n = 22)	−1.1 ± 0.22	−0.98 ± 0.13	−0.99 ± 0.26

LGE-MRI = late gadolinium-enhanced magnetic resonance imaging; ADS SR Visual = anatomic Doppler spectrum visual midsystolic segmental strain rate; ADS SR Slope = anatomic Doppler spectrum midsystolic segmental strain rate; TDI PSSR = tissue Doppler imaging peak systolic strain rate.

Values are expressed as the mean ± standard deviation.

* Significantly different from 0–12% and >12% ($p < 0.001$).

† Significantly different from >12% ($p = 0.008$).

DISCUSSION

In this study we demonstrated that SR by ADS was able to identify scarred myocardium and differentiate transmural from non-transmural distribution of myocardial scar on a segmental level. Furthermore, we found that analysis of SR by ADS was feasible in a larger number of segments compared with SR by conventional TDI. Tissue velocities measured by ADS indicate good accuracy compared with spectral Doppler velocity measurements by PW TDI, with a minor bias.

The display of spectral Doppler data has several advantages compared with analysis of velocity traces. As the entire spectrum of velocities rather than a weighted average can be visualized, data quality can easily be assessed. Furthermore, such visualization makes it possible to separate reverberation noise from signal from moving tissue. Finally, such spectral presentation of tissue velocity data makes estimation of the velocity gradient, that is, SR, feasible without the influence of noise, as it relies on tracing the spectral envelope, which remains visible in the presence of clutter (Fig. 2).

We correlated SR with scar tissue distribution determined by LGE-MRI. SR is a parameter of function rather than scar tissue. Dysfunction may be seen in peri-infarct areas, where scar is not detected by LGE-MRI. Therefore, LGE-MRI is suboptimal as a reference method in comparison to SR. However, LGE-MRI is the gold standard for imaging myocardial scar distribution, and as the extent of myocardial scarring correlates with reduced myocardial function (Jamal et al. 2002), it was chosen as reference method in this study. This may have contributed to the poor correlation between SR and scar at the segmental level. Both ADS methods exhibited significant correlations with LGE-MRI findings at the global level and between-group differences at the segmental level; however, the scatterplot revealed that there is a substantial variation in the measurements and that some of the large infarcts have high SRs. This indicates that there are still pitfalls to overcome with respect to SR by TDI and that SR remains a useful addition in an echocardiographic examination rather than its mainstay.

Table 4. Global correlation with LGE-MRI

Method	Pearson's correlation coefficient, r	p Value
LGE-MRI–mean ADS SR Visual	0.68	<0.001
LGE-MRI–mean ADS SR Slope	0.50	0.006
LGE-MRI–mean TDI PSSR	0.23	0.30
LGE-MRI–mean ADS S' (lateral and septal)	−0.56	0.002
LGE-MRI–mean PW S' (lateral and septal)	−0.56	0.002
LGE-MRI–ejection fraction	−0.3	0.1

LGE-MRI = late gadolinium-enhanced magnetic resonance imaging; ADS SR Visual = anatomic Doppler spectrum visual midsystolic segmental strain rate; ADS SR Slope = anatomic Doppler spectrum midsystolic strain rate; TDI PSSR = tissue Doppler imaging peak systolic strain rate; PW = pulsed wave.

Tissue Doppler imaging PSSR has previously exhibited a better correlation with transmurality of myocardial scar ($r = 0.63$ $p < 0.05$) (Zhang et al. 2005) compared with our findings ($r = 0.23$ $p = 0.30$). This difference may be a result of the variability of deformation by conventional TDI (Castro et al. 2000; Ingul et al. 2005), as well as misalignment of the LGE-MRI segments compared with ultrasound or poor image quality. Also, the infarcts investigated by Zhang et al. were larger than those in our study (5%–45% vs. 3%–21%), and they performed image acquisition within 6 d of infarct, potentially evaluating stunned myocardium. This differs from our study and may have contributed to the difference.

The results indicate that the semiquantitative method, ADS SR Visual, correlated better with scar than the quantitative methods, ADS SR Slope and TDI PSSR. This indicates that visual assessment of the Doppler spectrum might be superior to quantitative measurement of SR data. This is in line with previous studies in which semiquantitative methods were proven superior to quantitative methods (Voigt 2003). A possible explanation for

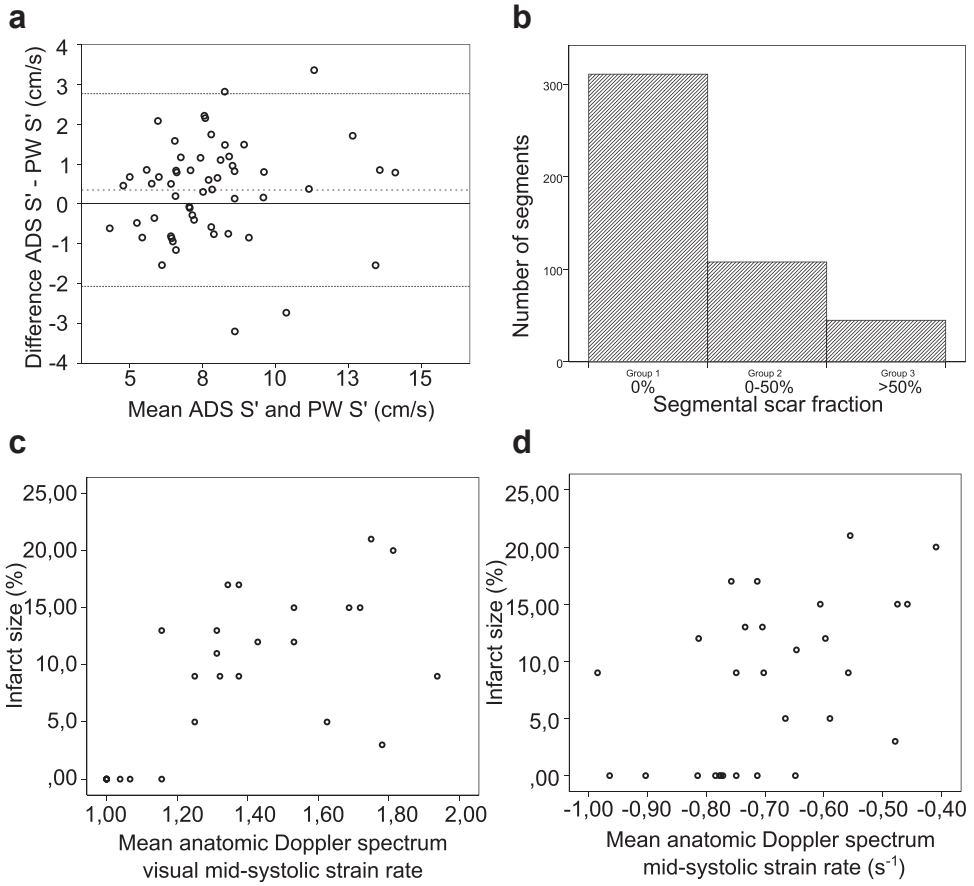

Fig. 7. (a) Bland–Altman plot: pulsed wave Doppler peak annular velocities (S') and anatomic Doppler spectrum (ADS). Peak annular velocities. (b) Segmental infarct fraction measured with late gadolinium-enhanced magnetic resonance imaging (LGE-MRI). y-Axis: number of segments, x-axis: different groups (group 1: 0%, group 2: 0–50%, group 3, >50% LGE-MRI). (c) Scatterplot with infarct size measured with LGE-MRI on y-axis and mean ADS SR Visual on the x-axis. (d) Scatterplot with infarct size measured with LGE-MRI on y-axis and mean ADS SR slope on the x-axis. SR = strain rate.

this could be that the semiquantitative assessment of the slope also allows visual assessment of the relative change in deformation between the adjacent segments in the same patient (Fig. 4). As there is a substantial variation in peak systolic SR by tissue Doppler, even in healthy patients selected with optimal image quality (Dalen et al. 2010), the quantitative reduction in deformation in ischemic myocardium with preserved contractile function may be hard to measure. A quantitative method does not take into account such between-patient variations and might therefore not be as suitable for evaluation of regional myocardial function as the semiquantitative approach.

Mitral annular velocities (peak S') was measured with ADS and PW TDI. There was a bias of 0.35 cm/s ($p = 0.04$). A possible explanation for this bias may be the length of the time window (*i.e.,* temporal smoothing) used for ADS (100 ms). A longer time window will reduce peak values (Gunnes et al. 2004).

The inter- and intra-observer COR and the mean error of global inter-observer ADS SR Slope measurements are

Table 5. Inter- and intra-observer data

Method	Mean	Mean difference ± SD	Limits of agreement (mean ± 1.96 SD)	COR	Mean error (%)
Inter-observer segmental ADS SR Slope	$-0.69\ s^{-1}$	0.070 ± 0.38	−0.68 to 0.82	0.76	42%
Inter-observer mean ADS SR Slope	$-0.71\ s^{-1}$	0.037 ± 0.05	−0.06 to 0.14	0.10	6%
Intra-observer segmental ADS SR Slope	$-0.75\ s^{-1}$	0.163 ± 0.31	−0.29 to 0.77	0.62	37%
Intra-observer mean ADS SR Slope	$-0.76\ s^{-1}$	0.172 ± 0.09	−0.01 to 0.35	0.18	22%

ADS SR Slope = anatomic Doppler spectrum midsystolic strain rate; SD = standard deviation; COR = Coefficient of repeatability.

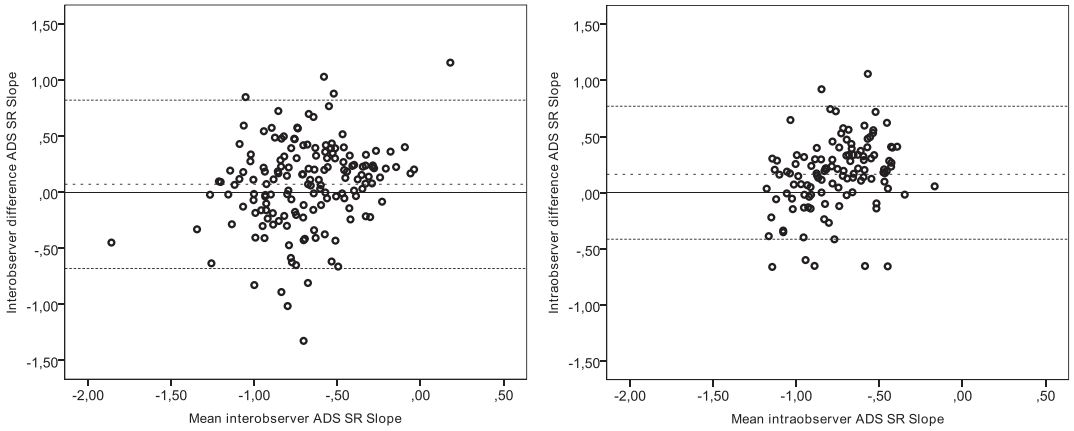

Fig. 8. Left: Bland–Altman plot for inter-observer ADS SR slope measurements. Right: Bland–Altmann plot for intra-observer ADS SR slope measurements. Units on the x- and y-axes on both left and right are s^{-1}. ADS = anatomic Doppler spectrum; SR = strain rate.

of the same order of magnitude as in previous findings (Thorstensen et al. 2010). The mean error of segmental ADS SR Slope and intra-observer global mean ADS SR Slope were, however, poorer (Thorstensen et al. 2010). The findings by Thorstensen et al. (2010) are based on speckle tracking rather than tissue Doppler and include healthy patients, which may explain some of the difference. Our findings are, however, of the same order of magnitude as described by Ingul et al. (2005), a study based on infarct patients and TDI strain rate data. Some of the variation in our findings may be attributed to the difference in the time point chosen as the basis for ADS; mid-systole is selected from an anatomic M-mode in a cine consisting of three cardiac cycles. Further, the differences in strain length and gain settings may also contribute to some variation in measurements.

Limitations

Anatomic Doppler spectrum represents velocities from a limited time window; events before or after the time of interest cannot be detected. Midsystole has, however, previously proven suitable for evaluation of infarct size (Thorstensen et al. 2012). The angle dependence of TDI also applies to ADS. The study has a small sample size, and the control group was not matched on age. The variation in time delay from infarction to image acquisition, and from LGE-MRI to ultrasound acquisition, is large; however, because image acquisition was performed after the acute phase, this should not introduce significant bias as the population had relatively small infarcts.

CONCLUSIONS

The anatomic Doppler spectrum can be used for quantitative and semiquantitative assessment of systolic SR. ADS allowed analysis of significantly more segments compared with TDI PSSR and was significantly correlated with myocardial scarring, whereas TDI PSSR was not. The results indicate that ADS could provide additional information when assessing SR by TDI, especially in patients with poor acoustic windows.

Acknowledgments—We appreciate valuable the comments on magnetic resonance analysis from P. Hala.—L.C.N.L., B.B. and B.H.A. are or were funded by the Medical Imaging Lab. The MI Lab was a Centre for Research-Based Innovation (SFI) appointed by the Research Council of Norway for the 8-y period 2007–2015. GE Vingmed was a partner in the MI Lab. S.A.A. is employed by GE Vingmed.

REFERENCES

Aase SA, Torp H, Amundsen BH, Bjåstad T, Støylen A. Peak systolic velocity by upper edge of pulsed wave tissue Doppler spectrums cause overestimation compared to M-mode in normal subjects. Eur J Echocardiogr 2008;9:S7–S8.

Bland JM, Altman D. Statistical methods for assessing agreement between two methods of clinical measurement. Lancet 1986;327: 307–310.

Brekke B, Nilsen LCL, Lund J, Torp H, Bjastad T, Amundsen BH, Stoylen A, Aase SA. Ultra-high frame rate tissue Doppler Imaging. Ultrasound Med Biol 2014;40:222–231.

Cain PA, Ugander M, Palmer J, Carlsson M, Heiberg E, Arheden H. Quantitative polar representation of left ventricular myocardial perfusion, function and viability using SPECT and cardiac magnetic resonance: Initial results. Clin Physiol Funct Imaging 2005;25: 215–222.

Castro PL, Greenberg NL, Drinko J, Garcia MJ, Thomas JD. Potential pitfalls of strain rate imaging: Angle dependency. Biomed Sci Instrum 2000;36:197–202.

Dalen H, Thorstensen A, Aase SA, Ingul CB, Torp H, Vatten LJ, Stoylen A. Segmental and global longitudinal strain and strain rate based on echocardiography of 1266 healthy individuals: The HUNT study in Norway. Eur J Echocardiogr 2010;11:176–183.

Fleming AD, Xia X, McDicken WN, Sutherland GR, Fenn L. Myocardial velocity gradients detected by Doppler imaging. Br J Radiol 1994;67:679–688.

Gjesdal O, Helle-Valle T, Hopp E, Lunde K, Vartdal T, Aakhus S, Smith HJ, Ihlen H, Edvardsen T. Noninvasive separation of large, medium, and small myocardial infarcts in survivors of reperfused ST-elevation myocardial infarction: A comprehensive tissue

Doppler and speckle-tracking echocardiography study. Circ Cardiovasc Imaging 2008;1:189–196.
Gunnes S, Storaa C, Lind B, Nowak J, Brodin LA. Analysis of the effect of temporal filtering in myocardial tissue velocity imaging. J Am Soc Echocardiogr 2004;17:1138–1145.
Heiberg E, Engblom H, Engvall J, Hedström E, Ugander M, Arheden H. Semi-automatic quantification of myocardial infarction from delayed contrast enhanced magnetic resonance imaging. Scand Cardiovasc J 2005;39:267–275.
Heiberg E, Ugander M, Engblom H, Götberg M, Olivecrona GK, Erlinge D, Arheden H. Automated quantification of myocardial infarction from MR images by accounting for partial volume effects: Animal, phantom, and human study. Radiology 2008;246:581–588.
Heimdal A, D'hooge J, Bijnens B, Sutherland G, Torp H. Effect of stationary reverberations and clutter filtering in strain rate imaging. 1998. IEEE Ultrason Symp Proc (Cat. No. 98CH36102). IEEE; 1998a. p. 1361–1364.
Heimdal A, Støylen A, Torp H, Skjærpe T. Real-time strain rate imaging of the left ventricle by ultrasound. J Am Soc Echocardiogr 1998b;11: 1013–1019.
Hoffmann S, Mogelvang R, Sogaard P, Iversen AZ, Hvelplund A, Schaadt BK, Fritz-Hansen T, Galatius S, Risum N, Biering-Sørensen T, Jensen JS. Tissue Doppler echocardiography reveals impaired cardiac function in patients with reversible ischaemia. Eur J Echocardiogr 2011;12:628–634.
Ingul CB, Torp H, Aase SA, Berg S, Stoylen A, Slordahl S. Automated analysis of strain rate and strain: Feasibility and clinical implications. J Am Soc Echocardiogr 2005;18:411–418.
Isaaz K, Thompson A, Ethevenot G, Cloez JL, Brembilla B, Pernot C. Doppler echocardiographic measurement of low velocity motion of the left ventricular posterior wall. Am J Cardiol 1989;64:66–75.
Jamal F, Kukulski T, Sutherland GR, Weidemann F, D'hooge J, Bijnens B, Derumeaux G. Can changes in systolic longitudinal deformation quantify regional myocardial function after an acute infarction? An ultrasonic strain rate and strain study. J Am Soc Echocardiogr 2002;15:723–730.
Jamal F, Strotmann J, Weidemann F, Kukulski T, D'hooge J, Bijnens B, Van de Werf F, De Scheerder I, Sutherland GR. Noninvasive quantification of the contractile reserve of stunned myocardium by ultrasonic strain rate and strain. Circulation 2001;104:1059–1065.
Kaluzynski K, Chen X, Emelianov SY, Skovoroda AR, O'Donnell M. Strain rate imaging using two-dimensional speckle tracking. IEEE Trans Ultrason Ferroelectr Freq Control 2001;48:1111–1123.
Kim RJ, Wu E, Rafael A, Chen EL, Parker MA, Simonetti O, Klocke FJ, Bonow RO, Judd RM. The use of contrast-enhanced magnetic resonance imaging to identify reversible myocardial dysfunction. N Engl J Med 2000;343:1445–1453.
Levene H. Robust tests for equality of variances. In: Olkin I, Ghurye SG, Hoeffding W, Madow WG, Mann HB, (eds). Contributions to probability and statistics: Essays in honor of Harold Hotelling. Stanford, CA: Stanford University Press; 1960. p. 278–292.
Lockie T, Nagel E, Redwood S, Plein S. Use of cardiovascular magnetic resonance imaging in acute coronary syndromes. Circulation 2009; 119:1671–1681.
Montalescot G, Sechtem U, Achenbach S, Andreotti F, Arden C, Budaj A, Bugiardini R, Crea F, Cuisset T, Di Mario C, Ferreira JR, Gersh BJ, Gitt AK, Hulot JS, Marx N, Opie LH, Pfisterer M, Prescott E, Ruschitzka F, Sabaté M, Senior R, Taggart DP, van der Wall EE, Vrints CJM, Zamorano JL, Baumgartner H, Bax JJ, Bueno H, Dean V, Deaton C, Erol C, Fagard R, Ferrari R, Hasdai D, Hoes AW, Kirchhof P, Knuuti J, Kolh P, Lancellotti P, Linhart A, Nihoyannopoulos P, Piepoli MF, Ponikowski P, Sirnes PA, Tamargo JL, Tendera M, Torbicki A, Wijns W, Windecker S, Valgimigli M, Claeys MJ, Donner-Banzhoff N, Frank H, Funck-Brentano C, Gaemperli O, Gonzalez-Juanatey JR, Hamilos M, Husted S, James SK, Kervinen K, Kristensen SD, Maggioni AP, Pries AR, Romeo F, Rydén L, Simoons ML, Steg PG, Timmis A, Yildirir A. 2013 ESC guidelines on the management of stable coronary artery disease. Eur Heart J 2013;34:2949–3003.
Sagberg E, Malm S, Ingul C, Torp H, Støylen A. Spatial velocity distribution for visualising velocity gradients. Feasibility and preliminary experience [poster]. Eur J Echocardiogr - Euroecho 2004;5(Issue Suppl 1):S152.
Smiseth OA, Stoylen A, Ihlen H. Tissue Doppler imaging for the diagnosis of coronary artery disease. Curr Opin Cardiol 2004;19: 421–429.
Stoylen A, Heimdal A, Bjornstad K, Torp HG, Skjaerpe T. Strain rate imaging by ultrasound in the diagnosis of regional dysfunction of the left ventricle. Echocardiography 1999;16:321–329.
Thorstensen A, Amundsen BH, Dalen H, Hala P, Kiss G, Aase SA, Torp H, Støylen A. Strain rate imaging combined with wall motion analysis gives incremental value in direct quantification of myocardial infarct size. Eur Heart J Cardiovasc Imaging 2012;13: 914–921.
Thorstensen A, Dalen H, Amundsen BH, Aase SA, Stoylen A. Reproducibility in echocardiographic assessment of the left ventricular global and regional function, the HUNT study. Eur J Echocardiogr 2010;11:149–156.
Urheim S, Edvardsen T, Torp H, Angelsen B, Smiseth OA. Myocardial strain by doppler echocardiography: Validation of a new method to quantify regional myocardial function. Circulation 2000;102: 1158–1164.
Voigt JU. Strain-rate imaging during dobutamine stress echocardiography provides objective evidence of inducible ischemia. Circulation 2003;107:2120–2126.
Voigt JU, Arnold MF, Karlsson M, Hübbert L, Kukulski T, Hatle L, Sutherland GR. Assessment of regional longitudinal myocardial strain rate derived from Doppler myocardial imaging indexes in normal and infarcted myocardium. J Am Soc Echocardiogr 2000; 13:588–598.
Weidemann F, Dommke C, Bijnens B, Claus P, D'hooge J, Mertens P, Verbeken E, Maes A, Van de Werf F, De Scheerder I, Sutherland GR. Defining the transmurality of a chronic myocardial infarction by ultrasonic strain-rate imaging: Implications for identifying intramural viability: An experimental study. Circulation 2003; 107:883–888.
Zhang Y, Chan AKY, Yu CMM, Yip GWK, Fung JWH, Lam WWM, So NMC, Wang M, Wu EB, Wong JT, Sanderson JE. Strain rate imaging differentiates transmural from non-transmural myocardial infarction: A validation study using delayed-enhancement magnetic resonance imaging. J Am Coll Cardiol 2005;46:864–871.

Appendix D

Paper IV - Color Tissue Doppler Imaging in Contrast Echocardiography - a Feasibility Study

Color Tissue Doppler Imaging in Contrast Echocardiography – a Feasibility Study

Mai Tone Lønnebakken, MD phd[a], Lars Christian Naterstad Lervik, MD[b], Asbjørn Støylen, MD phd[b].

[a]Department of Clinical Science, University of Bergen, Bergen, Norway and [b]Department of Circulation and Medical Imaging, Norwegian University of Science and Technology, Trondheim, Norway.

Running title: cTDI in Contrast Echocardiography

Corresponding author: Mai Tone Lønnebakken, MD phd,

Department of Clinical Science, University of Bergen

5021 Bergen

Norway

Phone: + 47 55 97 22 20

Fax: + 47 55 97 51 50

E-mail: Mai.Lonnebakken@uib.no

Word count: Abstract: 150 Total: 3233

Abstract

Color Tissue Doppler (cTD) Imaging (cTDI) and ultrasound contrast (UC) improves the diagnostic performance of echocardiography. UC might induce decorrelation of the cTD signals and enhancement of signals from the blood pool resulting in velocity overestimation. To assess the feasibility of cTDI during UC echocardiography, cTDI was performed before and repeated 10 minutes following an intravenous 2ml UC bolus injection in 20 patients with previous myocardial infraction. Longitudinal cTD velocities (S', e' and a') could be measured in 19 patients and 7% of LV segments had to be excluded due to poor image quality. There was no significant difference in longitudinal S', e' and a' prior to and after UC injection and the reproducibility were good with an intra-class correlation coefficient of 0.82, 0.85 and 0.89, respectively. This suggest that cTDI is feasible to perform after UC bolus injection.

Keywords: Color Tissue Doppler Imaging; Ultrasound contrast; Reproducibility; Contrast echocardiography.

Introduction

Ultrasound contrast (UC) is widely used during echocardiography to improve image interpretation, reproducibility, reader confidence and assess myocardial perfusion in patients with poor acoustic windows (Gonzalez-Gonzalez et al., 2014; Lonnebakken et al., 2009; Plana et al., 2008)(Larsson et al., 2016; Mulvagh et al., 2008; Senior et al., 2009). Color Tissue Doppler (cTDI), another advanced echocardiographic technique assessing regional myocardial velocity and hence regional myocardial function has also been demonstrated to improve the detection of myocardial dysfunction (Lang et al., 2015) . Combining these echocardiographic modalities may contribute to further optimization of echocardiographic assessment. However, previous studies combining cTDI and UC has been disappointing and the combination of UC and cTDI has in general not been recommended (Malm et al., 2006; Ressner et al., 2006; Ressner, Jansson, Cedefamn, Ask, & Janerot-Sjoberg, 2009). It has been suggested that decorrelation of the cTDI signals and the enhancement of signals from the blood pool by UC cause velocity overestimation (Gutberlet, Venz, Zendel, Hosten, & Felix, 1998; Logallo, Fromm, Waje-Andreassen, Thomassen, & Matre, 2014; Ressner et al., 2006; Ressner et al., 2009). Whether this can be avoided by 10 minutes of continuous ultrasound scanning to increase UC destruction will have important clinical implications, contribute to a more appropriate use of UC and improve the diagnostic performance of echocardiography.

Accordingly, in this study we tested the feasibility of performing cTDI during contrast echocardiography by assessing the reproducibility of cTD velocity signals after UC injection and 10 minutes of continuous ultrasound scanning.

Methods

Patient population

A total of 20 consecutive patients with first time ST-elevation myocardial infarction at least 4 weeks before, were included in the study. One patient had to be excluded from the analysis due to technical problems with the ultrasound scanner not allowing image acquisition after UC injection, leaving 19 patients for this analysis. All patients had been examined with acute coronary angiography, and percutaneous coronary intervention performed as appropriate during the acute phase. Patients with in-compensated heart failure, arrhythmias, severe valvular heart disease, mechanical valve prosthesis, severe pulmonary disease, renal failure or known allergy to the contrast agent used were excluded. All patients signed an informed consent to participate in the study. The study was approved by the regional ethical committee and performed in accordance with the Helsinki declaration.

Echocardiography

Echocardiography was performed using a Vivid E9 scanner (GE Vingmed, Horten, Norway) and a M5S-D probe (GE Vingmed, Horten, Norway). Apical 4-chamber view was used for image acquisition. cTDI was performed and 2 heart cycles were digitally stored for post-processing. After an intravenous injection of a 2 ml bolus of UC, SonoVue® (Bracco, Italy) and flushed by 10 ml of saline in a peripheral antecubital vein, followed by 10 minutes of continuous ultrasound scanning with a mechanical index (MI) of 0.8, a new cTD acquisition in the apical 4-chamber view including 2 heart cycles was performed and stored.

Following the joint European Association of Echocardiography and American Society of Echocardiography recommendations for left ventricular segmentation (Lang et al., 2015) and to avoid random noise, only the 2 basal and 2 mid LV segments in the apical 4-chamber view was analysed using the Echopac working station (GE Vingmed, Horten, Norway). Longitudinal cTD velocities, S', e' and a' was assessed in the 4 different LV segments in 2 consecutive heart beats prior to and following UC injection by two independent readers blinded to each other's results (MTL and LCNL) (Figure 1).

Statistics

IBM SPSS 23.0 software (IBM Corporation, Armonk, New York, USA) was used for data management and analysis. Continuous variables are presented as mean ± standard deviations (SD) and categorical variables as percentages. cTD velocities prior to and after contrast injection are compared using paired t-test. Equality of variance of cTD velocities before and after UC was tested by Levine's test. Intra- and inter-observer reproducibility of velocity measurements before UC, after UC and between measurements before and after UC was tested by intraclass correlations and presented as Bland-Altman plots.

Results

Study population

All patients had previous ST-elevation myocardial infarction, in which 50% had single vessel disease by coronary angiography. The infarct localisation was in the inferior wall in 50 % and in the anterior wall in 40%. There was abnormal wall motion by contrast echocardiography in 75% of the patients (Table 1). Additional patients' baseline characteristics are presented in Table 1.

In 7% of LV segments image quality did not allow cTD velocity measurement and had to be excluded from the analysis, the number of segments with poor image quality did not differ prior and after UC injection.

Intra- and inter-observer cTD reproducibility

The intra-observer reproducibility for the different cTDI measurements is presented in Table 2 and as a Bland-Altmans plot (Figure 2). The intraclass correlation coefficient of absolute agreement for repeated measurement of a single reader is excellent for all measurements both before and after UC injection (Table 2). In addition, the equality of variance was confirmed by the Levines' test both prior and after UC injection (p=ns).

Inter- observer reproducibility was good for S', e' and a' without significant differences in the measurements between the 2 readers(Table 3). However, the intraclass correlation coefficient for absolute agreement was poor but did not differ after introduction of UC (Table 3). The inter-observer reproducibility is presented as a Bland-Altman plot (Figure 3).

Reproducibility and variability between pre- and post-contrast cTDI measurements

The reproducibility of S', e' and a' measurement were optimal, there were no significant difference in the measurements prior to and 10 minutes after contrast injection (Table 4), and presented as a Bland Altman plot or a scatter plot ved correlations line in Figure 4. The intraclass correlation is also good (Table 4).

Discussion

The main finding is that in cTDI is feasible with good reproducibility after injection of UC and 10 minutes of continuous scanning. The clinical importance of our findings are underlined by the fact that according to current recommendations, UC should be added to improve left ventricular endocardial boarder delineation during echocardiography if ≥2 left ventricular segments could not be adequately visualized (Senior et al., 2009). Even though, UC is widely used in clinical echocardiography (Larsson et al., 2016; Senior et al., 2009) , a significant underuse of UC is reported from clinical practice. Consequently, the ability to assess cTDI after adding UC may contribute to improve diagnostic sensitivity and confidence during echocardiography and promote adherence to current recommendations.

However, previous experimental and clinical studies have documented that UC biases the autocorrelation phase shift of cTD velocity measurements, causing velocity overestimation (Malm et al., 2006; Ressner et al., 2006; Ressner et al., 2009). Also, as blood flow velocities are on the order of ten times tissue velocities, contrast-enhancing blood will

tend to increase the velocities in the receiver beams (Yokoyama et al., 2003). When velocities are used for deformation measurements, any increased variability will be magnified even more (Ressner et al., 2006). Consequently, UC has been regarded as rendering cTD velocity measurements unfeasible. In an ordinary echocardiography protocol, this can be solved by doing cTDI acquisitions before using contrast. In stress echocardiography, however, repeated acquisitions are necessary, and residual UC from baseline may affect cTDI recordings at peak stress. Recently, Nagy et al., report that both cTDI and speckle tracking based myocardial deformation imaging is feasible during contrast DSE (Nagy et al., 2015). This is in line with our findings. Further, our study adds to this by directly demonstrating a good reproducibility of cTD velocity measurement comparing tissue velocities before UC injection and 10 minutes after UC injection followed by continuous ultrasound scanning to potentiate UC destruction. These findings may give implications for concomitant use of UC and c TDI during DSE. cTD velocity measurements included in a DSE protocol has been demonstrated to improve the diagnostic performance of stress echocardiography to detect angiographic stenosis (Fujimoto et al., 2010; Ingul et al., 2007; Madler et al., 2003; Thorstensen, Dalen, Amundsen, Aase, & Stoylen, 2010). According to previous studies, reproducibility of cTD velocity measurements is good (Dalen, Thorstensen, Vatten, Aase, & Stoylen, 2010; Thorstensen et al., 2010), and the intra- and inter-observer reproducibility of this study was in line with these finding both prior to and 10 minutes after UC injection.

Whether cTDI can contribute to improve diagnosis in ischemic heart disease is mostly limited by image quality. Poor image quality and noise, in particularly in the apical and inferior wall of LV, may cause misinterpretation. When comparing reproducibility of cTD velocity measurements after UC, we therefore excluded LV regions known to be most prone to noise, and assessed velocities only in the mid- and basal 4 LV segments in the 4-chamber view (inferoseptal and anterolateral wall). It must be remarked, however, that cTDI is

generally vulnerable to noise, especially clutter. This means that in patients where UC is used due to image quality, it is less probable that cTDI will add anything.

Study limitations

This is a feasibility study with few participants, and, the results need to be confirmed in a larger study. Further, the study should be performed during an DSE protocol. The diagnostic impact of adding cTD velocity measurements in a contrast DSE protocol needs to be further explored. This study does not include analysis of deformation parameters, and implications about deformation parameters (ie strain and strain rate) cannot be made.

Conclusion

cTD velocities did not differ significantly 10 minutes after UC injection and continuous scanning, and had good reproducibility. This suggests that cTDI is feasible to include during contrast echocardiography, however, the diagnostic and clinical impact of performing cTD velocity assessment during contrast echocardiography needs further research.

Acknowledgements

Financial support was obtained from the MedViz Consortium, a collaboration between University of Bergen, Haukeland University Hospital and Christian Michelsen Research, Bergen, Norway, without any involvement in study design, collection, analysis or interpretation of data, writing the report, or in the decision to submit the article for publication. Lervik was funded by MI Lab. MI Lab was a Centre for Research-based Innovation (SFI) appointed by the Research Council of Norway for the 8-year period 2007-2015. GE Vingmed was a partner in MI-Lab.

Reference List

Dalen, H., Thorstensen, A., Vatten, L. J., Aase, S. A., & Stoylen, A. (2010). Reference values and distribution of conventional echocardiographic Doppler measures and longitudinal tissue Doppler velocities in a population free from cardiovascular disease. *Circ. Cardiovasc. Imaging, 3*(5), 614-622. doi:CIRCIMAGING.109.926022 [pii];10.1161/CIRCIMAGING.109.926022 [doi]

Dolan, M. S., Riad, K., El-Shafei, A., Puri, S., Tamirisa, K., Bierig, M., . . . Labovitz, A. J. (2001). Effect of intravenous contrast for left ventricular opacification and border definition on sensitivity and specificity of dobutamine stress echocardiography compared with coronary angiography in technically difficult patients. *Am Heart J, 142*(5), 908-915. doi:10.1067/mhj.2001.117608

Elhendy, A., O'Leary, E. L., Xie, F., McGrain, A. C., Anderson, J. R., & Porter, T. R. (2004). Comparative accuracy of real-time myocardial contrast perfusion imaging and wall motion analysis during dobutamine stress echocardiography for the diagnosis of coronary artery disease. *J Am Coll Cardiol, 44*(11), 2185-2191. doi:10.1016/j.jacc.2004.08.059

Fujimoto, H., Honma, H., Ohno, T., Mizuno, K., & Kumita, S. (2010). Longitudinal Doppler strain measurement for assessment of damaged and/or hibernating myocardium by dobutamine stress echocardiography in patients with old myocardial infarction. *J. Cardiol, 55*(3), 309-316. doi:S0914-5087(10)00009-2 [pii];10.1016/j.jjcc.2009.12.013 [doi]

Gonzalez-Gonzalez, A. M., Drakopoulou, M., Bhattacharyya, S., Chahal, N., Li, W., Roussin, I., . . . Shah, B. (2014). 144 The Incremental Prognostic Value of Myocardial Contrast Echocardiography in Clinical Practice: Follow-up Results from the Impact of Myocardial Perfusion Assessment in Clinical Tests of Stress Echocardiography (IMPACT-SE) Study. *Heart, 100 Suppl 3*, A84. doi:heartjnl-2014-306118.144 [pii];10.1136/heartjnl-2014-306118.144 [doi]

Gutberlet, M., Venz, S., Zendel, W., Hosten, N., & Felix, R. (1998). Do ultrasonic contrast agents artificially increase maximum Doppler shift? In vivo study of human common carotid arteries. *J Ultrasound Med, 17*(2), 97-102.

Ingul, C. B., Stoylen, A., Slordahl, S. A., Wiseth, R., Burgess, M., & Marwick, T. H. (2007). Automated analysis of myocardial deformation at dobutamine stress echocardiography: an angiographic validation. *J. Am. Coll. Cardiol, 49*(15), 1651-1659. doi:S0735-1097(07)00434-2 [pii];10.1016/j.jacc.2007.01.059 [doi]

Lang, R. M., Badano, L. P., Mor-Avi, V., Afilalo, J., Armstrong, A., Ernande, L., . . . Voigt, J. U. (2015). Recommendations for cardiac chamber quantification by echocardiography in adults: an update from the American Society of Echocardiography and the European Association of Cardiovascular Imaging. *J Am Soc Echocardiogr, 28*(1), 1-39.e14. doi:10.1016/j.echo.2014.10.003

Larsson, M. K., Da Silva, C., Gunyeli, E., Ilami, A. A., Szummer, K., Winter, R., & Bjallmark, A. (2016). The potential clinical value of contrast-enhanced echocardiography beyond current recommendations. *Cardiovasc Ultrasound, 14*(1), 2. doi:10.1186/s12947-015-0045-0

Logallo, N., Fromm, A., Waje-Andreassen, U., Thomassen, L., & Matre, K. (2014). Effect of microbubble contrast on intracranial blood flow velocity assessed by transcranial Doppler. *J Ultrasound, 17*(1), 21-26. doi:10.1007/s40477-014-0065-x

Lonnebakken, M. T., Bleie, O., Strand, E., Staal, E. M., Nygard, O. K., & Gerdts, E. (2009). Myocardial contrast echocardiography in assessment of stable coronary artery disease at intermediate dobutamine-induced stress level. *Echocardiography, 26*(1), 52-60. doi:10.1111/j.1540-8175.2008.00738.x

Madler, C. F., Payne, N., Wilkenshoff, U., Cohen, A., Derumeaux, G. A., Pierard, L. A., . . . Fraser, A. G. (2003). Non-invasive diagnosis of coronary artery disease by quantitative stress echocardiography: optimal diagnostic models using off-line tissue Doppler in the MYDISE study. *Eur. Heart J, 24*(17), 1584-1594. doi:S0195668X0300099X [pii]

Malm, S., Frigstad, S., Stoylen, A., Torp, H., Sagberg, E., & Skjarpe, T. (2006). Effects of ultrasound contrast during tissue velocity imaging on regional left ventricular velocity, strain, and strain rate measurements. *J. Am. Soc. Echocardiogr, 19*(1), 40-47. doi:S0894-7317(05)00670-X [pii];10.1016/j.echo.2005.07.017 [doi]

Mulvagh, S. L., Rakowski, H., Vannan, M. A., Abdelmoneim, S. S., Becher, H., Bierig, S. M., … Zoghbi, W. A. (2008). American Society of Echocardiography Consensus Statement on the Clinical Applications of Ultrasonic Contrast Agents in Echocardiography. *Journal of the American Society of Echocardiography*, *21*(11), 1179–1201. http://doi.org/10.1016/j.echo.2008.09.009

Nagy, A. I., Sahlen, A., Manouras, A., Henareh, L., da Silva, C., Gunyeli, E., . . . Winter, R. (2015). Combination of contrast-enhanced wall motion analysis and myocardial deformation imaging during dobutamine stress echocardiography. *Eur Heart J Cardiovasc Imaging, 16*(1), 88-95. doi:10.1093/ehjci/jeu171

Plana, J. C., Mikati, I. A., Dokainish, H., Lakkis, N., Abukhalil, J., Davis, R., . . . Zoghbi, W. A. (2008). A randomized cross-over study for evaluation of the effect of image optimization with contrast on the diagnostic accuracy of dobutamine echocardiography in coronary artery disease The OPTIMIZE Trial. *JACC Cardiovasc Imaging, 1*(2), 145-152. doi:10.1016/j.jcmg.2007.10.014

Ressner, M., Brodin, L. A., Jansson, T., Hoff, L., Ask, P., & Janerot-Sjoberg, B. (2006). Effects of ultrasound contrast agents on Doppler tissue velocity estimation. *J. Am. Soc. Echocardiogr, 19*(2), 154-164. doi:S0894-7317(05)00845-X [pii];10.1016/j.echo.2005.09.025 [doi]

Ressner, M., Jansson, T., Cedefamn, J., Ask, P., & Janerot-Sjoberg, B. (2009). Contrast biases the autocorrelation phase shift estimation in Doppler tissue imaging. *Ultrasound Med. Biol, 35*(3), 447-457. doi:S0301-5629(08)00434-1 [pii];10.1016/j.ultrasmedbio.2008.09.012 [doi]

Senior, R., Becher, H., Monaghan, M., Agati, L., Zamorano, J., Vanoverschelde, J. L., & Nihoyannopoulos, P. (2009). Contrast echocardiography: evidence-based recommendations by European Association of Echocardiography. *Eur J Echocardiogr, 10*(2), 194-212. doi:10.1093/ejechocard/jep005

Senior, R., & Shah, B. N. (2012). Myocardial contrast echocardiography for simultaneous assessment of function and perfusion in real time: a technique comes of age. *Circulation, 126*(10), 1182-1184. doi:CIRCULATIONAHA.112.129031 [pii];10.1161/CIRCULATIONAHA.112.129031 [doi]

Senior, R., Becher, H., Monaghan, M., Agati, L., Zamorano, J., Vanoverschelde, J. L., & Nihoyannopoulos, P. (2009). Contrast echocardiography: evidence-based recommendations by European Association of Echocardiography. *European Journal of Echocardiography : The Journal of the Working Group on Echocardiography of the European Society of Cardiology*, *10*(2), 194–212. http://doi.org/10.1093/ejechocard/jep005

Shah, B. N., Zacharias, K., Pabla, J. S., Karogiannis, N., Calicchio, F., Balaji, G., . . . Senior, R. (2016). The clinical impact of contemporary stress echocardiography in morbid obesity for the assessment of coronary artery disease. *Heart, 102*(5), 370-375. doi:10.1136/heartjnl-2015-308796

Sicari, R., Nihoyannopoulos, P., Evangelista, A., Kasprzak, J., Lancellotti, P., Poldermans, D., . . . Zamorano, J. L. (2009). Stress Echocardiography Expert Consensus Statement--Executive Summary: European Association of Echocardiography (EAE) (a registered branch of the ESC). *Eur. Heart J, 30*(3), 278-289. doi:ehn492 [pii];10.1093/eurheartj/ehn492 [doi]

Thorstensen, A., Dalen, H., Amundsen, B. H., Aase, S. A., & Stoylen, A. (2010). Reproducibility in echocardiographic assessment of the left ventricular global and regional function, the HUNT study. *Eur. J. Echocardiogr, 11*(2), 149-156. doi:jep188 [pii];10.1093/ejechocard/jep188 [doi]

Yokoyama, N., Schwarz, K. Q., Chen, X., Steinmetz, S. D., Becher, H., Schimpky, C., & Schlief, R. (2003). The effect of echo contrast agent on Doppler velocity measurements. *Ultrasound Med. Biol, 29*(5), 765-770. doi:S0301562902007706 [pii]

Figure legends

Figure 1: Color tissue velocity curves prior to ultrasound contrast injection (Panel A) and after ultrasound contrast injection (Panel B).

Figure 2: Intra-observer reproducibility of longitudinal tissue velocity S' prior to contrast injection and 10 minutes after contrast injection (Panel A), e' (Panel B) and a' (Panel C) demonstrated as a Bland Altman plots.

Figure 3: Inter-observer reproducibility of longitudinal tissue velocity prior to contrast injection and 10 minutes after contrast injection for S', e' and a' demonstrated as Bland Altman plots.

Figure 4: Reproducibility of S', e' and a' prior to and 10 minutes after contrast injection presented as Bland Altman plots and scatter plot demonstrating the correlation between measurements prior to and after ultrasound contrast injection.

Table 1: Patients characteristics

	N=19
Age (years)	62±6
Women (%)	10
Hypertension (%)	25
Diabetes	0
Current smoker (%)	30
Time since infarction (weeks)	20.3±14.3
Peak troponin T (ng/L)	5842±2828
Single vessel disease (%)	50
Anterior wall infraction (%)	40
Inferior wall infarction (%)	50
Other infract localisation (%)	10
Wall motion score index without UC	1.14 (1.00-1.56)
Wall motion score index with UC	1.21(1.00-1.67)
LAD (%)	40
CX (%)	25
RCA (%)	35

***UC: Ultrasound contrast; LAD: Left anterior decending CX: Circumflex ; RCA: Right coronary artery.**

Table 2: Intra-observer reproducibility of tissue velocity measurements before and after ultrasound contrast injection

Variables	First reading	Second reading	p-value	ICC (95% CI)
S' pre contrast	5.02±1.52	5.04±1.53	0.773	0.94 (0.90-0.96)
S' post contrast	4.84±1.44	4.72±1.41	0.147	0.94 (0.91-0.96)
e' pre contrast	-6.05±1.90	-5.97±1.78	0.468	0.94 (0.91-0.96)
e' post contrast	-5.78±1.80	-5.83±1.74	0.624	0.93 (0.88-0.95)
a' pre contrast	-5.90±2.12	-5.79±2.00	0.423	0.92 (0.91-0.96)
a' post contrast	-5.61±2.06	-5.54±2.05	0.515	0.94 (0.91-0.96)

Table 3: Inter-observer reproducibility of tissue velocity measurments before and after ultrasound contrast injection

Variables	Reader 1	Reader 2	p-value	ICC (95% CI)
S' pre contrast	4.95±1.57	4.67±1.79	0.305	0.21(-0.27-0.50)
S' post contrast	4.68±1.44	4.63±1.65	0.798	0.36 (-0.02-0.60)
e' pre contrast	-5.77±1.79	-5.46±1.88	0.263	0.31 (-0.97-0.57)
e' post contrast	-5.76±1.81	-5.65±1.83	0.692	0.27 (-0.17-0.54)
a' pre contrast	-5.63±2.11	-5.07±2.46	0.055	0.59 (0.35-0.74)
a' post contrast	-5.50±2.103	-5.24±2.17	0.287	0.71 (0.55-0.82)

Table 4: Reproducibility of Tissue velocity before and 10 minutes after contrast injection.

Variables	Before contrast	After contrast	p-value	ICC (95% CI)
S'	5.02±1.52	4.96±1.36	0.683	0.82 (0.71-0.89)
e'	-6.05±1.90	-5.90±1.76	0.359	0.84 (0.75-0.90)
a'	-5.90±2.12	-5.80±1.96	0.517	0.89 (0.82-0.93)

Panel A

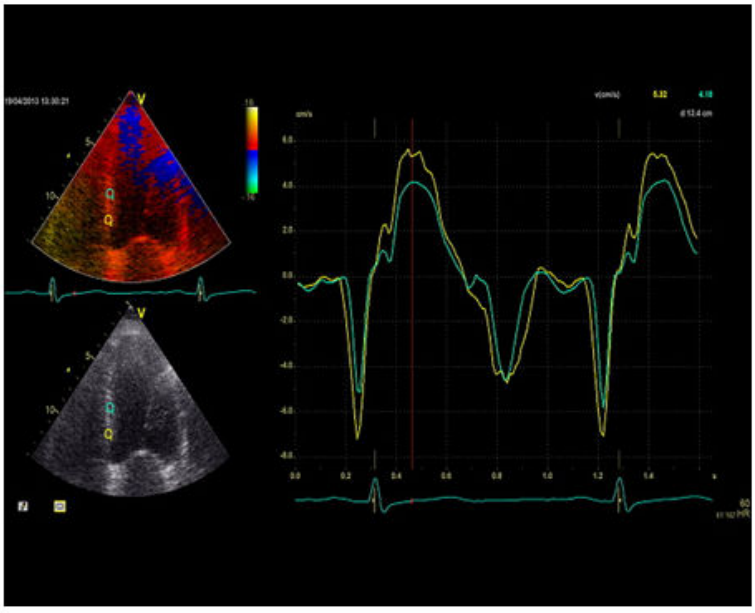

Panel B

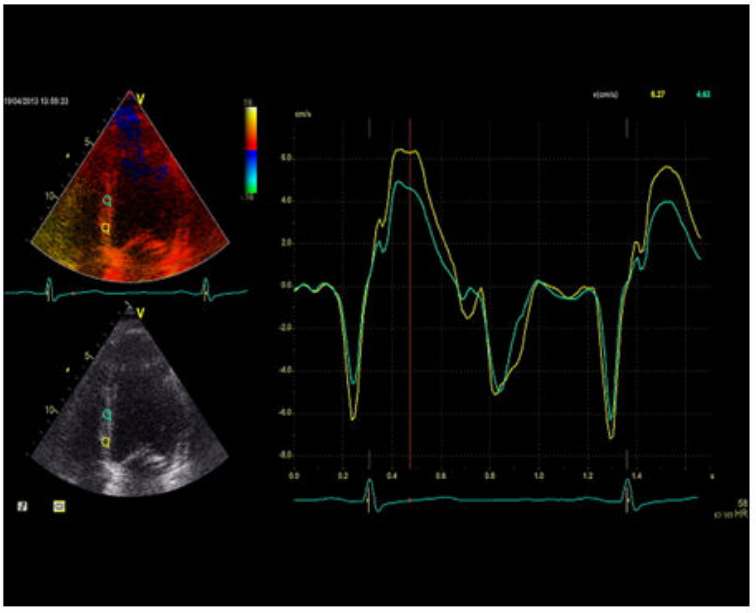

Intraindividual reproducibility prior to and after contrast

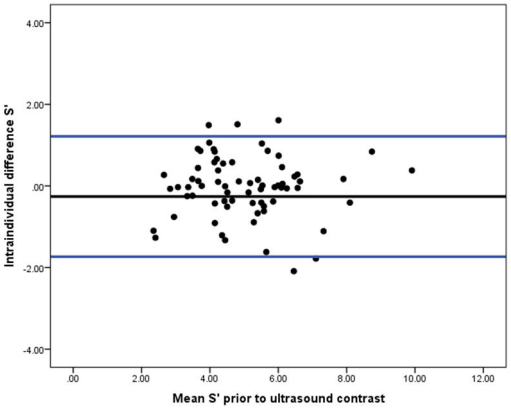

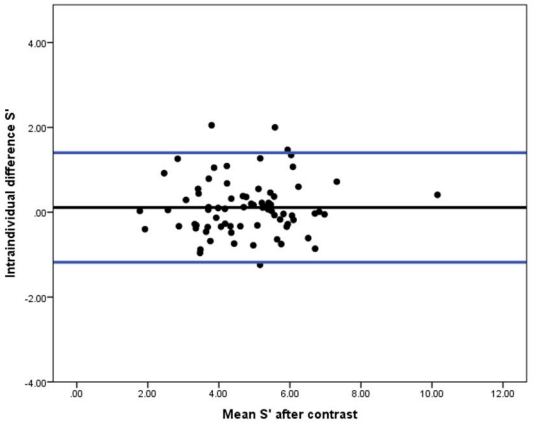

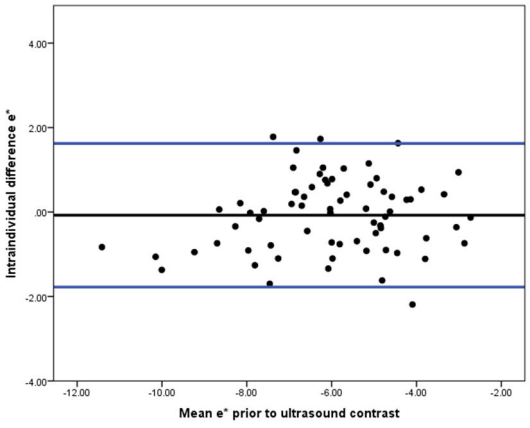

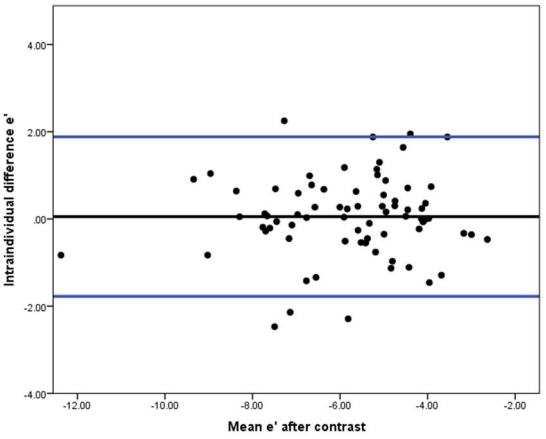

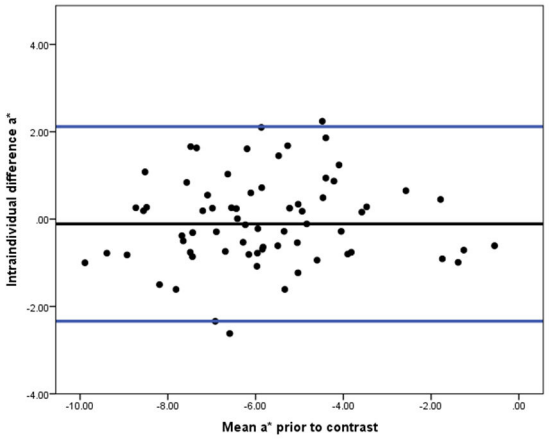

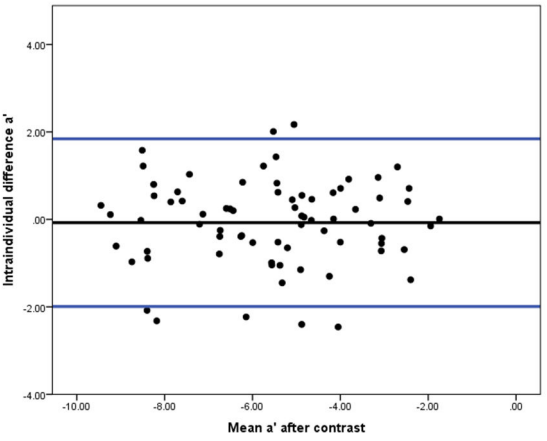

Interindividual reproducibility prior to and after contrast

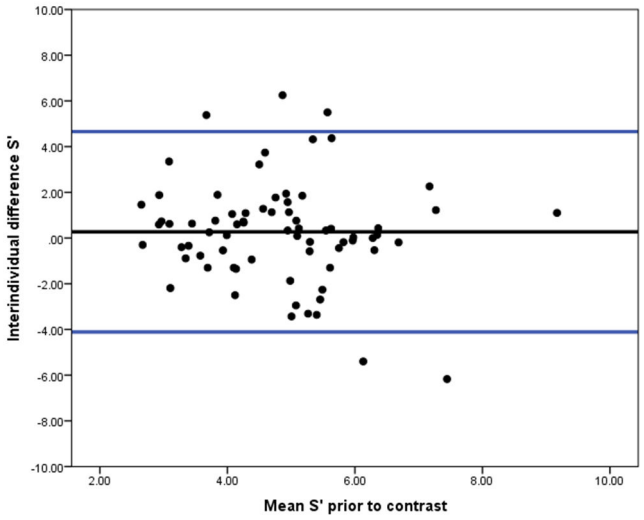

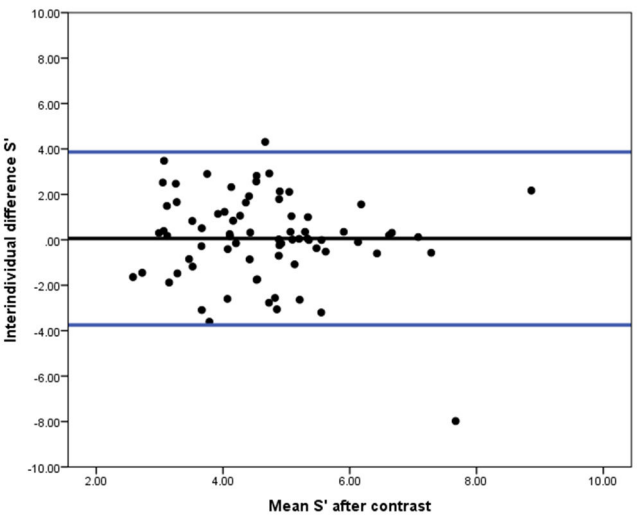

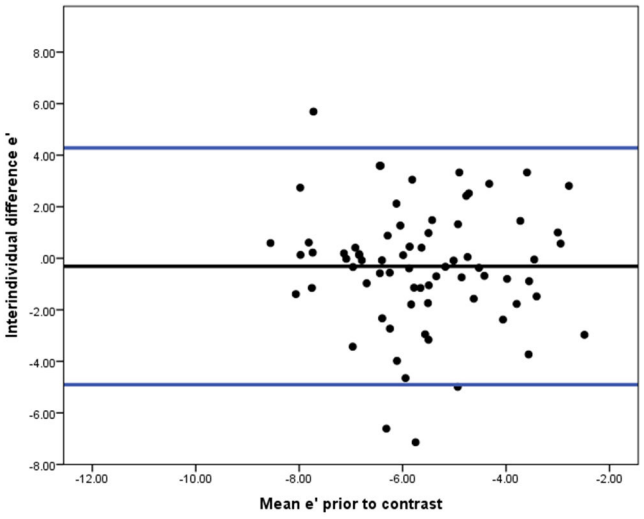

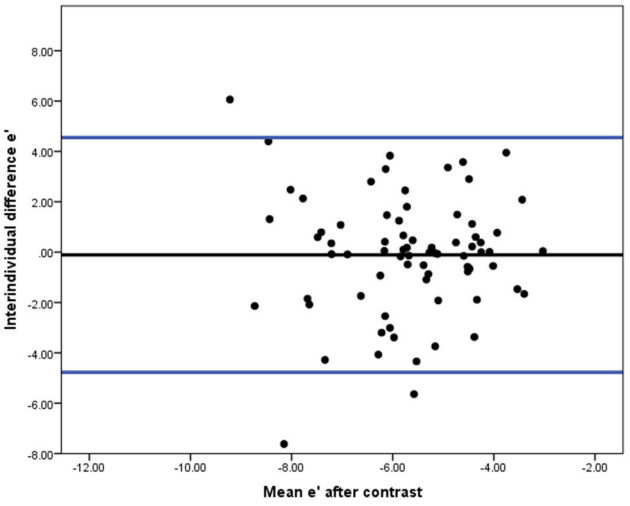

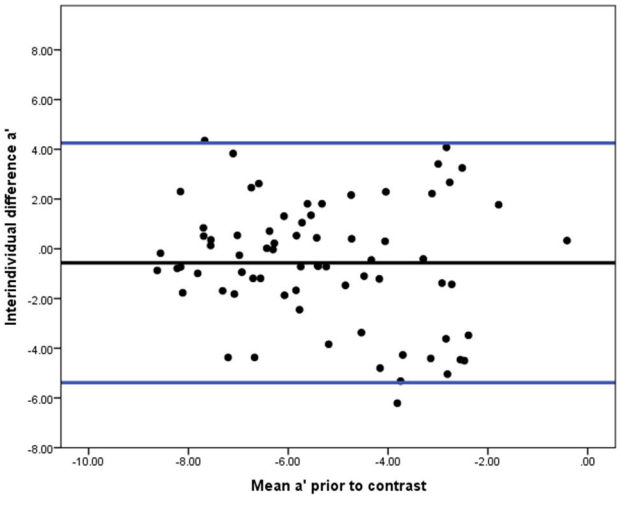

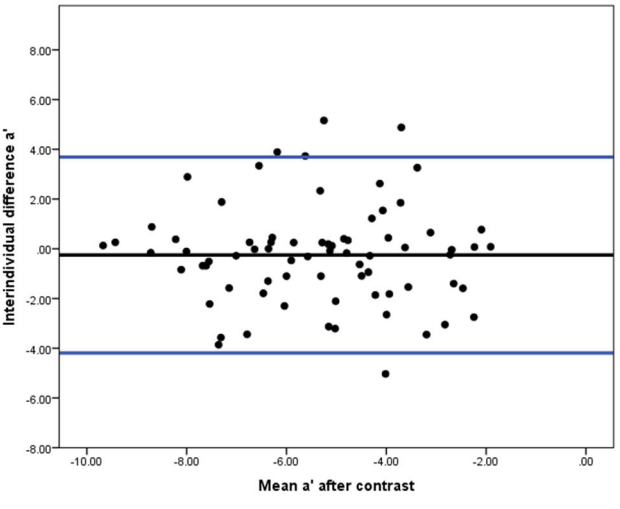

Reproducibility of cTV prior to and after ultrasound contrast

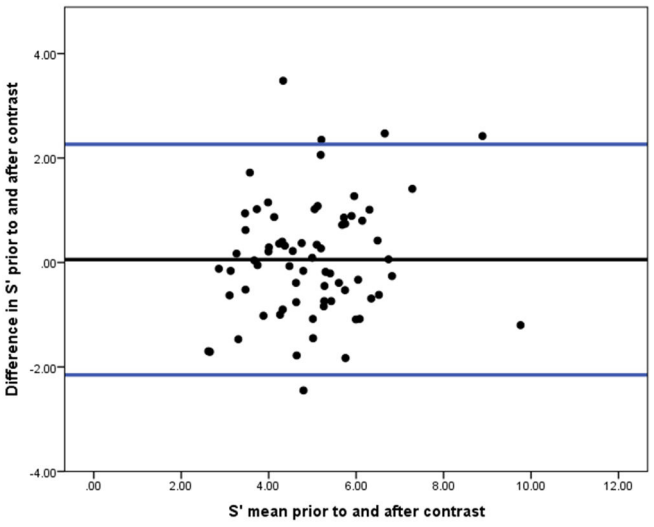

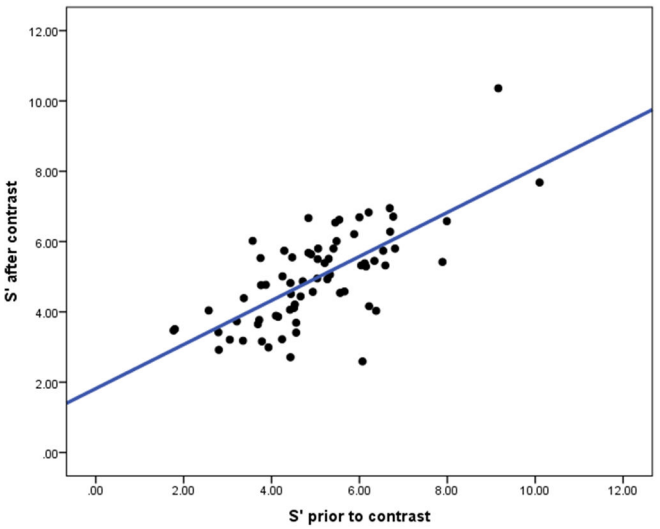

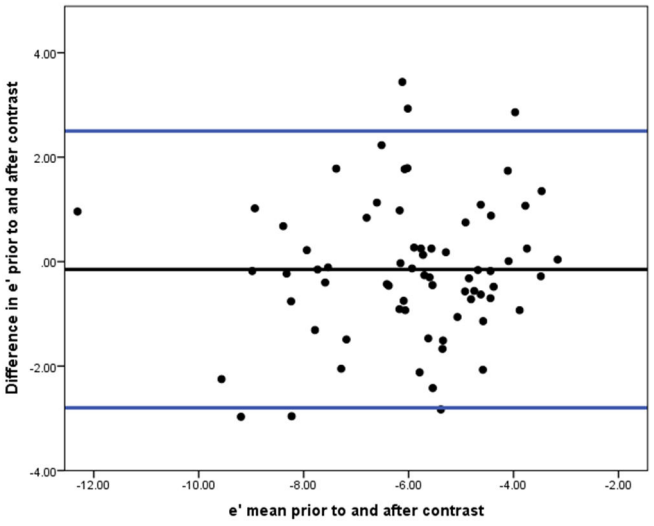

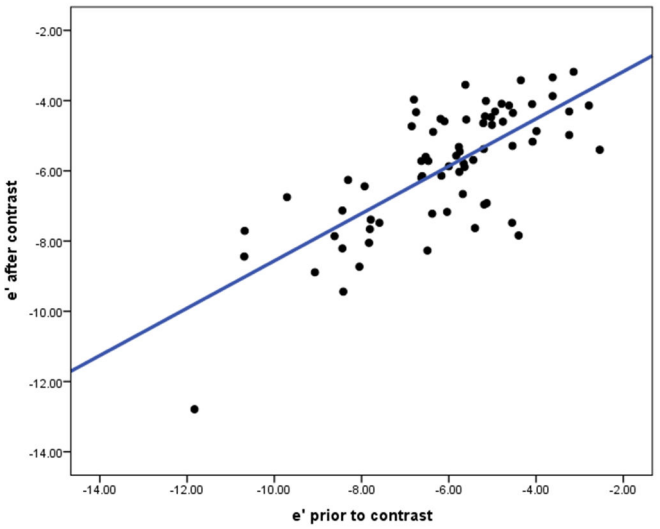

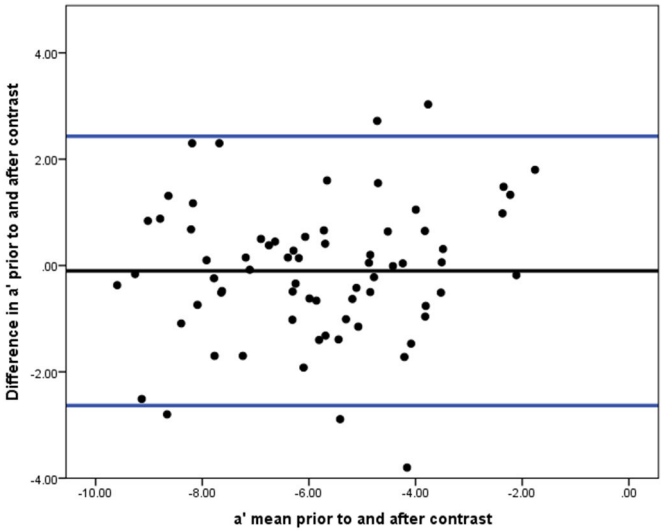

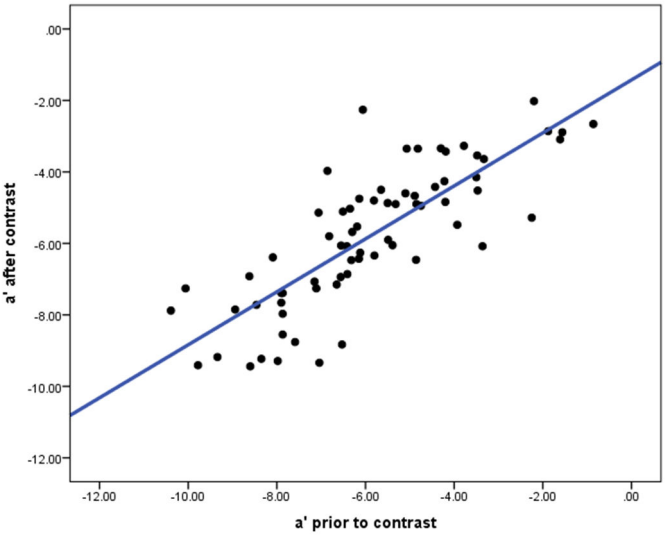

Bibliography

[1] Birger Brekke, Lars C.L. Nilsen, Joakim Lund, Hans Torp, Tore Bjastad, Brage H Amundsen, Asbjorn Stoylen, and Svein a Aase. Ultra-high Frame Rate Tissue Doppler Imaging. *Ultrasound in Medicine & Biology*, 40(1):222–231, jan 2014. ISSN 03015629. doi: 10.1016/j.ultrasmedbio.2013.09.012. URL http://www.ncbi.nlm.nih.gov/pubmed/24210859.

[2] Lars Christian Naterstad Lervik, Brekke Brekke, Carlo Missant, Peter Haemers, Ling Tong, Alejandra Ortega, Hans Torp, George R. Sutherland, Jan D'hooge, and Asbjørn Støylen. Detection of mechanical activation by two- and three-dimensional ultra-high frame rate tissue Doppler imaging in an open-chest pig model. *Manuscript submitted for review - Echocardiography*, 2017.

[3] Lars Christian Naterstad Lervik, Birger Brekke, Svein Arne Aase, Mai Tone Lønnebakken, Dordi Stensvåg, Brage H. Amundsen, Hans Torp, and Asbjørn Støylen. Myocardial Strain Rate by Anatomic Doppler Spectrum: First Clinical Experience Using Retrospective Spectral Tissue Doppler from Ultra-High Frame Rate Imaging. *Ultrasound in Medicine & Biology*, jun 2017. ISSN 03015629. doi: 10.1016/j.ultrasmedbio.2017.05.016. URL http://linkinghub.elsevier.com/retrieve/pii/S0301562917302399.

[4] MT Lønnebakken, Lars Christian Lervik Nilsen, and Asbjørn Støylen. Tissue Doppler Imaging in Contrast Echocardiography – a feasibility study. *Manuscript*, 2017.

[5] Siddharth Goyal and Abha Singh. The Origin of Echocardiography. *Texas Heart Institute Journal*, (34):431–438, 2007.

[6] Jacques Curie and Pierre Curie. Développement, par pression, de l'électricité polaire dans les cristaux hémièdres à faces inclinées. *Bulletin de la Société minérologique de France*, 3:294–295, 1880.

[7] Thomas L. Szabo. *Diagnostic Ultrasound Imaging - Inside Out*. 2004. ISBN 978-0-12-396487-8.

[8] Michael Ainslie. *Principles of Sonar Performance Modelling*. Springer Berlin Heidelberg, Berlin, Heidelberg, 2010. ISBN 978-3-540-87661-8. doi: 10.1007/978-3-540-87662-5. URL http://link.springer.com/10.1007/978-3-540-87662-5.

[9] D Kane, W Grassi, R Sturrock, and P V Balint. A brief history of musculoskeletal ultrasound: 'From bats and ships to babies and hips'. *Rheumatology (Oxford, England)*, 43(7):931–3, jul 2004. ISSN 1462-0324. doi: 10.1093/rheumatology/keh004. URL http://www.ncbi.nlm.nih.gov/pubmed/15213339.

[10] F. A. Firestone. The Supersonic Reflectoscope; an Instrument for Inspecting the Interior of Metal Parts by Means of Sound Waves. *The Journal of the Acoustical Society of America*, 16(1):100, 1944. ISSN 00014966. doi: 10.1121/1.1902363. URL http://scitation.aip.org/content/asa/journal/jasa/16/1/10.1121/1.1902363.

[11] Karl Theodor Dussik. On the possibility of using ultrasound waves as a diagnostic aid. *Neurol Psychiat*, 174:153–168, 1942.

[12] Inge Edler and Kjell Lindström. The history of echocardiography. *Ultrasound in medicine & biology*, 30(12):1565–644, dec 2004. ISSN 0301-5629. doi: 10.1016/S0301-5629(99)00056-3. URL http://www.ncbi.nlm.nih.gov/pubmed/15617829.

[13] Wolf-Dieter Keidel. Über die Verwendung des Ultraschalls in der klinischen Diagnostik. *Arztl. Forschg. (Worishofen)*, 1:349–357, 1947.

[14] Wolf-Dieter Keidel. Uber eine Methode zur Registrierung der Volumanderun- gen des Herzens am Menschen. *Zeitschr Kreislaufforsch*, 39:257, 1950.

[15] I Edler and C H Hertz. The use of ultrasonic reflectoscope for the continuous recording of the movements of heart walls. *Kungl Fysiografiska Sallskapets i Lund Forhandlingar*, may 1954. ISSN 1475-0961.

[16] Christian Andreas Doppler. Über das farbige Licht der Doppelsterne und einiger anderer Gestirne des Himmels. *Abh Königl Böhm Ges Wiss .*, 2:465–482, 1843.

[17] Buijs Ballot. Akustische Versuche auf der Niederländischen Eisenbahn, nebst gelegentlichen Bemerkungen zur Theorie des Hrn. Prof. Doppler. *Annalen der Physik und Chemie*, 142(11):321–351, 1845. ISSN 00033804. doi: 10.1002/andp.18451421102. URL http://doi.wiley.com/10.1002/andp.18451421102.

[18] A O Brubakk, B A Angelsen, and L Hatle. Diagnosis of valvular heart disease using transcutaneous Doppler ultrasound. *Cardiovascular research*, 11(5):461–9, sep 1977. ISSN 0008-6363. URL http://www.ncbi.nlm.nih.gov/pubmed/589636.

[19] J Holen, R Aaslid, K Landmark, and S Simonsen. Determination of pressure gradient in mitral stenosis with a non-invasive ultrasound Doppler technique. *Acta medica Scandinavica*, 199(6):455–60, jan 1976. ISSN 0001-6101. URL http://www.ncbi.nlm.nih.gov/pubmed/937070.

[20] J Holen, R Aaslid, K Landmark, S Simonsen, and T Ostrem. Determination of effective orifice area in mitral stenosis from non-invasive ultrasound Doppler data and mitral flow rate. *Acta medica Scandinavica*, 201(1-2):83–8, jan 1977. ISSN 0001-6101. URL http://www.ncbi.nlm.nih.gov/pubmed/835376.

[21] L Hatle, A Brubakk, A Tromsdal, and B Angelsen. Noninvasive assessment of pressure drop in mitral stenosis by Doppler ultrasound. *British heart journal*, 40 (2):131–40, feb 1978. ISSN 0007-0769. URL http://heart.bmj.com/content/40/2/131.

[22] L Hatle, B Angelsen, and A Tromsdal. Noninvasive assessment of atrioventricular pressure half-time by Doppler ultrasound. *Circulation*, 60(5):1096–104, nov 1979. ISSN 0009-7322. URL http://www.ncbi.nlm.nih.gov/pubmed/487543.

[23] L Hatle, B A Angelsen, and A Tromsdal. Non-invasive assessment of aortic stenosis by Doppler ultrasound. *British heart journal*, 43(3):284–92, mar 1980. ISSN 0007-0769. URL https://www.ncbi.nlm.nih.gov/pmc/articles/PMC482277.

[24] L Hatle. Noninvasive assessment and differentiation of left ventricular outflow obstruction with Doppler ultrasound. *Circulation*, 64(2):381–7, aug 1981. ISSN 0009-7322. URL http://www.ncbi.nlm.nih.gov/pubmed/7195785.

[25] L Hatle, B A Angelsen, and A Tromsdal. Non-invasive estimation of pulmonary artery systolic pressure with Doppler ultrasound. *British heart journal*, 45(2): 157–65, feb 1981. ISSN 0007-0769. URL https://www.ncbi.nlm.nih.gov/pmc/articles/PMC482504/.

[26] L Hatle and R Rokseth. Noninvasive diagnosis and assessment of ventricular septal defect by Doppler ultrasound. *Acta medica Scandinavica. Supplementum*, 645:47–56, jan 1981. ISSN 0365-463X. URL http://www.ncbi.nlm.nih.gov/pubmed/6940422.

[27] L K Hatle, C P Appleton, and R L Popp. Differentiation of constrictive pericarditis and restrictive cardiomyopathy by Doppler echocardiography. *Circulation*, 79 (2):357–70, feb 1989. ISSN 0009-7322. URL http://www.ncbi.nlm.nih.gov/pubmed/2914352.

[28] Karl Isaaz, Aubrey Thompson, Gerard Ethevenot, Jean L Cloez, Beatrice Brembilla, and Claude Pernot. Doppler echocardiographic measurement of low velocity motion of the left ventricular posterior wall. *The American Journal of Cardiology*, 64(1):66–75, jul 1989. ISSN 00029149. doi: 10.1016/0002-9149(89)90655-3. URL http://www.ncbi.nlm.nih.gov/pubmed/2741815.

[29] W N McDicken, G R Sutherland, C M Moran, and L N Gordon. Colour Doppler velocity imaging of the myocardium. *Ultrasound in medicine & biology*, 18(6-7): 651–4, jan 1992. ISSN 0301-5629. URL http://www.ncbi.nlm.nih.gov/pubmed/1413277.

[30] Arthur Guyton and John Hall. *Textbook of medical physiology*. 2011. ISBN 978-1-4160-4574-8.

[31] Sverre Holm. Medisinsk Ultralydavbildning. In *Fra Fysikkens Verden. 1999, oppdatert 2.okt 2008.*

[32] Asbjørn Stoylen. Strain rate imaging, 2014. URL http://folk.ntnu.no/stoylen/strainrate/.

[33] Helmut Baumgartner, Judy Hung, Javier Bermejo, John B. Chambers, Thor Edvardsen, Steven Goldstein, Patrizio Lancellotti, Melissa LeFevre, Fletcher Miller, and Catherine M. Otto. Recommendations on the Echocardiographic Assessment of Aortic Valve Stenosis: A Focused Update from the European Association of Cardiovascular Imaging and the American Society of Echocardiography. *Journal of the American Society of Echocardiography*, 30(4):372–392, apr 2017. ISSN 08947317. doi: 10.1016/j.echo.2017.02.009. URL http://linkinghub.elsevier.com/retrieve/pii/S0894731717301335.

[34] H. Nyquist. Certain Topics in Telegraph Transmission Theory. *Transactions of the American Institute of Electrical Engineers*, 47(2):617–644, apr 1928. ISSN 0096-3860. doi: 10.1109/T-AIEE.1928.5055024. URL http://ieeexplore.ieee.org/lpdocs/epic03/wrapper.htm?arnumber=5055024.

[35] Y Yoshitoshi, K Machii, H Sekiguchi, Y Mishina, S Ohta, Y Hanaoka, Y Kohashi, S Shimizu, and H Kuno. Doppler measurement of mitral valve and ventricle wall velocities. *Ultrasonics*, 4:27–8, jan 1966. ISSN 0041-624X. URL http://www.ncbi.nlm.nih.gov/pubmed/5931821.

[36] S Aase. *Methods for improving quality and efficiency in quantitative echocardiography: Aspects of using high frame rate*. PhD thesis, 2008. URL

[37] E Wu, J T Ortiz, P Tejedor, D C Lee, C Bucciarelli-Ducci, P Kansal, J C Carr, T A Holly, D Lloyd-Jones, F J Klocke, and R O Bonow. Infarct size by contrast enhanced cardiac magnetic resonance is a stronger predictor of outcomes than left ventricular ejection fraction or end-systolic volume index: prospective cohort study. *Heart (British Cardiac Society)*, 94(6):730–6, jun 2008. ISSN 1468-201X. doi: 10.1136/hrt.2007.122622. URL http://www.ncbi.nlm.nih.gov/pubmed/18070953.

[38] David Bello, Arnold Einhorn, Rishi Kaushal, Satish Kenchaiah, Aidan Raney, David Fieno, Jagat Narula, Jeffrey Goldberger, Kalyanam Shivkumar, Haris Subacius, and Alan Kadish. Cardiac magnetic resonance imaging: infarct size is an independent predictor of mortality in patients with coronary artery disease. *Magnetic resonance imaging*, 29(1):50–6, jan 2011. ISSN 1873-5894. doi: 10.1016/j.mri.2010.03.031. URL http://www.ncbi.nlm.nih.gov/pubmed/20980115.

[39] Robert J Burns, Raymond J Gibbons, Qilong Yi, Robin S Roberts, Todd D Miller, Gary L Schaer, Jeffrey L Anderson, and Salim Yusuf. The relationships of left ventricular ejection fraction, end-systolic volume index and infarct size to six-month mortality after hospital discharge following myocardial infarction treated by thrombolysis. *Journal of the American College of Cardiology*, 39(1):30–6, jan 2002. ISSN 0735-1097. URL http://www.ncbi.nlm.nih.gov/pubmed/11755283.

[40] Michael Dandel, Hans Lehmkuhl, Christoph Knosalla, Nino Suramelashvili, and Roland Hetzer. Strain and strain rate imaging by echocardiography - basic concepts and clinical applicability. *Current cardiology reviews*, 5(2):133–48, may 2009. ISSN 1875-6557. doi: 10.2174/157340309788166642. URL https://www.ncbi.nlm.nih.gov/pmc/articles/PMC2805816/.

[41] Asbjørn Støylen and Terje Skjaerpe. Systolic long axis function of the left ventricle. Global and regional information. *Scandinavian cardiovascular journal : SCJ*, 37 (5):253–8, sep 2003. ISSN 1401-7431. URL http://www.ncbi.nlm.nih.gov/pubmed/14534065.

[42] Anders Thorstensen, Brage Høyem Amundsen, Håvard Dalen, Pavel Hala, Gabriel Kiss, Svein Arne Aase, Hans Torp, and Asbjørn Støylen. Strain rate imaging combined with wall motion analysis gives incremental value in direct quantification of myocardial infarct size. *European heart journal cardiovascular Imaging*, 13 (11):914–21, nov 2012. ISSN 2047-2412. doi: 10.1093/ehjci/jes070. URL http://www.ncbi.nlm.nih.gov/pubmed/22499406.

[43] Asbjørn Støylen. *Strain rate imaging of the left ventricle by ultrasound. Feasibility , clinical validation and physiological aspects*. PhD thesis, 2001.

[44] I. Mirsky and W. W. Parmley. Assessment of passive elastic stiffness for isolated heart muscle and the intact heart. *Circulation research*, 33(2):233–43, aug 1973. ISSN 0009-7330. doi: 10.1161/01.RES.33.2.233. URL http://www.ncbi.nlm.nih.gov/pubmed/4269516.

[45] J D'hooge, A Heimdal, F Jamal, T Kukulski, B Bijnens, F Rademakers, L Hatle, P Suetens, and G R Sutherland. Regional strain and strain rate measurements by cardiac ultrasound: principles, implementation and limitations. *European journal of echocardiography : the journal of the Working Group on Echocardiography of the*

European Society of Cardiology, 1(3):154–70, sep 2000. ISSN 1525-2167. doi: 10.1053/euje.2000.0031. URL http://www.ncbi.nlm.nih.gov/pubmed/11916589.

[46] Brian D Hoit. Strain and strain rate echocardiography and coronary artery disease. *Circulation. Cardiovascular imaging*, 4(2):179–90, mar 2011. ISSN 1942-0080. doi: 10.1161/CIRCIMAGING.110.959817. URL http://www.ncbi.nlm.nih.gov/pubmed/21406664.

[47] Charlotte Ingul, Hans Torp, Svein Arne Aase, Sigrid Berg, Asbjorn Stoylen, and Stig Slordahl. Automated Analysis of Strain Rate and Strain: Feasibility and Clinical Implications. *Journal of the American Society of Echocardiography*, 18 (5):411–418, may 2005. ISSN 08947317. doi: 10.1016/j.echo.2005.01.032. URL http://www.ncbi.nlm.nih.gov/pubmed/15891750.

[48] Fadi Jamal, Tomasz Kukulski, George R. Sutherland, Frank Weidemann, Jan D'hooge, Bart Bijnens, and Geneviève Derumeaux. Can changes in systolic longitudinal deformation quantify regional myocardial function after an acute infarction? An ultrasonic strain rate and strain study. *Journal of the American Society of Echocardiography*, 15(7):723–730, jul 2002. ISSN 08947317. doi: 10.1067/mje.2002.118913. URL http://linkinghub.elsevier.com/retrieve/pii/S0894731702000238.

[49] Tomasz Kukulski, Fadi Jamal, Lieven Herbots, Jan D'hooge, Bart Bijnens, Liv Hatle, Ivan De Scheerder, and George R Sutherland. Identification of acutely ischemic myocardium using ultrasonic strain measurements. *Journal of the American College of Cardiology*, 41(5):810–819, mar 2003. ISSN 07351097. doi: 10.1016/S0735-1097(02)02934-0. URL http://linkinghub.elsevier.com/retrieve/pii/S0735109702029340.

[50] Asbjorn Stoylen, Andreas Heimdal, Knut Bjornstad, Hans G. Torp, and Terje Skjaerpe. Strain Rate Imaging by Ultrasound in the Diagnosis of Regional Dysfunction of the Left Ventricle. *Echocardiography (Mount Kisco, N.Y.)*, 16(4):321–329, may 1999. ISSN 1540-8175. URL http://www.ncbi.nlm.nih.gov/pubmed/11175157.

[51] Yan Zhang, Anna K Y Chan, Cheuk-Man Yu, Gabriel W K Yip, Jeffrey W H Fung, Wynnie W M Lam, Nina M C So, Mei Wang, Eugene B Wu, John T Wong,

and John E Sanderson. Strain rate imaging differentiates transmural from non-transmural myocardial infarction: a validation study using delayed-enhancement magnetic resonance imaging. *Journal of the American College of Cardiology*, 46 (5):864–71, sep 2005. ISSN 0735-1097. doi: 10.1016/j.jacc.2005.05.054. URL http://www.ncbi.nlm.nih.gov/pubmed/16139138.

[52] Jonathan Chan, Lizelle Hanekom, Chiew Wong, Rodel Leano, Goo-Yeong Cho, and Thomas H Marwick. Differentiation of subendocardial and transmural infarction using two-dimensional strain rate imaging to assess short-axis and long-axis myocardial function. *Journal of the American College of Cardiology*, 48 (10):2026–33, nov 2006. ISSN 1558-3597. doi: 10.1016/j.jacc.2006.07.050. URL http://www.ncbi.nlm.nih.gov/pubmed/17112992.

[53] Theodore P. Abraham, Veronica L. Dimaano, and H.-Y. Hsin-Yueh Liang. Role of Tissue Doppler and Strain Echocardiography in Current Clinical Practice. *Circulation*, 116(22):2597–2609, nov 2007. ISSN 0009-7322. doi: 10.1161/CIRCULATIONAHA.106.647172. URL http://www.ncbi.nlm.nih.gov/pubmed/18040039.

[54] Havard Dalen, Anders Thorstensen, Svein a Aase, Charlotte B Ingul, Hans Torp, Lars J Vatten, and Asbjorn Stoylen. Segmental and global longitudinal strain and strain rate based on echocardiography of 1266 healthy individuals: the HUNT study in Norway. *European journal of echocardiography : the journal of the Working Group on Echocardiography of the European Society of Cardiology*, 11 (2):176–83, mar 2010. ISSN 1532-2114. doi: 10.1093/ejechocard/jep194. URL http://www.ncbi.nlm.nih.gov/pubmed/19946115.

[55] Malin K. Larsson, Cristina Da Silva, Elif Gunyeli, Ali Akebat Bin Ilami, Karolina Szummer, Reidar Winter, and Anna Bjällmark. The potential clinical value of contrast-enhanced echocardiography beyond current recommendations. *Cardiovascular Ultrasound*, 14(1):2, dec 2015. ISSN 1476-7120. doi: 10.1186/s12947-015-0045-0. URL http://www.cardiovascularultrasound.com/content/14/1/2.

[56] Marcus Ressner, Tomas Jansson, Jonny Cedefamn, Per Ask, and Birgitta Janerot-Sjoberg. Contrast Biases the Autocorrelation Phase Shift Estimation in Doppler Tissue Imaging. *Ultrasound in Medicine & Biology*, 35(3):447–457, mar 2009. ISSN

03015629. doi: 10.1016/j.ultrasmedbio.2008.09.012. URL http://linkinghub.elsevier.com/retrieve/pii/S0301562908004341.

[57] Marcus Ressner, Lars-Ake Brodin, Tomas Jansson, Lars Hoff, Per Ask, and Birgitta Janerot-Sjoberg. Effects of Ultrasound Contrast Agents on Doppler Tissue Velocity Estimation. *Journal of the American Society of Echocardiography*, 19 (2):154–164, feb 2006. ISSN 08947317. doi: 10.1016/j.echo.2005.09.025. URL http://linkinghub.elsevier.com/retrieve/pii/S089473170500845X.

[58] Siri Malm, Sigmund Frigstad, Asbjorn Stoylen, Hans Torp, Einar Sagberg, and Terje Skjarpe. Effects of Ultrasound Contrast During Tissue Velocity Imaging on Regional Left Ventricular Velocity, Strain, and Strain Rate Measurements. *Journal of the American Society of Echocardiography*, 19(1):40–47, jan 2006. ISSN 08947317. doi: 10.1016/j.echo.2005.07.017. URL http://www.ncbi.nlm.nih.gov/pubmed/16423668.

[59] B. F. Hoffman, P. F. Cranefield, J. H. Stuckey, N. S. Amer, R. Cappelletti, and R. T. Domingo. Direct Measurement of Conduction Velocity in In situ Specialized Conducting System of Mammalian Heart. *Experimental Biology and Medicine*, 102(1):55–57, oct 1959. ISSN 1535-3702. doi: 10.3181/00379727-102-25141. URL http://ebm.sagepub.com/lookup/doi/10.3181/00379727-102-25141.

[60] Jonathan M Cordeiro, Lindsey Greene, Cory Heilmann, Daniel Antzelevitch, and Charles Antzelevitch. Transmural heterogeneity of calcium activity and mechanical function in the canine left ventricle. *American journal of physiology. Heart and circulatory physiology*, 286(4):H1471–9, apr 2004. ISSN 0363-6135. doi: 10.1152/ajpheart.00748.2003. URL http://www.ncbi.nlm.nih.gov/pubmed/14670817.

[61] David P. Shattuck, M D Weinshenker, S W Smith, and O T von Ramm. Explososcan: a parallel processing technique for high speed ultrasound imaging with linear phased arrays. *The Journal of the Acoustical Society of America*, 75(4):1273–82, apr 1984. ISSN 0001-4966. doi: 10.1121/1.390734. URL http://www.ncbi.nlm.nih.gov/pubmed/6725779.

[62] Hiroshi Kanai and H Satoh. A new method for measuring small local vibrations in the heart using ultrasound. *... , IEEE Transactions on*, 40(12):1233–1242, 1993. URL http://ieeexplore.ieee.org/xpls/abs{_}all.jsp?arnumber=250580.

[63] Jan D'hooge, Elisa Konofagou, Fadi Jamal, Andreas Heimdal, Laurentino Barrios, Bart Bijnens, Jan Thoen, Frans Van de Werf, George Sutherland, and Paul Suetens. Two-dimensional ultrasonic strain rate measurement of the human heart in vivo. *IEEE transactions on ultrasonics, ferroelectrics, and frequency control*, 49(2):281–6, feb 2002. ISSN 0885-3010. doi: 10.1109/58.985712. URL http://www.ncbi.nlm.nih.gov/pubmed/11885685.

[64] Jiqi Cheng and Jian-yu Lu. Extended high-frame rate imaging method with limited-diffraction beams. *IEEE transactions on ultrasonics, ferroelectrics, and frequency control*, 53(5):880–99, may 2006. ISSN 0885-3010. URL http://www.ncbi.nlm.nih.gov/pubmed/16764444.

[65] Hideyuki Hasegawa and Hiroshi Kanai. High-frame-rate echocardiography with reduced sidelobe level. *IEEE transactions on ultrasonics, ferroelectrics, and frequency control*, 59(11):2569–75, nov 2012. ISSN 1525-8955. doi: 10.1109/TUFFC.2012.2490. URL http://www.ncbi.nlm.nih.gov/pubmed/23192821.

[66] Yasunori Honjo, Hideyuki Hasegawa, and Hiroshi Kanai. Two-Dimensional Tracking of Heart Wall for Detailed Analysis of Heart Function at High Temporal and Spatial Resolutions. *Japanese Journal of Applied Physics*, 49(7):07HF14, jul 2010. ISSN 0021-4922. doi: 10.1143/JJAP.49.07HF14. URL http://stacks.iop.org/1347-4065/49/07HF14.

[67] Yasunori Honjo, Hideyuki Hasegawa, and Hiroshi Kanai. Accurate ultrasonic measurement of myocardial regional strain rate at high temporal and spatial resolutions. In *2008 IEEE Ultrasonics Symposium*, pages 1995–1998. IEEE, nov 2008. ISBN 978-1-4244-2428-3. doi: 10.1109/ULTSYM.2008.0492. URL http://ieeexplore.ieee.org/lpdocs/epic03/wrapper.htm?arnumber=4803512.

[68] Jian-yu Lu, Jiqi Cheng, and Jing Wang. High frame rate imaging system for limited diffraction array beam imaging with square-wave aperture weightings high frame rate imaging system for limited diffraction array beam imaging with square-wave aperture weightings. *IEEE Transactions on Ultrasonics, Ferroelectrics and Frequency Control*, 53(10):1796–1812, oct 2006. ISSN 0885-3010. doi: 10.1109/TUFFC.2006.112. URL http://ieeexplore.ieee.org/lpdocs/epic03/wrapper.htm?arnumber=4012864.

[69] Jean Provost, Wei-Ning Lee, Kana Fujikura, and Elisa E Konofagou. Imaging the electromechanical activity of the heart in vivo. *Proceedings of the National Academy of Sciences of the United States of America*, 108(21):8565–70, may 2011. ISSN 1091-6490. doi: 10.1073/pnas.1011688108. URL https://www.ncbi.nlm.nih.gov/pmc/articles/PMC3102378/.

[70] M. Tanter, J. Bercoff, L. Sandrin, and M. Fink. Ultrafast compound imaging for 2-D motion vector estimation: application to transient elastography. *IEEE Transactions on Ultrasonics, Ferroelectrics and Frequency Control*, 49(10):1363–1374, oct 2002. ISSN 0885-3010. doi: 10.1109/TUFFC.2002.1041078. URL http://ieeexplore.ieee.org/lpdocs/epic03/wrapper.htm?arnumber=1041078.

[71] Jean Provost, Clement Papadacci, Juan Esteban Arango, Marion Imbault, Mathias Fink, Jean-Luc Gennisson, Mickael Tanter, and Mathieu Pernot. 3D ultrafast ultrasound imaging in vivo. *Physics in medicine and biology*, 59(19): L1–L13, oct 2014. ISSN 1361-6560. doi: 10.1088/0031-9155/59/19/L1. URL http://www.ncbi.nlm.nih.gov/pubmed/25207828.

[72] B Lind, J Nowak, J Dorph, J. van der Linden, and L-A. Brodin. Analysis of Temporal Requirements for Myocardial Tissue Velocity Imaging. *European Heart Journal - Cardiovascular Imaging*, 3(3):214–219, sep 2002. ISSN 2047-2404. doi: 10.1053/euje.3.3.214. URL http://ehjcimaging.oxfordjournals.org/cgi/doi/10.1053/euje.3.3.214.

[73] Camilla Storaa, Britta Lind, and Lars-Åke Brodin. Distribution of left ventricular longitudinal peak systolic strain and impact of low frame rate. *Ultrasound in Medicine & Biology*, 30(8):1049–1055, aug 2004. ISSN 03015629. doi: 10.1016/j.ultrasmedbio.2004.06.006. URL http://linkinghub.elsevier.com/retrieve/pii/S0301562904001590.

[74] Victor Mor-Avi, Roberto M Lang, Luigi P Badano, Marek Belohlavek, Nuno Miguel Cardim, Genevieve Geneviève Derumeaux, Maurizio Galderisi, Thomas Marwick, Sherif F Nagueh, Partho P Sengupta, Rosa Sicari, Otto a Smiseth, Beverly Smulevitz, Masaaki Takeuchi, James D Thomas, Mani Vannan, Jens-Uwe Voigt, and Jose Luis José Luis Jose Luis Zamorano. Current and evolving echocardiographic techniques for the quantitative evaluation of cardiac mechanics: ASE/EAE consensus statement on methodology and indications endorsed by

the Japanese Society of Echocardiography. *Journal of the American Society of Echocardiography : official publication of the American Society of Echocardiography*, 24(3):277–313, mar 2011. ISSN 1097-6795. doi: 10.1016/j.echo.2011.01.015. URL http://www.ncbi.nlm.nih.gov/pubmed/21385887.

[75] Maja Cikes, Ling Tong, George R Sutherland, and Jan D'hooge. Ultrafast cardiac ultrasound imaging: Technical principles, applications, and clinical benefits. *JACC: Cardiovascular Imaging*, 7(8):812–823, aug 2014. ISSN 18767591. doi: 10.1016/j.jcmg.2014.06.004. URL http://www.ncbi.nlm.nih.gov/pubmed/25124014.

[76] Elisa E Konofagou, Jianwen Luo, Deepak Saluja, Daniel O Cervantes, James Coromilas, and Kana Fujikura. Noninvasive electromechanical wave imaging and conduction-relevant velocity estimation in vivo. *Ultrasonics*, 50(2):208–15, feb 2010. ISSN 1874-9968. doi: 10.1016/j.ultras.2009.09.026. URL http://www.ncbi.nlm.nih.gov/pubmed/19863987.

[77] Elisa E Konofagou and Jean Provost. Electromechanical wave imaging for noninvasive mapping of the 3D electrical activation sequence in canines and humans in vivo. *Journal of biomechanics*, 45(5):856–64, mar 2012. ISSN 1873-2380. doi: 10.1016/j.jbiomech.2011.11.027. URL http://www.ncbi.nlm.nih.gov/pubmed/22284425.

[78] Jean Provost, Alok Gambhir, John Vest, Hasan Garan, and Elisa E Konofagou. A clinical feasibility study of atrial and ventricular electromechanical wave imaging. *Heart rhythm : the official journal of the Heart Rhythm Society*, 10(6):856–62, jun 2013. ISSN 1556-3871. doi: 10.1016/j.hrthm.2013.02.028. URL http://www.ncbi.nlm.nih.gov/pubmed/23454060.

[79] Jean Provost, Viatcheslav Gurev, Natalia Trayanova, and Elisa E Konofagou. Mapping of cardiac electrical activation with electromechanical wave imaging: an in silico-in vivo reciprocity study. *Heart rhythm : the official journal of the Heart Rhythm Society*, 8(5):752–9, may 2011. ISSN 1556-3871. doi: 10.1016/j.hrthm.2010.12.034. URL https://www.ncbi.nlm.nih.gov/pmc/articles/PMC3100212/.

[80] Alexandre Costet, Jean Provost, Alok Gambhir, Yevgeniy Bobkov, Peter Danilo, Gerard J J Boink, Michael R Rosen, and Elisa E Konofagou. Electromechanical wave imaging of biologically and electrically paced canine hearts in vivo. *Ultrasound in medicine & biology*, 40(1):177–87, jan 2014. ISSN 1879-291X. doi: 10.1016/j.ultrasmedbio.2013.08.019. URL http://www.sciencedirect.com/science/article/pii/S0301562913009794.

[81] Shougang Wang, Wei-Ning Lee, Jean Provost, Jianwen Luo, and Elisa E Konofagou. A composite high-frame-rate system for clinical cardiovascular imaging. *IEEE transactions on ultrasonics, ferroelectrics, and frequency control*, 55 (10):2221–33, oct 2008. ISSN 1525-8955. doi: 10.1109/TUFFC.921. URL http://www.ncbi.nlm.nih.gov/pubmed/18986870.

[82] Hiroshi Kanai. 9A-4 Ultrasonic Imaging of Propagation of Electric Excitation in Heart Wall. In *Ultrasonics Symposium, 2007. IEEE*, pages 753–756. Ieee, oct 2007. ISBN 978-1-4244-1383-6. doi: 10.1109/ULTSYM.2007.193. URL http://ieeexplore.ieee.org/lpdocs/epic03/wrapper.htm?arnumber=4409766.

[83] Julien Grondin, Alexandre Costet, Ethan Bunting, Alok Gambhir, Hasan Garan, Elaine Wan, and Elisa E. Konofagou. Validation of electromechanical wave imaging in a canine model during pacing and sinus rhythm. *Heart rhythm*, 13(11):2221–2227, nov 2016. ISSN 1556-3871. doi: 10.1016/j.hrthm.2016.08.010. URL http://www.ncbi.nlm.nih.gov/pubmed/27498277.

[84] Espen W Remme, Erik Lyseggen, Thomas Helle-Valle, Anders Opdahl, Eirik Pettersen, Trond Vartdal, Asgrimur Ragnarsson, Morten Ljosland, Halfdan Ihlen, Thor Edvardsen, and Otto a Smiseth. Mechanisms of preejection and postejection velocity spikes in left ventricular myocardium: interaction between wall deformation and valve events. *Circulation*, 118(4):373–80, jul 2008. ISSN 1524-4539. doi: 10.1161/CIRCULATIONAHA.107.748491. URL http://www.ncbi.nlm.nih.gov/pubmed/18606917.

[85] Jan D'hooge, Elisa Konofagou, Fadi Jamal, Andreas Heimdal, Laurentino Barrios, Bart Bijnens, Jan Thoen, Frans Van de Werf, George Sutherland, and Paul Suetens. Two-dimensional ultrasonic strain rate measurement of the human heart in vivo. *IEEE transactions on ultrasonics, ferroelectrics, and frequency control*,

49(2):281–6, feb 2002. ISSN 0885-3010. URL http://www.ncbi.nlm.nih.gov/pubmed/11885685.

[86] George R. Sutherland, Liv Hatle, Piet Claus, Jan D'hooge, and Bart Bijnens. *Doppler Myocardial Imaging, A Textbook*. BSWK bvba, Scientific Consulting and Publishing. Hasselt, Belgium., 2008. ISBN 9789081059213.

[87] Birger Brekke, Hans Torp, Tore Bjastad, Asbjorn Stoylen, and Svein A. Aase. 3D Tissue Doppler imaging with ultra high frame rate. In *2011 IEEE International Ultrasonics Symposium*, pages 717–720. IEEE, oct 2011. ISBN 978-1-4577-1252-4. doi: 10.1109/ULTSYM.2011.0174. URL http://ieeexplore.ieee.org/lpdocs/epic03/wrapper.htm?arnumber=6293074.

[88] Arnold M Weissler, Willard S Harris, and D Clyde. Systolic time intervals in heart failure in man. *Circulation*, 37(37):149–159, 1968. doi: 10.1161/01.CIR.37.2.149.

[89] R G Pai and K S Gill. Amplitudes, durations, and timings of apically directed left ventricular myocardial velocities: I. Their normal pattern and coupling to ventricular filling and ejection. *Journal of the American Society of Echocardiography : official publication of the American Society of Echocardiography*, 11(2):105–11, feb 1998. ISSN 0894-7317. URL http://www.ncbi.nlm.nih.gov/pubmed/9517548.

[90] Fredrik Orderud, Gabriel Kiss, and Hans G. Torp. Automatic coupled segmentation of endo- and epicardial borders in 3D echocardiography. In *2008 IEEE Ultrasonics Symposium*, volume m, pages 1749–1752. IEEE, nov 2008. ISBN 978-1-4244-2428-3. doi: 10.1109/ULTSYM.2008.0429. URL http://ieeexplore.ieee.org/document/4803188/.

[91] Tim Lockie, Eike Nagel, Simon Redwood, and Sven Plein. Use of cardiovascular magnetic resonance imaging in acute coronary syndromes. *Circulation*, 119(12):1671–81, mar 2009. ISSN 1524-4539. doi: 10.1161/CIRCULATIONAHA.108.816512. URL https://www.ncbi.nlm.nih.gov/pmc/articles/PMC2730545/.

[92] Peter A. Cain, Martin Ugander, John Palmer, Marcus Carlsson, Einar Heiberg, and Hakan Arheden. Quantitative polar representation of left ventricular myocardial perfusion, function and viability using SPECT and cardiac magnetic resonance: initial results. *Clinical Physiology and Functional Imaging*, 25(4):215–222, jul 2005. ISSN 1475-0961. doi: 10.1111/j.1475-097X.2005.00618.x. URL

http://doi.wiley.com/10.1111/j.1475-097X.2005.00618.x.

[93] Einar Heiberg, Henrik Engblom, Jan Engvall, Erik Hedström, Martin Ugander, and Håkan Arheden. Semi-automatic quantification of myocardial infarction from delayed contrast enhanced magnetic resonance imaging. *Scandinavian Cardiovascular Journal*, 39(5):267–275, jan 2005. ISSN 1401-7431. doi: 10.1080/14017430500340543. URL http://www.tandfonline.com/doi/full/10.1080/14017430500340543.

[94] Einar Heiberg, Martin Ugander, Henrik Engblom, Matthias Götberg, Göran K Olivecrona, David Erlinge, and Håkan Arheden. Automated quantification of myocardial infarction from MR images by accounting for partial volume effects: animal, phantom, and human study. *Radiology*, 246(2):581–8, feb 2008. ISSN 1527-1315. doi: 10.1148/radiol.2461062164. URL http://www.ncbi.nlm.nih.gov/pubmed/18055873.

[95] R J Kim, E Wu, A Rafael, E L Chen, M A Parker, O Simonetti, F J Klocke, R O Bonow, and R M Judd. The use of contrast-enhanced magnetic resonance imaging to identify reversible myocardial dysfunction. *The New England journal of medicine*, 343(20):1445–53, nov 2000. ISSN 0028-4793. doi: 10.1056/NEJM200011163432003. URL http://www.ncbi.nlm.nih.gov/pubmed/11078769.

[96] Howard Levene. Robust testes for equality of variances. In Contributions to Probability and Statistics: Essays in Honor of Harold Hotelling. *Stanford University Press*, pages 278–292, 1960. ISSN 00063452. doi: 10.1002/bimj.19630050119.

[97] J. Martin Bland, DouglasG. G Altman, J M Bland, and DouglasG. G Altman. Statistical methods for assessing agreement between two methods of clinical measurement. *Lancet (London, England)*, 1(8476):307–10, feb 1986. ISSN 0140-6736. doi: 10.1016/S0140-6736(86)90837-8. URL http://www.ncbi.nlm.nih.gov/pubmed/2868172.

[98] T. Bjastad, S.A. Aase, and H. Torp. The impact of aberration on high frame rate cardiac B-mode imaging. *IEEE Transactions on Ultrasonics, Ferroelectrics and Frequency Control*, 54(1):32–41, jan 2007. ISSN 0885-3010. doi: 10.1109/TUFFC.2007.209. URL http://ieeexplore.ieee.org/document/4037298/.

[99] A G Tsakiris, D A Gordon, R Padiyar, and D Fréchette. Relation of mitral valve opening and closure to left atrial and ventricular pressures in the intact dog. *The American journal of physiology*, 234(2):H146–51, feb 1978. ISSN 0002-9513. URL http://www.ncbi.nlm.nih.gov/pubmed/623315.

[100] Wolfgang a Goetz, Emmanuel Lansac, Hou-Sen Lim, Patricia a Weber, and Carlos M G Duran. Left ventricular endocardial longitudinal and transverse changes during isovolumic contraction and relaxation: a challenge. *American journal of physiology. Heart and circulatory physiology*, 289(1):H196–201, jul 2005. ISSN 0363-6135. doi: 10.1152/ajpheart.00867.2004. URL http://www.ncbi.nlm.nih.gov/pubmed/15708963.

[101] M J Garcia, L Rodriguez, M Ares, B P Griffin, a L Klein, W J Stewart, and J D Thomas. Myocardial wall velocity assessment by pulsed Doppler tissue imaging: characteristic findings in normal subjects. *American heart journal*, 132(3):648–56, sep 1996. ISSN 0002-8703. URL http://www.ncbi.nlm.nih.gov/pubmed/8800038.

[102] D Pellerin, L Cohen, F Larrazet, F Pajany, S Witchitz, and C Veyrat. Preejectional left ventricular wall motion in normal subjects using Doppler tissue imaging and correlation with ejection fraction. *The American journal of cardiology*, 80(5):601–7, sep 1997. ISSN 0002-9149. URL http://www.ncbi.nlm.nih.gov/pubmed/9294989.

[103] C Pislaru, C J Bruce, M Belohlavek, J B Seward, and J F Greenleaf. Intracardiac measurement of pre-ejection myocardial velocities estimates the transmural extent of viable myocardium early after reperfusion in acute myocardial infarction. *Journal of the American College of Cardiology*, 38(6):1748–56, nov 2001. ISSN 0735-1097. URL http://www.ncbi.nlm.nih.gov/pubmed/11704391.

[104] Partho P Sengupta, Bijoy K Khandheria, Josef Korinek, Jianwen Wang, and Marek Belohlavek. Biphasic tissue Doppler waveforms during isovolumic phases are associated with asynchronous deformation of subendocardial and subepicardial layers. *Journal of applied physiology (Bethesda, Md. : 1985)*, 99(3):1104–11, sep 2005. ISSN 8750-7587. doi: 10.1152/japplphysiol.00191.2005. URL http://www.ncbi.nlm.nih.gov/pubmed/15905326.

[105] Hiroshi Kanai. Propagation of vibration caused by electrical excitation in the normal human heart. *Ultrasound in medicine & biology*, 35(6):936–48, jun 2009. ISSN 1879-291X. doi: 10.1016/j.ultrasmedbio.2008.12.013. URL http://www.ncbi.nlm.nih.gov/pubmed/19251357.

[106] M Marciniak, B Bijnens, a Baltabaeva, a Marciniak, C Parsai, P Claus, and G R Sutherland. Interventricular interaction as a possible mechanism for the presence of a biphasic systolic velocity profile in normal left ventricular free walls. *Heart (British Cardiac Society)*, 94(8):1058–64, aug 2008. ISSN 1468-201X. doi: 10.1136/hrt.2007.126938. URL http://www.ncbi.nlm.nih.gov/pubmed/17984214.

[107] Jonathan M Cordeiro, Lindsey Greene, Cory Heilmann, Daniel Antzelevitch, and Charles Antzelevitch. Transmural heterogeneity of calcium activity and mechanical function in the canine left ventricle. *American journal of physiology. Heart and circulatory physiology*, 286(4):H1471–9, apr 2004. ISSN 0363-6135. doi: 10.1152/ajpheart.00748.2003. URL http://www.ncbi.nlm.nih.gov/pubmed/14670817.

[108] Ethan Bunting, Litsa Lambrakos, Paul Kemper, William Whang, Hasan Garan, and Elisa Konofagou. Imaging the Propagation of the Electromechanical Wave in Heart Failure Patients with Cardiac Resynchronization Therapy. *Pacing and clinical electrophysiology : PACE*, oct 2016. ISSN 1540-8159. doi: 10.1111/pace.12964. URL http://www.ncbi.nlm.nih.gov/pubmed/27790723.

[109] Alexandre Costet, Elaine Wan, Ethan Bunting, Julien Grondin, Hasan Garan, and Elisa Konofagou. Electromechanical wave imaging (EWI) validation in all four cardiac chambers with 3D electroanatomic mapping in canines in vivo. *Physics in Medicine and Biology*, 61(22):8105–8119, 2016. ISSN 0031-9155. doi: 10.1088/0031-9155/61/22/8105. URL https://www.ncbi.nlm.nih.gov/pubmed/27782003.

[110] P L Castro, N L Greenberg, J Drinko, M J Garcia, and J D Thomas. Potential pitfalls of strain rate imaging: angle dependency. *Biomedical sciences instrumentation*, 36:197–202, 2000. ISSN 0067-8856. URL http://www.ncbi.nlm.nih.gov/pubmed/10834232.

[111] J.-U. Voigt. Strain-Rate Imaging During Dobutamine Stress Echocardiography Provides Objective Evidence of Inducible Ischemia. *Circulation*, 107

(16):2120–2126, apr 2003. ISSN 00097322. doi: 10.1161/01.CIR.0000065249.69988.AA. URL http://circ.ahajournals.org/cgi/doi/10.1161/01.CIR.0000065249.69988.AA.

[112] Sigurd Gunnes, Camilla Storaa, Britta Lind, Jacek Nowak, and Lars-Ake Brodin. Analysis of the effect of temporal filtering in myocardial tissue velocity imaging. *Journal of the American Society of Echocardiography : official publication of the American Society of Echocardiography*, 17(11):1138–45, nov 2004. ISSN 0894-7317. doi: 10.1016/j.echo.2004.06.006. URL http://www.ncbi.nlm.nih.gov/pubmed/15502787.

[113] A. Thorstensen, H. Dalen, B. H. Amundsen, S. A. Aase, and A. Stoylen. Reproducibility in echocardiographic assessment of the left ventricular global and regional function, the HUNT study. *European Journal of Echocardiography*, 11(2): 149–156, mar 2010. ISSN 1525-2167. doi: 10.1093/ejechocard/jep188. URL http://ehjcimaging.oxfordjournals.org/cgi/doi/10.1093/ejechocard/jep188.

[114] Nilsen, Lars Christian Lervik, Joakim Lund, Birger Brekke, and Asbøjrn Støylen. Strain rate measurements with ultra-high frame rate tissue doppler imaging. *European Heart Journal - Cardiovascular Imaging*, 14(suppl 2):ii208–ii236, 2013. ISSN 2047-2404. doi: 10.1093/ehjci/jet207. URL http://ehjcimaging.oxfordjournals.org/cgi/doi/10.1093/ehjci/jet207.

[115] W G Hopkins. Measures of reliability in sports medicine and science. *Sports medicine (Auckland, N.Z.)*, 30(1):1–15, jul 2000. ISSN 0112-1642. URL http://www.ncbi.nlm.nih.gov/pubmed/10907753.

[116] J Schmid, R Kaufmann, M R Grübler, N Verheyen, F Weidemann, and J S Binder. Strain Analysis by Tissue Doppler Imaging: Comparison of Conventional Manual Measurement with a Semiautomated Approach. *Echocardiography*, 33(3):372–378, 2016. ISSN 1540-8175. doi: 10.1111/echo.13100. URL https://www.ncbi.nlm.nih.gov/pubmed/26515731.

[117] Charlotte Bjork Ingul, Asbjorn Stoylen, Stig A. Slordahl, Rune Wiseth, Malcolm Burgess, and Thomas H. Marwick. Automated Analysis of Myocardial Deformation at Dobutamine Stress Echocardiography. *Journal of the American College of Cardiology*, 49(15):1651–1659, apr 2007. ISSN 07351097. doi:

10.1016/j.jacc.2007.01.059. URL http://linkinghub.elsevier.com/retrieve/pii/S0735109707004342.

[118] Naoyuki Yokoyama, Karl Q Schwarz, Xucai Chen, Sherry D Steinmetz, Harald Becher, Christina Schimpky, and Reinhard Schlief. The effect of echo contrast agent on Doppler velocity measurements. *Ultrasound in medicine & biology*, 29 (5):765–70, may 2003. ISSN 0301-5629. URL http://www.ncbi.nlm.nih.gov/pubmed/12754076.

[119] H Okura, K Yoshida, T Akasaka, T Hozumi, T Takagi, S Morioka, and J Yoshikawa. Improved transvalvular continuous-wave Doppler signal intensity after intravenous Albunex injection in patients with prosthetic aortic valves. *Journal of the American Society of Echocardiography : official publication of the American Society of Echocardiography*, 10(6):608–12. ISSN 0894-7317. URL http://www.ncbi.nlm.nih.gov/pubmed/9282350.

[120] R. Senior, H. Becher, M. Monaghan, L. Agati, J. Zamorano, J. L. Vanoverschelde, and P. Nihoyannopoulos. Contrast echocardiography: evidence-based recommendations by European Association of Echocardiography. *European Journal of Echocardiography*, 10(2):194–212, aug 2008. ISSN 1525-2167. doi: 10.1093/ejechocard/jep005. URL http://ehjcimaging.oxfordjournals.org/cgi/doi/10.1093/ejechocard/jep005.

[121] Nicola Logallo, Annette Fromm, Ulrike Waje-Andreassen, Lars Thomassen, and Knut Matre. Effect of microbubble contrast on intracranial blood flow velocity assessed by transcranial Doppler. *Journal of Ultrasound*, 17(1):21–26, mar 2014. ISSN 1876-7931. doi: 10.1007/s40477-014-0065-x. URL http://link.springer.com/10.1007/s40477-014-0065-x.

[122] Anikó I Nagy, Anders Sahlén, Aristomenis Manouras, Loghman Henareh, Cristina da Silva, Elif Günyeli, Astrid A Apor, Béla Merkely, and Reidar Winter. Combination of contrast-enhanced wall motion analysis and myocardial deformation imaging during dobutamine stress echocardiography. *European heart journal cardiovascular Imaging*, pages 1–8, sep 2014. ISSN 2047-2412. doi: 10.1093/ehjci/jeu171. URL http://www.ncbi.nlm.nih.gov/pubmed/25187604.

[123] Havard Dalen, Anders Thorstensen, Lars J Vatten, Svein A Aase, and Asbjorn Stoylen. Reference values and distribution of conventional echocardiographic Doppler measures and longitudinal tissue Doppler velocities in a population free from cardiovascular disease. *Circulation. Cardiovascular imaging*, 3(5):614–22, sep 2010. ISSN 1942-0080. doi: 10.1161/CIRCIMAGING.109.926022. URL http://www.ncbi.nlm.nih.gov/pubmed/20581050.

[124] Krishna K. Kadappu and Liza Thomas. Tissue Doppler Imaging in Echocardiography: Value and Limitations. *Heart, Lung and Circulation*, 24(3):224–233, mar 2015. ISSN 14439506. doi: 10.1016/j.hlc.2014.10.003. URL http://linkinghub.elsevier.com/retrieve/pii/S1443950614007331.

[125] Christian Seiler. *Collateral Circulation of the Heart*. Springer London, London, 2009. ISBN 978-1-84882-341-9. doi: 10.1007/978-1-84882-342-6. URL http://link.springer.com/10.1007/978-1-84882-342-6.

[126] R. E. Kerber, M. L. Marcus, J. Ehrhardt, R. Wilson, and F. M. Abboud. Correlation between echocardiographically demonstrated segmental dyskinesis and regional myocardial perfusion. *Circulation*, 52(6):1097–1104, dec 1975. ISSN 0009-7322. doi: 10.1161/01.CIR.52.6.1097. URL http://circ.ahajournals.org/cgi/doi/10.1161/01.CIR.52.6.1097.

[127] Eugene S Chung, Angel R Leon, Luigi Tavazzi, Jing-Ping Sun, Petros Nihoyannopoulos, John Merlino, William T Abraham, Stefano Ghio, Christophe Leclercq, Jeroen J Bax, Cheuk-Man Yu, John Gorcsan, Martin St John Sutton, Johan De Sutter, and Jaime Murillo. Results of the Predictors of Response to CRT (PROSPECT) trial. *Circulation*, 117(20):2608–16, may 2008. ISSN 1524-4539. doi: 10.1161/CIRCULATIONAHA.107.743120. URL http://www.ncbi.nlm.nih.gov/pubmed/18458170.

[128] E Silva, M Sitges, L Mont, V Delgado, D Tamborero, B Vidal, M Godoy, S Poyatos, C Pare, M Azqueta, and J Brugada. Quantification of left ventricular asynchrony throughout the whole cardiac cycle with a computed algorithm: application for optimizing resynchronization therapy. *Journal of cardiovascular electrophysiology*, 20(10):1130–6, oct 2009. ISSN 1540-8167. doi: 10.1111/j.1540-8167.2009.01507.x. URL http://www.ncbi.nlm.nih.gov/pubmed/19549037.

[129] Jeroen J Bax, Sander G Molhoek, Thomas H Marwick, Lieselot Van Erven, Paul J Voogd, Soeresh Somer, Eric Boersma, Paul Steendijk, and Martin J Schalij. Usefulness of Myocardial Tissue Doppler Echocardiography to Evaluate Left Ventricular Dyssynchrony Before and After Biventricular Pacing in. 91(02):94–97, 2003.

[130] Hideaki Kanzaki, Didier Jacques, L.Elif Sade, Donald a. Severyn, David Schwartzman, and John Gorcsan. Regional correlation by color-coded tissue Doppler to quantify improvements in mechanical left ventricular synchrony after biventricular pacing therapy. *The American Journal of Cardiology*, 92(6):752–755, sep 2003. ISSN 00029149. doi: 10.1016/S0002-9149(03)00848-8. URL http://linkinghub.elsevier.com/retrieve/pii/S0002914903008488.

[131] Serkan Ozturk, Aytekin Alcelik, Mehmet Ozyasar, Oguz Dikbas, and Selim Ayhan. Evaluation of left ventricular systolic asynchrony in patients with subclinical hypothyroidism. 19(4):374–380, 2012.

[132] Henryk Dreger, Adrian C Borges, Bruno Ismer, Sebastian Schattke, Berthold Stegemann, Gert Baumann, and Christoph Melzer. A modified echocardiographic protocol with intrinsic plausibility control to determine intraventricular asynchrony based on TDI and TSI. *Cardiovascular ultrasound*, 7(Lv):46, jan 2009. ISSN 1476-7120. doi: 10.1186/1476-7120-7-46. URL https://www.ncbi.nlm.nih.gov/pubmed/23121169.

[133] Berthold Stegemann, Henryk Dreger, Bruno Ismer, Gert Baumann, and Christoph Melzer. Left ventricular asynchrony in patients with right bundle branch block and normal ejection fraction. *Pacing and clinical electrophysiology : PACE*, 36 (1):63–8, jan 2013. ISSN 1540-8159. doi: 10.1111/pace.12043. URL http://www.ncbi.nlm.nih.gov/pubmed/23121169.

[134] Jonathan a Kirk and David a Kass. Electromechanical dyssynchrony and resynchronization of the failing heart. *Circulation research*, 113(6):765–76, aug 2013. ISSN 1524-4571. doi: 10.1161/CIRCRESAHA.113.300270. URL https://www.ncbi.nlm.nih.gov/pubmed/23989718.

[135] Kristina H Haugaa, Marit Kristine Smedsrud, Torkel Steen, Erik Kongsgaard, Jan Pål Loennechen, Terje Skjaerpe, Jens-Uwe Voigt, Rik Willems, Gunnar Smith, Otto a Smiseth, Jan P Amlie, and Thor Edvardsen. Mechanical dispersion assessed

by myocardial strain in patients after myocardial infarction for risk prediction of ventricular arrhythmia. *JACC. Cardiovascular imaging*, 3(3):247–56, mar 2010. ISSN 1876-7591. doi: 10.1016/j.jcmg.2009.11.012. URL http://www.ncbi.nlm.nih.gov/pubmed/20223421.

[136] Hiroyuki Iwano, Satoshi Yamada, Masaya Watanabe, Hirofumi Mitsuyama, Hisao Nishino, Shinobu Yokoyama, Sanae Kaga, Mutsumi Nishida, Hisashi Yokoshiki, Hisao Onozuka, Taisei Mikami, and Hiroyuki Tsutsui. Novel strain rate index of contractility loss caused by mechanical dyssynchrony. - A predictor of response to cardiac resynchronization therapy-. *Circulation journal : official journal of the Japanese Circulation Society*, 75(9):2167–75, jan 2011. ISSN 1347-4820. doi: 10.1253/circj.CJ-10-1099. URL http://www.ncbi.nlm.nih.gov/pubmed/21757822.

[137] Hiroyuki Iwano, Satoshi Yamada, Masaya Watanabe, Hirofumi Mitsuyama, Kazuya Mizukami, Hisao Nishino, Shinobu Yokoyama, Sanae Kaga, Kazunori Okada, Mutsumi Nishida, Hisashi Yokoshiki, Taisei Mikami, and Hiroyuki Tsutsui. Strain Rate Dispersion Index Can Predict Changes in Left Ventricular Volume and Adverse Cardiac Events Following Cardiac Resynchronization Therapy. *Circulation Journal*, 77(11):2757–2765, 2013. ISSN 1346-9843. doi: 10.1253/circj.CJ-13-0483. URL http://jlc.jst.go.jp/DN/JST.JSTAGE/circj/CJ-13-0483?lang=en{&}from=CrossRef{&}type=abstract.

[138] Hiroshi Ashikaga, Steven R Mickelsen, Daniel B Ennis, Ignacio Rodriguez, Peter Kellman, Han Wen, and Elliot R McVeigh. Electromechanical analysis of infarct border zone in chronic myocardial infarction. *American journal of physiology. Heart and circulatory physiology*, 289(3):H1099–105, sep 2005. ISSN 0363-6135. doi: 10.1152/ajpheart.00423.2005. URL http://www.ncbi.nlm.nih.gov/pmc/articles/PMC2396317/.

[139] Mohamed Fahmy Elnoamany, Hala Mahfouz Badran, Tarek Helmy Abo Elazm, and Eslam Shawky Abdelaziz. Asynchrony of left ventricular systolic performance after the first acute myocardial infarction in patients with narrow QRS complexes: Doppler tissue imaging study. *Journal of the American Society of Echocardiography : official publication of the American Society of Echocardiography*, 19(12):1449–57, dec 2006. ISSN 1097-6795. doi: 10.1016/j.echo.2006.06.012. URL http://www.ncbi.nlm.nih.gov/pubmed/17138028.

[140] K Fukuda, T Oki, T Tabata, a Iuchi, and S Ito. Regional left ventricular wall motion abnormalities in myocardial infarction and mitral annular descent velocities studied with pulsed tissue Doppler imaging. *Journal of the American Society of Echocardiography : official publication of the American Society of Echocardiography*, 11(9):841–8, sep 1998. ISSN 0894-7317. URL http://www.ncbi.nlm.nih.gov/pubmed/9758375.